



ScuDo
Scuola di Dottorato ~ Doctoral School
WHAT YOU ARE, TAKES YOU FAR



Doctoral Dissertation
Doctoral Program in Chemical Engineering (31st Cycle)

Enhancement of bioenergy production (H₂ + CH₄) from organic waste in anaerobic fermentation processes

Carlos Enrique Gómez Camacho

* * * * *

Supervisor

Prof. Bernardo Ruggeri

Politecnico di Torino
May, 2019

This thesis is licensed under a Creative Commons License, Attribution - Noncommercial - NoDerivative Works 4.0 International: see www.creativecommons.org. The text may be reproduced for non-commercial purposes, provided that credit is given to the original author.

I hereby declare that, the contents and organisation of this dissertation constitute my own original work and does not compromise in any way the rights of third parties, including those relating to the security of personal data.

.....
Carlos Enrique Gómez Camacho
Turin, May the 16th, 2019

Outline of the Thesis

The question about energy security is increasingly urgent, especially due to the ever-growing societal energy consumption patterns. Therefore, it is necessary to evaluate the different options and/or alternatives that are framed under the precepts of sustainability and which can compete with traditional energy sources, aiming not only to guarantee the needs of the current population, but also considering future scenarios. One of the most promising alternatives, which is widely spread, is Anaerobic Digestion (AD). AD exploits different biogeochemical cycles for the transformation of organic material (i.e. different organic waste and wastewaters) into products of interest, such as bioenergy carriers (H_2 and CH_4) and the digestate and compost for the agricultural industry.

This thesis consists of a compendium of experimental works that are framed in different areas of interest of the Chemical Engineering field regarding the production of bioenergy through anaerobic fermentation process, which can potentially allow an enhanced energy-recovery: the use of *Process Analytical Tools* (PAT), *Microbial Communities Engineering* (MCE) and *Energy Sustainability Analysis* (ESA), in detail:

Chapter I is introductory and presents a brief background and the major milestones that allowed the technical and scientific development of Anaerobic Digestion. In addition, the current panorama of energy production at a European level from biogas is presented, highlighting the different quotas of primary energy, as well as the correspondent power and heat production figures of the major players at regional level.

Chapter II presents a brief theoretical review of the hydrolysis process and the difficulties associated with the modelling of this phase of the AD. The experimental part includes the effect of comminution pre-treatments (i.e. ultrasonication, bead milling and rotor-stator degradation) on the Particle Size Distribution, using a PAT probe (i.e. single mode fiber in-situ laser back reflection) along with Image

Analysis to determine the effect on the different phases of interest: biotic phase, using model microorganisms (*Clostridium acetobutylicum* and *Bacillus subtilis*), complex feedstocks (i.e. mixture of grass silage, soil and water) and an AD broth from an on-going digester. The effects of the different parameters for each pre-treatment were assessed in terms of specific cuts of interest (D0-D50, D50-D90) as well as the specific energy consumption.

In **Chapter III**, two experimental techniques that are the *state-of-the-art* in the field of Microbial Communities (i.e. Frequency-Dependent Polarizability Anisotropy measurements and Flow Cytometry) for bioenergy production are tested to monitor the activity of the microorganisms involved in the process of biohydrogen production through Dark Fermentation, giving attention to cellular viability, metabolic products, the physiological state of fermentative bacteria and about the dynamics of the involved microbial groups.

Chapter IV examines the synergistic interactions between Anaerobic Corrosion (AC) of Fe^0 particles and Dark Fermentation (DF) systems, using a Hydrogen Producing Bacteria (HPB) consortium and different Fe^0 doses. An increased bio- H_2 production for the Fe^0 dosed samples coupled to a significant CO_2 -sink was observed. Moreover, the dynamics of H_2 production for supplemented and non-supplemented samples were modelled using a modified Gompertz equation; while Fe^0 supplemented samples exhibit a longer lag phase, which suggests that the biological phase requires a longer time for the adaptation to the presence of Fe^0 , the achieved biohydrogen production rates and yields increased significantly. Additionally, a literature review is provided with the possible mechanisms of the synergistic interactions.

Chapter V provides insights into the continuous operation of Two-Stage Anaerobic Digestion (TSAD) systems, in order to physically segregate the microbial community into Hydrogen Producing Bacteria (HPB) and Hydrogen Consuming Bacteria (HCB), under optimized environments for the production of each bioenergy carrier (i.e. bio- H_2 and bio- CH_4). The energetic performance resulted in an enhanced energy-recovery in TSAD compared to classical one-stage processes, due to the energy produced as hydrogen, the higher methane production and the role of the first stage as biological pre-treatment. A reliable energy-recovery is assured through operational parameters, in each stage, such as pH, temperature, mixing rate, Organic Loading Rate (OLR), Red-Ox potential, Hydraulic Retention Time (HRT) and kinetic selection of the microorganisms.

Lastly, in **Chapter VI**, an Energy Sustainability Analysis (ESA) methodology was developed and applied to evaluate the convenience of distributed H_2 production. This methodology serves to rationalize the main energy flows which

cross the technological boundaries, considering the diverted energy from other societal purposes to run a facility, for the construction of the plant, for the production of the required chemicals among other indirect energy flows. Three technologies are analysed: Steam Methane Reforming (SMR), Solar-Powered Water Electrolysis (SPWE) and TSAD. The results of the ESA are expressed through dedicated indicators: Energy Sustainability Index (ESI), Energy Return on Investment (EROI) and Energy Payback-Time (EPT), which reflect the intrinsic performance of a given technology based on the required energy flows.

Publications included in the Thesis

The topics which are addressed in following publications are extended in this Thesis, which are part of the results of my PhD research activities, including the conception, the experimental procedure, the interpretation of the results and the writing:

- **Chapter 3** is based on a Proceedings Publication: “Monitoring the impact of pH regulation in Dark Fermentation of Agricultural Waste: effects on product distribution and cell viability,” presented at the *7TH International Symposium on Energy from Biomass and Waste* (Venice, 2018), by **C. E. Gomez Camacho**, K. Pellicer Alborch, A. Bockisch, S. Junne, P. Neubauer. and B. Ruggeri.
- **Chapter 4** is based on a Journal Publication: “Macro approach analysis of dark biohydrogen production in the presence of zero valent powdered Fe⁰”, published in *Energy*, volume 159, pp. 525-533, September 2018, by **C. E. Gomez Camacho**, Francesco I. Romano and B. Ruggeri.
- **Chapter 5** is based on a draft Journal Publication: “Continuous Two-Step Anaerobic Digestion (TSAD) of Organic Market Waste: rationalising process parameters” submitted to the *International Journal of Energy and Environmental Engineering (IJEEE)* in March 2019, by **C. E. Gomez Camacho**, Lorenzo Mangialardi, M. Persico, A. C. Luongo Malavé and B. Ruggeri.

Other publications produced during the PhD research activities, which are non-directly included in the Thesis:

- “Experimental tests on commercial Sweet Product Residue (SPR) as a suitable feed for anaerobic bioenergy ($H_2 + CH_4$) production” published in *Waste Management*, volume 71, pp. 626-635, January 2018, by A.C. Luongo Malavé, **C.E. Gómez Camacho**, D. Fino and B. Ruggeri.
- “Syntrophic Microorganisms Interactions in Anaerobic Digestion (AD): a Critical Review in the Light of Increase Energy Production” published in *Chemical Engineering Transactions*, volume 64, May 2018, by **C.E. Gomez Camacho** and B. Ruggeri.
- “Electrical energy network efficiencies evaluation as milestones for smart grids development: Italy’s case study,” presented at the *IEEE PES Innovative Smart Grid Technologies Conference Europe* (Turin, 2017), by **C. E. Gomez Camacho**, G. Muto, and B. Ruggeri.
- “Enhanced Biohydrogen Production and CO_2 Sink by Powered Fe^0 Addition in Dark Fermentation,” presented at the *10TH International Conference on Sustainable Energy and Environmental Protection: Renewable Energy Sources* (Bled, 2017), by **C. E. Gomez Camacho**, F. I. Romano, and B. Ruggeri.
- “Shear stress as phylogenetic control of microbial population dynamics in Dark Fermentation (DF) systems,” presented at the *7TH International Symposium on Energy from Biomass and Waste* (Venice, 2018), by L. Mangialardi, **C.E. Gomez Camacho** and B. Ruggeri.

Acknowledgments

First of all, I would like to thank God for giving me an extra supply of strength, health, imagination and clarity during my PhD work, for accompanying me during the whole path, and for never letting me down, even in the most-demanding episodes. Equally important for me was the support of my parents, for which I will not find words to accordingly thank, my Mom (Maria Trinidad), my Dad (Hugo Emmanuel), as well as my sisters (Brenda and Sofia) and aunts (Ruth† and Helina); because my family kindly supported me, made me the person that I am today and shared with me the correct values which help me to endure daily life.

I should always acknowledge the Universidad Central de Venezuela (*UCV*), “*La Casa que vence la sombra*”, for my initial contact with science and academic training and the opportunity to grow in one of the most, if not the most, democratic place in our national territory.

At Politecnico di Torino, my current *alma mater*, I had the opportunity to learn and expand my horizons, acquiring a wide variety of multidisciplinary skills, therefore I would like to especially thank Prof. Bernardo Ruggeri, whose constant support, advise and large experience in the field of process engineering, biotechnology, sustainability and policy-making has provided me global insights of energy-recovery and production systems and have also been invaluable for the development of the present work. My gratitude goes also to the different students who I had the pleasure to guide (and to learn from) through their Master theses: Suzana, Francesco, Lorenzo, Mauro and Chiara whose contributions, results and dedication are present, at some extend, in the present work. I also thank other collaborators of Prof. Ruggeri’s research group: Andrea, Giorgia, Marco, Giancarmine, Giuseppe, Carlotta and Stefano since the discussions in the group always fostered my scientific curiosity.

Part of the experimental work was conducted at the Technische Universität Berlin (TU Berlin), in the Chair of Bioprocess Engineering under the supervision of Professor Peter Neubauer and Dr.-Ing Stefan Junne, who I kindly thank for the opportunity to work in their facilities, learn from the cutting-edge research that they

conduct and become part of the team that they lead. I also extend my gratitude to the other members of the team, Anna Maria, Anika, David, Klaus, Lara and Marly whose help and good disposition positively influenced my doctoral stay.

Last but not least, I really appreciate the support of the large family of Venezuelan people living in Turin, especially Jaime and Felix, because we together share the immigrant's fate full of twists and bump and support each other in difficult times.

*“Estudia niño, sin cesar estudia,
Es puerta de luz un libro abierto:
Entra por ella, niño, y de seguro
Que para ti serán en lo futuro
Dios más visible, su poder más cierto.*

*El ignorante vive en el desierto
Donde es el agua poca, el aire impuro;
Un grano le detiene el pie inseguro;
Camina tropezando; ¡vive muerto!*

*En ese de tu edad abril florido,
Recibe el corazón las impresiones
Como la cera el toque de las manos:*

*Estudia, y no serás, cuando crecido,
Ni el juguete vulgar de las pasiones,
Ni el esclavo servil de los tiranos.”*

*Elias Calixto Pompa
(1834-1887)*

Contents

1.Introduction	1
1.1 Brief historic background of Anaerobic Digestion	1
1.2 State of Biogas production in Europe	4
References	9
2.Effects of mechanical pre-treatments on the different phases of Anaerobic Digestion broths	11
2.1 Introduction	11
2.2 Theoretical background.....	14
2.2.1 Hydrolysis	14
2.2.2 Cellulases.....	15
2.2.3 Lipases.....	15
2.2.4 Proteases	16
2.2.5 Hydrolysis Models	17
2.3 Experimental procedure	21
2.3.1 Bacteria cultivation.....	21
2.3.2 Feedstocks: Agricultural Waste (AW)	22
2.3.3 Mechanical pre-treatments	22
2.3.4 Analytical Measurements	24
2.4 Results	25
2.4.1 Effect of mechanical pre-treatments on the biotic phase (<i>Bacillus subtilis</i> cultures).....	25
2.4.2 Specific Energy input and cell viability	28
2.4.3 Effects of continuous-flow ultrasonication on the particle size distribution of <i>Clostridium acetobutylicum</i> samples	29
2.4.4 Effects on the feedstock: Agricultural Waste (AW)	33
2.5 Conclusions	39
References	40

3. Monitoring the state of mixed cultures used for bioenergy production	43
3.1 Introduction	43
3.2 Theoretical background	45
3.2.1 Biofuels and Biorefineries:	45
3.2.2 Physiological status and cell viability of mixed cultures	48
3.2.3 Flow Cytometry (FC)	51
3.2.4 Frequency-Dependent Polarizability Anisotropy (FDPA)	53
3.3 Materials and methods	55
3.3.1 Experimental set-up of the DF system	55
3.3.2 Preparation of the Hydrogen Producing Bacteria (HFB) inoculum	55
3.3.3 Feedstock and pre-treatment	56
3.3.4 Analytical Measurements	57
3.4 Results and discussion	59
3.4.1 Course of fermentation and metabolic products	59
3.4.2 Anisotropic Polarizability (AP) measurements	61
3.4.3 Flow cytometry (FC)	62
3.5 Conclusions	70
References	72
4. Macro-approach analysis of biohydrogen production in the presence of powdered Fe°	75
4.1 Introduction	75
4.2 Materials and methods	77
4.2.1 Experimental tests	77
4.2.2 Preparation of the substrate	77
4.2.3 Preparation of the inoculum	78
4.2.4 Analytical measurements	78
4.2.5 Relaxation time approach	79
4.2.6 Fe° Anaerobic Corrosion (AC)	81
4.2.7 Dark fermentation (DF)	83
4.3 Results and discussion	84
4.3.1 Anaerobic corrosion	84
4.3.2 Dark Fermentation	86

4.3.3 Synergic effects and dynamic interaction of the involved phenomena	88
4.3.4 Discussion on the nature of the synergic effects	90
4.4 Conclusions	94
References	95
5. Continuous Two-Step Anaerobic Digestion (TSAD) of Organic Market Waste: rationalising process parameters	101
5.1 Introduction	101
5.2. Materials and methods	103
5.2.1 Experimental set-up of the TSAD system	103
5.2.2 Preparation and pre-treatment of the substrate	105
5.2.3 Preparation of the inocula	105
5.2.4 Analytical Measurements	106
5.2.5 Start-up of the TSAD system	106
5.2.6 Screening of the different Hydraulic Retention Times (HRT)	107
5.2.7 Kinetic selection of the microorganisms based on HRT	107
5.2.8 Efficiency (η) and Efficacy (ζ) evaluations	109
5.3. Results and discussion	110
5.3.1 Volatile Solid (VS) concentrations along the TSAD system	110
5.3.2 H ₂ and CH ₄ production in S1 and S2 for different HRT	112
5.3.3 Statistical analysis of the TSAD in a pseudo-steady-state condition	113
5.3.4 Energetic Performance of the TSAD	115
5.4. Conclusion	119
References	120
6. Energy Sustainability Analysis (ESA) of distributed H ₂ production	123
6.1 Introduction	123
6.2 Methodology	126
6.2.1 <i>Energy Sustainability Analysis (ESA)</i>	126
6.2.2 Boundaries of analysis	126
6.2.3 <i>Energy Sustainability Index (ESI)</i>	127
6.2.4 Analogical Model (AM)	128
6.2.5 Energy Return on Invested (EROI) and Energy Payback Time (EPT)	130

6.3 Case study: distributed H ₂ production	130
6.3.1 Steam-Methane Reforming (SMR)	130
6.3.2 Solar-Powered Water Electrolysis (SPWE)	132
6.3.3 Two-Stage Anaerobic Digestion (TSAD)	134
6.4 Results and Discussion.....	135
6.5 Conclusions	140
References	142
List of Figures	145
List of Tables.....	149

1. Introduction

1.1 Brief historic background of Anaerobic Digestion

The history of biogas has many successive chapters, which made it possible to develop what is nowadays known as Anaerobic Digesters and constitutes a technique of sanitation/stabilization of wastewaters as well as a model energy-recovery process with an enormous presence in the world and an even greater potential to be exploited.

In the history of mankind, the presence of fermentative processes has been largely limited to the production phase, especially in the food and beverages industry. In ancient times, different cultures fermented different substrates and produced mead (using glucose and fructose from honey), wine and beers (using sugars to produce ethanol), vinegar (producing acetic acid through the aerobic oxidation of ethanol), yogurts (lactic acid fermentation from milk), kefir, bread, cheese, among others [1]. Most of these processes were focused on the transformations occurring in the solid and/or liquid phases, without complex considerations about the gas phase. Even before the appearance of the microscope, artisans and workers followed recipes and intuitive and experiential-based heuristics in order to reproduce the production processes.

The term *fermentation* has its roots in the Latin verb *fervēre*, which means to boil or to be hot or agitated, probably derived from the physical observable effects of CO₂ production in liquid media during this phenomenon. According to [2], the term first appeared around the 14th century, but the common scientific sense was coined around the 17th century. Van Helmont (1660) formally introduced the word *gas* (from the greek word *kaos*, which means disorder) [3], establishing the difference between air, gas and condensable vapours and recognized the evolution of CO₂ (*gas sylvestre*) from inorganic reactions and also during the production of wine and beer [4]. Furthermore, Van Helmont first noticed the production of flammable gases due to decaying organic matter.

Another important milestone in the story of biogas were the contributions of Volta (1777) [5], conducted in a marshy area of Lake Maggiore (Italy). Volta observed an *inflammable air native of marshes* (methane) bubbling from the bottom of the lake and associated the production of this gas to the decomposition of organic plants and vegetables in the water. Volta additionally experimented on flammability, which led to the development of the *Pistola di Volta*, a device to assess the flammability of gases (i.e. an early combustion chamber) based on the noise that the explosion produces and he first compared the energy content of methane with other gases, concluding that *the air of swamps* ignites and explodes most loudly than other combustible airs, even than hydrogen [6].

Fourcroy (1787) introduced the modern sense of the term fermentation, associated to the production of carbonic acid gas (i.e. CO₂), first proposing the existence of 5 types of vegetable fermentations: saccharine (sugars), vinous, acetous, colouring and putrid [7]. Lavoisier and Gay-Lusac studied alcoholic fermentations in detailed, where sugars in the presence of oxygen were transformed into alcohols, releasing CO₂ and organic acids [8], even trying to summarize in simple chemical equations the observed yields associated to fermentation. Their observations served as reference to Louis Pasteur, who further questioned if succinic acid and glycerine trace production during alcoholic fermentation could be due to a secondary and accidental action [9]. In 1789, Lavoisier published “*Traité élémentaire de chimie*”, reporting different experiments and first stating the famous mass conservation principle. In fact, it was the observations and quantification of an alcoholic fermentation process that led Lavoisier to formulate the principle, considering the balances of sugar, alcohol and carbon dioxide. Moreover, an innovative concept brought to the scientific community by Lavoisier was the resemblance between respiration and combustion because, according to him, respiration could be conceived as a slow combustion that takes place in the lungs [10].

The *flammable air* reported by Volta was later (1806) identified independently as carburetted hydrogen by Henry and methane by Dalton. In 1863, a manuscript presenting Louis Pasteur observations during the period 1861-1863, titled “*A Novel Instance of the Production of Fermentation by the Presence of Infusoria capable of existing without free Oxygen and deprived of all Access of Atmospheric Air*” [11], first suggested the distinction of aerobic and anaerobic microorganisms which later, in 1878 [8], was extended to exclusively aerobic, at once aerobic and anaerobic, or exclusively anaerobic. Pasteur findings were controversial at the time, since according to his theory, framed within a *vitalism* optic, certain processes are carried on in living organisms, as the case of fermentation. Especially known are the differences between Pasteur and Liebig, since the latter affirmed that fermentation had a *mechanist* nature and claimed that it was a pure mechanical and chemical phenomenon, triggered by oxygen that promotes an unstable behaviour in the structure of compounds, that propagates, thus generating the decay of organic matter and fermentation products. However, Liebig first related rotting organic substances (i.e. manure, urine) to classic fermentative processes, such as wine and beer production, and also to digested food [12].

Methane production from ethanol under anaerobic laboratory conditions was first evidenced by Béchamp in 1868, who ascribed methane production to a little ferment observed in the microscope, named by him as *Microzyma create* [13]. During this time period, in the 19th century, the concept of enzyme was also first introduced, linked to the on-going developments in the field of fermentation. Kühne (1876) suggested the term *enzyme*, which derives from Greek (ἐνζυμῶν) and means “*in leavean*” or “*in yeast*” [14], to name the structures denominated at the time as *non-organized ferments*. This definition is probably based on Bertholet (1860) experiments, which evinced the transformation of sucrose into glucose and fructose using an extract from yeast by the action of *soluble ferments*, now believed to be

extracellular invertases (β -fructofuranosidases) from *Saccharomyces cerevisiae* [13].

The independent experiments of Tappeiner (1882) and, a student of Pasteur, Gayon (1884), provided more experimental insights into biomethane formation. Teppeiner studied different anaerobic cultures from plants organic materials, using ruminant intestinal fluids as inoculum and applying different treatments (i.e. promoting heat and chemical inhibitions) and concluded that only untreated samples were able to produce methane [13]. On the other hand, Gayon and Pasteur collected horse and cattle manure and produced biogas at 100 L/m³, even conjecturing that this gas could be sufficient to light up the streets of Paris [15].

Molecular hydrogen produced by bacterial activity was first reported by Popoff (1885), who studied the anaerobic decomposition of cellulose in presence of river mud, and tracked the gaseous products, confirming that methane, carbon dioxide and hydrogen were formed [13]. The first differences among acidogenic and methanogenic fermentations were observed by Hoppe-Seyler (1887), who investigated cellulose decomposition and studied the acidogenic degradation of formic acid to hydrogen and carbon dioxide and the conversion of acetic acid into carbon dioxide and methane using sewer sludges as inoculum [13]. His work also introduced the concept of reduction associated to fermentation, exemplified by the passage from galactose to mannitol or the conversion from lactic acid into propionic acid.

In the year 1876, Gibbs published the manuscript “*On the Equilibrium of Heterogeneous Substances*” [16] and Helmholtz presented in 1882 “*Thermodynamik chemischer Vorgänge*” building the foundations of modern thermodynamics, which has also served for describing, understanding and designing processes and phenomena occurring in biological systems. Other important contribution was made by Nernst (1888), who further worked on thermodynamics and electrochemistry, developing the equation that correlates the cell potential to reactants and which is also useful in biology, biotechnology, molecular chemistry and medicine.

Omeliński (1897) started observing by accident mixed acidogenic cultures (named by him as *aroma producing bacteria*), and hydrogen production when he experimented with the decomposition of pieces of raw potato in water [17]. He classified (1923) aroma producing bacteria based in the type of fermentation as: yeasts, acetic acid bacteria, lactic acid bacteria, butyric acid bacteria, putrefactive bacteria, pathogenic bacteria and mold fungi. Following Omeliński, Söhngen further researched on the activity of mixed cultures, especially the role of carbon dioxide and hydrogen, and their combination to produce methane. He first provided temporal differences between fermentations yielding hydrogen and methane and he drew gas production rates of methane from butyrate and formate [18] as well as the first formulations of the hydrogenotrophic and acetoclastic pathways for methane generation.

In 1930, Buswell introduced his empirical equation to estimate the theoretical amount of biogas that can be stoichiometrically formed from any kind of organic matter, characterized in terms of its elemental constituents. This model and its

further additions became the baseline for the further development of more complex models aiming at predicting the theoretical yield of organic substrates in methane and other products [19].

In 1967 Bryant et al. first proposed the “*Interspecies Electron Transfer*” theory, while studying a culture of *Methanobacillus omelianskii* that was thought to be pure, but later it was established that two strains were involved in CH₄ generation due to syntrophic relations established between acidogenic bacteria and methanogens [20].

From the engineering point of view, during the 19th century, different AD plants were reported to be built in different parts of the world. Historical references diverge on the exact date, however, some of them point New Zealand (1840) as the first commercial digester, although it was built initially to treat whale fat [21]. Another early successful application (1859) of biogas was implemented in Matunga (Mumbai, India) to provide water sanitation and gas for an engine (i.e. lightening purposes) for an asylum-hospital facility for leprosy patients. Meanwhile (1881), Mouras in France presented the *automatic scavenger*, an airtight chamber aimed at treating suspended organic matter. Later in 1896, in Exeter (England), an AD plant was constructed to treat sewage, also providing gas for public lightening.

1.2 State of Biogas production in Europe

Biogas production can be considered now a consolidate technology worldwide, and the different configurations that fermenters for Anaerobic Digestion (AD) might present at industrial level, e.g. stirred tanks reactors (CSTR), Plug flow digesters (PFR), Up flow Anaerobic Sludge Blanket (UASB) have reached a Technology Readiness Level (TRL) certainly in the range 7-9. For instance, *The State of Renewable Energies in Europe*, in its the 15th edition, reports 17.240 operative biogas plants in Europe in the year 2015 [22] and for the year 2016, biogas primary energy production reached 16.1 Million tonne of oil equivalent (Mtoe) [23], with more of 77 % of the production coming from Germany, United Kingdom and Italy (see **Figure 1.1**) [24]. The primary energy, in this case, corresponds to the energy embedded in the mix of gases that are produced in Anaerobic Digesters. The main energy carriers associated to the AD process are bio-H₂ and bio-CH₄. In most of the cases, H₂ is produced biologically via *Dark Fermentation* (DF), although hydrogen can also be produced by biophotolysis of water using *algae* and photosynthetic bacteria, photodecomposition of organic compounds by photosynthetic organisms or a mixture between fermentative and photosynthetic microorganisms [25] and CH₄ via *methanogenesis* in AD; both processes encompass a series of steps that lead in each case to either H₂ and/or CH₄.

Biogas specific composition, and therefore its energy content, depend on many factors, such as the type of microbial consortia, the composition of the feed (i.e. substrate), operational conditions, accumulation of inhibitory compounds, seasonality, among others. However, the referential values for biogas range from 40-70 % v/v in CH₄ and 60-30 % of CO₂.

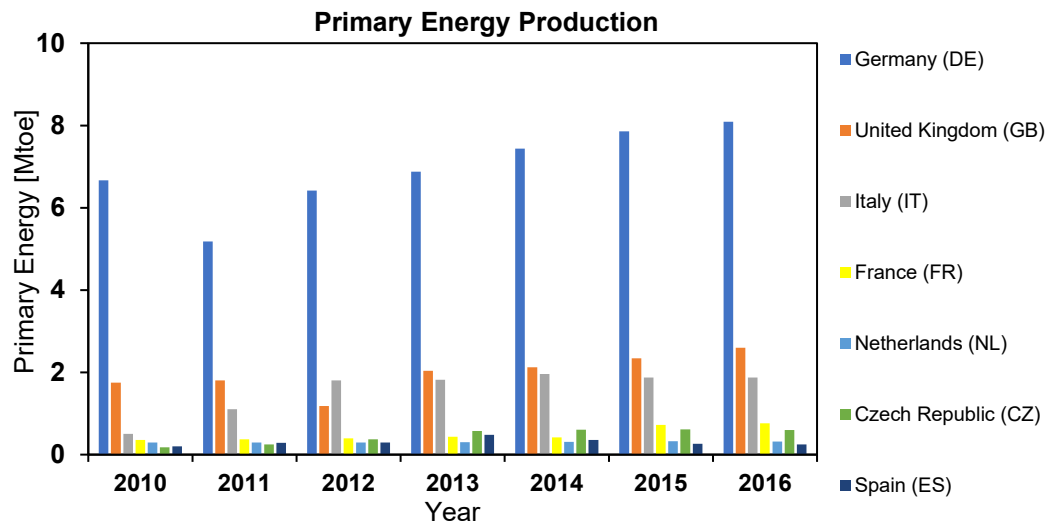


Figure 1.1 Primary energy production from biogas for the main European players during 2010-2016 [26].

Similar to oil, biogas is not a standard product, whose chemical composition is always fixed. Fossil fuels, such as gasoline, kerosene or jet fuel are characterized by their energetic power and oil prices are set according to the variation of a determined crude compared to a standard (e.g. Brent or West Texas Intermediate), based on the chemical assay, where properties such as API density, fuels yields, Sulphur content, salinity, viscosity, asphaltene/aromatics/paraffins contents are assessed.

For the case of AD, the main energy content of biogas is due to H_2 and CH_4 . Rasi et al. [27] examined data from different biogas plants (landfills, sewage digesters and farm plants) and found an average methane content of 48% - 65%, carbon dioxide ranging from 36% to 41% and other trace gases: O_2 (<1 %), N_2 (1-17%), H_2S (15.1–427.5 ppm), Volatile Organic Compounds (VOC) such as benzene (0.1-35.6 mg/m^3) and toluene (0.2 – 171.6 mg/m^3) and in a lower degree organic silicon compounds (0.4 – 10.6 mg/m^3). According to their results, high N_2 and O_2 contents were found in landfills, especially during winter, which is probably due to air infiltration and low methane yields at low temperatures; moreover, sewage sludges and landfills exhibited more variable traces composition than farm plant, which can be related to the higher heterogeneity in the feed for each case. Arnold and Kajolinna [28] further investigated the composition of biogas and reported traces of hexamethylcyclotrisiloxane (2.29 mg/m^3), ammonia (3-4 ppmv) and Sulphur compounds (700-900 mg/m^3) from landfills, octamethylcyclotetrasiloxane (4.3 mg/m^3) and decamethylcyclopentasiloxane (27.05 mg/m^3) from sewage sludges and decamethylcyclopentasiloxane (4.46 mg/m^3) and Sulphur compounds (30 ppmv) from the co-digestion of sewage sludges with different industrial, municipal and kitchen wastes.

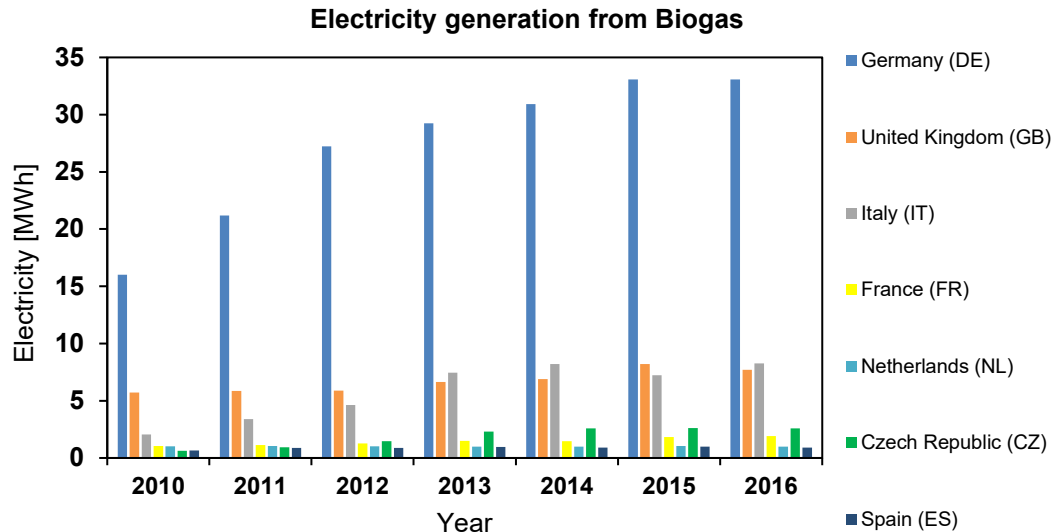


Figure 1.2 Electricity generation from biogas for the main European players during 2010-2016 [26].

In one-stage Anaerobic Digesters, or classical AD plants, H_2 is not a desired product, and it is internally consumed in the digester by hydrogen-scavenger bacteria. However, in multi-step anaerobic digestion, such as TSAD [29] or in complex wastewater treatment plants, hydrogen production can be significant in the previous stages to the methanogenic reactor, and therefore it contributes in a lesser extend to the produced primary energy. The trace compounds in biogas, as noted before, correspond only to a negligible fraction of it; in some cases, it is required downstream treatment, but the presence of these trace elements do not significantly contribute to the primary energy produced in these systems.

The main application of biogas is to be used as fuel, hence the final energy that is used by final consumers are either electricity (**Figure 1.2**) or heat, or both combined. According to [30], the life stages of energy can be considered as: *primary energy*, extracted from the soil, sun, air, or the sea (i.e. either renewable or non-renewable) which becomes a *secondary energy* through refinement or industrial processing that represents an energy carrier (or *refined fuel*) to be finally delivered to the end use point as *final energy*.

At European level, the most important reference in the energy field is nowadays the ambitious Energy Efficiency Directive (EED) 2012/27/EU. The primary objective was to save 20% of the primary energy used in the Union, with a limit of 1474 Mtoe of primary energy and 1078 Mtoe in terms of final consumption by 2020. The goal of the EED is to shift energy production, transformation and utilization towards rational and innovative technologies, thus increasing energy security and mitigating environmental impacts. In addition, EED encourages the use of localized power generation systems (i.e. less than 20 MW) that are capable of improving the overall efficiency of the system, not only due to their greater generation efficiency, but also due to the reduced losses in the transmission and distribution stages.

Table 1.1. Produced primary energy and electrical and thermal efficiency from biogas in Europe during 2016 [26].

	Primary Energy [Mtoe]	Electricity [MWh]	Heat [ktoe]	$\eta_{electric}$ [%]	$\eta_{thermal}$ [%]	η_{total} [%]
<i>Germany</i>	8.094	33.073	222.553	35.13	2.75	37.88
<i>United Kingdom</i>	2.601	7.706	-	25.47	-	-
<i>Italy</i>	1.875	8.259	207.987	37.87	11.09	48.97
<i>France</i>	0.760	1.901	40.604	21.51	5.34	26.85
<i>Netherlands</i>	0.319	0.993	6.520	26.77	2.04	28.81
<i>Czech Republic</i>	0.601	2.589	14.331	37.04	2.38	39.43
<i>Spain</i>	0.245	0.906	6.544	31.80	2.67	34.47

In this respect, the recent trends of primary energy production from biogas (**Figure 1.1**) and power generation (**Figure 1.2**) are promising facts which reflect the increasing interest which is given to this type of energy recovery technologies.

Table 1.2 Total primary energy consumption [31] and biogas share for 2016 in Europe.

	Total Consumption [Mtoe]	Biogas Production [Mtoe]	Share [%]
<i>Germany</i>	322.5	8.094	2.51
<i>United Kingdom</i>	188.1	2.601	1.38
<i>Italy</i>	151.3	1.875	1.24
<i>France</i>	235.9	0.760	0.32
<i>Netherlands</i>	84.5	0.319	0.38
<i>Czech Republic</i>	39.9	0.601	1.51
<i>Spain</i>	135.0	0.245	0.18
<i>Total</i>	1 157.2	14.495	1.25

As suggested by the EED, energy efficiency is a major concern which can be addressed only by applying simultaneous strategies, due to the inextricable complexity of the nature of energy efficiency. However, increased biogas production is a global trend, and other major economic players [32][33] as well as developing countries have started to implement AD systems at different scales for biogas production. AD provides a technological solution that is able to fulfil economic feasibility of the process in an energetically sustainable manner, hence the use of AD to treat and revalorize different organic wastes has influenced the practices and policies not only of different countries, regions and large companies, but also of small farmers and users. Thus, recovering power and heat (**Table 1.1**), from biogas production processes is an adequate strategy which offers the possibility to apply top-down and bottom-up approaches; national governments (**Table 1.2**) and regional bodies propose directives which are applied, enhanced or modify by locals since the generation organic waste is localized and distributed across countries. Moreover, coupling organic waste management and energy production aims at reusing and recycling, which are two fundamental concepts for the study of environmental sustainability and also complies with the criterion of *proximity*.

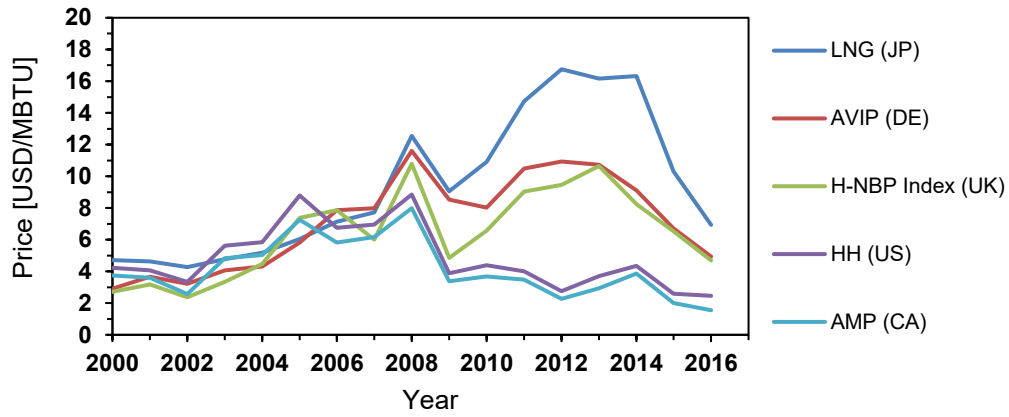


Figure 1.3 Historic [2000-2016] prices of regional standards of Natural Gas: Liquefied Natural Gas (LNG) in Japan, Average German Import Price (AVIP) in Germany, Heren National Balancing Point Index (H-NBP) in the United Kingdom, Henry Hub Index (HH) in the United States and the Alberta Market Price (AMP) in Canada [34].

Traditional fossil fuels, and specially oil and its derivatives, have played a very complex role in our modern civilization responding to production quotas, demand, prices and socio-political interests that are, in some cases, unpredictable (**Figure 1.3**). On the other hand, the use of renewable energies, especially localized- and self-produced, serves to promote environmental improvements and stability in energy services, which is of interest in the design of future energy systems, combining local power generation, mix of primary sources and assessment of variabilities for renewable sources.

References

- [1] Y. H. Hui, *Handbook of Food and Beverage Fermentation Technology*. New York: Marcel Dekker, 2004.
- [2] “Online Etymology Dictionary,” May-2018. [Online]. Available: <http://www.dictionary.com/browse/fermentation>.
- [3] “Online Etymology Dictionary,” May-2018. [Online]. Available: <http://www.dictionary.com/browse/gas>.
- [4] H. S. Redgrove, *Joannes Baptista van Helmont; alchemist, physician and philosopher*. London: William Rider & Son, Ltd., 1922.
- [5] A. Volta, *Lettere del Signor Don Alessandro Volta Sull’ Aria Inflammabile Nativa delle Paludi*. Milano: Giuseppe Marelli, 1777.
- [6] R. S. Wolfe, “Recreating Volta’s dramatic 19th-century displays of energy released from methane provides insights into anaerobic microbial metabolism,” *ASM News*, vol. 70, no. 1, pp. 15–18, 2004.
- [7] S. Parkes, *A Chymical Catechism, Or, The Application of Chymistry to the Arts: For the Use of Young People, Artists, Tradesmen and the Amusement of Leisure Hours*. New York: James Humphreys, 1807.
- [8] M. Sebald and D. Hauser, “Pasteur, oxygen and the anaerobes revisited,” *Anaerobe*, vol. 1, no. 1, pp. 11–16, 1995.
- [9] L. Pasteur, “On alcoholic fermentation,” *London, Edinburgh, Dublin Philos. Mag. J. Sci.*, vol. 18, no. 119, pp. 239–240, 1859.
- [10] M. H. Stipanuk and M. A. Caudill, *Biochemical, Physiological, and Molecular Aspects of Human Nutrition*. St. Louis: Saunders Elsevier, 2012.
- [11] L. Pasteur, “A novel instance of the production of fermentation by the presence of Infusoria capable of existing without free oxygen and deprived of all access of atmospheric air,” *Ann. Mag. Nat. Hist.*, vol. 11, pp. 313–317, 1863.
- [12] A. García-Carmona and J. Acevedo-Díaz, “The controversy between Pasteur and Liebig on fermentation – A story to understand some features of the Nature of Science,” *Working Paper* (doi: 10.13140/RG.2.2.11612.18565), 2016.
- [13] J. G. Ferry, *Methanogenesis: Ecology, Physiology, Biochemistry & Genetics*. New York: Springer Science & Business Media, 2012.
- [14] “Online Etymology Dictionary,” May-2018. [Online]. Available: <http://www.dictionary.com/browse/enzyme>.
- [15] C. J. Cleveland and C. G. Morris, *Handbook of Energy: Chronologies, Top Ten Lists, and Word Clouds*. Amsterdam: Elsevier Science, 2013.
- [16] J. W. Gibbs, “On the equilibrium of heterogeneous substances,” *Am. J. Sci.*, vol. 16, pp. 441–458, 1878.
- [17] V. L. Omelianski, “Aroma-Producing Microorganisms,” *J. Bacteriol.*, vol. 8, no. 4, pp. 393–419, Jul. 1923.
- [18] N. L. Söhngen, “Sur le rôle du Méthane dans la vie organique,” *Recl. des Trav. Chim. des Pays-Bas la Belgique*, vol. 29, no. 7, pp. 238–274, 1910.
- [19] A. M. Buswell and F. W. Sollo, “The Mechanism of the Methane Fermentation,” *J. Am. Chem. Soc.*, vol. 70, no. 5, pp. 1778–1780, 1948.
- [20] M. P. Bryant, E. A. Wolin, M. J. Wolin, and R. S. Wolfe, “*Methanobacillus omelianskii*, a symbiotic association of two species of bacteria,” *Arch. Mikrobiol.*, vol. 59, no. 1, pp. 20–31, 1967.
- [21] J. Bundschuh and G. Chen, *Sustainable Energy Solutions in Agriculture*. London: CRC Press/Balkema, 2014.

- [22] EurObserv'ER, "The State of Renewable Energies in Europe," Paris, 2015.
- [23] EurObserv'ER, "Press Release: Biogas Barometer," Paris, 2017.
- [24] EurObserv'ER, "The State of Renewable Energies in Europe," Paris, 2016.
- [25] D. Das and T. N. Veziroglu, "Hydrogen production by biological processes: a survey of literature," *Int. J. Hydrogen Energy*, vol. 26, no. 1, pp. 13–28, 2001.
- [26] EurObserv'ER, "Cartographic Module," 2018. [Online]. Available: http://observer.cartajour-online.com/barosig/Interface_Standard/cart@jour.phtml?NOM_PROJET=barosig&NOM_USER=&Langue=Langue2&Login=OK&Pass=OK. [Accessed: 23-Apr-2018].
- [27] S. Rasi, A. Veijanen, and J. Rintala, "Trace compounds of biogas from different biogas production plants," *Energy*, vol. 32, no. 8, pp. 1375–1380, 2007.
- [28] M. Arnold and T. Kajolinna, "Development of on-line measurement techniques for siloxanes and other trace compounds in biogas," *Waste Manag.*, vol. 30, no. 6, pp. 1011–1017, 2010.
- [29] A. C. Luongo Malave, D. Fino, C. E. Gomez Camacho, and B. Ruggeri, "Experimental tests on commercial Sweet Product Residue (SPR) as a suitable feed for anaerobic bioenergy (H₂+ CH₄) production," *Waste Manag.*, vol. 71, pp. 626–635, 2018.
- [30] A. B. Lovins, "Energy Efficiency, Taxonomic Overview," *Encyclopedia of Energy*. Elsevier Academic Press, pp. 383–401, 2004.
- [31] British Petroleum (BP), "Primary energy consumption in Europe | Statistics," 2017.
- [32] X. Jiang, S. G. Sommer, and K. V. Christensen, "A review of the biogas industry in China," *Energy Policy*, vol. 39, no. 10, pp. 6073–6081, 2011.
- [33] S. K. Lohan *et al.*, "Biogas: A boon for sustainable energy development in India's cold climate," *Renew. Sustain. Energy Rev.*, vol. 43, pp. 95–101, 2015.
- [34] British Petroleum (BP), "Statistical Review of World Energy 2017," 2017.

2. Effects of mechanical pre-treatments on the different phases of Anaerobic Digestion broths

2.1 Introduction

Anaerobic fermentation processes, such as Dark fermentation (DF) or Anaerobic Digestion (AD), which produce gas energy carriers such as H_2 and CH_4 , are considered useful techniques for sustainable energy recovery. Moreover, the versatility of these systems allows a wide range of complex feedstock to be used; agricultural, municipal and industrial waste as well as wastewaters (i.e. from tannery, fishing, slaughterhouse industries), sludges and different combination of them can be fed into the digesters. Anaerobic Digestion generally comprehends four stages, i.e. *hydrolysis*, *acidogenesis*, *acetogenesis* and *methanogenesis*. On the other hand, Dark Fermentation can be seen as a truncated version of AD, where methanogenesis is suppressed, hence the system only produces biohydrogen. However, both techniques present different optimal conditions, and therefore the process configuration of Two-Stage Anaerobic Digestion (TSAD) enhances the energy recovery by splitting the system into two steps [1] (see **Figure 2.1**).

In classical AD, H_2 is a key metabolite and regulator for the methane-producing process through anaerobic fermentation. It is present at different concentrations for each stage of the anaerobic digestion, interacts in different metabolic pathways and strongly influences methane production. Thauer et al. [2] summarized the main dehydrogenation reactions (i.e. H_2 -forming reactions of energy metabolism) and the hydrogenation reactions (i.e. H_2 -consuming reactions of energy metabolism) and assessed the energetic requirements for each of them. Particularly, hydrogen is used in diverse metabolic reactions, during the degradation or synthesis of different compounds, such as: carboxylic acids, α -Keto acids, α - and β -unsaturated acids, aldehydes and alcohols. Hence, the microbiome of the AD process can be classified in two large groups: Hydrogen Producing Bacteria (HPB) and Hydrogen Consuming Bacteria (HCB), based on the relation between the key metabolite H_2 and the biological phase for each case.

On the other hand, the Two-Stage Anaerobic Digestion (TSAD) process is divided in two physically-separated stages: the first reactor is aimed at maximizing the hydrogen concentration in the gas output of this stage (i.e. through HPB selection of the microbial population, mainly fermentative, hydrolytic and acidogenic bacteria) and a second reactor where the effluent from the first is fed

and methane is produced from the later phases of the AD process (i.e. methanogenesis).

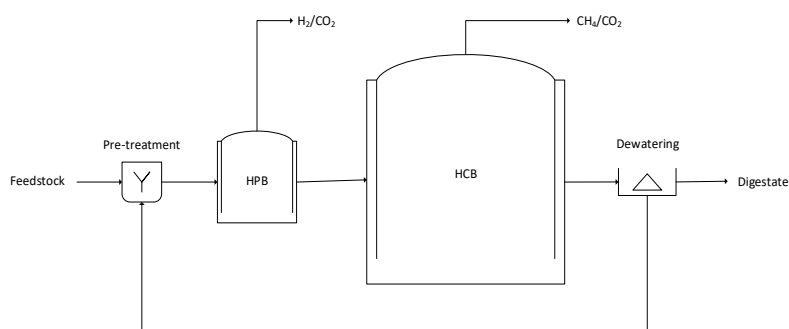


Figure 2.1 General scheme of the Two-Stage Anaerobic Digestion (TSAD) process; HPB: Hydrogen Producing Bacteria, HCB: Hydrogen Consuming Bacteria.

The correct operation of TSAD systems requires process parameters to be precisely controlled (e.g. pH, redox potential, total solids, hydraulic retention time, etc.), since process parameters exert a *selective pressure* on the biological systems, hence allowing the enrichment of HPB in the first stage and a balance between HPB and HCB in the second.

TSAD systems represent not only a sustainable option for energy recovery from different types of waste, but also it is in line with other environmental sustainability constrains, such as water consumption. As observed in **Figure 2.1**, the effluent of the process, which is the output of the methanogenic reactor, is called digestate and undergoes a separation step to recover water (dewatering) and produces the dried digestate. Then, water is recycled and mixed with the fresh feed to avoid unnecessary water expenditures and to meet the water content requirements for the AD process, either dry or wet fermentation [3]. However, the water recycling stream also contains in some extent HCB concentrations, which in the case of TSAD should be taken into consideration due to the characteristics of each stage, to avoid significant perturbations in the microbial composition in the first stage due to fraction coming from the second bioreactor.

The first phase, hydrolysis, which is common for DF and AD, is often mentioned as the rate-limiting step of the trophic chain that is established between the microbial species that are present in the digester's consortia, particularly for the case of wet fermentation (Total Solids, TS < 15%). For semi-solid or solid-state fermentations (TS > 15%), diffusion processes gain importance and therefore, under these conditions, can also be rate-limiting [4]. Complex feedstocks can be digested due to the wide variety of microorganism and enzymes that are present in mixed consortia, which progressively degrade substrates into organic constituents: carbohydrates, proteins and lipids. Large macromolecules are first hydrolysed and subsequently fermented; polysaccharides and starches are converted to small chain carbohydrates, proteins to amino acids and lipids to long-chain fatty acids (LCFA).

In general, the adopted strategy towards the reduction of the hydrolysis reaction time is the use of pre-treatments. Pre-treatments can be mechanical, chemical, biological or a combination of them. The main scope of such treatments is to

enhance the biodegradability, which is reached by surface modification, size reduction, tuning of key chemical properties, supplementation of adequate enzymatic pools, thermal degradation, among others.

In the context of TSAD, the application of pre-treatment and the use of recirculated water streams (see **Figure 2.1**) can also help to maintain the stability of the microbiome of the first stage. After the dewatering step, the feed can be diluted with the recirculated water stream (i.e. prior or after the pre-treatment) in order to meet the Total Solids specifications of the AD plant, however, the recirculated stream contains an important fraction of HPB and HCB, which can be also affected due to the pre-treatment and disturb the microbial culture present in the first stage. Hence, for multi-stage configurations with water recirculation (i.e. containing also biotic phases), the pre-treatment step has two main objectives: the preparation of the organic substrate (e.g. reduction of particle size) and can be used to control the microbial populations of interest. In the first stage, the dominant population is composed by fermentative microorganisms that are responsible for the initial degradation of the feed (HPB). On the other hand, the population of HCB is not required for the first bioreactor and the existence of structural differences among the two groups can be exploited, such as, the different thresholds of mechanical stress that HPB and HCB are able to withstand.

Certain similarities can be seen between bacteria, archaeal and eukaryotic membranes, which can be understood from an evolutionary point of view and from the energetic requirements of each dominion [5]. In AD and DF systems, the predominant dominion of interest are Bacteria and Archaea; there are also important structural differences which can be exploited in order to select a determined group of them. For example, bacterial membranes present glycerol-3-phosphate ester lipids, while archaeal membranes are constituted by glycerol-1-phosphate ether lipids. Moreover, in gram-positive bacteria, peptidoglycan layers (i.e. murein) contain an important amount of functionalized teichoic acid, while gram-negative present a thinner peptidoglycan layer and an additional outer membrane with lipopolysaccharides. On the other hand, several methanogens also present pseudomurein, which is composed by L-amino acids and N-acetyltalosaminuronic acid, while for bacteria murein walls contain D-amino acids and N-acetylmuramic acids.

In this chapter a general theoretical background about hydrolysis is presented and the effects of mechanical pre-treatment are reviewed from two important perspectives: i) the influence on the biological phase, tested on the facultative anaerobe *B. subtilis* as a model microorganism of HPB which belongs to the phyla of Firmicutes, through agar plating and image processing to assess the impact on the *cell viability* and ii) the study of Particle Size Distribution (PSD) using an *in situ* laser back-reflection probe to monitor the effects of different mechanical pre-treatment on fermentation broths and the phases of interest.

The comminution technologies or mechanical pre-treatments that are studied in this chapter on model fermentative bacteria (HPB), whose resistance to shear stress tends to be higher than that of methanogens (HCB), as noted above. Considering that in TSAD the produced water is recirculated in the first bioreactor to meet the

adequate concentration (avoiding additional water expenditures) and to limit the quantity of water to be depolluted for the final discharge. Hence, it is a must to limit the quantity of active HCB arriving in the first bioreactor that could accumulate in the time disturbing the HPB predominant role within the microbiome. In this regard, continuous ultrasonication is been studied as an intermediate operation, which can help the hydrolysis phase on recirculation loops, and to reduce the population of HCB which is fed to the first stage. To this aim, experimental ultrasonication tests, either batch or continuous, were conducted and compared to 2 other typical comminution methods used for cell lysis and particle size reduction, namely bead milling and rotor-stator degradation.

2.2 Theoretical background

2.2.1 Hydrolysis

Hydrolysis encompasses the phenomena of disintegration, solubilization and enzymatic degradation [6]. Hydrolysis can be broadly classified into two types [7]: i) the release of hydrolytic enzymes to the bulk liquid by suspended biomass and/or ii) the attachment of biomass to partially soluble substrate and the subsequent degradation of the substrate by nearly produced enzymes. Enzymes are of protein nature, sometimes presenting prosthetic groups and active metal centres. Gerardi [8] broadly classify enzymes into endoenzymes and exoenzymes, according to site of action of the enzyme; endoenzymes carry their catalytic activity within the cell, hence using soluble substrates that are able to penetrate or diffuse across the cell membrane, while exoenzyme are produced inside the cells but are released in order to bind with insoluble substrates or to first modify these particles and substrates, so that they can enter the cell. Hence, hydrolytic enzymes present high degree of specificity, due to the stereochemical conditions that each substrate should have in order to be hydrolysed.

Table 2.1 Main hydrolases responsible for the degradation of specific organic substrates ^{a)}

SUBSTRATE	ENZYME FAMILY	EXAMPLES	PRODUCTS
<i>Polysaccharides</i>	Saccharolytic	Cellobiohydrolases	Monosaccharides
		Endoglucanases	
		Glucosidases	
		Xylanase	
		Amylase	
<i>Proteins</i>	^{b)} Proteolytic (Protease)	Endopeptidase	Polypeptides
		Exopeptidase	Amino acids
<i>Lipids</i>	Lipolytic	Lipase	Fatty acids

a) Modify from [8]

a) Data from [9]

Hydrolases is a large family of enzymes (**Table 2.1**) that catalyses hydrolysis by splitting large molecules into shorter chains using water molecules (H₂O), where one (H) is attached to one cleaved fraction, while an (OH) group is added to the second one.

2.2.2 Cellulases

A fundamental factor in hydrolytic degradations is the cooperation or synergism between endo- and exo-enzymes, initially identified by Reese et al. in 1950 [10], which suggested that the cellulose degradation process is constituted by two steps: in the first step soluble poly-anhydroglucose chains are generated that are then converted in the second step into short chain sugars. As mentioned above, the solubility of the substrate to be degraded, the structure, the type of bonds and its size greatly influence the type of enzyme or the pool of enzymes that are required to degrade the compound. For example, exoenzymes have a larger specificity towards key bonds that allow the solubilization of large molecules, while endoenzymes tend to be less specific since the substrate is already located at the cytoplasm (already solubilized) and can, therefore, be degraded easier. The mechanisms of cellulose hydrolysis are still under revision since no unified theory have successfully enclosed all experimental evidences [11].

In mixed cultures, this phenomenon has been studied very little due to the great complexity associated to the estimation of the production quota of hydrolytic enzymes belonging to each microbial specie in play.

For example, [10] studied a co-culture between two moulds, *Trichoderma reesei* and *Aspergillus terreus* to determine if there was a positive effect on the degradation of sugar cane bagasse in a solid-state fermentation. Their results indicated that for this pair of microorganisms, the degradation of substrate was negatively influenced, achieving an overall halved substrate degradation, but with an increased concentration of reducing sugars, produced during the first step of hydrolysis. Conversely, [12] used an hypercellulolytic mutant of *Trichoderma reesei* in co-culture with *Aspergillus niger*, also using sugar cane as substrate, and reported more than 60 % increased enzymes concentrations of cellulases, endoglucanases and β -glucosidase than the pure culture. Microbial consortia present different enzymatic activity for each cellulase, depending on the origin and type of substrate. Tantayotai et al. [13] examined mixed cultures from two different matrixes and observed the activity of key enzymes, obtaining: 0.417 and 0.434 U/mg for β -glucanase, 0.116 and 0.184 U/mg for exo- β -glucanase and 1.069 and 3.184 U/mg for β -glucosidase, coming from horse manure and from decomposed wood, respectively.

2.2.3 Lipases

Natural sources of microbial lipases are fungi, bacteria and archaea. Lipases are reversible enzymes, able to catalyse hydrolysis and synthetic reactions. They are involved in several chemical reactions, such as trans- and inter-esterification, lysis of acids, amino acids, alcohols and acylation [14].

The source of lipases confers some specific characteristics to the enzymes. The collection of enzymes from extreme environments tends to result in thermostable

[15], salt, alkaline [16] and acid tolerant lipases, that can be further used for different applications.

Lipases are naturally produced by bacteria in AD consortia; however, animal produced lipases can be also used for biogas production, especially for high fat content residues. Lipases are mainly exocellular enzymes and exhibit an interesting activation mechanism that is triggered at the water-oil interface, where the α -helix of the lipase is folded back in the presence of lipidic substrates. The hydrolysis of triglycerides yields di- or mono-glycerides, glycerol and fatty acids.

An early study [17] observed the production of biogas from the co-digestion of fleshing residues and tannery wastewater, directly supplementing the culture broth with steapsin in order to enhance the hydrolytic step. Although lipases dosages were significantly high, ranging from 0 to 1 g (for 7.5 g of VS), biogas generation increased more than 15% and the required time for the anaerobic digestion process was reduced by 30%, compared to the non-amended control. Another experiment assessed the effect of lipase pre-treatment for animal fats, vegetable oil and floatable grease using three types of lipases, at different dosages, extracted from different sources: fungi (*Aspergillus*), yeast (*Candida*) and animal (pancreatic porcine) and obtained enhanced hydrolysis and biomethane production rates for fungi and yeast lipases, and modest improvements due to animal lipase addition [18].

2.2.4 Proteases

Proteases are the third families of enzymes, which are essential for hydrolysis in AD systems. Proteases are a key factor in the hydrolytic step because they are responsible not only for the degradation of the protein fraction present in the substrate, but also for recycling death biomass and particular proteins and enzymes that have already served in the biological system. Proteolytic reactions cleave peptides bonds (C-N), generating smaller chain amino acids.

Müller et al. [19] tested the performance at laboratory scale, in batch and semi-continuous AD systems supplemented with four different types of proteases, at low (10-100 μ L/batch) and high dosages (100-1000 μ L/batch). Their results showed that the addition in batch tests brings improvements in terms of biogas productions (9-52 %), while for semi-continuous operation no positive effects were found, even decreasing, for two out of the four proteases tested, the biogas yield. However, typical operation of AD plants avoids large protein-rich substrates overloading, since an optimal relation C:N in the range of 25:1 to 35:1 should be maintained. Nitrogen rich substrates, above the average range, can lead to ammonia/ammonium-inhibition, which is detrimental to many microbial species present in the bioreactor due to its permeability across the cytoplasmic membrane which derives in intracellular pH and cations imbalances [20].

On the other hand, experimental evidence suggests that protein-rich feedstocks could be used for biogas generation if the inoculum is adapted to them, generating an environment where proteases exhibit increased activity and correlate well with biogas production [21].

2.2.5 Hydrolysis Models

Since hydrolysis is a rather complex process, different mathematical models have long tried to describe such type of reactions. Models are either pure chemical, biological or combined (see **Table 2.2**). The most common empirical model is the First Order Kinetics, where the rate of hydrolysis (dS/dt) is considered to exclusively depend on the hydrolytic constant (k_H) and the degradable substrate concentration (S), as shown in **Equation 2.1**:

$$\frac{dS}{dt} = -k_H \cdot S \quad (2.1)$$

Which can be stoichiometrically coupled to biogas production rate (dP/dt), considering the yield coefficient ($Y_{P/S}$) for the substrate in biogas as follow:

$$\frac{dP}{dt} = Y_{P/S} \cdot k_H \cdot S \quad (2.2)$$

And can be integrated in the time dominion, yielding:

$$P = P_0 + Y_{P/S} \cdot S_0 \cdot (1 - e^{-k_H \cdot t}) \quad (2.3)$$

This set of equations is only valid for constant conditions, such as pH, temperature, redox potential, applied pre-treatment, substrate-inoculum ratio (S/I) and initial particle size distribution.

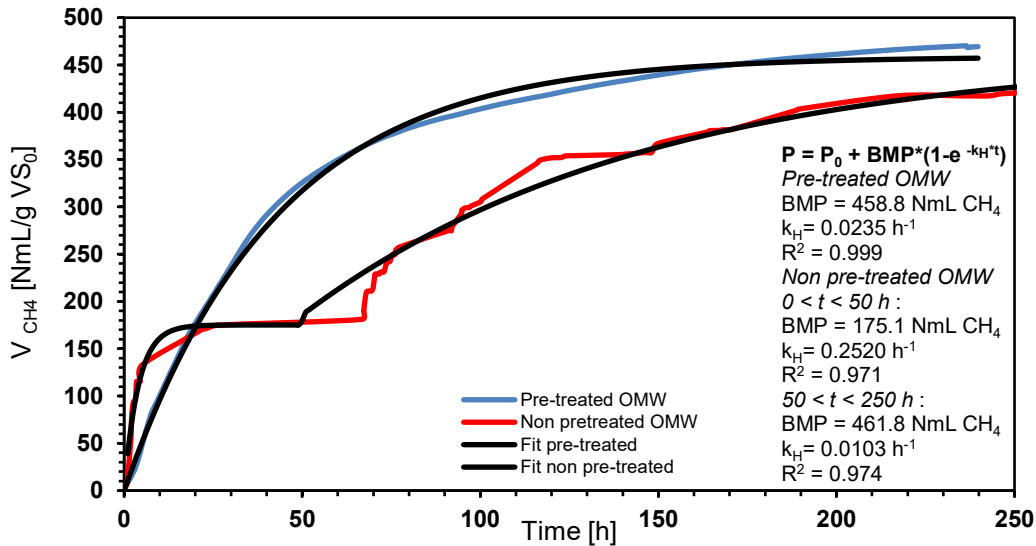


Figure 2.2 Hydrolysis first order kinetics for pre-treated and non-pre-treatment Organic Market Waste (OMW). Own experimental data presented for illustration purposes: 35 °C, anaerobic conditions, mixing rate 100 rpm and $S/I = 1$; pre-treated substrate and adapted inoculum (blue line) and non-pre-treated substrate and non-adapted inoculum (red line).

Hence, first order constants are found widely in literature but rarely applicable to different systems. For example, in **Figure 2.2**, first order kinetic models are applied to two systems using Organic Market Waste (OMW) as substrate (i.e. a mixture of fruits and vegetables residues) one with a thermal basic pre-treatment (55 °C for 24 h at pH =12) compared to a non-pre-treated system. This type of substrate is rich in water, carbohydrates, proteins and lipids with a variable fraction of hemicellulose and lignin. The application of the pre-treatment serves to make the substrate more available for microorganisms, in particular for enzymes which are the responsible structures for the hydrolytic degradation. Moreover, as observed in **Figure 2.2**, for the non-pre-treated feedstock, the different raw constituents divide the hydrolysis phase into subsections, with different *apparent* first order kinetic constants as a result of the variable degradability of each fraction. Literature data present a wide range for hydrolytic constants, measured from different organic wastes and process conditions. For example, in [22], the calculation of the hydrolytic constant yielded 0.0046 h⁻¹ at 20 °C for the Organic Fraction of Municipal Solid Waste (OFMSW). Nielfa et al. [23] assumed first order kinetics for the hydrolysis of bio-waste and OFMSW at 35 °C and obtained values in the range between 0.0133 – 0.0200 and 0.0004 – 0.0079 h⁻¹, respectively.

For the cases where an important fraction of recalcitrant or non-degradable substrate is present (φ), an additional correction can be made to **Equation 2.1**:

$$\frac{dS}{dt} = -k_H * (S - \varphi \cdot S_0) \quad (2.4)$$

Other type of models that can be used for describing hydrolysis, particularly in the cases where the concentration of enzymes is not in excess in respect to the available substrate (i.e. equivalent to the case where the S/I ratio is too high); for those cases a Monod-type equation results more adequate to describe the hydrolytic step:

$$\frac{dS}{dt} = V_{H,max} \cdot \frac{S}{k_s + S} \quad (2.5)$$

In **Equation 2.5**, the hydrolysis rate (dS/dt) is described as a function of the substrate concentration (S), using a saturation model that includes two constants: *i*) the maximum hydrolysis rate $V_{H,max}$ and *ii*) the half-saturation constant, k_s .

However, other type of models has also been introduced, based on the available surface of the substrate and its characteristic Particle Size Distributions (PSD). The presence of insoluble fractions in the feedstocks for AD or DF can also be seen as a reduction of the available surface for the hydrolytic reactions to take place.

Table 2.2 Literature review of Hydrolysis Models

<i>Model</i>	<i>Equation</i>	<i>Reference</i>
First Order (soluble substrate) – Chemical	$dS/dt = -k_H \cdot S$	[24]
First Order (partially soluble substrate) – Chemical	$dS/dt = -k_H \cdot (S - \phi \cdot S)$	[25]
First Order – Chemical & Biological	$dS/dt = -k_H \cdot S \cdot X$	[26]
Monod-type – Chemical	$dS/dt = V_{H,max} \cdot S / (k_s + S)$	[6]
Monod-type – Chemical & Biological	$dS/dt = \mu_{max} \cdot S \cdot X / (k_s + S)$	[27]
Contois	$dS/dt = \mu_{max} \cdot S \cdot X / (k_s \cdot X + S)$	[24]
Diffusion Model	$dS/dt = -k_H \cdot S^{0.5}$	[26]
Tessier	$dS/dt = \mu_{max} \cdot X \cdot (1 - e^{-S/k_s})$	[27]

dS/dt : hydrolysis rate, S : substrate concentration, ϕ : fraction of non-degradable substrate, X : biomass concentration, k_H : hydrolytic constant, $V_{H,max}$: maximum specific rate, μ_{max} : maximum specific growth rate, k_s : half saturation constant.

As the solubility of the substrate increases, the available area increases; entirely soluble substrates represent the limit case, with a very large available surface and therefore other type of models (i.e. first order or biological models) are more suitable than classic surface models such as:

$$\frac{dS}{dt} = -k_{SH} \cdot A_S \quad (2.6)$$

Considering perfect spherical particles, with uniform density among layers, the mass of substrate can be written as $S = (4/3)\pi n \rho r^3$, where n represents the number of particle, ρ the mean particle density and r the mean radius of the substrate particle. The total available surface can be then described as for perfect spherical particles as $A_S = 4\pi n r^2$. Hence, **Equation 2.6** can be reformulated as follow:

$$\frac{d(\rho \cdot r)}{dt} = -3 \cdot k_{SH} \quad (2.7)$$

Assuming a constant particle density, and rewriting the surface hydrolytic kinetic constant as $3k_{SH} = k'_{sh}$, then the particle size can be obtained as function of time:

$$r(t) = r_0 - \frac{k'_{SH}}{\rho} \cdot t \quad (2.8)$$

Moreover, some authors have studied the influence of the particle size distribution (PSD) during hydrolysis, in particular the dependence of the hydrolytic constant on the initial particle size. Experimental data from [28] have shown an inverse relationship between the particle diameter and the hydrolysis coefficient; a reduction from 600 μm to 200 μm in the mean diameter of casein particles resulted in an increase of the first order hydrolytic constant from 0.0410 d^{-1} to 0.0868 d^{-1} . Similar results were provided by [24], which used smaller cellulose particles, and found an increase in the hydrolytic constant from 0.19 h^{-1} to 0.44 h^{-1} for particles of 70 and 20 μm , respectively. Whereas in [29], the enzymatic hydrolysis of rice flour was studied using porcine pancreatic α -amylase and two types of starch particles (i.e. short grain and long grain); the results suggested that the percentage of

hydrolysed starch can be enhance, from c. 70 % up to more of 90 % decreasing the particle size from 180 to 80 μm .

Different experimental observations have also hypothesized an exponential relation between the ratio of mean particle diameter and the hydrolytic kinetic constant as:

$$k_{SH}(D_n) = k_{SH}(D_0)\exp\left(-\frac{D_n}{\alpha}\right) \quad (2.9)$$

which is an Arrhenius-type model, where the relation between the kinetic constant for particles of a specific diameter $k_{SH}(D_n)$ is inverse to the particle diameter D_n , considering as pre-exponential factor the hydrolytic constant for particles of reduced diameter approaching to zero - $k_{SH}(D_0)$ - and a substrate-dependent factor (α).

However, not only the particle diameter is fundamental, the shape of the substrate particles and the active sites on the surface are also relevant parameters. The dependence of the hydrolysis rate on particulate diameter is inverse, i.e. when the substrate exhibits larger diameters, then the rate is reduced. The specific surface area (m^2/g) provides a more adequate framework, since not only the substrate particle geometry (radius) is considered, but also the mass of each particle. In this respect, the aforementioned reference [28] also correlated the hydrolytic constant to the specific surface area and obtained more than 750% increase in the hydrolytic rate, from 0.034 to 0.298 day^{-1} , as the specific surface area rose from 0.01 to 0.19 m^2/g .

In the context of energy-recovery processes, pre-treatments either mechanical, thermal or biological should also consider the energy expenditures of these steps in order to improve the process. Although hydrolysis is a very complex phenomenon, there are opportunities to enhance degradation rates and degradation degrees of particulate substrates, considering the factors mentioned above, which can be summarized as:

- The interactions of the biological phase (microorganisms and particularly enzymes) with the organic substrates,
- The nature of the substrate: type of constituents which are present, the degradability and solubility of each fraction, initial PSD, porosity and available surface area and presence of inhibitory compounds (or release during hydrolysis),
- The effects of pre-treatments and the modification which are caused in the substrate, aimed at improving energy expenditures by enhancing degradation rates and degradation degrees in AD processes.

2.3 Experimental procedure

The experimental approach of this work consists in evaluating the effects of the mechanical pre-treatments on the different phases of interest within the anaerobic fermentation broths: *i)* the biotic phase, through model fermentative microorganisms and evaluating the respective reduction of cell viability for each comminution treatment and *ii)* the abiotic phase (substrate), in terms of reduction of the particulate diameter.

2.3.1 Bacteria cultivation

2.3.1.1 Liquid pure cultures preparation

Two liquid stock cultures were prepared, using bacteria strains belonging to the phylum of Firmicutes, which were tested in different systems: *Clostridium acetobutylicum* (strain ATCC824) and *Bacillus subtilis* (strain DSM 21393). The correspondent taxonomic classification for each specie is shown in **Table 2.3**, while the composition of the liquid media for each specie is reported in **Table 2.4**.

Table 2.3 Taxonomic classification of the fermentative microorganisms used during the tests.

Domain	Bacteria	Bacteria
Phylum	Firmicutes	Firmicutes
Class	Clostridia	Bacilli
Order	Clostridiales	Bacillales
Family	Clostridiaceae	Bacillaceae
Genus	<i>Clostridium</i>	<i>Bacillus</i>
Species	<i>C. acetobutylicum</i>	<i>B. subtilis</i>
Strain	ATCC824	DSM 21393

Table 2.4 Medium composition for *Clostridium acetobutylicum* and *Bacillus subtilis* cultures.

<i>Clostridium Growth Medium (CGM)</i>			<i>Bacillus Growth Medium (BGM)</i>		
Compound	Concentration		Compound	Concentration	
KH ₂ PO ₄	0.0750	% w/w H ₂ O	Tryptone	10.00	g/L
K ₂ HPO ₄ ·3H ₂ O	0.0982	% w/w H ₂ O	Yeast extract	7.50	g/L
NaCl	0.1100	% w/w H ₂ O	Sodium chlorate	5.00	g/L
MnSO ₄ ·H ₂ O	0.0010	% w/w H ₂ O	Glucose	2.50	g/L
MgSO ₄	0.0348	% w/w H ₂ O	Thiamine	0.05	g/L
FeSO ₄ ·7H ₂ O	0.0010	% w/w H ₂ O	Biotin	0.05	g/L
Asparagine	0.2000	% w/w H ₂ O	Sigma 204 antifoam	1.00	mL
Yeast extract	0.5000	% w/w H ₂ O			
(NH ₄) ₂ SO ₄	0.2000	% w/w H ₂ O			
Glucose	8.0000	% w/w H ₂ O			
p-Aminobenzoic-acid	0.0004	% w/w H ₂ O			
Sigma 204 antifoam	0.0010	% w/w H ₂ O			

The liquid cultures were prepared in sterile bottom-baffled Ultra Yield Flasks (Thomson Instrument Company, Oceanside, USA), with a total volume of 2500 mL, operated with a working volume of 10 % v/v (i.e. 250 mL).

2.3.1.2 Petri-dish cultivation on agar

Samples were plated on agar in order to assess the effect of the different pre-treatments on cell viability for *B. subtilis*. The semi-solid/gel-like medium consisted in *Lysogeny broth* or *Luria Broth* (LB); the composition consisted in: Tryptone 10.00 g/L, Yeast extract 5.00 g/L, Sodium chlorate 5.00 g/L and Agar 14.00 g/L. The agar media was autoclaved and poured into the Petri dishes and placed in refrigerated storage (i.e. -20 °C) until used in the further cultivations.

2.3.2 Feedstocks: Agricultural Waste (AW)

The substrate for the tests was a mixture of agricultural waste composed by maize silage (i.e. 40.7 g TS/L and 39.2 g VS/L) and grass silage (i.e. 43.1 g TS/L and 40.5 g VS/L), mixed in a proportion of 9:1 (w/w). Raw substrate was diluted with tap water, reaching a concentration of dry biomass of approximately 20 % w/w.

2.3.3 Mechanical pre-treatments

2.3.3.1 Bead Milling

The wet bead milling tests were conducted in batch-mode using a Retsch 400 MM mixer mill (Retsch GmbH, Haan, Germany), shown in **Figure 2.3**. The device contains two working chambers or stations, i.e. steel cylindrical vessels, and each chamber was filled with glass beads and the sample, hence batch experiments were conducted in duplicates. Prior to each test, the selected glass beads (i.e. approx. 0.5 mm) and the working chamber were sterilized with a 70 % v/v ethanol solution. The nominal station volume is 25 mL, while the loaded glass beads volume was kept constant at 4 mL (i.e. 16 % v/v filling volume) and the sample volume was approximately 16 mL for the AW, while for the *B. Subtilis* samples laid around 8 mL.



Figure 2.3 Picture of the Retsch MM 400 bead milling device.

2.3.3.2 Rotor-Stator degradation

Rotor-stator degradation was tested in batch-mode using an Ultra-Turrax T25 (IKA-Werke, Staufen, Germany), coupled to a dispersing element (a rotor-stator), as presented in **Figure 2.4**. The nominal diameters of the rotor and stator are 14 and 18 mm, respectively. Prior to each batch, the rotor and the stator were cleaned with a 70 % v/v ethanol solution. The selected frequencies for the tests correspond to 800 min^{-1} and 20 500 min^{-1} , to cover a wide range of attainable values with the experimental equipment, which represent roughly 5 and 80 % of the maximal values, respectively of the device.

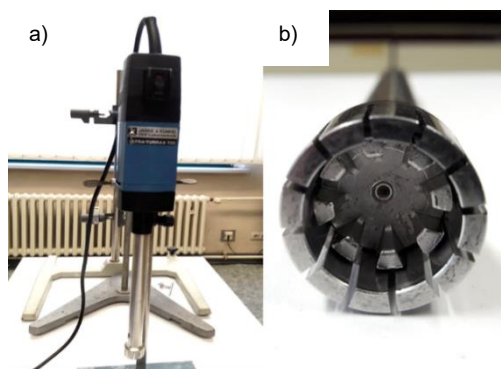


Figure 2.4 Photograph of the rotor-stator system: a) dispersing instrument Ultra-Turrax T25 and b) dispersing rotor-stator shaft.

2.3.3.3 Batch and continuous-flow ultra sonication

The instrument used for the sonication pre-treatment was an UP200St transducer unit (Hielscher Ultrasonics, Teltow, Germany) coupled to a 2 mm S26d2 sonotrode (Hielscher Ultrasonics, Teltow, Germany). Two configurations (i.e. batch and continuous) of the direct ultrasonication pre-treatment method were tested. The ultrasonic apparatus consisted of generator, converter, booster and the sonotrode, as shown in **Figure 2.5a**, while for the continuous-flow tests an ultrasonic chamber is required, as well as a pump (for the continuous flow of feedstock) and a cooling system for the ultrasonic chamber (**Figure 2.5b**).

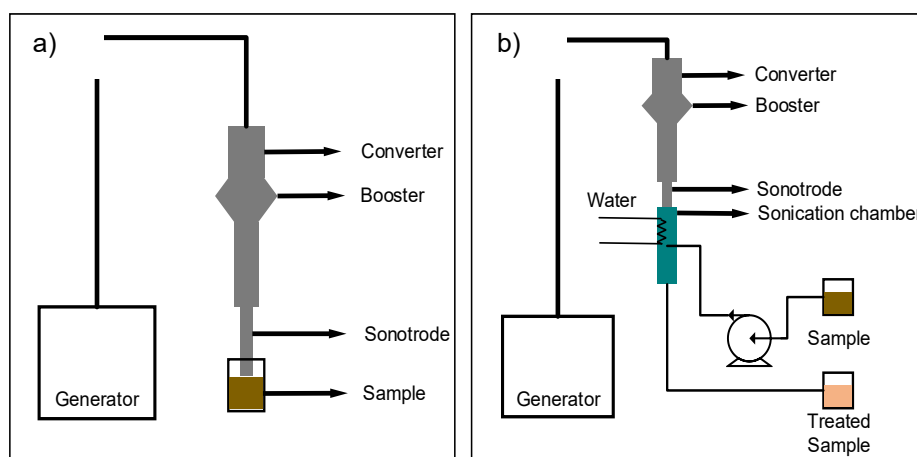


Figure 2.5. Graphical representation of the key components of the ultrasonication device for the different types of operation: **a)** batch and **b)** continuous-flow

The relevant parameters that must be specified are the amplitude and the time of application of the pre-treatment. In the case of continuous ultrasonication, the flow rate (i.e. and indirectly the residence time) also plays an important role. The power of the ultrasonication system corresponds to 200 W, while the frequency is 26 kHz. Prior to each batch, the sonotrode was cleaned with a 70 % v/v ethanol solution, while for the continuous-flow mode, the device was sterilized only at the beginning. Experiments were conducted in triplicate to have statistical significance.

2.3.4 Analytical Measurements

2.3.4.1 Image analysis software for cell counting

Plates with *B. subtilis* cultures were photographed and analysed using *Fiji* (version 1.4) [29], an open source dedicated image processing package used for biotechnological purposes developed by *ImageJ*. An inner square was cropped, circumscribed on the area of the circumference, where the diameter of the plate (approx. 5.2 cm) matched the diagonal of the square, as shown in **Figure 2.6a**. The set equivalence for the image processing was 1:1 pixel to cm. For the quantitative assessment, each photograph was first inverted to black and white, and then the area occupied by cells was calculated (see **Figure 2.6b**). Finally, the corresponding percentage (%) of the surface of the plate occupied by biomass was estimated through the aforementioned relation; single cells quantification was not performed due to the accuracy of the method, which cannot satisfactorily discriminate within aggregated cells.

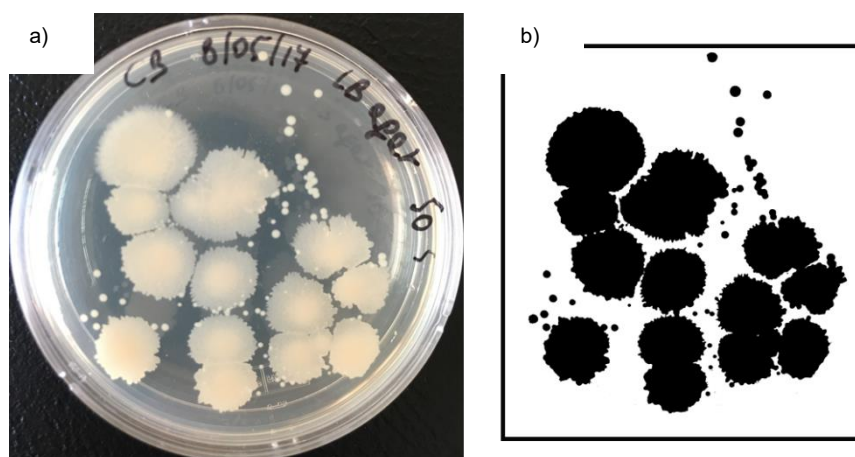


Figure 2.6 Photograph of a cultivating plate (A) and binary contrast image of the area occupied by the cells on the same plate (B).

2.3.4.2 *In situ* laser back-reflection

The Particle Size Distribution was observed using an *in situ* laser back-reflection single-mode fiber transmission probe (Sequip S+E GmbH, Dusseldorf, Germany), whose focus area, a sapphire window, can be set for the required range

of observation (i.e. 0.5 – 1000.0 μm). Samples were placed in circular glass dishes along with the measuring probe and a magnetic stirrer, under adequate mixing conditions (80 – 100 rpm) to have statistical significance on the total number of analysed particles (see **Figure 2.7**).

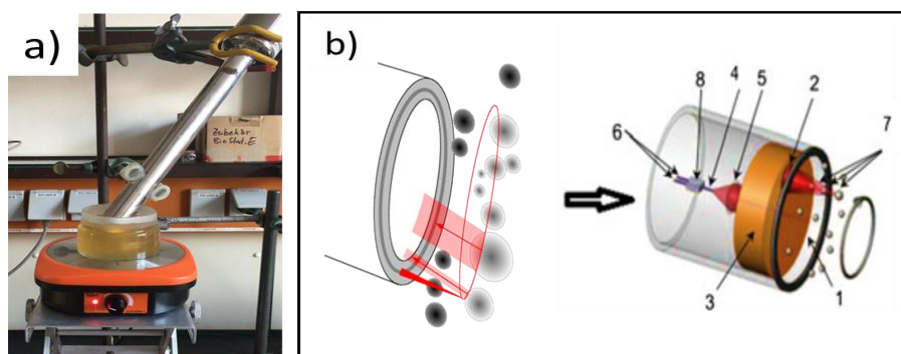


Figure 2.7 a) Photograph of the front view of the experimental set-up used for the *in situ* laser black reflection measurements and b) Schematic design of the working principle and main components of the probe: 1) sapphire window, 2) focusing lens, 3) rotating optical system, 4) single mode fiber, 5) coupling in lens, 6) single mode fiber, 7) dynamic focus and 8) fiber optic coupler (modified from [30]).

The Particle Size Distribution (PSD) in this chapter are intended to be number based (using data in the range of $10^3 - 10^4$ *events*) and the mean experimental values are calculated on the base of 10 measurements.

2.4 Results

2.4.1 Effect of mechanical pre-treatments on the biotic phase (*Bacillus subtilis* cultures)

Even though the microbial communities that are within the AD systems present a large diversity, the fermentative activity is carried out mostly by the phyla of Bacteroidetes and Firmicutes. Particularly, different studies suggest that the relative abundance of Firmicutes is in the range 40-80 % out of the total consortium [32][33], with stable dynamics in presence of different type of substrates [33]. *Bacillus subtilis* was chosen for tests, due to its role as model microorganisms and growth capacity under aerobic conditions, which is necessary for some of the mechanical tested in this section. The strain which is used in this study (reported in **Table 2.3**) is a genetically modified microorganism with suppressed capacity of forming endospores. Sporulation is a process which is generally induced by reduced levels of nutrients (starvation) and/or extreme environmental conditions (i.e. abrasion, heat, toxic chemicals and radiations) [35][36]; hence, spores are dormant or vegetative metabolic states that can survive for extended periods with very little or no nutrients and which under appropriate environmental conditions can return to an active growing state, through the reverse process which is known as germination [37].

This section focuses attention on the effect of mechanical pre-treatments on metabolic active growing cells of *B. subtilis*, as an indicator to quantify the impact

of each experimental technique and compare them in terms of energy expenditure and damage to the biotic phase. Besides, taking into account that the hydrolysis process is very complex, the measurement of cell viability in this case also serves as an indirect measurement to understand if the quantity of enzymes necessary for the hydrolytic process will be affected.

2.4.1.1 Bead Milling

As noted above, suspensions of *Bacillus subtilis* cultures were pre-treated to assess the effect on this type of bacteria. Cell viability was evaluated using the normalized colonized area on agar plates, due to the characteristics of the samples (see section 2.3.4.1).

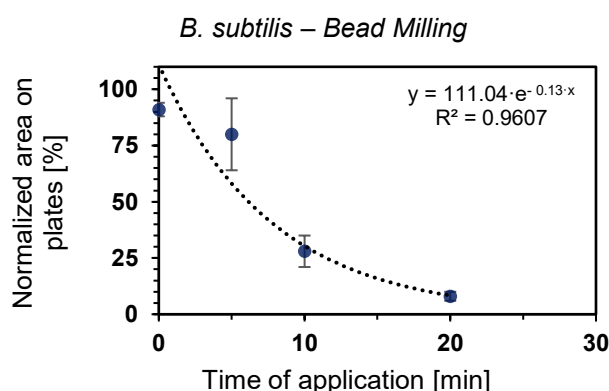


Figure 2.8 Colonized area on cultivation plates a function of the application time of the bead milling pre-treatment on a culture of *B. subtilis*.

The mechanical stress that bead milling produces in the cells was observed through colonies formation, plating the liquid samples that were comminuted using glass bead and comparing to the untreated control (i.e. $t=0$ min). The observed trend in **Figure 2.8** presents how at longer application times the viability of the *B. subtilis* is significantly compromised. The results also showed that almost 11 % of viability (compared to the control samples) is lost during the first 5 min of milling, while for 10 minutes almost 70 % of the colonies were not present and at 20 min the reduction reached up to 83 %.

2.4.1.2 Rotor-Stator degradation

The pre-treatment tests with the rotor-stator device were conducted at two different frequencies, namely 800 min^{-1} and 20500 min^{-1} , scanning distinct application times (i.e. 0, 5, 10 and 20 min), as observed in **Figure 2.9**.

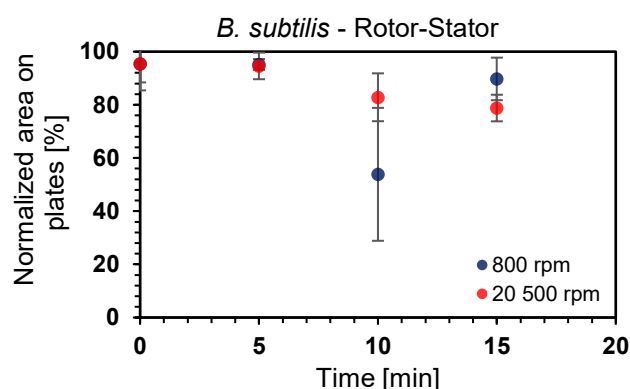


Figure 2.9 Normalized area of colonized area on agar plates after the application of rotor-stator pre-treatment at different intensity conditions.

Cell viability was assessed using the normalized colonized area in the plates, inoculated with aliquots from the samples before and after the pre-treatment. Another important factor that should be considered is the ice bath, which is necessary in order to reduce thermal stresses on biomass. The results showed that rotor-stator degradation resulted in decreased cell viability at longer application times, with negligible reduction for the application time of 5 minutes.

For $t=10$ min, no clear trend was observed, since the lowest rotor speed (800 rpm) resulted in lower cell viability, although with large standard deviation, compared to the obtained value for 20 500 rpm. For the tested time 15 minutes, the area occupied by the *B. subtilis* cultures reduced in c. 10 % for 800 rpm tests, while a 20 % reduction was obtained from the 20 500 rpm speed.

2.4.1.3 Batch ultrasonication

First, all application times correspond to three intervals of the same length, to avoid excessive overheating of the samples and hence thermal degradation; i.e. 30 s correspond to 3 cycles of 10 s, 60 s to 3 cycles of 20 s while 2 minutes to 3 cycles of 40 s.

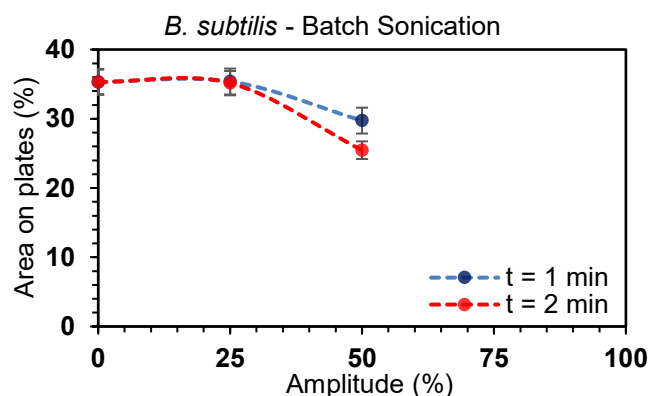


Figure 2.10 Percentage of colonized area on agar plates after the application of batch sonication at different conditions

For the batch and continuous tests, the frequency is kept constant (see **section 2.3.3.3**), while application times and the amplitude of the ultrasound probe, which is a parameter that serves to adjust the maximum power rating of the generator,

were scanned. Amplitude values of 0 % (i.e. control sample, without pre-treatment), 25 % and 50 % (referred to the maximum horn extension of the sonotrode) were compared for each application time. At 25 % amplitude, no marked differences in the cell viability were observed for the different application times nor compared the untreated sample (0 %). This result indicates that at low amplitude values (0-25 %), the application time does not play a fundamental role since the differences in the colonized area on plates are less than 1 % (see **Figure 2.10**). However, for the 50 % amplitude case, an application time of 1 min resulted 16 % reduction of the colonized area on plates and for 2 minutes it reached almost 28 %.

2.4.1.4 Continuous-flow ultrasonication

For continuous-flow ultrasonication, the flow rate was kept constant, hence the application time is fixed and equal to the residence time in the chamber. As noted in **section 2.3.3.3**, the configuration of the systems differs from the batch tests and in this part the influence of different values of amplitude (i.e. 0, 20, 30 and 50 %) on *B. subtilis* was studied.

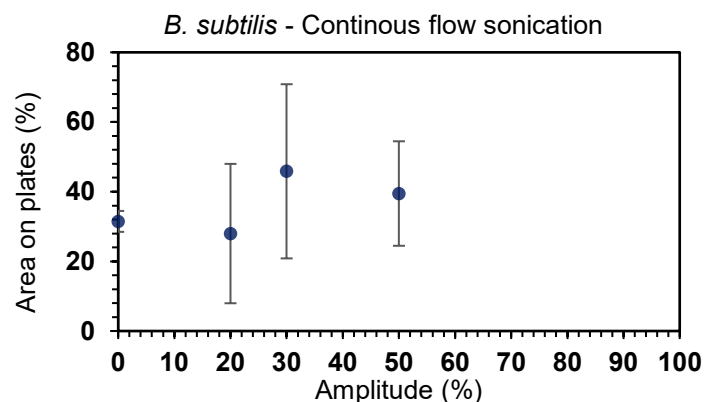


Figure 2.11 Percentage of colonized area on agar plates after the application of continuous sonication at different conditions of amplitude.

The results obtained for the case of continuous sonication did not follow a clear trend. It was observed that increasing the amplitude of the sonication caused variable effects on the biomass; in some cases (e.g. 30 and 50%) the colonized area on petri dishes was greater than the obtained value of the non-pre-treated sample. This result is in agreement with batch tests (**section 2.4.1.3**), since at constant application time, the amplitude of the sonotrode does not significantly reduce the colonized area on plates. However, the results showed rather large experimental uncertainties, which hinders a more complex analysis (**Figure 2.11**).

2.4.2 Specific Energy input and cell viability

In **Figure 2.12**, a comparison among the different mechanical pre-treatments is presented. Cell viability was normalized for each case and plot against the total amount of energy that was given in each case per mass unit of dry cell weight. As

shown in **Figure 2.12**, bead milling is the most detrimental for the *B. Subtilis* cells, followed by rotor-stator and finally ultrasonication.

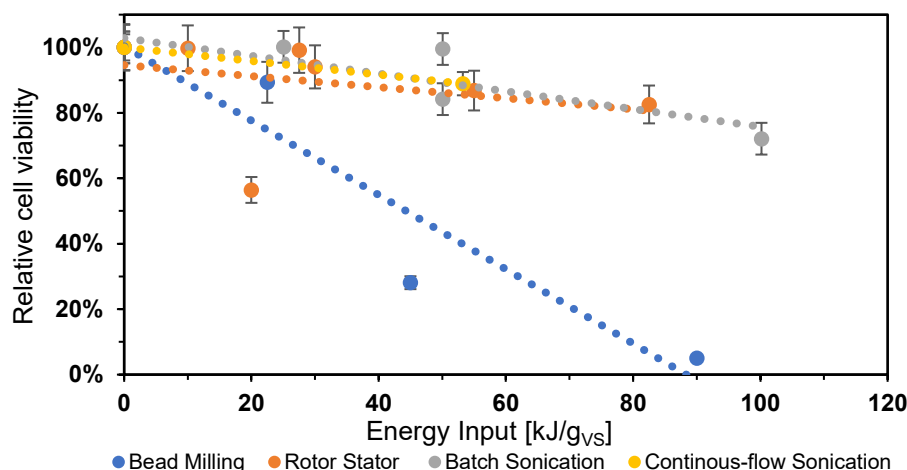


Figure 2.12 Comparison of residual cell viability at different threshold of energy input for the different mechanical pre-treatments.

In fact, these three techniques under analysis have long served as downstream processing operation units in the biotechnological field, mainly for cell disruption, lysis and extraction of compounds of interest [38]. Particularly, bead mill is used for applications targeting cell lysis (i.e. release of intracellular compounds), applying an intensive solid shear stress using glass, ceramic or steel beads. Rotor-stator and ultrasonication exert a hydrodynamic stress rather than solid shear stress compared to the case of bead milling, which explains the observed trends in Figure 2.11. In fact, *Bacillus* species (i.e. *Bacillus subtilis*, *sphaericus*, *licheniformis*, *cohnii*) are known to survive high shear stress conditions, sometimes involving also sporulation mechanisms, and therefore are being intensively studied for the production of self-healing concretes [39][40].

Between batch and continuous-flow ultrasonication, no significant differences were appreciated; however, continuous-flow ultrasonication has the advantage to be conducted without time delays which is the case for the batch mode. Nevertheless, it should be noted that there is no standard test for the evaluation of the mechanical stress that is given to a biological system, these measurements rely on try and error approaches. The evaluation of the different threshold is important because it provides an idea of the resistance of biomass against shear stress, and therefore it could be used as external stressor to select and maintain the microbial consortia (i.e. mainly HPB) which is recirculated from methanogenic stage into the hydrogen bioreactor (see **Figure 2.1**).

2.4.3 Effects of continuous-flow ultrasonication on the particle size distribution of *Clostridium acetobutylicum* samples

The second microorganism that was tested to observe the effects of mechanical pre-treatments on biomass is the well-characterized *Clostridium acetobutylicum*. It

is a model microorganism, belonging to the phyla of Firmicutes and to the class of Clostridia (**Table 2.3**), which is also an important player in the microbiome of AD, particularly involved in the degradation of cellulose and sugars and in the production of hydrogen. *C. acetobutylicum* is an anaerobic bacterium, which have been long present in the biotechnological industry, in the context of ABE (Acetone, Butanol, Ethanol) fermentation processes due to the wide range of carbon sources that can use and the valuable fermentation products which can be obtained to be used as biofuels.

Considering that *C. Acetobutylicum* is a strict anaerobe, contrary to *B. subtilis* which is believed to be facultative microorganism, batch pre-treatments such as bead milling, rotor stator and batch sonication were excluded for the former due to the experimental difficulties to perform tests under anaerobic conditions. For *C. acetobutylicum* cells, continuous ultrasonication was chosen to avoid the effects of the aerobic shock and in order to assess the effects only regarding the pre-treatment. Moreover, due to the difficulties of maintaining anaerobic conditions and plating cell samples on agar for the different mechanical pre-treatments, it was decided to monitor, in this case, the particle size distribution (PSD) of the cell suspensions by means of the *in-situ* laser back reflection probe testing the effects of continuous-flow ultrasonication. The system was tested using two values of amplitude, namely 20 and 50 %.

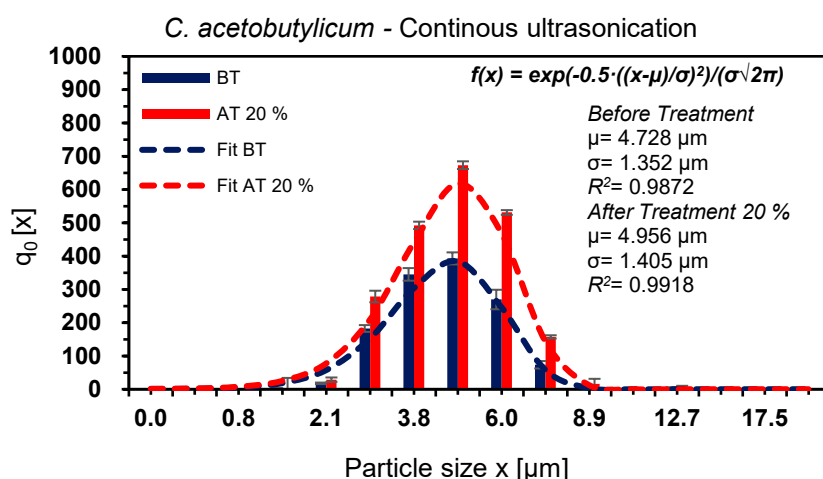


Figure 2.13 Particle size distribution (PSD) of *C. acetobutylicum* samples treated with ultrasonication at 20 % amplitude

As observed in **Figure 2.13**, the initial PSD of the sample consisted in a unimodal normal distribution before the application of the pre-treatment. Moreover, the distribution could be modelled following a Gauss distribution; the fitting parameters and correlation coefficients are also reported in **Figure 2.13**. The obtained initial values of PSD (i.e. before treatment), showed a population centred in $4.728 \pm 1.352 \mu\text{m}$, while for the treated samples at 20 % amplitude laid around $4.956 \pm 1.405 \mu\text{m}$. Nonetheless, it should be considered that the *in-situ* laser back reflection probe has a minimal resolution of $0.5 \mu\text{m}$ (see **section 2.3.4.2**), which means that the application of ultrasonication with an amplitude of 20 % did not affect significantly the system, and the PSDs can be considered almost equivalent.

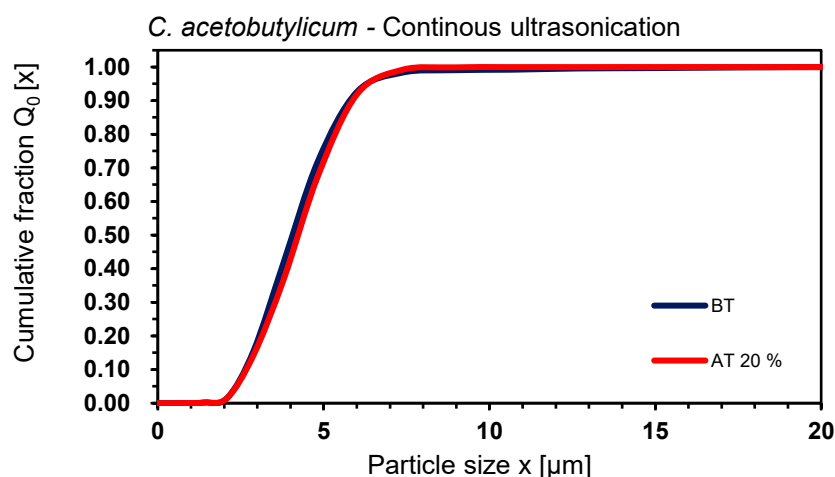


Figure 2.14 Cumulative Particle size distribution (PSD) of *C. acetobutylicum* samples treated with ultrasonication at 20 % amplitude.

These obtained values for *C. acetobutylicum* PSD are in agreement with literature data concerning the size of this bacterial specie [41]. Additionally, the cumulative PSD (**Figure 2.14**) before and after the application of the pre-treatment showed similar trends, with marginal deviation between the d10 and d80 cuts.

On the other hand, when the amplitude was set at 50 %, the PSD distribution significantly changed after the application of the pre-treatment. As presented in **Figure 2.15**, the mean cell diameter passed from $4.728 \pm 1.352 \mu\text{m}$ to $6.865 \pm 2.141 \mu\text{m}$, which represents an increment of more than 45.2 % in the mean cell size. The same trend is also observable from the cumulative PSD plot (**Figure 2.17**), where the curves before treatment and after treatment exhibit a large difference in the whole range, from cut d0 up to almost d100.

Although *clostridium* species are known to exhibit different physiological states and morphologies [42], the time scale of the experiments ($< 5 \text{ min}$) suggests that the obtained differences in the cell size are not a result of genetic regulations. For example, Jiao et al. [43] studied cultures of *Clostridium beijerinckii* under different conditions and calculated the cell size; it yielded around $8\text{--}10 \mu\text{m}$ at acidogenic phase, while during solventogenesis the obtained measurements resulted in $8\text{--}12 \mu\text{m}$.

Since *C. acetobutylicum* is capable of forming aggregates, which could be visually observed during the culture preparation, the increased cell diameter after ultrasonication could be due to the breakup of cell aggregates, which initially have a larger dimension beyond the sensitivity of the probe. Hence, it is possible to hypothesize that *clostridium* cells which were contained in the cell aggregates (macro-flocs) presented a larger cell size compared to the single-cells measured before the pre-treatment and therefore a different mean value was obtained after the application of the sonication treatment (see **Figure 2.16**).

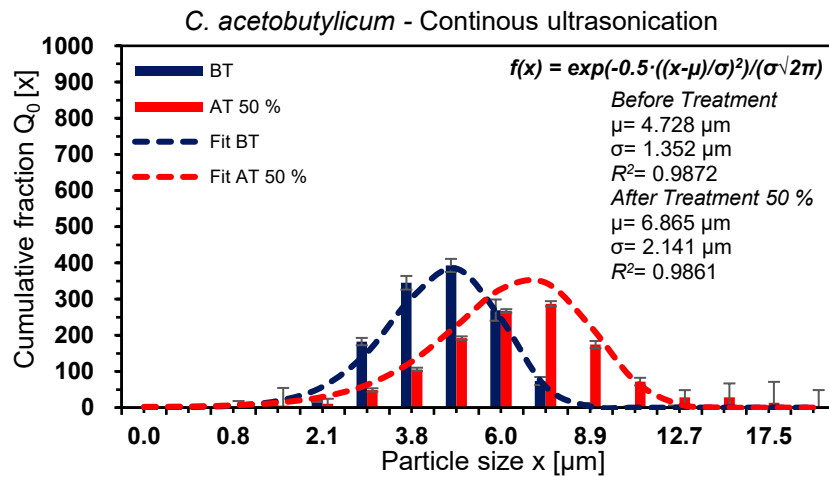


Figure 2.15 Particle size distribution (PSD) of *C. acetobutylicum* samples treated with ultrasonication at 50 % amplitude

The comparison between the tests at 20 and 50% of amplitude (with application time of 2.5 min), resulted in different PSD: at 20% of amplitude, no significant effect was observed in the samples, presenting very similar PSD. On the other hand, the tests at 50% showed an increase in the mean diameter of the cells, which at first glance might seem counter-intuitive but it is probably due to breakage of microbial aggregates containing bacterial cells of larger dimensions, which could not be detected initially due to the range of observation of the probe. The values of the standard deviation, reported in each chart, also shed light about the dispersion of the measurements.



Figure 2.16. Photograph of the macro-flocs present in the stock culture of *C. acetobutylicum*

For the case before treatment and 20 % amplitude, the presented data exhibited very similar dispersion with a little increment of less than 4 % after the application of sonication, while for 50 % amplitude the relative error among the measurements was more than 58 %. In any case, it is necessary to highlight that none of the 2 tests showed a shift towards smaller diameters, which could indicate the absence of cell rupture due to this type of pre-treatment. Moreover, if the ultrasonication treatment had strong effects on the cells (cell lysis or sporulation), it would have been

appreciated as an increased fraction of cell debris count, below the mean initial diameter.

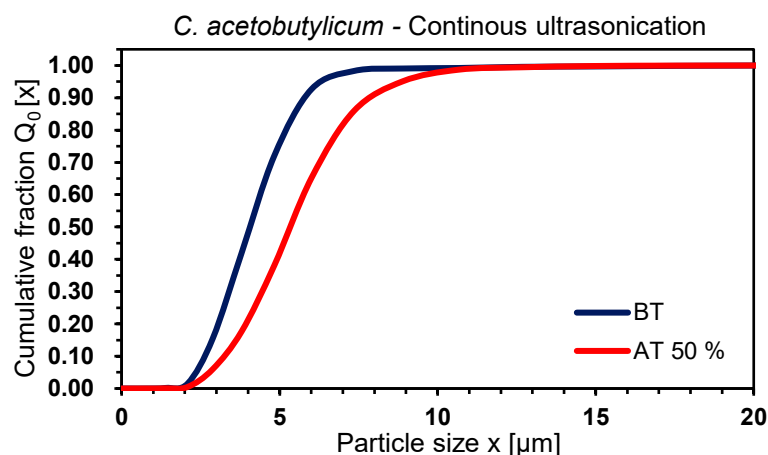


Figure 2.17 Cumulative Particle size distribution (PSD) of *C. acetobutylicum* samples treated with ultrasonication at 50 % amplitude.

These results obtained for *C. acetobutylicum* are congruent with the research presented in [44], where sonication was studied for activated sludges and the authors proposed that sonication differently affected micro-flocs (<4.4 μm) and macro-flocs (>4.4 μm). In their study, the effect of sonication in PSD was almost performed during the first minute and micro-flocs resulted less susceptible to ultrasonication treatment than macro-flocs, probably due to the nature of the binding forces in each case.

2.4.4 Effects on the feedstock: Agricultural Waste (AW)

2.4.4.1 Continuous-flow ultrasonication

The effects of the mechanical pre-treatments were also assessed on the abiotic phase. As mentioned above, the intrinsic characteristics of the substrate and the modifications that are brought up due to external stresses (mechanical, chemical, enzymatic or combined) might significantly influence the hydrolytic rate. In particular, this section is concerned the effects of mechanical abrasion on agricultural waste (AW), constituted by a mixture of maize and grass silage (see **section 2.3.2**). First of all, it should be noted that the raw PSD of AW (i.e. before treatment) considerably differs from the PSD for *C. acetobutylicum*. The PSD of agricultural waste is rather complex (**Figure 2.18**), with a multimodal distribution due to the great diversity of dimensions and fractions present in the mixture.

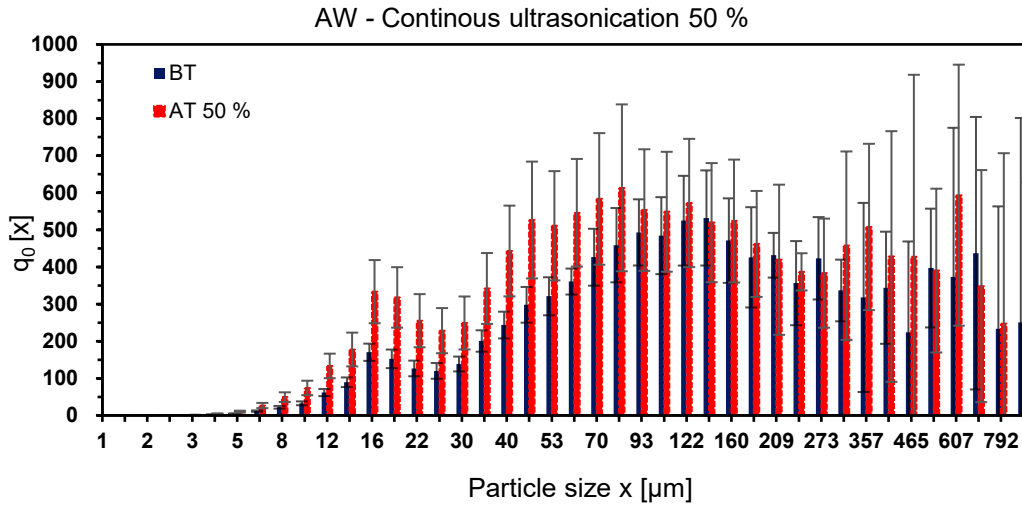


Figure 2.18 Particle size distribution (PSD) of Agricultural Waste samples treated with ultrasonication at 50 % amplitude.

The data also presented a high degree of polydispersity even for the samples before treatment, with low relative error (< 15-20%) for the measurements below 350 μm , while for longer particle's diameters the standard deviation significantly increases. These effects are more marked after sonication, which was tested for this type of substrate at 50 % amplitude, under similar conditions to the previous tests. The ultrasonication pre-treatment served to enrich small and medium particles cuts, particularly in the range 16 -350 μm .

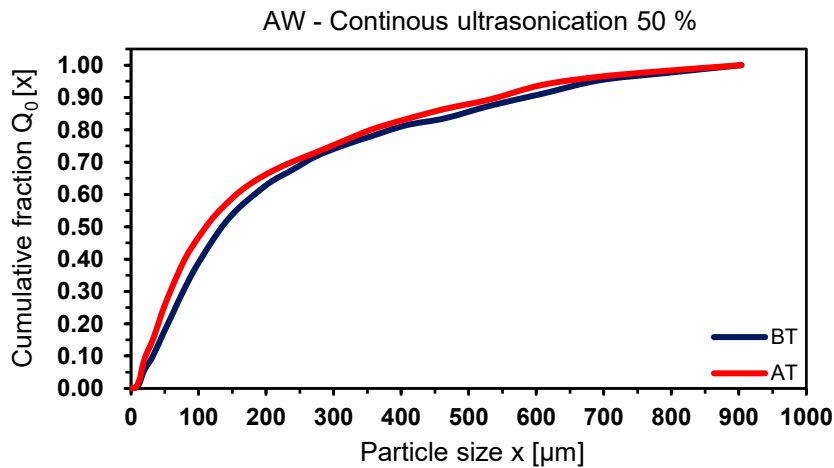


Figure 2.19 Particle size distribution (PSD) of Agricultural Waste samples treated with ultrasonication at 50 % amplitude.

On the other hand, the cumulative PSD presented in **Figure 2.19** shows a significant shift towards smaller particles diameter over the whole studied range. For practical purposes, three important meshes were defined to assess the effects on the distinct groups of interest. The highest reduction was achieved for the d10 cut, which is the diameter of the cumulative fraction of particles corresponding to 10 % of the total sample; the application of the pre-treatment reduced the diameter from this cut from 49.14 to 21.63 μm , which represents a percentage reduction of

c. 56%. For the d50 cut, the reduction amounted 17.67 %, with the diameter passing from 135.12 μm to 111.24 μm . Lastly, the d90 cut presented the smallest decrement, of about 7.4 %, going from 585.03 to 541.96 μm (see **Table 2.5**). This decreasing reduction observed in the different cuts could be explained from the point of view of the cavitation phenomena involved in ultrasonication.

Table 2.5 Characteristic *D* values of interest for the ultrasonication pre-treatment on Agricultural Waste

	BT [μm]	AT [μm]	Reduction [%]
<i>d10</i>	49.14	21.63	55.98
<i>d50</i>	135.11	111.24	17.67
<i>d90</i>	585.03	541.96	7.36

The ultrasonication technique is based on the application of alternating cycles of compression and rarefaction. During these cycles, nuclei bubbles are formed that coalesce and form: *i*) stable bubbles, which grow to a characteristic dimension and at the end escape the liquid phase and *ii*) bubbles in a transitory regime that grow over the cycles of rarefaction and compression until they reach an unstable dimension and undergo violent collapse, creating localized spots with high temperatures (>5000 K) and pressure (>500 atm). The frequency of the applied ultrasound is fairly low (26 kHz) and it corresponds to a theoretical critical or resonant dimension of cavitation bubbles in the range 0.1-100 μm [45]. Larger particles (>200 μm) might not be intensively affected due the ultrasonication pre-treatment, because transient bubbles cannot fully entrain large biomass particles, hence these bubbles slip over the AW particles surface and promote a partial rupture.

2.4.4.2 Bead Milling

Since bead milling was tested using a batch configuration, samples were filtered using 125 μm sieves in order to delimit the particle size and avoid over-estimations during the transfer of the samples.

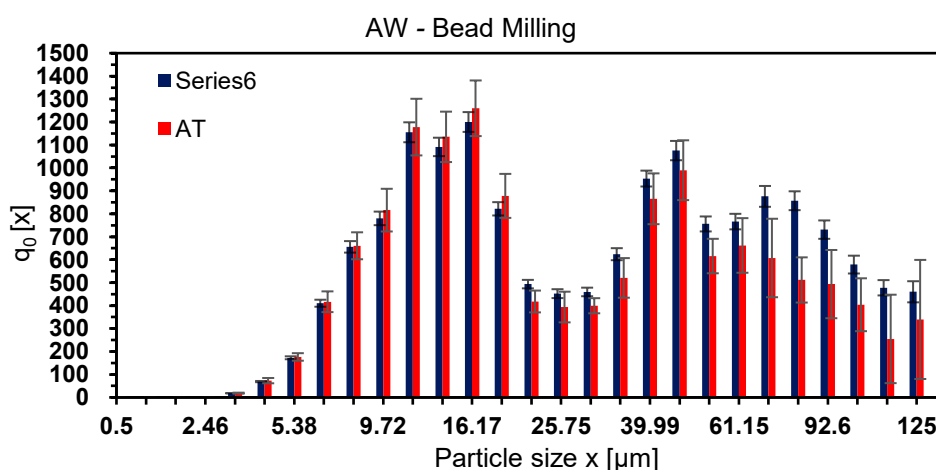


Figure 2.20 Particle size distribution (PSD) of Agricultural Waste samples treated with bead mill.

Hence, the PSD was obtained for a demarcate fraction between 0 and 125 μm , with the correspondent modifications to the probe lenses to enhance accuracy in the aforementioned range. The tests were carried out in conditions similar to *B. subtilis* tests (see **section 2.4.1.1**), using an application time of 10 minutes.

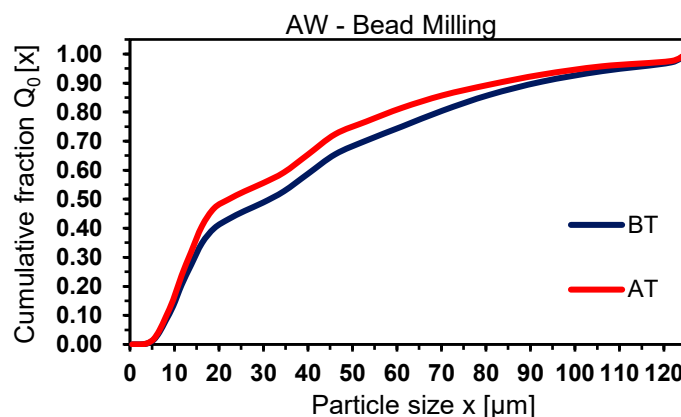


Figure 2.21 Cumulative Particle size distribution (PSD) of Agricultural Waste samples pre-treated with bead mill.

The obtained trends for the samples show that both PSDs are multimodal (**Figure 2.20** and **Figure 2.21**), with a relatively low initial dispersion (average relative error $< 5\%$), which after pre-treatment increased $> 15\%$ (as presented in **Table 2.6**).

Table 2.6 Characteristic D values of interest for the bead mill pre-treatment on Agricultural Waste.

	BT [μm]	AT [μm]	Reduction [%]
d_{10}	8.64	8.31	3.87
d_{50}	31.31	22.26	28.89
d_{90}	91.34	82.70	9.46

It is important to note that there was a significant increase in the number count of particles in the range 0 - 18.95 μm after the application of the pre-treatment, while for the 22.13 μm - 125 μm range, the number of particles captured by the probe decreased, which is consistent with the expected effect in this type of comminution process.

2.4.4.3 Rotor-Stator

Finally, the last comminution treatment which was tested on AW was rotor-stator degradation. Samples were also filtered using the 125 μm sieve and successively measured with the probe. As shown in **Figure 2.22**, the initial PSD was concentrated in a narrow range, mainly between 0 and 30 μm , and after the application of the pre-treatment it remained in the same range, but the particles count substantially increased.

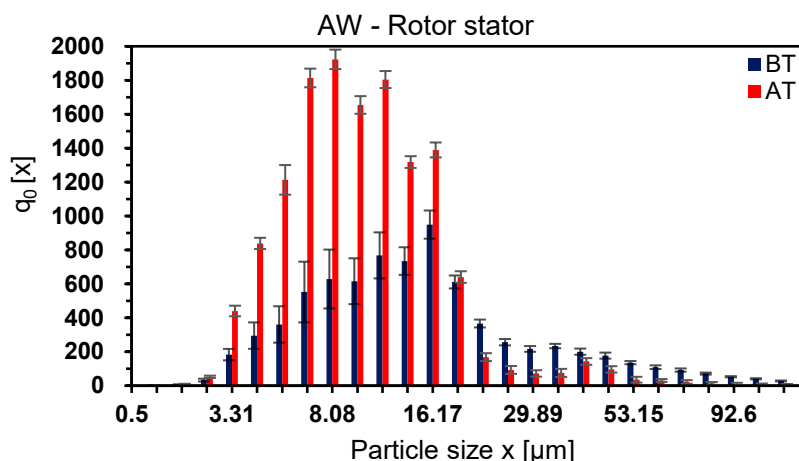


Figure 2.22 Particle size distribution (PSD) of Agricultural Waste samples pre-treated with rotor-stator.

The cumulative PSD exhibited a similar trend, with a marked difference between the d_{20} and d_{90} (**Figure 2.23**), particularly in the range d_{50} - d_{90} .

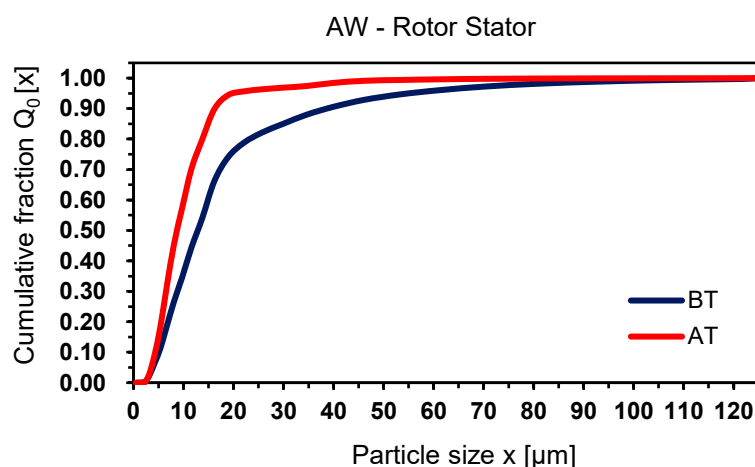


Figure 2.23 Particle size distribution (PSD) of Agricultural Waste samples pre-treated with rotor-stator.

The reduction of the comminuted particles amounted 14.63 % in the d_{10} slot, while for d_{50} in was around 32.11 % and d_{90} roughly halved, with a reduction of 58.06 % (**Table 2.7**).

Table 2.7 Characteristic D values of interest for the rotor-stator pre-treatment on Agricultural Waste

	BT [μm]	AT [μm]	Reduction [%]
d_{10}	5.06	4.32	14.63
d_{50}	12.84	8.72	32.11
d_{90}	38.79	16.27	58.06

In addition, it should be noted that the cumulative curve (**Figure 2.23**) after pre-treatment is quite steep, reaching a high percentile ($> 95\%$) at relatively low diameters, close to 20 μm . In addition, the relative error of the measurements

decreases for the samples after the treatment, which also indicates the effectiveness of the pre-treatment in respect to homogenizing the dispersion of the particle size.

2.4.4.4 Energy expenditure of mechanical pre-treatments

The energetic expenses for the pre-treatment steps are fundamental in energy-recovery processes. Upstream processing is almost always necessary for second generation feedstocks and therefore the energy cost should be a discriminating parameter of the process. Although for mechanical pre-treatments it is more evident, since the energy costs can be linked to the power input of the machinery which is used, in the case of chemical pre-treatment it is also necessary to perform this type of analysis. For example, different studies [46][47] have evaluated the energetic costs of the basic pre-treatment, using the Gross Energy Requirement (GER) of the NaOH production and comparing it to the increased energy recovery, under the form of enhanced biogas yield after the application of the alkaline pre-treatment.

The specific energy costs can be expressed using different indicators; for this particular case, it was decided to perform an analysis in terms of: *i)* spent energy per gram of dry matter (i.e. SE_m), as - $SE_m = \text{Energy} / \text{grams of treated dry matter}$ -, expressed in J/g_{DM} and spent energy on the D50 relative reduction (i.e. SE_l), as - $SE_l = \text{Energy} / \Delta D50$ - expressed in J/ μm . In addition, SE_m was compared to the Lower Heating Value (LHV) of the substrate under analysis (c. 14500 J/g_{DM}), in order to evaluate which fraction of the embedded energy is necessary for the application of the pre-treatment.

Table 2.8 Specific Energy consumption for each tested pre-treatment on Agricultural Waste

	Nominal Power [W]	Occupation fraction	Time [min]	$\Delta D50$ [μm]	SE_l - Specific Energy [J/ μm]	SE_m - Specific Energy [J/g _{DM}]	Relative Energy [-]
Bead Milling	150	0.70	10.0	23.88	3.77	7.04	0.579
Rotor-stator	500	0.55	10.0	9.05	18.24	8.59	0.707
Ultrasonication	200	0.50	2.5	4.12	3.64	4.69	0.386

The results of the energy analysis (**Table 2.8**) suggest that sonication is the most convenient pre-treatment, in the conditions under examination. The mass specific energy (SE_m) and the length specific energy (SE_l) resulted in lower energy consumption, with a requirement of 38.6 % of the embedded energy. On the other hand, rotor-stator degradation was the most energy-intensive, with length specific energy of 18.24 J/ μm and a relative expense 70.7 % of the LHV. Bead Mill resulted in intermediate values, with a consumption of 57.9 % of the LHV of the substrate. Although these values are reference values, which correspond to the applied conditions in this study, the methodology can serve to rationalize the use of them in industrial context.

A more comprehensive analysis could include the experimental calculation of the energy obtained, under the form of methane, and compare it with the energetic expenditure of the pre-treatment. In addition, the process conditions could also be optimized using the increase in methane production ($\Delta \text{mL CH}_4/\text{g}_{\text{DM}}$) as a reference and comparing it with the increase in energy delivered in the pre-treatment ($\Delta \text{kWh/g}$); the enhancement of energy-recovery will then be given by the maximization of the former and the minimization of the latter.

2.5 Conclusions

This chapter reviews the hydrolysis phase, which is critical for the anaerobic fermentation process. One of the most critical points is the increasing pressure on feedstocks that can be used; the hydrolytic phase requires a more detailed analysis in the context of lignocellulosic substrates or with high recalcitrant fraction as well as a revision to energy expenditures.

Additionally, in more advanced configurations, such as the case of the TSAD or Plug Flow reactors, pre-treatment and the time of application also play a key role for the biological phase. The hydrolytic phase is quite complex, since it involves chemical and biological phenomena and can be described according to certain parameters of interest depending on the biomass characteristics. Hence comminution is fundamental, but the existence of enzymes complements the process, catalysing hydrolysis and making possible the release of the soluble substrates for bacterial intake. When wet mechanical pre-treatments are applied to process streams, which also contain the biological phase, shear stress can be used as an external stressor promoting the selection of bacterial population of interest, for example increasing HPB and the decreasing HBC due to the different threshold of each group. For the model microorganisms tested, *B. subtilis* and *C. acetobutylicum*, bead mill resulted more detrimental to cell viability, while sonication, either in batch or continuous mode, and rotor-stator degradation had a gentler effect. Cell viability, in the context of this chapter, is not only useful to determine the survival of microbial species to abrasion but also to understand if the generation of enzymes will continue to take place since a damaged or non-viable microorganism will certainly compromise its ability to produce hydrolytic enzymes.

Another important aspect is the use of process analytical tools to monitor the comminution phase and understand, even in real time, the metabolic state and/or the particle size distribution in fermentation broths. Some of the experiments presented in this chapter were carried out using image analysis (after plating) to estimate cell viability and *in situ* laser back reflection. Particularly the latter method can provide high-throughput measurements which can help improve the performance of the hydrolytic phase and to develop new mathematical models to enhanced bioenergy recovery, therefore the experimental conditions were selected to maintain an acceptable range of uncertainty and provide valuable information about the process for each test.

References

- [1] B. Ruggeri, T. Tommasi, and S. Sanfilippo, *BioH₂ & BioCH₄ Through Anaerobic Digestion: From Research to Full-scale Applications*. Springer London, 2015.
- [2] R. K. Thauer, K. Jungermann, and K. Decker, "Energy conservation in chemotrophic anaerobic bacteria.," *Bacteriol. Rev.*, vol. 41, no. 1, pp. 100–180, 1977.
- [3] E. Angelonidi and S. R. Smith, "A comparison of wet and dry anaerobic digestion processes for the treatment of municipal solid waste and food waste," *Water Environ. J.*, vol. 29, no. 4, pp. 549–557, 2015.
- [4] D. J. Martin, "Mass transfer limitations in solid-state digestion," *Biotechnol. Lett.*, vol. 21, no. 9, pp. 809–814, 1999.
- [5] V. Sojo, A. Pomiankowski, and N. Lane, "A Bioenergetic Basis for Membrane Divergence in Archaea and Bacteria," *PLoS Biol.*, vol. 12, no. 8, pp. 1–12, 2014.
- [6] V. A. Vavilin, B. Fernandez, J. Palatsi, and X. Flotats, "Hydrolysis kinetics in anaerobic degradation of particulate organic material: An overview," *Waste Manag.*, vol. 28, no. 6, pp. 939–951, 2008.
- [7] D. J. Batstone *et al.*, "The IWA Anaerobic Digestion Model No 1 (ADM1)," *Water Sci. Technol.*, vol. 45, no. 10, pp. 65–73, 2002.
- [8] M. H. Gerardi, *The Microbiology of Anaerobic Digesters*. Hoboken: Wiley, 2003.
- [9] A. J. Barrett and J. K. McDonald, "Nomenclature: protease, proteinase and peptidase.," *Biochem. J.*, vol. 237, no. 3, p. 935, 1986.
- [10] E. T. Reese, R. G. H. Siu, and H. S. Levinson, "The biological degradation of soluble cellulose derivatives and its relationship to the mechanism of cellulose hydrolysis.," *J. Bacteriol.*, vol. 59, no. 4, pp. 485–497, 1950.
- [11] J. Jalak, M. Kurašin, H. Teugjas, and P. Väljamäe, "Endo-exo synergism in cellulose hydrolysis revisited," *J. Biol. Chem.*, vol. 287, no. 34, pp. 28802–28815, 2012.
- [12] M. Gutierrez-Correa, L. Portal, P. Moreno, and R. P. Tengerdy, "Mixed culture solid substrate fermentation of *Trichoderma reesei* with *Aspergillus niger* on sugar cane bagasse," *Bioresour. Technol.*, pp. 173–178, 1999.
- [13] P. Tantayotai, P. Pornwongthong, C. Muenmuang, T. Phusantisampan, and M. Sriariyanun, "Effect of Cellulase-producing Microbial Consortium on Biogas Production from Lignocellulosic Biomass," *Energy Procedia*, vol. 141, pp. 180–183, 2017.
- [14] A. Salihu and M. Z. Alam, "Solvent tolerant lipases: A review," *Process Biochem.*, vol. 50, no. 1, pp. 86–96, 2015.
- [15] D. Lee *et al.*, "Isolation and characterization of a thermophilic lipase from *Bacillus thermoleovorans* ID-1," *FEMS Microbiol. Lett.*, vol. 179, no. 2, pp. 393–400, 1999.
- [16] E. H. Ghanem, H. A. Al-Sayed, and K. M. Saleh, "An alkalophilic thermostable lipase produced by a new isolate of *Bacillus alcalophilus*," *World J. Microbiol. Biotechnol.*, vol. 16, no. 5, pp. 459–464, 2000.
- [17] K. Sri Bala Kameswari, C. Kalyanaraman, S. Porselvam, and K. Thanasekaran, "Enhancement of Biogas Generation by Addition of Lipase in the Co-Digestion of Tannery Solid Wastes," *CLEAN - Soil, Air, Water*, vol. 39, no. 8, pp. 781–786, 2011.
- [18] Y. Meng, F. Luan, H. Yuan, X. Chen, and X. Li, "Enhancing anaerobic

- digestion performance of crude lipid in food waste by enzymatic pretreatment,” *Bioresour. Technol.*, vol. 224, pp. 48–55, Jan. 2017.
- [19] L. Müller, J. Kretzschmar, J. Pröter, J. Liebetrau, M. Nelles, and F. Scholwin, “Does the addition of proteases affect the biogas yield from organic material in anaerobic digestion?,” *Bioresour. Technol.*, vol. 203, pp. 267–271, 2016.
 - [20] O. Yenigün and B. Demirel, “Ammonia inhibition in anaerobic digestion: A review,” *Process Biochem.*, vol. 48, no. 5–6, pp. 901–911, 2013.
 - [21] E. Kovács, R. Wirth, G. Maróti, Z. Bagi, G. Rákhely, and K. L. Kovács, “Biogas production from protein-rich biomass: fed-batch anaerobic fermentation of casein and of pig blood and associated changes in microbial community composition,” *PLoS One*, vol. 8, no. 10, pp. 1–18, 2013.
 - [22] D. Bolzonella, F. Fatone, P. Pavan, and F. Cecchi, “Anaerobic fermentation of organic municipal solid wastes for the production of soluble organic compounds,” *Ind. Eng. Chem. Res.*, vol. 44, no. 10, pp. 3412–3418, 2005.
 - [23] A. Nielfa, R. Cano, and M. Fdz-Polanco, “Theoretical methane production generated by the co-digestion of organic fraction municipal solid waste and biological sludge,” *Biotechnol. Reports*, vol. 5, no. 1, pp. 14–21, 2015.
 - [24] A. Valentini, G. Garuti, A. Rozzi, and A. Tilche, “Anaerobic degradation kinetics of particulate organic matter: A new approach,” *Water Sci. Technol.*, vol. 36, no. 6–7, pp. 239–246, 1997.
 - [25] K. Masoud, “Biodegradability of the organic fraction of municipal solid waste in a high-solids anaerobic digester,” *Waste Manag. Res.*, vol. 13, no. 2, pp. 123–136, 1995.
 - [26] F. Cecchi, J. M. Alvarez, P. G. Traverso, F. Medici, and G. Fazzini, “A new approach to the kinetic study of anaerobic degradation of the organic fraction of municipal solid waste,” *Biomass*, vol. 23, no. 2, pp. 79–102, 1990.
 - [27] R. O. Owihondah *et al.*, “Assessment and parameter identification of simplified models to describe the kinetics of semi-continuous biomethane production from anaerobic digestion of green and food waste,” *Bioprocess Biosyst. Eng.*, vol. 39, no. 6, pp. 977–92, Jun. 2016.
 - [28] S. Aldin, G. Nakhla, and M. B. Ray, “Modeling the influence of particulate protein size on hydrolysis in anaerobic digestion,” *Ind. Eng. Chem. Res.*, vol. 50, no. 18, pp. 10843–10849, 2011.
 - [29] E. de La Hera, M. Gomez, and C. M. Rosell, “Particle size distribution of rice flour affecting the starch enzymatic hydrolysis and hydration properties,” *Carbohydr. Polym.*, vol. 98, no. 1, pp. 421–427, 2013.
 - [30] J. Schindelin *et al.*, “Fiji: an open-source platform for biological-image analysis,” *Nat. Methods*, vol. 9, no. 7, pp. 676–682, 2012.
 - [31] A. Brognaux, J. Bugge, F. H. Schwartz, P. Thonart, S. Telek, and F. Delvigne, “Real-time monitoring of cell viability and cell density on the basis of a three dimensional optical reflectance method (3D-ORM): Investigation of the effect of sub-lethal and lethal injuries,” *J. Ind. Microbiol. Biotechnol.*, vol. 40, no. 7, pp. 679–686, 2013.
 - [32] J. De Vrieze *et al.*, “The full-scale anaerobic digestion microbiome is represented by specific marker populations,” *Water Res.*, vol. 104, pp. 101–110, 2016.
 - [33] R. Wirth, E. Kovács, G. Maróti, Z. Bagi, G. Rákhely, and K. L. Kovács, “Characterization of a biogas-producing microbial community by short-read next generation DNA sequencing,” *Biotechnol. Biofuels*, vol. 5, pp. 1–16, 2012.
 - [34] K. Kampmann, S. Ratering, I. Kramer, M. Schmidt, W. Zerr, and S. Schnell,

- “Unexpected stability of Bacteroidetes and Firmicutes communities in laboratory biogas reactors fed with different defined substrates,” *Appl. Environ. Microbiol.*, vol. 78, no. 7, pp. 2106–2119, 2012.
- [35] C. A. Jones, N. L. Padula, and P. Setlow, “Effect of mechanical abrasion on the viability, disruption and germination of spores of *Bacillus subtilis*,” *J. Appl. Microbiol.*, vol. 99, pp. 1484–1494, 2005.
- [36] P. Setlow, “Spores of *Bacillus subtilis*: their resistance to and killing by radiation, heat and chemicals,” *J. Appl. Microbiol.*, vol. 101, pp. 514–525, 2006.
- [37] D. Higgins and J. Dworkin, “Recent progress in *Bacillus subtilis* sporulation,” *FEMS Microbiol. Rev.*, vol. 36, no. 1, pp. 131–148, 2012.
- [38] R. Seetharam, *Purification and Analysis of Recombinant Proteins*. New York: Marcel Dekker, 1991.
- [39] H. M. Jonkers and E. Schlangen, “Development of a bacteria-based self healing concrete,” in *Tailor Made Concrete Structures —new solutions for our society*, 2008, pp. 425–430.
- [40] M. Seifan, A. K. Sarmah, A. K. Samani, A. Ebrahiminezhad, Y. Ghasemi, and A. Berenjian, “Mechanical properties of bio self-healing concrete containing immobilized bacteria with iron oxide nanoparticles,” *Appl. Microbiol. Biotechnol.*, vol. 102, no. 10, pp. 4489–4498, May 2018.
- [41] B. P. Tracy, S. W. Jones, and E. T. Papoutsakis, “Inactivation of σ^E and σ^G in *Clostridium acetobutylicum* illuminates their roles in clostridial-cell-form biogenesis, granule synthesis, solventogenesis, and spore morphogenesis,” *J. Bacteriol.*, vol. 193, no. 6, pp. 1414–1426, 2011.
- [42] D. T. Jones, A. Van Der Westhuizen, S. Long, E. Allcock, S. Reid, and D. Woods, “Solvent production and morphological changes in *Clostridium acetobutylicum*,” *Appl. Environ. Microbiol.*, vol. 43, no. 6, pp. 1434–1439, 1982.
- [43] S. Jiao *et al.*, “Transcriptional analysis of degenerate strain *Clostridium beijerinckii* DG-8052 reveals a pleiotropic response to CaCO_3 -associated recovery of solvent production,” *Sci. Rep.*, vol. 6, pp. 1–14, 2016.
- [44] K. Show, T. Mao, and D. Lee, “Optimisation of sludge disruption by sonication,” *Water Res.*, vol. 41, no. 20, pp. 4741–4747, 2007.
- [45] A. Brothie, F. Grieser, and M. Ashokkumar, “Effect of Power and Frequency on Bubble-Size Distributions in Acoustic Cavitation,” *Phys. Rev. Lett.*, vol. 102, no. 8, pp. 1–4, 2009.
- [46] B. Ruggeri, S. Sanfilippo, T. Tommasi, and D. Fino, “Process Energy Sustainability Evaluation through a LCA Approach,” *Chem. Eng. Trans.*, vol. 25, pp. 629–634, 2011.
- [47] A. C. Luongo Malave, D. Fino, C. E. Gomez Camacho, and B. Ruggeri, “Experimental tests on commercial Sweet Product Residue (SPR) as a suitable feed for anaerobic bioenergy ($\text{H}_2 + \text{CH}_4$) production,” *Waste Manag.*, vol. 71, pp. 626–635, 2018.

3. Monitoring the state of mixed cultures used for bioenergy production

3.1 Introduction

The shift from oil-based economies and their derivatives to circular economic models that can promote the better use of available resources, especially different types of wastes, is a growing concern of the biotechnological industry. Europe accounts 224 biorefineries [1], that use different feedstocks such as bio-waste, lignocellulosic material, waste fats and oils and different sugar- and starch-rich residues. Traditional refineries are constituted by several sequential unit operations, which use oil, i.e. an unspecified complex mixture of hydrocarbons, as the main input. Once in the refinery, oil undergoes first pre-treatment steps, that aim at removing contaminants and water, and is subsequently sent to the distillation units, where the main products pools and cuts are obtained. After distillation, the petrochemical industry uses catalytic units to transform a share of these products into higher added value products.

On the other hand, biorefineries share some similarities with traditional refineries. Biorefineries are being classified according to the specific activity, either for the generation of energy or for the production of specific bio-based products. The field of biotechnology has tried to adopt the principle of *Quality by Design (QbD)* as a benchmark, not only for the pharmaceutical and food industry, but also for the conceptualization of biorefineries, which significantly increases the challenges associated to reliable process monitoring and control strategies. According to the International Council for Harmonisation of Technical Requirements for Pharmaceuticals for Human Use (ICH), *QbD* represents “a systematic approach to process development that begins with predefined objectives and emphasizes product and process understanding and process control, based on sound science and quality risk management’ [2], which basically includes:

- identification of the product’s critical quality attributes that are of significant importance to the product;
- design of the process to deliver these attributes;
- a robust control strategy to ensure consistent process performance;
- validating the process demonstrating the effectiveness of the control strategy;
- continuous monitoring to ensure robust process performance over the life cycle of the product.

In the biorefineries context, Dark Fermentation (DF) of organic waste is one of the most versatile techniques that can be integrated in several process configurations. Dark fermentation processes are mixed acidic fermentations, which use undefined microbiomes or mixed consortia of hydrolytic and fermentative bacteria, that convert sugars and starches into small chain carbohydrates, proteins into amino acids and lipids to glycerol, long-chain and short-chain carboxylic acids, along with the production of H_2 and CO_2 .

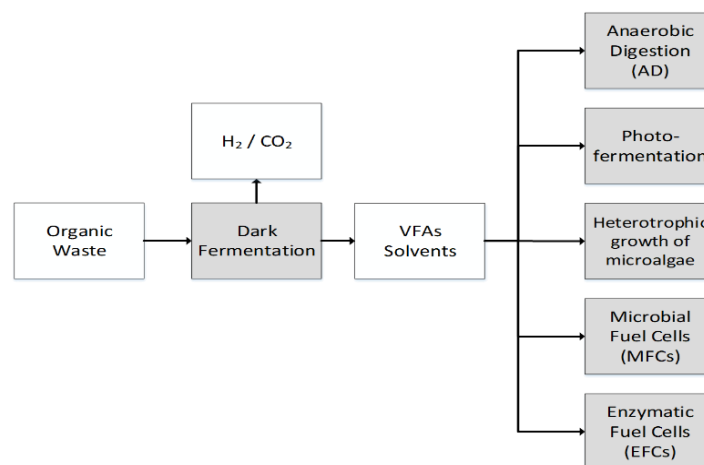


Figure 3.1 Possible process integration for Dark Fermentation (DF).

Traditionally, DF has been coupled to Anaerobic Digestion (AD), mostly in two-stage Anaerobic Digestion (TSAD) configurations, recovering both gaseous energy carriers, bio- H_2 in the first step and bio- CH_4 in the second [3]. Furthermore, the liquid residues from the DF process contain a pool of carboxylic acids and also solvents that can be fed into different processes for value addition (see **Figure 3.1**), such as Microbial Fuel Cells (MFC) [4], algae and microalgae cultivations [5], or combined steps [6][7][8].

The modern biotechnological industry relies in two workhorses: *i*) metabolic engineering, which is based on the study and modification of cellular properties of pure cultures through genetic modifications and *ii*) microbial community engineering (MCE), based on co-cultures or mixed cultures exploiting natural diversity and interactions between groups of microorganisms. Both branches actively research on the topic of bioenergy recovery [9][10], although for most cases the use of pure cultures tends to be cost-intensive (i.e. which is especially critical for energy-recovery processes) and therefore mixed cultures are preferred, using selection and evolutionary techniques and coupled to adequate process parameters and selective pressures. As a matter of fact, MCE is gaining ground not only for energy production but also for the production of food, chemicals and materials [11][12][13].

Although microbial communities have been long studied in ecology, the rise of throughput technologies have broadened the field of interest and applications. However, the determination of live/dead cells or the identification of metabolic

status of each microbial cell is an endeavouring task. This is a problem for both branches of biotechnology, since discriminating between a living, inactive or dead microorganism is fundamental in disciplines such as biorefineries, ecology, aeronautics, environmental health, medicine, among others.

DNA sequencing is today a powerful tool which is available to identify microbial species and strains but high-throughput tests in regard to viability are rather scarce. DNA sequencing offers valuable information about genetic material but in the context of mixed cultures, the information can lead to inaccurate conclusions. For example, the presence of DNA fragments of a particular microorganism within a microbiome does not give information on the viability and/or the physiological state of this microorganism or its role in the community dynamics. Therefore, there are still challenges associated to determine whether a microorganism or a group of them is present in the consortium and have a physiologically active state.

In general, culture-based techniques are used to determine viability discriminating among live/dead microorganisms, commonly relying on agar plating or liquid cultures using simple, complex or synthetic medium for growth. However, the dynamics of mixed cultures include species-species and environment-species interactions that are difficult to reproduce under controlled laboratory conditions. Some electro-optical tools which are available nowadays are interesting candidates in the field of monitoring the physiological status of mixed consortia for bioenergy production. One of the major advantages is that certain electro-optical techniques can be used at single-cell level for a high-throughput detection and discrimination among hundreds of thousands or millions of cells within a sample.

This chapter addresses the use of two experimental techniques, Flow Cytometry (FC) and Frequency-Dependent Polarizability Anisotropy (FDPA) measurements to monitor the Dark Fermentation process, carried out with a mixed acidogenic culture. Flow cytometry is a laser-based electrooptical technique that measures two scatter signals Forward Scatter (FSC) and Side Scatter (SSC), and is equipped with different fluorescence detector channels that serve to assess both, qualitatively and quantitatively the physiological state of several thousand cells per second, using specific dyes (i.e. which bound to certain molecules or structures) or exploiting auto-fluorescent properties of different cell types [14]. The other electrooptical technique is the measurement of the Polarizability Anisotropy (AP) of a cell suspension, where the outer layer of the cellular membrane exhibits anisotropic polarizability when an electric field (EF) of a certain frequency is applied in the normal and tangential direction.

3.2 Theoretical background

3.2.1 Biofuels and Biorefineries:

The rise of biorefineries in Europe, which reached the number of 224 in November 2017 [1], is an important milestone at European level. As presented in **Figure 3.2**, there are different types of feedstocks that are used in each refinery

type, and the distribution of the plants is more concentrated in west and central Europe.

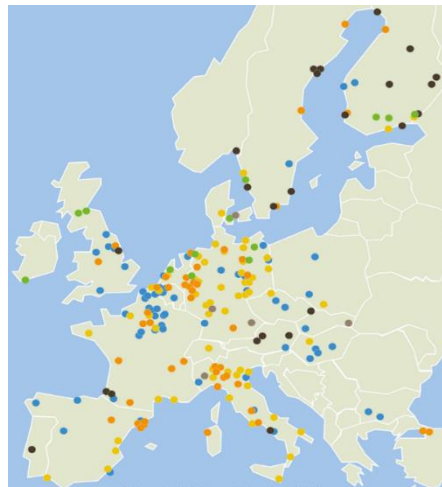


Figure 3.2 Map showing the geographical location of different types of biorefineries in Europe for the year 2017: ● General Bio-waste, ● Lignocellulosic (not wood), ● Oil/fats – biodiesel, ● Oil/fats – oleo chemistry, ● Sugar/starch – bioethanol and chemicals and ● Wood-based (modified from [1]).

Biorefineries and the re-use of different types of waste at industrial level is an important step towards circular economic models. Biorefineries can be widely classified according to the industrial purpose, hence there are two major classifications: *energy* and *bio-based chemicals* biorefineries. However, there are also process configuration where both types are present (see **Figure 3.3**).

Nowadays, the classification of biofuels considers four generations, which are briefly introduced hereafter [15][16]:

- I. *First Generation Biofuels*: derived from food crops and therefore pose the question of competition between arable land for human sustenance agriculture and biofuels, typically involving traditional chemical and mechanical processing (grinding, milling, distillation, transesterification, among others), but also a small share of biotechnological processes, such as fermentation of sugarcane for the production of bioethanol or the enzymatic transesterification of oil/fats into diesel.
- II. *Second Generation Biofuels*: encompass the use of organic waste/residues, which do not compete for arable land. However, due to the high content of cellulose and lignin present in this type of feedstock, pre-treatment steps (chemical, thermal, mechanical and/or biological) are required to improve the yield of these systems. The production can be either chemical (i.e. gasification, pyrolysis) or biological to produce biomethane, biohydrogen, butanol, ethanol and other important volatile fatty acids (VFA) and solvents.
- III. *Third Generation Biofuels*: corresponds to the cultivation of biomass, particular algae. This generation differs from the two previous because it targets carbon dioxide (CO₂) fixation. In this context, autotrophic microorganisms that present higher growth rates than plants, are seen as advantageous, particular algae since its metabolic pathways also includes

high lipids production (i.e. which can be further converted into other biofuels such as biodiesel and kerosene oil). An important challenge of this type of biofuels is the direct energy expenditure for the cultivation and down-stream processing of algae biomass, as well as microbial contamination problems in algae cultivations that significantly slow down the growth and yield.

- IV. *Fourth generation*: the state-of-the-art or current generation of biofuels, which includes the use of advanced technology for biofuels productions. From the biotechnological point of view, these technologies include the use of genetically modified microorganisms (GMO) to enhance carbon capture, improve yields and modify important features of microorganisms (i.e. substrate utilization, lower water consumption, aerobic/anaerobic physiology, removal of inhibitions, etc.) as well as engineered microbial communities to target specific products or exploit symbiotic associations.

The rise of biorefineries should be welcomed as a major step towards sustainability and therefore the field of biotechnology has faced, and will continue to address, many challenges to adapt itself to the growing requirements. Traditional oil refineries can be classified according to the *Nelson Complexity Index* (NCI), which considers the diversity of refined products obtained through medium and deep conversion units compared to the obtained products from the main distillation units.

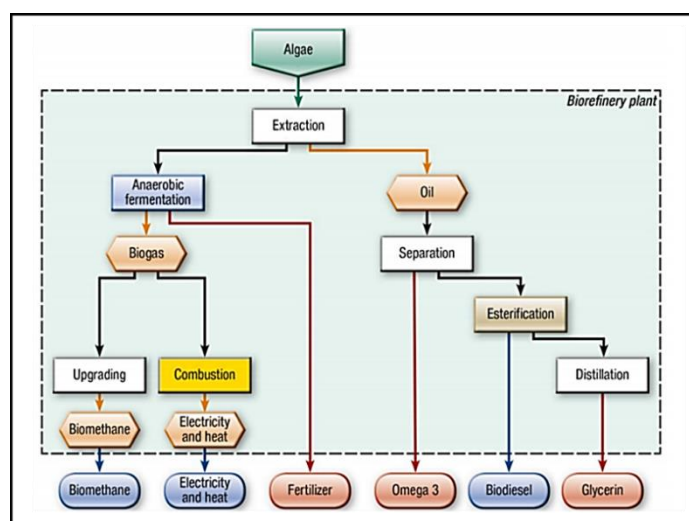


Figure 3.3 Basic reference scheme of a third generation biorefinery, producing chemicals and energy: biomethane (upgraded biogas with more than 95 % v/v CH₄), electricity and heat from CHP units fed with raw biogas, fertilizers (the digestate from AD), omega-3 extracted from algae biomass, lipids pool that can be trans-esterified into biodiesels obtaining also, after distillation, glycerol as a by-product (modified from [17]).

Recent efforts have tried to establish a similar indicator for biorefineries the – *Biorefinery Complexity Index (BCI)* –, based on the Technology Readiness Level (TRL) of four key elements that are present in biorefineries: platforms, feedstocks, products and processes (**Figure 3.3**) [17]. In classic petrochemical processes, the performance of conversion processes strongly depends on the state of the catalysts. Nevertheless, catalyst deactivation is an ubiquitous and well-studied phenomenon that takes place in every refinery conversion process; deactivation can be either due

to chemical, mechanical or thermal stress over time and some of the common mechanisms of catalyst deactivation include poisoning, sintering, coking, masking, among others [18][19]. In the case of biorefineries, the control and monitoring of the biotic phase, i.e. tracking the physiological status of microbial cultures (pure, co-cultures or mixed cultures) is fundamental to maintain an optimal performance.

3.2.2 Physiological status and cell viability of mixed cultures

In the biotechnological field, the verification of whether a microorganism is *alive* or *dead* is generally made through cultivation-dependent methods. As noted by Davey [20], these methods can lead to inaccurate conclusions since the absence of colonies growth in a given medium does not always guarantee that all microorganisms are dead, and that growth will not be resumed when conditions are changed. Moreover, in pure cultures, growth can be followed online through optical density measurements, direct microscopic count or by calculating the dry cell weight. In mixed cultures, for example those used in the production of bioenergy as Anaerobic Digestion or Dark Fermentation, the calculation of the growth rate is much more difficult due to the heterogeneity of microorganisms present and the complexity of fermentation broths, which contain dissolved and suspended substrates.

The definition of life in a microbiological context (i.e. microscopic level), is much more complex than the typical conception at macroscopic level. Following Hammes et. al [21] the basic elements (**Figure 3.4b**) for the existence of life (i.e. excluding viruses), and therefore tightly linked to viability, are:

- I. the existence of non-severely damaged or fully functional nucleic acids, involved in the transcription/translation processes and in DNA replication;
- II. the presence of cellular metabolism, for the basic functioning of cell;
- III. the presence of an intact and functional cellular membrane, able to maintain a suitable intracellular environment.

There are different states of viability, in which a certain microorganism can be found, in addition to the typical *alive* condition (see **Figure 3.4a**). For example, there are damage conditions that are potentially reversible, such as starvation and sublethal injuries induced by physical or chemical stresses [22]. A microorganism can be subjected to conditions of substrate limitations, normally entering a dormant state but can then recover its metabolic activity when placed in a different media or it can activate regulatory mechanisms that trigger the expression of genes [23] that allow the uptake of another type of substrate (i.e. diauxic growth) [24].

Different mechanical or chemical stresses can cause sublethal damages when certain properties of the cells are compromised, such as the decrease of enzymatic synthesis or damage to nucleic acids. Although protein and DNA damage are rather difficult to quantify, there is evidence to suggest that some of these stresses may be

reversible or irreversible and depend on the application intensity and the response of the biological system [25].

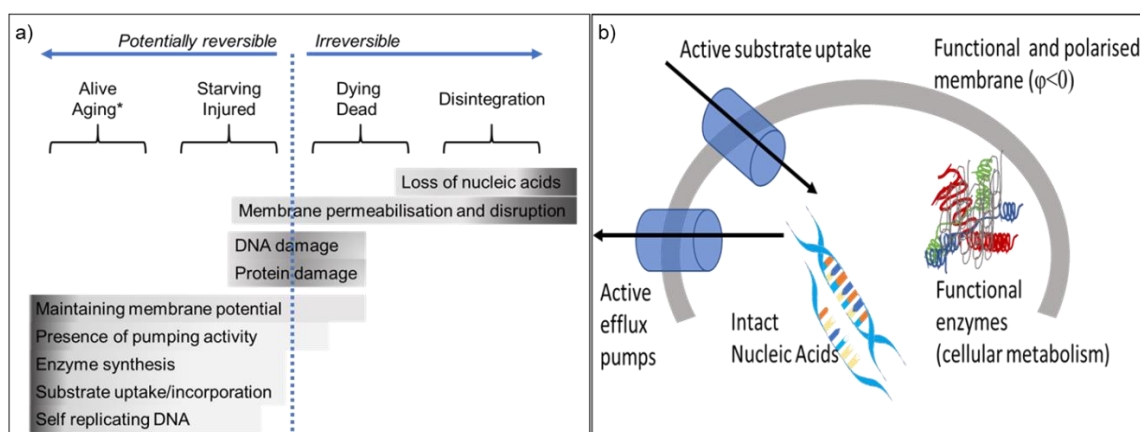


Figure 3.4 a) Proposed cellular stages of bacterial viability, comprehending reversible and irreversible damages and **b)** bacterial features which can be used to track cell viability (modify from [21]).

Another important factor is the state of the cell membranes. Perhaps, the most universal parameter to quantify and study cell viability is the state of cell membranes, since it defines the limits of individual cells and/or of specific compartments within cells and represents the interface with the environment. Hence, the presence of different membrane types and structures is a common feature in all existing life domains. In fact, also certain types of viruses possess envelopes that confer key properties and modulate its action mechanisms [26].

As shown in **Figure 3.4a**, membrane permeabilization (internal or external) encompasses states of reversible and irreversible damage, but it is generally linked to irreversible phenomena that lead to the solubilization of the membranes and ultimately to cellular lysis and disintegration. Certain applications, such as the transport of drugs at the intracellular level need solubilizing agents that allow the passage of molecules but that do not generate irreversible damage. On the other hand, the extraction of molecules of interest in the medical and biotechnological fields intensely focuses on the correct solubilization of membranes to recover the desired products. An element that is related to membrane permeabilization which is important to understand the transition from reversible to irreversible damage and represents a key property that can be exploited in viability measurements is the membrane potential (Ψ) or ($\Delta\Psi$). The membrane potential is given by the total difference in concentration of ionic species between the inside of the cell (or organelle) and the outside and by the individual transport of each ion. At bacterial level, and also at mitochondrial level, it is fundamental because it is responsible for generating ATP and is related to the transport of ions (mainly protons) from inside and outside the cell.

Early studies have suggested that electrochemical concept of proton-motive force (*pmf*) in bacteria is constituted by two components: the electric potential ($\Delta\Psi$) and difference in the concentration of protons on both sides of the membrane (ΔpH),

and that ionic changes in the culture media are compensated via the interconversion of these components [27].

A common approach that is used to understand the main components of the *pmf* is based on the transport thermodynamics across the cellular membrane.

Gibbs free energy of formation (ΔG_f) for a charged specie (i) can be obtained through the thermodynamic relation:

$$\Delta G_{f,i} = \Delta G_{f,i}^0 + R \cdot T \cdot \ln \left(\frac{C_i^{Z_i}}{C_i^{Z_i,0}} \right) + Z_i \cdot F \cdot \Psi \quad (3.1)$$

where the $\Delta G_{f,i}$ (kJ/mol) at the operative conditions can be calculated from $\Delta G_{f,i}^0$ (i.e. the reference state at $P_i^0 = 1$ bar, $T^0 = 298$ K and $C_i^{Z_i,0} = 1$ mol/L), corrected by: *i*) a chemical concentration term $R \cdot T \cdot \ln(C_i^{Z_i}/1)$, which is a function of actual temperature T (K), the gas constant R (8.314 kJ/(kmol·K)), the concentration of the i -specie C_i (mol/L) and its valency (Z_i) and *ii*) an electrical potential term $Z_i \cdot F \cdot \Psi$, which depends on the valency Z_i , the Faraday constant (96.5 kJ/(V·mol Z_i)) and the electrical potential Ψ (V).

Considering that the free energy change for the translocation across the membrane (i.e. from the inner part to the outside) of the charged specie under analysis (ΔG_{pmf}), protons ($i = H^+$), can be calculated as the difference between the inner and outer formation energies of the compound, the following equation can be written:

$$\Delta G_{pmf} = \Delta G_{f,H^+,out} - \Delta G_{f,H^+,in} \quad (3.2)$$

Since:

- $\Psi_{out} = 0$ (considering the outside of the cell the reference state)
- $\Delta G_{f,in}^0 \cong \Delta G_{f,out}^0$
- For $i = H^+$, $Z_i = +1$
- $\ln(C_i) \cong \ln(10) \cdot pH$

Combining **Equation 3.1** and **3.2**, the free energy change of protons translocation can be rewritten as:

$$\Delta G_{pmf} = R \cdot T \cdot \ln(C_{H^+,out}) - [R \cdot T \cdot \ln(C_{H^+,in}) + F \cdot \Psi_{in}] \quad (3.3)$$

Hence, the membrane potential can be written as:

$$\Psi_{in} = \frac{1}{F} \cdot [\ln(10) \cdot R \cdot T \cdot (pH_{in} - pH_{out}) - \Delta G_{pmf}] \quad (3.4)$$

The proton-motive force (*pmf*) can also be seen as the *energy gain per transported proton*, taking into account the transmembrane difference of ions concentration. According to [28], bacteria exert control mechanisms to maintain

constant values of pmf , balancing both components, $\Delta\Psi$ and ΔpH (see **equation 3.3** and **3.4**).

Generally, a polarised viable cell would have an electric potential $\Psi_m < 0$, but the variations (and punctual depolarization conditions) in this electric potential are balanced by the proton transport component. Hence, depolarized cells cannot always be considered irreversibly damaged, while cells presenting a significant decreased in the energetic metabolism ($pmf \rightarrow 0$) would fall into this category. This approach is being studied recently in the design of anti-pathogenic agents and in the development of antibiotics for better efficacy in the medical field. For example, Farha et al. [28] used different selective agents aiming either to counter $\Delta\Psi$ or to deplete ΔpH and assessed the inhibitory effects on *Staphylococcus aureus*; they found a synergistic effect when both factors are attacked simultaneously also generating lower cytotoxicity effects. Another study, presented by Epanand et al. [29], studied the antimicrobial effect of ceragenin agents on the depolarization of cytoplasmic membranes. For this, different gram-positive and gram-negative bacteria were tested, under different ceragenin types and concentrations and the results suggested that antimicrobial action is linked to the permeability and composition of the cell membranes, and that similar mechanisms operate in both types of bacteria, with increased diffusion constraints due to the outer membranes of gram-negative bacteria.

The most common methods for estimating cell viability through the state of membranes is done, nowadays, through electro-optical techniques, some of them are already consolidated in certain fields and others are emerging, particularly in the field of Processes Analytical Chemistry. This field develops instruments, which are different from the typical sensors of pressure, temperature or humidity, that provide greater capacity at scientific and engineering level to monitor and analyse key chemical and physical properties and provide enhanced on-line, off-line and at-line controls [30]. Some of the properties that can be exploited in electro-optical measurements are related, for the case of membrane potential, with the use of fluorescent dyes. As early introduced by Roos et. al [31], for the measurement of the membrane potential and its variations in axons cells, properties such as absorption, fluorescence, circular dichroism or birefringence offer a broad range of possibilities.

3.2.3 Flow Cytometry (FC)

Flow cytometry is an electro-optic technique or an analysis platform, based on light scattering. The optical system comprises the use of a light source, typically a laser and a set of lenses, where the corresponding data about the light scatter in different directions or the emission of fluorescence can be collected at the single-cell level.

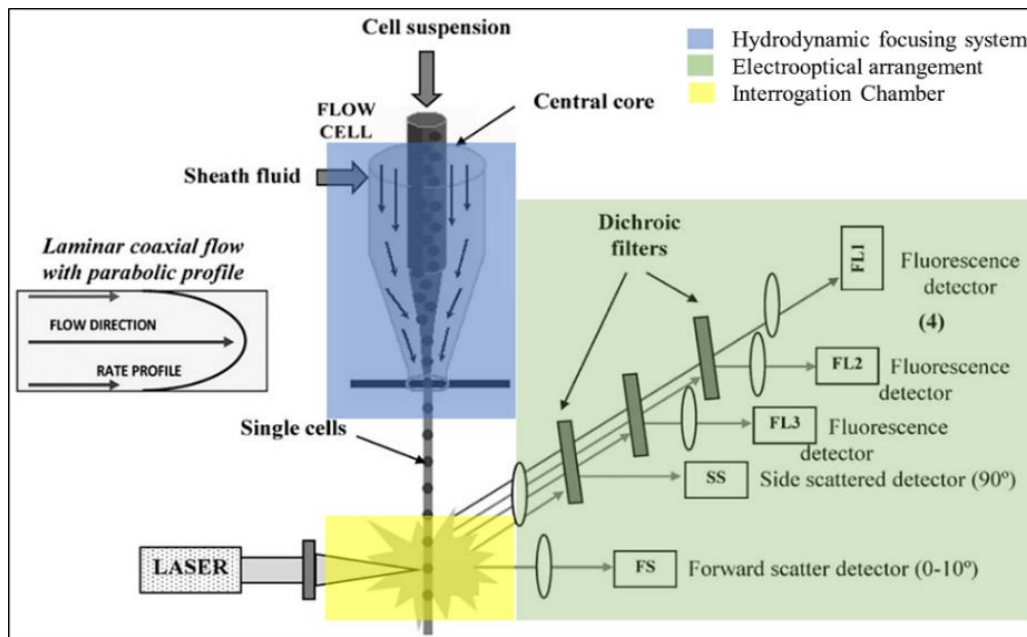


Figure 3.5 Schematic representation of the flow cytometry apparatus (modified from [32]).

The main advantage of flow cytometry (i.e. over other techniques such as fluorescent microscopy), is the capacity to conduct high-throughput analysis, measuring up to $10^6 - 10^7$ events for each sample in very short times. The resolution in this type of measurements is achieved through the use of a hydrodynamic focusing system (see **Figure 3.5**), which comprehends a particular geometry and the coaxial flow of a sheath fluid and the sample stream. The sheath stream is aimed at confining without clogging, within a short length channel to avoid diffusion, a core stream containing the sample particles through an interrogation chamber. Both streams flow at laminar conditions, however, in order to achieve an acceptable focused width and length of the sample stream useful to discriminate cells within the interrogation chamber, an optimal ratio between the sheath flow velocity and the sample flow velocity must be set, normally in the range 5-70. In this interrogation chamber, where particles or cells pass ideally as single cells or single particles, two orthogonal lasers intercept the sample and record the scatter light in both directions. These two signals are the base parameters for flow cytometry analysis: *i*) Forward SCatter (FSC), which is measured in a plane parallel (0-10°) to the laser beam, and corresponds mostly to diffracted light in the forward direction, which is normally associated to the cell size and *ii*) Side SCatter (SSC), which is collected from the refracted and reflected light of a perpendicular laser beam (i.e. at 90°) as a result of refractive index changes on the cell surface. The refractive index is an important biophysical parameter, which provides information on the cell structure, granularity, complexity among other internal features. When both signals, FSC and SSC, are combined and plot together, it allows the morphological discrimination of particles within heterogenous populations containing different cells types and debris.

The electrooptical arrangement (**Figure 3.5**) uses for the FSC channel a photodiode, which converts the scattered light signals for each particle into an electrical current, while the signal of the SSC passes through photomultiplier tubes

to amplify the signal and divert it to the detectors using different mirrors and filters (i.e. bandpass, shortpass and longpass filters). These filters are responsible for allowing only a determined spectral band to be recovered in the photodiode for each channel, which is useful while using fluorochromes and collecting multi-parameter signals. Hence, flow cytometry analyses often include staining with single fluorochromes or the use of multiple dyes. The use of this type of compounds is aimed at labelling specific enzymes, identifying different structures or monitoring key parameters or properties, which complement the information about the cell structure, gained through the FSC/SSC channels.

Since the use of fluorescent dyes can interfere with the biological system, and potentially bias the gathered information, the choice of staining compounds is critical for this type of analysis. Following [32], the selection of fluorochrome should consider: biological inert compounds with low cytotoxicity, elevated extinction coefficient and quantum yield (i.e. to be detected even at low concentrations), well-defined and narrow emission spectrum, photostability at the involved wavelengths and adequate water solubility (to facilitate diffusion).

However, very few data are available regarding the application of flow cytometry for unspecified mixed cultures, especially in the field of bioenergy production, although the versatility of the technique suggests large potential [33]. One of the few applications found in literature [34] is the use of FC in a long-term experiment, tracking the composition of the community present in AD bioreactors, combining FSC with DAPI-staining (i.e. a DNA-binding dye, to differentiate between debris and DNA-possessing particles). The results revealed that more than 20 microbial sub-groups were involved in the process, and that the variation of the Organic Loading Rate (OLR), by two or four folds the initial value, yielded a noticeable increase in three main sub-populations, which also positively correlated with Volatile Fatty Acids (VFA) production in the system. Additionally, the feasibility case study of biogas production monitored with FC was presented by [35], considering sample acquisition time, operational costs and automatization potential, among other important factors.

3.2.4 Frequency-Dependent Polarizability Anisotropy (FDPA)

Another important method which might be useful for process monitoring of cell viability is based in the measurement of electrooptical responses of complex polyelectrolyte solutions. The frequency-dependent dielectric properties of polyelectrolytes and colloids suspensions are difficult to describe in accurate manner, since the mobility of charged species, the particle's morphology and the surrounding interface highly and complexly influence the measurements. Cell suspensions (i.e. as well as other important suspensions of biological material such as proteins, tissues or nucleic acids) are heterogenous systems, with important differences in conductivity (σ) and permittivity (ϵ) between the suspension media and the inner part of the cells, due to ionic concentrations. The different ionic concentrations are the responsible for the membrane potential (see **section 3.2.2**), but the charges distribution and ion transport mechanisms also contribute to the

total measured dielectric properties. However, this difference in the dielectric constants causes different polarization mechanisms under the influence of external electrical fields [36] applied at different thresholds or frequencies.

According to [37], the three principal dielectric responses of interest are:

- α -dispersion: which is mainly due to the ionic character of the constituents, the cytoplasm and the suspension medium, accounting for the polarization of the ionic atmosphere around the cell surface, probably due to surface conductivity (at very low frequencies) and characterized for minimal conductivities values;
- β -dispersion: which results from the mismatch of the electric properties at the cell-medium interface (i.e. Maxwell-Wagner effect), where the system is governed by permittivity values;
- γ -dispersion: generally found at higher frequencies than the radio-spectrum (> 1 GHz) and takes into account the polarization of water molecules.

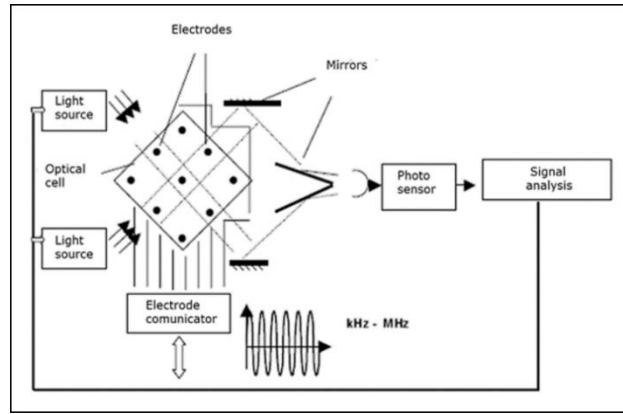


Figure 3.6. Schematic representation of the measuring cell for polarizability anisotropy measurements (modified from [38]).

Bacterial cells can be considered ellipsoidal particles, whose cytoplasmic membrane exhibit polarizability anisotropy when an electric field (EF) of a certain frequency is applied in the normal and tangential direction due to the charge differences in its structure. The EF is applied at low and/or medium frequencies (i.e. in the radiofrequencies spectrum) and it causes a rotational momentum on cells, which promotes an orientation effect and can be used for the calculation of the tensor of polarizability $\alpha_{ijk}(\omega)$. Considering the assumption of axially symmetrical single-shell ellipsoidal cells, it follows that $\alpha_{\perp j} = \alpha_{\perp k} = \alpha_{\perp}$, hence the polarizability anisotropy can be simplified to $\Delta\alpha(\omega) = \alpha_{\parallel}(\omega) - \alpha_{\perp}(\omega)$ [39].

Different studies have sought to use the measurements of FDPA as indicator for cell viability. Asami et al. [40] early studied the applicability of such models to study the properties of a pure culture of *E. coli*, while [41] developed a realistic model for the properties of red blood cells suspensions, of about $7.8 \mu\text{m}$ length and 8 nm thickness of cell membrane. Junne et al. [39] used an automatic sampling systems, which included a measuring chamber similar to the represented in **Figure 3.6** to monitor the physiological status of aerobic *E. Coli* cultivations. As shown in

Figure 3.6, an optical cell was placed in an electrooptical arrangement, where the EFs were applied in orthogonal directions, and the signals were captured by photosensors and converted into relative units of FDPA. The use of automatic-sampling during cultivation allowed high-throughput data to be obtained and the differentiation among four metabolic phases during the growth of batch *E. coli* cultures based on the dynamic behaviour of the FDPA, which also served to estimate cell length based on the relaxation time that took the biological phase to return to the non-polarized or relaxed state. Recently, different studies have tried to test the applicability of FDPA to monitor physiological status and cell viability of mixed cultures. Habermann et al. [38] measured the FDPA of different AD systems using corn silage as feedstock and observed a decreased of polarizability in the systems which suffered an intentional acidification, suggesting that the viability and/or vitality of fermentations broths and sewage sludges can be monitor through FDPA measurements.

3.3 Materials and methods

3.3.1 Experimental set-up of the DF system

Fermentation tests were conducted using two EloFerm bioreactors (EloSystems, Berlin, Germany) with a total volume of 1 L and a working volume of 0.4 L. Both bioreactors operated in parallel under anaerobic conditions achieved by flushing N₂ for 10 minutes into the liquid phase; the working temperature was in the mesophilic range (35 °C) and magnetic stirrers were used for the tests at 200 rpm. Due to the settings of the tests, the first fermenter (A) had a fixed pH set-point of 6.0, controlled with an integrated control loop in the EloFerm system using a 30 % (w/w) NaOH solution, while in the second bioreactor (B), the pH remained uncontrolled throughout the course of fermentation, which lasted c. 42 hours.

3.3.2 Preparation of the Hydrogen Producing Bacteria (HFB) inoculum

Since the test were concerned the production of biohydrogen through Dark Fermentation, the inoculum consisted of a microbial consortium enriched in spore-forming Hydrogen Producing Bacteria (HPB), prepared using a 100 ml sample of AD sludge from an on-going digester and treated at pH 3.0 with 1 M HCL solution at 35 °C, to inhibit the growth of methanogens as reported in [3]. The treatment was applied in anaerobic conditions for 24 h in a Multitron II incubation chamber (Infors HT, Bottmingen, Switzerland).

3.3.3 Feedstock and pre-treatment

The selected feedstock for these tests consisted in a mixture of agricultural waste; a co-digestion of corn and grass silage (see **Figure 3.7**), mixed in a proportion of 9:1 (w/w), whose characterization is presented in **Table 3.1**. The fresh feedstock was first diluted with tap water in a ratio 4:11 w/w and the particle size was decreased using a laboratory batch mill (IKA-10 Werke, Staufen, Germany), in order to facilitate mixing and sampling during the fermentation process. The prepared feedstock solution was treated with a 30 % w/w NaOH solution, to reach a pH=12 and incubated at 35 °C (Infors HT, Bottmingen, Switzerland) for a period of 24 h. At the beginning of the DF tests, the Dry Matter (DM) concentration of the system was around 90.05 ± 2.30 g/L.



Figure 3.7 Agricultural waste used as substrate: corn silage (left) and grass silage (right).

Table 3.1 Fresh feedstock characterization

	Corn Silage [g/kg FM]	Grass Silage [g/kg FM]
<i>Dry Matter (DM)</i>	371.0	491.0
<i>Organic Matter (OM)</i>	356.9	443.4
<i>Moisture</i>	629.0	509.0
<i>Total Ash</i>	14.1	47.6
<i>Crude Protein (CP)</i>	23.4	82.0
<i>Crude Fiber</i>	76.4	118.3
<i>Carbohydrates</i>	123.9	-
<i>Crude Fats</i>	10.4	15.7
<i>ELOS</i>	252.3	317.2
<i>ADF</i>	89.4	143.9
<i>NDF</i>	154.0	232.7
<i>NFC</i>	169.2	112.9
<i>Avail. CP</i>	46.7	66.3
<i>Ammonia</i>	0.6	1.8
<i>NH₃-N of Total N [%]</i>	12.6	11.5
<i>pH</i>	3.9	4.5
<i>BGP [m³ biogas/t_{FM}]</i>	234.8	286.1
<i>BMP [m³ CH₄/t_{FM}]</i>	123.3	150.2

FM, fresh matter; **DM**, dry matter; **OM**, organic matter; **CP**, crude protein; **ELOS**, enzymatic soluble organic matter; **ADF**, acid-detergent fiber; **NDF**, neutral detergent fiber; **NFC**, non-fibrous carbohydrates; **BGP**, biogas potential; **BMP**, biomethane potential.

3.3.4 Analytical Measurements

3.3.4.1 Gas Analysis

The qualitative analysis of the produced gases was performed, after the gas output was dried in a silica-gel bed, using an *ad-hoc* built array consisting in three in-series connected gas sensors (BlueSens, Herten, Germany), BPC-CO₂ and BPC-CH₄ (i.e. which take advantage of Infrared beam weakening as measuring principle for CO₂ and CH₄), and one BPC-H₂, which uses the difference in thermal conductivity (compared to air), to estimate the percentage of H₂ (see **Figure 3.8**).

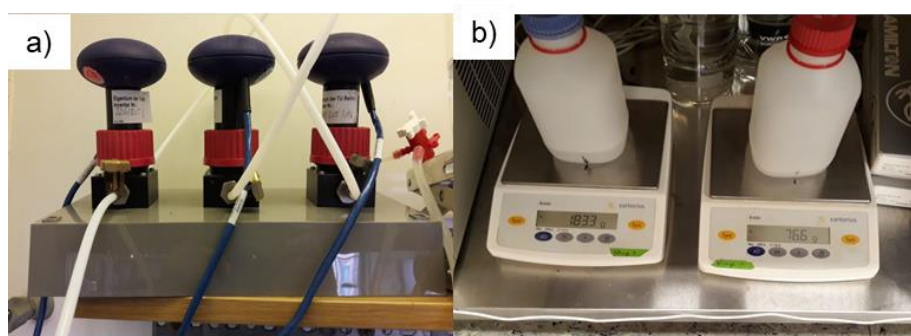


Figure 3.8 Photograph of Gas Analysis system: **a)** the gas measuring array, from left to right CO₂, CH₄ and H₂ sensors and **b)** collector bottles on analytical balances for the quantification of the gas flow.

The total flow and the flow rate were estimated using the acidic water (pH = 3) displacement method, connecting the output of the gas measurement array to a gas-meter flask and then to a collector bottle placed on an analytical balance (**Figure 3.8b**).

3.3.4.2 Liquid products - Volatile Fatty Acids (VFA) and solvents

Liquid samples were taken from both systems at different time points during the course of fermentation. Samples were filtered first with 125 μm nylon filters (Carl Roth GmbH, Karlsruhe, Germany) to remove large particles and then with 0.45 μm filters and diluted (1:1) with ultra-deionized water (i.e. resistivity > 18 $\text{M}\Omega\cdot\text{m}$ and conductivity < 0.055 $\mu\text{S}/\text{cm}$) provided by an Easypure II RF device (Barnstead, Iowa, USA). Aliquots of 200 μL were taken and poured into close vials for the HPLC (High-Performance Liquid Chromatography) measurements. The device, a 1200-series HPLC (Agilent Technologies, Waldbronn, Germany), is equipped with a Refractive Index Detector (RID) and a 300x7.7mm, 8 μm HyperRezTM XP Carbohydrate H⁺ column (Fisher Scientific, Schwerte, Germany) and it was operated at a temperature of 65 °C. The selected mobile phase for this type of tests was a 5 mM H₂SO₄ isocratic solution, at a flow rate of 0.6 mL/min for a cycle time of 50 min. Prior to the analysis, for the purpose of identification of VFA and solvents, a calibration was performed, which included formate, acetate,

propionate, butyrate, ethanol, propanol and butanol in an adequate range for DF tests of 0 to 4 g/L.

3.3.4.3 Flow cytometry (FC) analysis

Samples taken from both bioreactors, at different time points, were initially filtered with 125 µm nylon filters (Carl Roth GmbH, Karlsruhe, Germany) in order to remove large debris and inert particles and subsequently filtered under vacuum using 0.2 µm filters, which were previously wetted with a Phosphate-Buffered Saline (PBS) solution (136.9 mM NaCl, 2.7 mM KCl, 8.1 mM Na₂HPO₄·2H₂O and 1.8 mM KH₂PO₄, pH = 7.2). Each sample was washed with 5 rinsing cycles of 1 mL PBS buffer. The retained cells on the filter paper were re-suspended in 10 mL PBS by vortexing and the cell concentration was adjusted to about $1 \cdot 10^6$ cells/mL prior to the staining step. BOX, also called DiBAC₄(3) or bis-(1,3-dibutylbarbituric acid) trimethine oxonol, was used as labelling dye for 200 µL samples using BOX concentrations of 0.5 µg/mL together with dissolved EDTA (~ 29.75 µg/mL), at room temperature (20 °C) for 4 minutes to assess the number of depolarized cells and the state of membrane potential. Additionally, positive controls for BOX were prepared by applying a thermal treatment (80 °C) to the sample for 1 hour and subsequent staining with BOX using the same conditions. Samples were analysed by means of a MACSQuant Analyzer (Milteny Biotech, Bergisch-Gladbach, Germany) equipped with three lasers (violet 405 nm, blue 488 nm and red 635 nm), two scatter detectors (FSC, SSC), and eight fluorescent channels equipped with multiple filters.

3.3.4.4 AP evaluation by FDPA measurements

Samples taken from both bioreactors, at different time points, were initially filtered with 125 µm nylon filters (Carl Roth GmbH, Karlsruhe, Germany) in order to remove large debris and inert particles. Subsequently, an aliquot of 10 mL of the filtrate was centrifuged at 4 °C and 600 rpm for 5 minutes. The supernatant was diluted with distilled water to adjust the initial electrical conductivity to an adequate range compatible with AP measurements (approx. 1:10 v/v). AP measurements were conducted *atline*, using an EloTrace device (EloSystems, Berlin, Germany). The AP-levels of each sample were acquired at four different frequencies: 210, 400, 900 and 2100 kHz, based on the type of broth under analysis and previous exploratory tests. Mean values are presented together with the standard deviation of the triplicates measured for each sample. AP values are displayed using arbitrary units of the equipment, scaled by a factor of $5 \cdot 10^{-31}$ F·m² (i.e. farad square meters), for easier representation and comparison with literature values.

3.4 Results and discussion

3.4.1 Course of fermentation and metabolic products

Dark fermentations tests were performed following the procedure as described above: one bioreactor with (A) and one without pH control (B). First of all, the acid-treatment applied to the AD sludge proved to be effective, since no methane production was observed throughout the fermentation tests. The pH development in both experiments is presented in **Figure 3.9**, where the three different sampling points are depicted in Roman numerals. Firstly, a short lag phase of adaptation to the environmental conditions (first 3 hours), with reproducible pH evolution of both fermentations, can be observed. During the first hours (around 8-9 h after the cultivation started), pH shortly dropped below the set-point and therefore few drops of sodium hydroxide were dosed in the system A. However, the natural adaptation of the mixed culture to this type of substrate promotes a relative stable pH during the first hours, probably due to the poor degradability of the substrate. Then, a growth phase of about 13-14 h, which mainly produced organic acids that significantly reduced the pH value, along with gas production ($H_2 + CO_2$) for both bioreactors, can be seen. An important share of hydrogen is produced by fermentative microorganisms (e.g. *Enterobacteriaceae*, *Clostridia*, among others) during the decarboxylation of pyruvate into acetyl-CoA, a common step in metabolic pathways producing acetic acid, butyric acid and ethanol, which are some of the identified products during DF. Finally, cells entered the stationary phase (after 33-34 h), and thus the evolution of gas ceased, in parallel with the production of VFA.

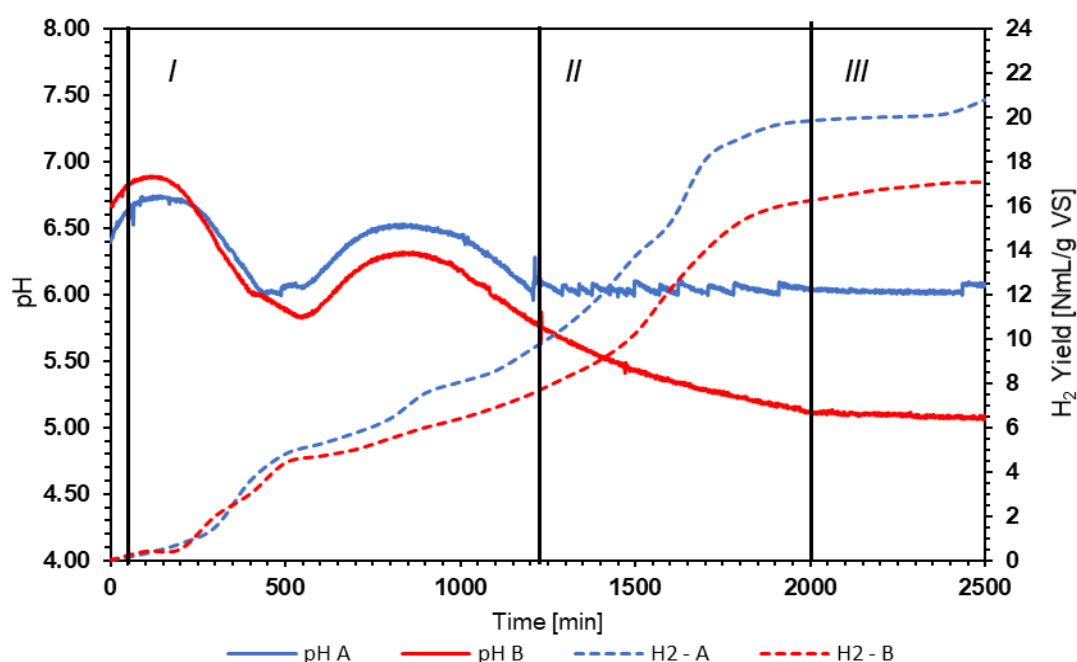


Figure 3.9 Behaviour of pH and hydrogen yield throughout a dark fermentation with (A) and without (B) pH control (roman numerals stand for sampling points during the experiments).

The VFA analysis during both dark fermentations (**Figure 3.10**) revealed important differences and titres variations over time between the system without pH control (B) and the one with pH control (A). For both systems, the butyric-fermentation dominated, but the pH-controlled reactor produced a higher amount of acetic acid and ethanol towards the end of the fermentation, while the production of these two compounds in the non-pH regulated system was rather modest throughout the fermentation. Formic and propionic acid concentrations, in both systems, did not notably change during the experiments.

Moreover, gas production reached 20.80 ± 0.05 and 17.08 ± 0.05 NmL H_2 /gV_{Sadded} at the end of fermentation tests (see **Figure 3.9**), with mean hydrogen concentrations of 28.3 ± 0.5 and 26.0 ± 0.8 % for the system A and B, respectively; these values are also in agreement with literature values for this type of substrate. The composition of the produced biogas can be considered rather similar for both systems (i.e. increased c. 8.8 % for the pH regulated system) while the H_2 yield, as shown in **Figure 3.9**, for the pH-regulated system (A) increased around 21.8 % compared to B. Since the composition of the substrate is equal for both systems, the H_2 fraction in the produced gas seems to be related to the elemental composition of the substrate, while the yield, in the time window of the experimental fermentation tests, exhibited a greater variation probably due to the different operative conditions (pH in this case).

Although it is generally believed that low pH values can trigger the shift from acidogenesis to solventogenesis, in our experiment solvents such as acetone or butanol were not found during the HPL-chromatographic analysis, however the final pH for the non-controlled system reached values close to 5, which is still a relative high value for solventogenesis [42].

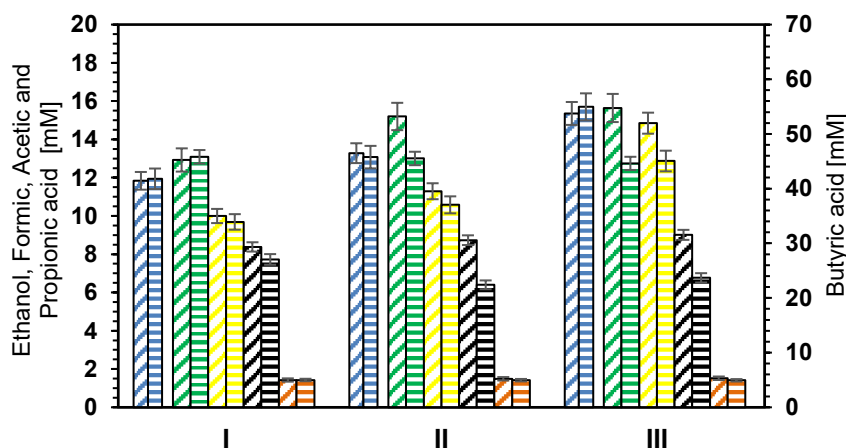


Figure 3.10 Ethanol (green), formic (black), acetic (yellow), propionic (orange) and butyric (blue) acid concentrations throughout dark fermentation with (A, diagonal filled bars) and without (B, horizontal filled bars) pH control. Roman numerals stand for sampling points during the experiments.

As noted by [43], the production of carboxylic acids and solvents represents approximately 65 % weight based of the consumed organic matter, while H_2 represents around 3 % and CO_2 and biomass amounts around 35 %, hence liquid metabolites constitute the largest fraction of the converted substrate.

3.4.2 Anisotropic Polarizability (AP) measurements

The results of electrooptical measurements of cell polarizability throughout both A and B fermentations can be observed in **Figure 3.11**. It should be noted that AP measurements are very sensitive to the presence of ions (see **section 3.2.4**). Typical fermentation broths in AD and DF exhibit high conductivities values (i.e. in the range 10-40 mS/cm), which is a parameter that is periodically monitored to avoid osmotic stresses on biomass. At medium and high frequencies, the electrical conductivity of the media could have an important effect on the anisotropy measurements. As stated in **section 3.3.4.4**, a washing step was first applied to adjust initial conductivity values. However, system A had a constant pH loop connected so that NaOH was frequently dosed in this bioreactor. This may be the explanation of a higher standard deviation of measurements from reactor A in contrast to reactor B, observed through both fermentations and across the four frequencies under analysis (**Figure 3.11**).

At the beginning of fermentation tests (point I), the AP measurements, particularly at low frequencies, were similar for both systems. In the second measuring point (II), bioreactor A showed a higher AP than system B, especially at low frequencies (i.e. 210 and 400 kHz), probably due to the fixed pH that guaranteed a constant environment for the mixed culture to grow and allows cells to maintain a constant membrane potential. These lower values of the AP for the non-controlled system (B) can be also correlated to the lower cumulative biohydrogen yields showed in **Figure 3.9**. In fact, a low intracellular pH has an important effect on the cell viability [44] as it reduces the *pmf* in different types of bacteria (see **section 3.2.2**). Hence, changes in extracellular or intracellular pH have a strong impact in transmembrane potential, mainly due to bacterial responses to the external stresses and the balance of both components of the *pmf*, which generates a noticeable change of the Maxwell-Wagner polarizability [45][46].

Additionally, the non-dissociated form of organic acids is favoured under acidic conditions (system B). In this case, cells use their energy mainly to counteract this stress to maintain homeostasis rather than for growth, which can also partly explain the lower hydrogen yields in the gas output and reduced titres found in the liquid broth. For the last point (III), where the stationary phase was achieved, AP values are also similar for both systems (A and B), with slightly higher values at lower frequencies for system B.

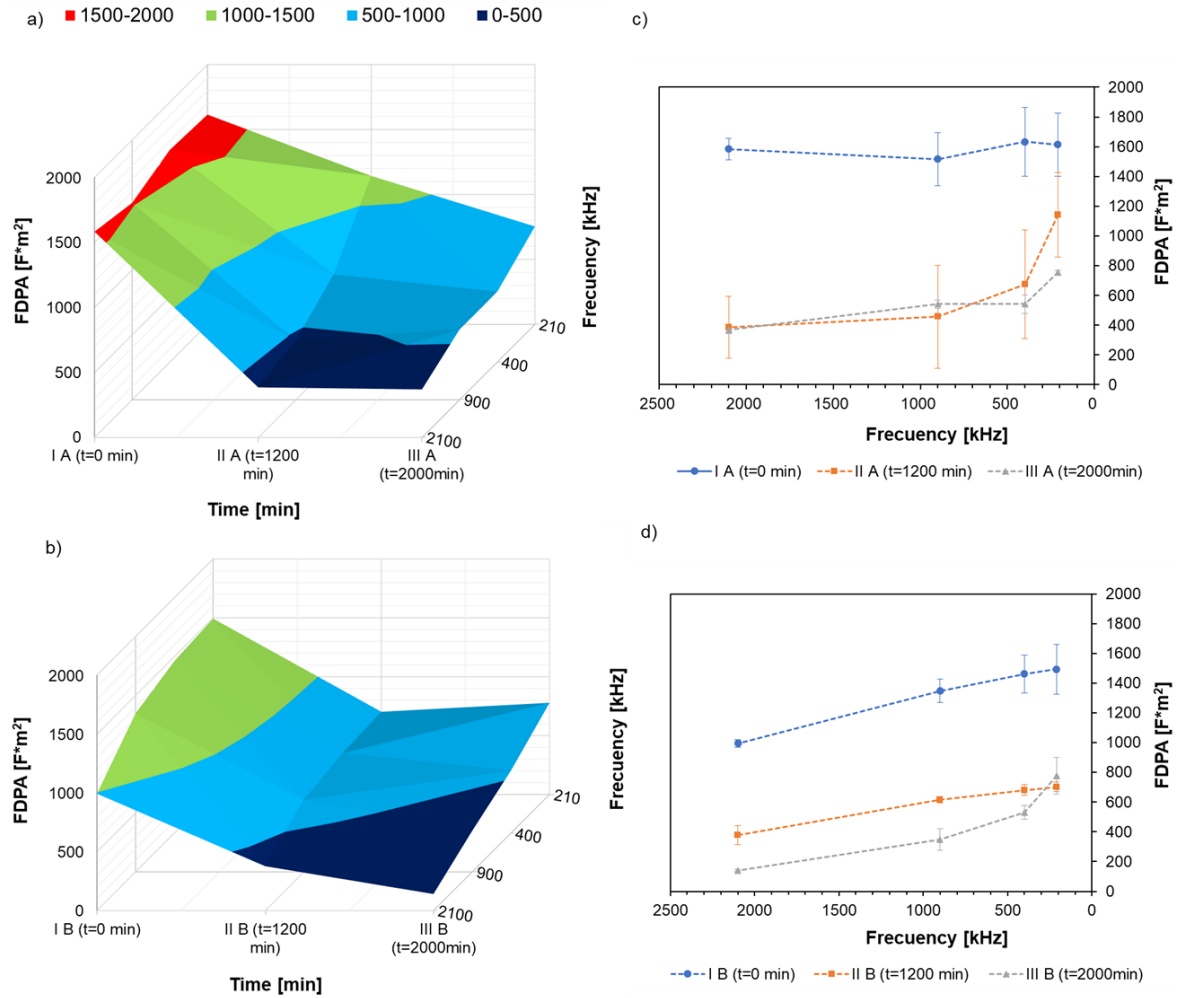


Figure 3.11 Results of the FDPA measurements 3D (a, b) and 2D (c, d) electrooptical measurements of cell polarizability at 200, 400, 900 and 2100 kHz of DF with (left plots) and without (right plots) pH control.

3.4.3 Flow cytometry (FC)

3.4.3.1 Populations Dynamics

For the FC analysis, samples were collected at the beginning of the fermentation to set the optimal detector sensitivities (by voltage adjustment) for each channel that allow the monitoring of cells during the process. First of all, measurements were conducted in triplicate for statistical significance. The Flow Cytometry protocol optimized for complex fermentations broths, as reported in **section 3.3.4.3**, provided robustness and reproducibility to the performed analysis (see **Figure 3.12**).

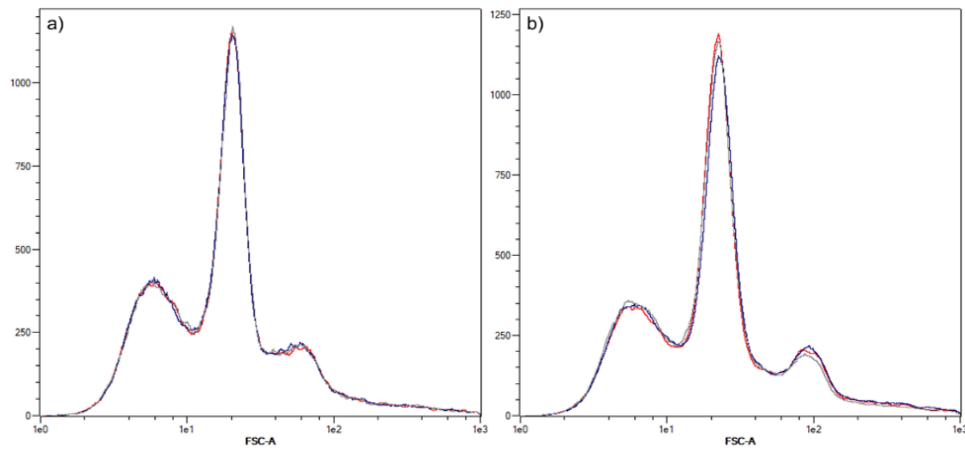


Figure 3.12 Histogram plots of the Forward Scatter Channel (triplicates), at time point I (the beginning of fermentation) for the system A and B, respectively (*events-based* chart).

Electrical pulses from the scattered light are converted to voltage and can be given as height (peak signal), width (length of the path through the laser) or as the cumulative scattered light (area-based); in the present study the latter was used for the analysis of the data. Each cell that passes through the interrogation chamber generates electrical pulses, due to the scattered light, and are registered as events in the corresponding channel. Data obtained from the cytometer can then be plotted using univariate or bivariate charts, using dot plots, density plot or histograms. Axes can be defined as linear or logarithmic to present data, in the present case three decades logarithmic resulted as the most suitable for the differentiation of subpopulation within samples.

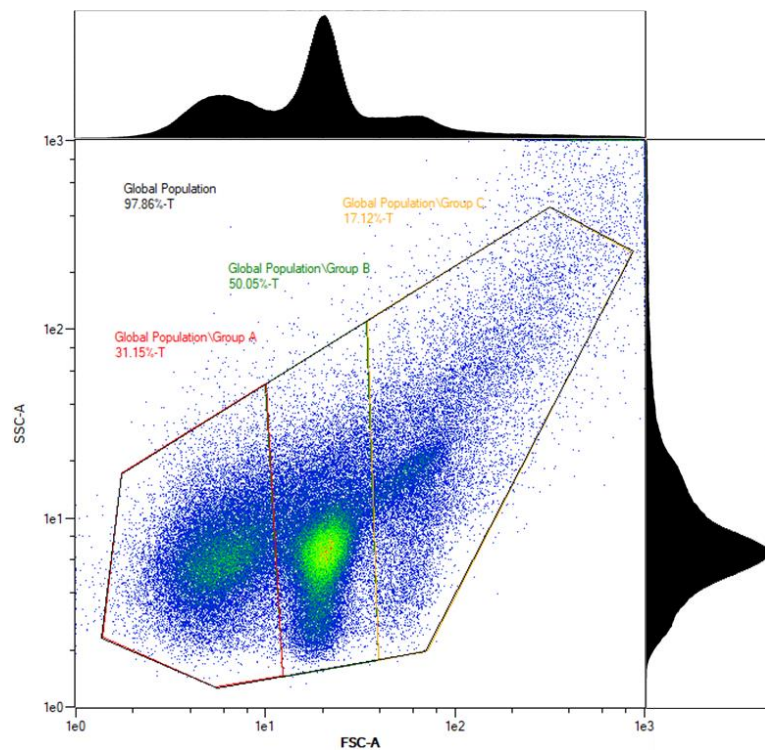


Figure 3.13 Combined plot of the bivariate FSC vs SSC signals (*events based*), along with histograms for each channel.

The histogram of the FSC channel, at the beginning of the tests, shows three differentiable subpopulations. Moreover, the triplicates of each sample showed good replicability, presenting very low values of relative error (below 3 % in each case). The comprehensive analysis of the population was performed using the density bivariate chart of the FSC vs SSC channels. The total number of events per measurement was around 10^6 and an adequate gating strategy was applied (i.e. named *global population*) to encompass more than 95 % of the collected events in each case, shown in **Figure 3.13**.

The gating procedure was applied to each sample for both bioreactors and tracked over time. Matching the data of the histograms and the density plots, three key sub-populations were identified (*Group A*, *Group B* and *Group C*). The relative abundance of each group was calculated for each system and time point.

Table 3.2 Relative abundance of each sub-population for both systems.

	Time [min]	Relative abundance [%]		
		Group A	Group B	Group C
System A (pH control)	0	31.73 ± 0.02	50.78 ± 0.14	17.50 ± 0.07
	1200	36.53 ± 0.15	45.98 ± 0.05	17.49 ± 0.07
	2000	55.50 ± 0.34	32.11 ± 0.21	12.38 ± 0.18
System B (no pH control)	0	28.07 ± 0.06	52.53 ± 0.98	19.40 ± 0.11
	1200	34.14 ± 0.11	44.79 ± 0.50	21.06 ± 0.16
	2000	54.05 ± 0.26	30.66 ± 0.19	15.29 ± 0.31

The three studied subpopulations showed a dynamic behaviour over time; the values are presented in **Table 3.2**. Interestingly, the microbial population in both bioreactors, for pH controlled and the non-controlled system exhibited similar trends for each of the tracked groups. That is, at the beginning of the fermentation, the relative abundance of *events* found in each gate was similar for both bioreactors and then *Group A* increased over time, while *Group B* and *Group C* decreased. Only *Group C* for the reactor without pH control slightly increased during the 0-1200 minutes interval and then decreased in the 1200 – 2000 minutes slot.

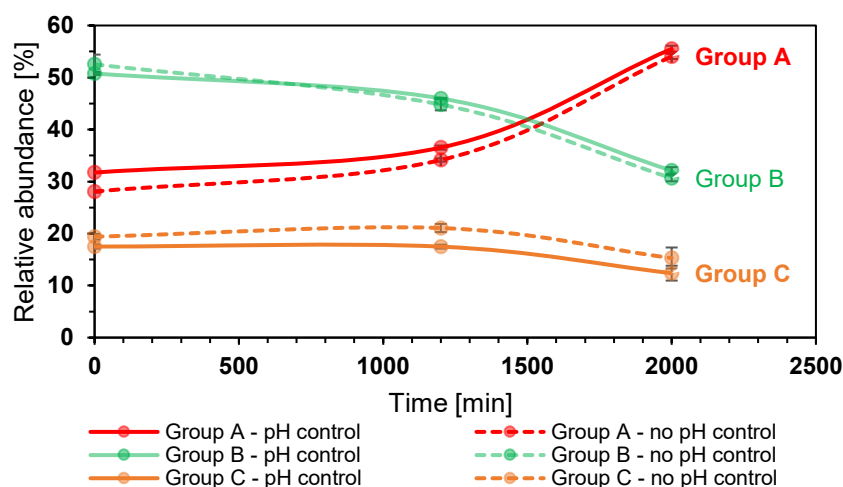


Figure 3.14 Evolution of the percentual relative abundance of each sub-population.

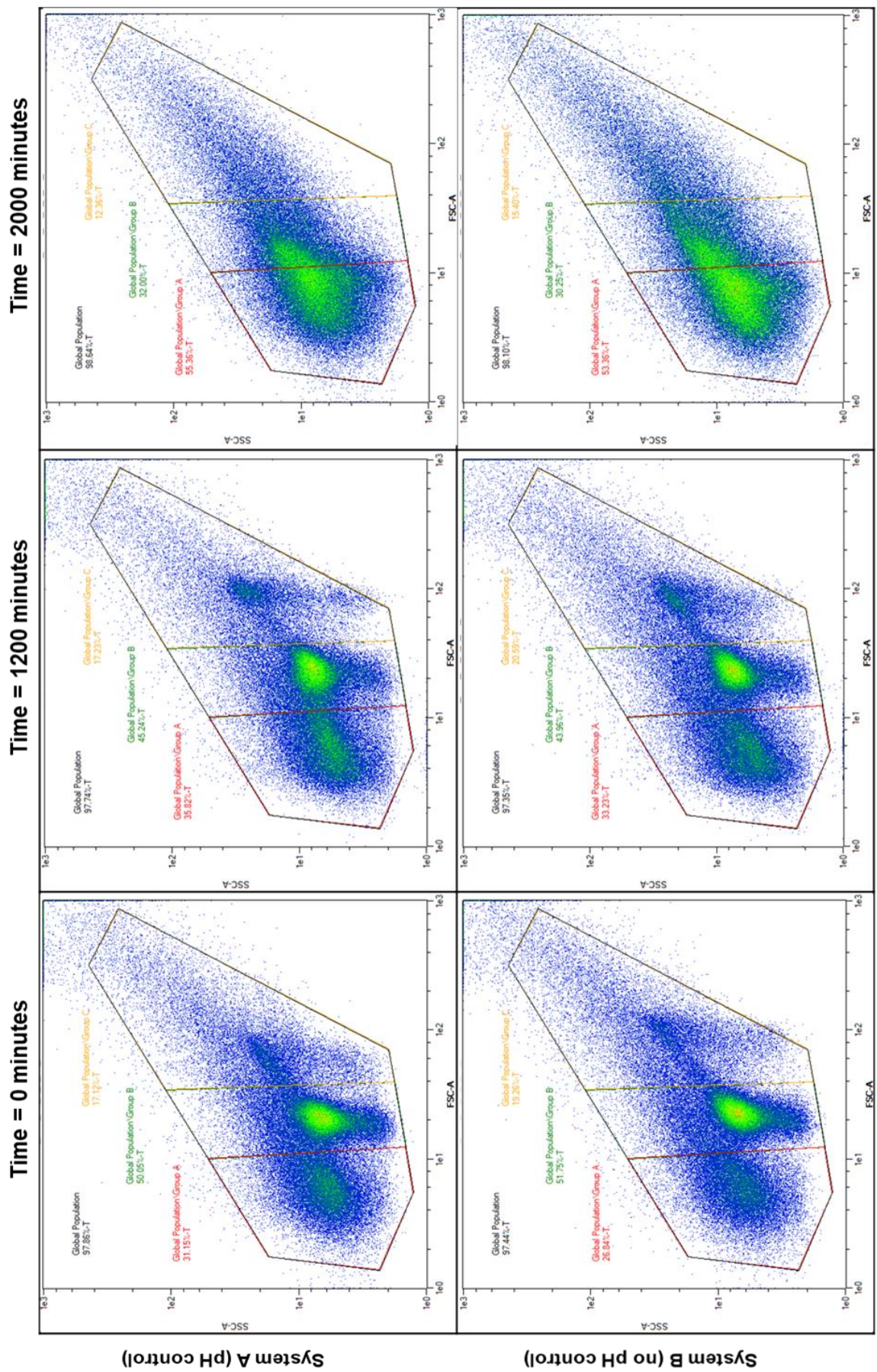


Figure 3.15 Bivariate (FSC vs SSC) density plots at different time points showing the evolution of sub-populations.

The evolution of the sub-populations can be seen in **Figure 3.14**, while FC fingerprints of the time points under analysis (I, II and III) for the system with (A) and without (B) pH control are presented in **Figure 3.15**.

The FSC vs SSC plots showed also that the microbiome was dominated by three key species at time point I ($t = 0$ min) as well as in the second sampling time II ($t = 1200$ min), while for III ($t = 2000$ min) no key dominating groups were observed, i.e. the density plot for FSC/SSC channels showed a heterogenous population with a high variation in relative cell size and granularity. When compared with the statistical data, Group A went from 31.73 % and 28.07 % to 55.50 % and 54.05 %, for system A and B respectively. These significant variations mean that at the end of fermentation this sub-population amount around half of the single-cells present in the culture broth.

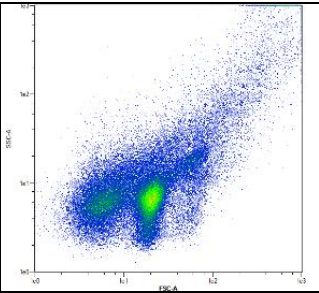
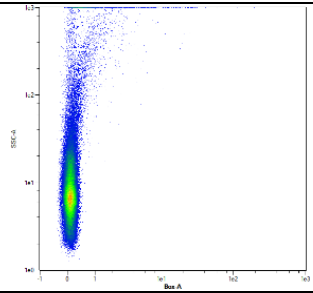
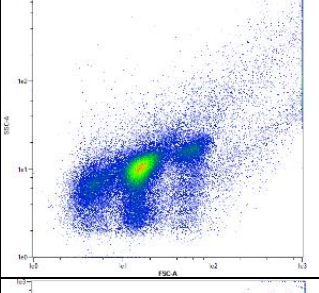
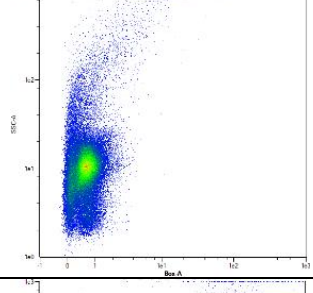
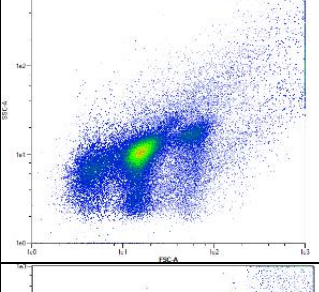
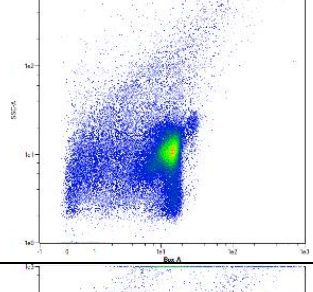
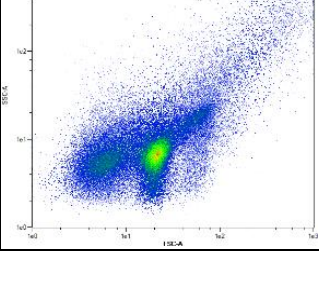
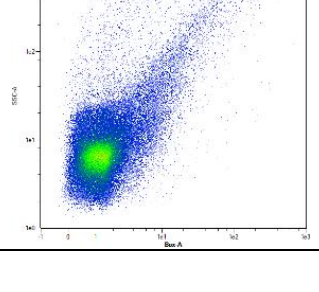
3.4.3.2 Depolarized cells – Box Staining

In this phase, DiBAC₄(3) or BOX fluorescent staining agent was used to calculate the percentage of depolarized cells. In order to establish a baseline in the experiments, which served as an internal standard, positive and negative controls were performed on the samples. It consisted in a thermal treatment at 80 °C for 1 hour to simulate a perturbation in the membrane potential, mainly by means of the depolarization of the membrane. This can be detected using BOX staining and the BOX-A channel (i.e. excitation at 488 nm and emission maximum at 525 nm). The comparison between the controls and the samples can be seen in **Table 3.3**.

It shows the cytometric fingerprint of the FSC vs SSC channels to ensure that the composition of the population remained constant and also presents the bivariate plot of the signals BOX vs SSC. The response in the FSC vs SSC plots are similar in all cases, while the channel BOX offers a trend that allows to discriminate between samples.

The comparison between the non-treated and unstained sample and the positive control suggests that the SSC/BOX FC fingerprint could be used as an indicator of *vitality* within mixed consortia of microorganisms, as it reflects comprehensively the state of the membrane potential. BOX is a hydrophobic, negatively charged dye, which is used to investigate the membrane status of microbial cells; the addition of EDTA (see **section 3.2.4.3**) increases the range of action of the dye, since it facilitates the uptake of the dye through the outer membrane. This is especially useful for gram-negative bacteria, which in turn provides more reliable data about the whole bacterial mixed culture used for this study (i.e. composed by different fermentative bacteria, either gram-positive or -negative) [46]. In conditions of hyperpolarization or normal polarization of the cells, BOX is excluded from cells. On the other hand, when changes in the membrane potential occur, towards positive values, it enters the depolarized cells; however, no further information can be provided to assess whether the cellular damage (depolarization) is reversible or irreversible.

Table 3.3 Settings for the BOX dye on treated, non-treated and control samples.

Description	FSC vs SSC	BOX vs SSC
<ul style="list-style-type: none"> Unstained Sample as acquired (untreated) 		
<ul style="list-style-type: none"> Unstained Positive Control (treated sample) 		
<ul style="list-style-type: none"> Stained (with BOX) Positive Control (treated sample) 		
<ul style="list-style-type: none"> Stained (with BOX) Sample as acquired (untreated) 		

Another important feature of the flow cytometric analysis, besides gating, is the creation of regions that also allow the classification of the different populations and subpopulations. In order to quantify the number of depolarized cells, a region was established based on the information given by the signal intensity response of the fluorescent channel, i.e. where the BOX fluorochrome information is collected. An example is shown in **Figure 3.16**; on the left, the response of a stained sample (for the system A, at the beginning of the fermentation) and that of the stained positive control (same sample which underwent the thermal treatment) is presented. The results for samples A and B at different time points are shown in **Figure 3.17**.

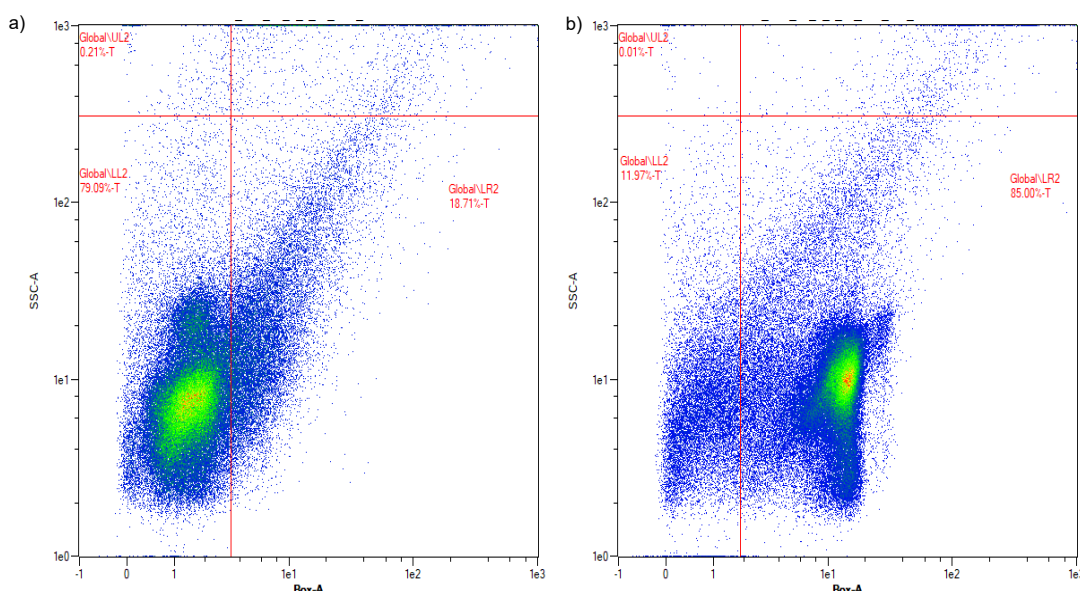


Figure 3.16 Regions of polarized and depolarized cells discriminated using the SSC vs BOX plots in FC: a) polarized cells and b) depolarized cells according to the set trigger

Box has been proved to be useful discriminating damaged (depolarized) cells, through its accumulation mechanism from the extracellular medium and the increase of the quantum yield upon binding to key intracellular structures in plants cells [47], bacteria and archaea [48] and even in the community members of the human gut microbiota [49]. The stained untreated sample (see **Figure 3.16**) yielded a percentage of depolarized cells close to 18.71%, while in the positive control (thermally treated control) it was around 85.00% (time point I, system A). This same discrimination by regions was applied to all the time points for both systems under study, using the triplicates results for each sample.

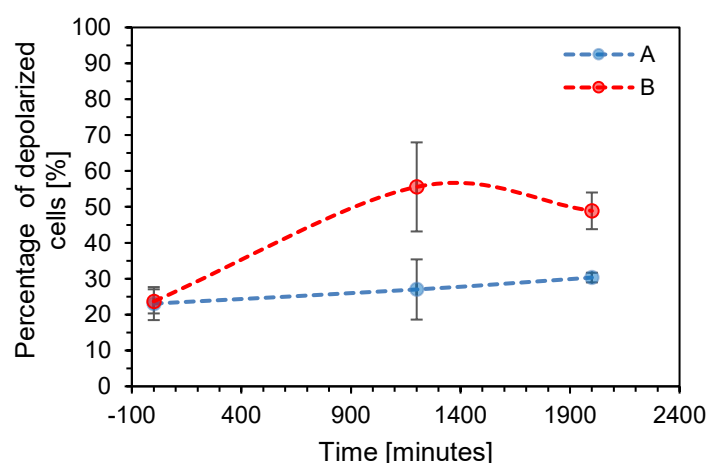


Figure 3.17 Fraction of depolarized cells for each system at different time points, calculated using the BOX probe in FC analysis.

In this respect, the percentage of depolarised cells quantified through triplicates FC measurements (see **Figure 3.17**) resulted in 23.06 ± 4.60 and 23.68 ± 3.36 % for

A and B, respectively, at the beginning of the tests (time point I). These values represent the percentage of BOX-stained cells, which is very similar for both bioreactors at the beginning of the dark fermentation tests. For the time point II, the system with uncontrolled pH (B), exhibited a greater number of depolarised cells around 55.57 ± 12.41 , while system A had a percentage around 26.99 ± 8.39 . The final state of each system (i.e. timepoint III) resulted in a slight increment of depolarised cells for A (30.31 ± 1.34), while for B a modest decrement of depolarised cells (48.9 ± 5.11) was found.

3.4.3.3 Correlation between FC and FDPA

Although the two techniques presented in this chapter, for the monitoring of cell viability are based on different physical measurement principles, a correlation between the methods can be established. The measurements of FDPA are based on the ionic properties of the microorganism's suspensions and the obtained values are relative for each system under analysis.

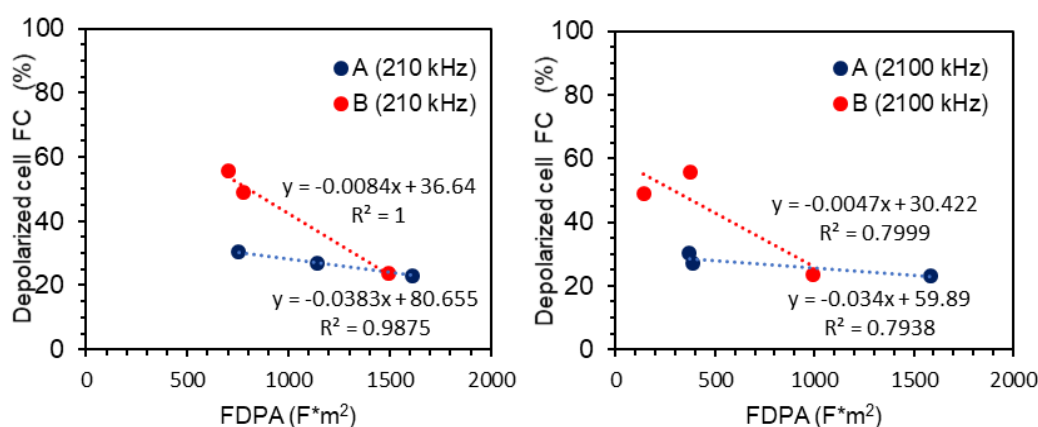


Figure 3.18 Correlation of FDPA measurements vs % of BOX stained cells.

Moreover, the variations of the AP values offer, as mentioned above, valuable information about the physiological state, and presumable also indirectly on the *pmf* for the case of bacteria. Hence, it could be said that the FDPA values are a combined signal reflecting the energetic state and the state of transport mechanisms, while BOX measurements in FC is an ON/OFF indicator of the membrane potential ($\Delta\Psi$) that indicates the fraction of polarized/depolarized cells, without further considerations. In the present study, acceptable correlation coefficients were found between the obtained variations in the FDPA and the percentage of depolarized cells calculated using FC; the calculated values of R^2 at the lowest frequency (210 kHz) amounted 0.9875 and 1.000 for system A and B, as reported in **Figure 3.18a**, while at the highest tested frequency (2100 kHz) lay around 0.7938 and 0.7999, respectively (**Figure 3.18b**). These high correlation values can also be observed by comparing **Figure 3.11** and **Figure 3.17**. The AP values (**Figure 3.11**) at 210 kHz for system A showed an almost linear decrease over time, while AP values of

system B had a minimum at time point II. These trends in AP measurements are similar to the trends obtained in the percentage of depolarized cells in FC measurements (**Figure 3.17**); for system A, the percentage of depolarized cells increases continuously over time (although modestly), while for system B there is a maximum in the number of depolarized cells for time point II. Moreover, the cumulative specific hydrogen evolution for each system (see **Figure 3.9**) is also in agreement with the resulting trends of AP and FC measurements; at time point I, the yield was similar for both systems, while for II, the system B only achieved a 77 % of the yield of system A (i.e. the most critical condition as shown in AP and FC), and for the condition III (i.e. the final state), B achieved 82 % of the yield obtained in A. Finally, it should be taken into consideration that the *probe parameter* for these tests was the pH influence, which might present similar effects on both techniques, therefore yielding fair correlation coefficients; while for other stress conditions, the information independently provided by each measurement can be rather supplementary.

3.5 Conclusions

The development of biorefineries is a growing need of our modern society. In this respect, some of the classical biotechnological processes, such as Anaerobic Digestion or Dark Fermentation, play an important role since these are the most consolidated technologies of this type of processes. As presented at the beginning of this chapter, both have great potential to be integrated into process configurations that include better use of resources and the reuse of organic feedstocks, closing the circle that is vital for sustainable modern economies. The case of DF is of great interest because it offers a great potential for process integration, with recovery of bioenergy both in gaseous form (biohydrogen), as well as a liquid metabolites pool of fuels and/or chemicals of high valorisation potential.

DF, on the other hand, is based on the use of unspecified microbiomes, whose operation tends to be acceptable but without complex biological controls. In this respect, the use of electro-optical techniques for biological systems offers the possibility of monitoring the physiological state of the biotic phase through indirect measurements, using high-throughput techniques such as Flow Cytometry (i.e. based on light scattering properties), whose versatility and different combinations with fluorescent dyes provide information not only about the morphology of the involved microbial groups, but also about the reversible and/or irreversible stress conditions whose impact can be seen in changes of membrane potential, the integrity of the cellular membrane, the presence of nucleic acids and the existence of metabolic activity and its relative changes. On the other hand, at-line measurements of the tensor of polarizability of the biotic phase (i.e. based on the differences in the refractive index) as a frequency-dependant property, particularly in the range 210-400 kHz, provided information concerning the complex response of electric properties, whose changes can also be related to the physiological state of mixed cultures through the membrane potential. These techniques are candidated

for the monitoring of the activity of the biotic phase, and the cross-correlation among them, which has been established in this chapter, can help to improve the current knowledge. The lack of information about the physiological state in complex microbiome often leads to substrate and/or product inhibitions, undesired population shifts, low metabolic activity (i.e. suboptimal product yields) among other factors that ultimately reduce the performance of the process. These factors can induce both reversible and irreversible damage to the biotic phase; monitoring the process through adequate tools following the *Quality by Design* paradigm could facilitate the tasks in biorefineries providing information about the state of mixed cultures and serve to determine better integration approaches with other process units. The present study used pH influence on the microbiome as *probe parameter*, which was useful to understand the behaviour of the DF system using as carbon sources agricultural waste. The applied approach for DF seems to be an adequate indicator for mixed cultures, since quantitative analyses in term of relative abundance of microorganism groups could be performed encompassing the wide range of microorganisms that are present in the mixed consortia. However, more research is needed to assess the potential of these techniques to be used in continuous and large-scale processes and the development of control strategies for the DF and other relevant biorefineries processes.

References

- [1] NOVA Institut, “Biorefineries in Europe 2017,” Hürth, 2017.
- [2] A. S. Rathore, V. R. Chopda, and J. Gomes, “Knowledge management in a waste based biorefinery in the QbD paradigm,” *Bioresour. Technol.*, vol. 215, pp. 63–75, 2016.
- [3] B. Ruggeri, T. Tommasi, and S. Sanfilippo, *BioH₂ & BioCH₄ Through Anaerobic Digestion: From Research to Full-scale Applications*. Springer London, 2015.
- [4] A. Wang *et al.*, “Integrated hydrogen production process from cellulose by combining dark fermentation, microbial fuel cells, and a microbial electrolysis cell,” *Bioresour. Technol.*, vol. 102, pp. 4137–4143, 2010.
- [5] V. Turon, E. Trably, E. Fouilland, and J.-P. Steyer, “Growth of *Chlorella sorokiniana* on a mixture of volatile fatty acids: The effects of light and temperature,” *Bioresour. Technol.*, vol. 198, pp. 852–860, 2015.
- [6] I. Valdez-Vazquez and A. Sanchez, “Proposal for biorefineries based on mixed cultures for lignocellulosic biofuel production: a techno-economic analysis,” *Biofuels, Bioprod. Biorefining*, vol. 12, no. 1, pp. 56–67, 2018.
- [7] A. Xia *et al.*, “Improvement of the energy conversion efficiency of *Chlorella pyrenoidosa* biomass by a three-stage process comprising dark fermentation, photofermentation, and methanogenesis,” *Bioresour. Technol.*, vol. 146, pp. 436–443, 2013.
- [8] A. Schievano *et al.*, “Dark fermentation, anaerobic digestion and microbial fuel cells: An integrated system to valorize swine manure and rice bran,” *Waste Manag.*, vol. 56, pp. 519–529, 2016.
- [9] P. Majidian, M. Tabatabaei, M. Zeinolabedini, M. P. Naghshbandi, and Y. Chisti, “Metabolic engineering of microorganisms for biofuel production,” *Renew. Sustain. Energy Rev.*, vol. 82, pp. 3863–3885, 2018.
- [10] F. Liew, A. M. Henstra, M. Köpke, K. Winzer, S. D. Simpson, and N. P. Minton, “Metabolic engineering of *Clostridium autoethanogenum* for selective alcohol production,” *Metab. Eng.*, vol. 40, pp. 104–114, 2017.
- [11] N. A. Bokulich, Z. T. Lewis, K. Boundy-Mills, and D. A. Mills, “A new perspective on microbial landscapes within food production,” *Curr. Opin. Biotechnol.*, vol. 37, pp. 182–189, 2016.
- [12] J. Bader, E. Mast-Gerlach, M. K. Popović, R. Bajpai, and U. Stahl, “Relevance of microbial coculture fermentations in biotechnology,” *J. Appl. Microbiol.*, vol. 109, no. 2, pp. 371–387, 2010.
- [13] C. S. S. Oliveira, C. E. Silva, G. Carvalho, and M. A. Reis, “Strategies for efficiently selecting PHA producing mixed microbial cultures using complex feedstocks: Feast and famine regime and uncoupled carbon and nitrogen availabilities,” *N. Biotechnol.*, vol. 37, pp. 69–79, 2017.
- [14] J. Lambrecht, N. Cichocki, T. Hübschmann, C. Koch, H. Harms, and S. Müller, “Flow cytometric quantification, sorting and sequencing of methanogenic archaea based on F420 autofluorescence,” *Microb. Cell Fact.*, vol. 16, no. 1, pp. 1–15, 2017.
- [15] J. Ben-Iwo, V. Manovic, and P. Longhurst, “Biomass resources and biofuels potential for the production of transportation fuels in Nigeria,” *Renew. Sustain. Energy Rev.*, vol. 63, pp. 172–192, 2016.
- [16] K. Dutta, A. Daverey, and J. G. Lin, “Evolution retrospective for alternative fuels: First to fourth generation,” *Renew. Energy*, vol. 69, pp. 114–122, 2014.
- [17] G. Jungmeier, H. Jørgensen, E. de Jong, H. Stichnothe, and M. Wellisch,

- “IEA - The Biorefinery Complexity Index,” 2014.
- [18] M. D. Argyle and C. H. Bartholomew, “Heterogeneous Catalyst Deactivation and Regeneration: A Review,” *Catalysts*, vol. 5, pp. 145–269, 2015.
 - [19] P. Forzatti and L. Lietti, “Catalyst deactivation,” *Catal. Today*, vol. 52, no. 2–3, pp. 165–181, 1999.
 - [20] H. M. Davey, “Life, death, and in-between: meanings and methods in microbiology,” *Appl. Environ. Microbiol.*, vol. 77, no. 16, pp. 5571–6, 2011.
 - [21] F. Hammes, M. Berney, and T. Egli, “Cultivation-independent Assessment of Bacterial Viability,” *Adv. Biochem. Eng. Biotechnol.*, vol. 124, pp. 123–150, 2012.
 - [22] V. C. H. Wu, “A review of microbial injury and recovery methods in food,” *Food Microbiol.*, vol. 25, no. 6, pp. 735–744, 2008.
 - [23] A. Narang and S. S. Pilyugin, “Bacterial gene regulation in diauxic and non-diauxic growth,” *J. Theor. Biol.*, vol. 244, no. 2, pp. 326–348, 2007.
 - [24] A. Jöers and T. Tenson, “Growth resumption from stationary phase reveals memory in *Escherichia coli* cultures,” *Sci. Rep.*, vol. 6, no. 1, p. 24055, 2016.
 - [25] A. M. Wesche, J. B. Gurtler, B. P. Marks, and E. T. Ryser, “Stress, sublethal injury, resuscitation, and virulence of bacterial foodborne pathogens,” *J. Food Prot.*, vol. 72, no. 5, pp. 1121–1138, 2009.
 - [26] J. P. Buchmann and E. C. Holmes, “Cell Walls and the Convergent Evolution of the Viral Envelope,” *Microbiol. Mol. Biol. Rev.*, vol. 79, no. 4, pp. 403–418, 2015.
 - [27] E. P. Bakker and W. E. Mangericht, “Interconversion of Components of the Bacterial Proton Motive Force by Electrogenic Potassium Transport,” *J. Bacteriol.*, vol. 147, no. 3, pp. 820–826, 1981.
 - [28] M. A. Farha, C. P. Verschoor, D. Bowdish, and E. D. Brown, “Collapsing the Proton Motive Force to Identify Synergistic Combinations against *Staphylococcus aureus*,” *Chem. Biol.*, vol. 20, no. 9, pp. 1168–1178, 2013.
 - [29] R. F. Epand, J. E. Pollard, J. O. Wright, P. B. Savage, and R. M. Epand, “Depolarization, bacterial membrane composition, and the antimicrobial action of ceragenins,” *Antimicrob. Agents Chemother.*, vol. 54, no. 9, pp. 3708–13, 2010.
 - [30] K. A. Bakeev, Ed., *Process Analytical Technology: Spectroscopic Tools and Implementation Strategies for the Chemical and Pharmaceutical Industries*, 1st ed. Oxford: Blackwell Publishing Ltd, 2005.
 - [31] W. N. Ross *et al.*, “Changes in absorption, fluorescence, dichroism, and birefringence in stained giant axons: Optical measurement of membrane potential,” *J. Membr. Biol.*, vol. 33, no. 1, pp. 141–183, 1977.
 - [32] M. Díaz, M. Herrero, L. A. García, and C. Quirós, “Application of flow cytometry to industrial microbial bioprocesses,” *Biochem. Eng. J.*, vol. 48, no. 3, pp. 385–407, 2010.
 - [33] T. L. da Silva, J. C. Roseiro, and A. Reis, “Applications and perspectives of multi-parameter flow cytometry to microbial biofuels production processes,” *Trends Biotechnol.*, vol. 30, no. 4, pp. 225–231, 2012.
 - [34] [1] C. Koch, I. Fetzer, T. Schmidt, H. Harms, and S. Müller, “Monitoring functions in managed microbial systems by cytometric bar coding,” *Environ. Sci. Technol.*, vol. 47, no. 3, pp. 1753–1760, 2013.
 - [35] C. Koch, S. Müller, H. Harms, and F. Harnisch, “Microbiomes in bioenergy production: From analysis to management,” *Curr. Opin. Biotechnol.*, vol. 27, pp. 65–72, 2014.

- [36] C. T. O’Konski, “Electric properties of macromolecules. (V). Theory of ionic polarization in polyelectrolytes,” *J. Phys. Chem.*, vol. 64, no. 5, pp. 605–619, 1960.
- [37] A. Di Biasio, L. Ambrosone, and C. Cametti, “The Dielectric Behavior of Nonspherical Biological Cell Suspensions: An Analytic Approach,” *Biophys. J.*, vol. 99, pp. 163–174, 2010.
- [38] B. Habermann, E. Ritzi, and F. Schulze, “Monitoring of biogas plants - experiences in laboratory and full scale,” *Carbon – Sci. Technol.*, vol. 7, no. 2, pp. 1–7, 2015.
- [39] S. Junne, M. Nicolas Cruz-Bournazou, A. Angersbach, and P. Götz, “Electrooptical monitoring of cell polarizability and cell size in aerobic *Escherichia coli* batch cultivations,” *J. Ind. Microbiol. Biotechnol.*, vol. 37, no. 9, pp. 935–942, 2010.
- [40] K. Asami, T. Hanai, and N. Koizumi, “Dielectric analysis of *Escherichia coli* suspensions in the light of the theory of interfacial polarization,” *Biophys. J.*, vol. 31, no. 2, pp. 215–228, 1980.
- [41] J. L. Sebastián, S. Muñoz, M. Sancho, G. Martínez, and K. V. I. S. I. S. Kaler, “Polarizability of red blood cells with an anisotropic membrane,” *Phys. Rev. E*, vol. 81, no. 2, pp. 022901–022904, 2010.
- [42] T. Millat, H. Janssen, H. Bahl, R. Fischer, and O. Wolkenhauer, “The pH-induced Metabolic Shift from Acidogenesis to Solventogenesis in *Clostridium acetobutylicum* – From Experiments to Models,” in *Experimental Standard Conditions of Enzyme Characterization*, 2011, pp. 33–54.
- [43] J. R. Bastidas-Oyanedel, F. Bonk, M. H. Thomsen, and J. E. Schmidt, “Dark fermentation biorefinery in the present and future (bio)chemical industry,” *Rev. Environ. Sci. Biotechnol.*, vol. 14, no. 3, pp. 473–498, 2015.
- [44] M. Valli, M. Sauer, P. Branduardi, N. Borth, D. Porro, and D. Mattanovich, “Improvement of lactic acid production in *Saccharomyces cerevisiae* by cell sorting for high intracellular pH,” *Appl. Environ. Microbiol.*, vol. 72, no. 8, pp. 5492–5499, 2006.
- [45] A. M. Zhivkov and A. Y. Gyurova, “Influence of cytoplasm electrolyte concentration on Maxwell-Wagner polarizability of bacteria *E. coli*,” *J. Phys. Chem. B*, vol. 113, no. 24, pp. 8375–8382, 2009.
- [46] M. H. Nezhad, M. Knight, and M. L. Britz, “Evidence of changes in cell surface proteins during growth of *Lactobacillus casei* under acidic conditions,” *Food Sci. Biotechnol.*, vol. 21, no. 1, pp. 253–260, 2012.
- [47] H. Sträuber and S. Müller, “Viability States of Bacteria-Specific Mechanisms of Selected Probes,” *Cytom. Part A*, vol. 77A, pp. 623–634, 2010.
- [48] K. R. Konrad and R. Hedrich, “The use of voltage-sensitive dyes to monitor signal-induced changes in membrane potential – ABA triggered membrane depolarization in guard cells,” *Plant J.*, vol. 55, pp. 161–173, 2008.
- [49] P. Beck and R. Huber, “Detection of cell viability in cultures of hyperthermophiles,” *FEMS Microbiol. Lett.*, vol. 148, no. 1, pp. 11–14, 2006.
- [50] C. F. Maurice, H. J. Haiser, and P. J. Turnbaugh, “Xenobiotics shape the physiology and gene expression of the active human gut microbiome,” *Cell*, vol. 152, no. 1–2, pp. 39–50, 2013.

4. Macro-approach analysis of biohydrogen production in the presence of powdered Fe⁰

4.1 Introduction

Iron cycles are being studied extensively in different fields, from groundwater remediation techniques [1] to iron fertilization in water bodies due to geobiochemical effects [2]. Recent research in the area of Anaerobic Digestion (AD) has addressed metals supplementation to biological systems as a possible technique to enhance biomethane production [3]. The aim of metals addition is to raise the methane yields *in situ*, thus making the energy-recovery in AD processes even more attractive. However, the effects of metal particles and the interactions with the biotic phase of AD has not been fully elucidated, because of the great variety of microorganisms within the mixed cultures involved in these types of bioenergy production process. Mixed adapted consortia are the standard inoculum in AD plants since pure cultures for waste treatment are cost-intensive. These cultures tend to be composed of four main microbial groups, named accordingly to their function (i.e. *hydrolytic*, *acidogenic*, *acetogenic* and *methanogens*); each group encompasses hundreds of different microorganisms, whose dynamics can be affected in different ways by the addition of Fe⁰.

AD is present worldwide, not only in developed countries, but also in developing countries, where alternative energies are emerging, at different scales [4], for energy-recovery and sanitation of wastewaters and organic refuses [5].

Energy recovery in Dark Fermentation (i.e. a truncated version of AD, where methanogens are not present and the system produces only bio-H₂) and AD systems is of biological nature, in which the collective action of the aforementioned microbial groups leads to the degradation of organic material, which in turn produces energy bio-carriers, namely bio-H₂ and bio-CH₄, and a solid residue (i.e. digestate), which can be used for different applications.

Biogas has no standard composition, its composition reaches a maximum of about 70 % v/v of methane; however, in most real cases, it is around 40-60 % v/v, with an important fraction of carbon dioxide (> 30%). On the other hand, biomethane refers to biogas which undergoes an upgrading treatment (e.g. absorption, adsorption, membranes processes, cryogenic separation and their combinations), increasing the concentration of CH₄, up to 90% - 95 % v/v, but at the expense of additional energy, which could affect the overall energetic convenience of the process [6]. Nowadays, the call for the decarbonization of the energy sector exerts a great deal of pressure on renewable energies, where CO₂-

emissions play a fundamental role in distinguishing between *biogenic* and *industrial* CO₂ emissions, especially from the socio-economic point of view. As introduced by Jensen and Skovsgaard in [7], the real quantification and proper allocation of CO₂ emissions can help in the transition from natural gas to biogas and/or biomethane; they evaluated different scenarios for Denmark and concluded that the CO₂-cost is fundamental to increase the use of biogas, and that biogas heating power could be upgraded through the use of hydrogen.

The supplementation of different conductive materials, mainly metals, and nano-or micro-structured zero-valent iron, has shown positive effects in different experimental works that investigated their use to improve the generation of biogas [8][9] or the enhance the energy recovery at low costs, particularly with retrieved and/or recycled metals. Recent studies have shown common results: the addition of zero-valent metals positively influences the generation of methane in AD. One of the first studies by Yang et al. (2013) [10], showed that methane production can be increased, even for low doses of nano-structured zero valent iron (i.e. a concentration below 1.7 g/L) by up to 10%. More encouraging threshold were obtained by Hu et al. [11], who achieved an increase of more than 60% in CH₄ yield through the use of different doses of up to 20 g/L, of either nanostructured Fe⁰ or of waste iron scraps. Abdelsalam et al. [12] have recently found raised yields of biogas and biomethane of about 50% with different nano-structured metallic materials (i.e. cobalt, nickel, iron and magnetite), supplemented in moderate concentrations (1-20 mg/L). Meng et al. [13] tested an acidogenic culture during the degradation of propionate into acetate adding Fe⁰ particles of approximately 200 µm and observed the activity of some key enzymes involved in the process. Their results suggested that the addition of Fe⁰, and its anaerobic corrosion (AC) with the generation of Fe²⁺ ions within the acidogenic microbiome, might be correlated to a significant enhancement in the activity and concentration of different iron-containing enzymes. Among the enzymatic pool under analysis, the significant enhanced activity of Pyruvate: ferredoxin oxidoreductase (PFOR), which contains active iron sites and is involved in hydrogen production as a supplier of electrons from the decarboxylation of pyruvate to hydrogenases, should be highlighted [14].

Since the different phases of AD can be segregated in different reactors (DF and AD), such as Two-Stage Anaerobic Digestion (TSAD) [15][16] in order to increase the overall energy production [17], the present aims to study the effects of the addition of Fe⁰ in the dynamics of the first stage, that is, the fermentative stage in which H₂ is produced in order to understand the possible interactions. For this purpose, experimental tests were conducted with and without the addition of Fe⁰ to DF systems. Due to the inherent complexity of mixed microbial cultures, a macro-approach was chosen for the study, where experimental data were analysed using the Roels approach to identify dynamic interactions between anaerobic corrosion (AC) and dark fermentation (DF). This method allows complex phenomena, whose analytical description could require several equations and the evaluation of many parameters, to be studied through a simple and effective description of the dynamics of the process called relaxation times (τ_R) approach.

4.2 Materials and methods

4.2.1 Experimental tests

Tests were conducted in batch mode and were divided into two types: AC and DF tests. AC tests were performed at two different Fe° concentrations: 1 g/L (AC_1) and 2 g/L (AC_2), conducted under the same operative conditions as DF, that is, equal pH, temperature and mixing rate and in the absence of any organic substrate or biological phase. The DF tests included the biological phase (adapted inoculum) and the substrate, and were divided into three sets:

- i) non-supplemented Fe° DF test (0 g/L), as control reference (DF_C)
- ii) DF test supplemented with Fe° at a concentration of 1 g/L (DF_1)
- iii) DF test supplemented with Fe° at a concentration of 2 g/L (DF_2)

All the tests were conducted in triplicate in air tight 500 mL serum bottles, using a working volume of 100 mL of deionised water and adding acidic-treated (i.e. 30 min with 2 M HCL to eliminate surface rust, under anaerobic conditions) powdered Fe° (Kremer Pigmente GmbH & Co. 54600, nominal size 315 μm) to reach the above-stated concentrations of 1 g/L and 2 g/L. The pH was adjusted over the 6.6-7.2 range with a solution of 2M HCl, N_2 was flushed for 10 minutes to reach anaerobic conditions and the bottles were sealed with rubber bungs and silicone to avoid gas leaks. The tests were carried out in a thermostatic chamber at $30 \pm 1^\circ\text{C}$, in the low limit of the optimal mesophilic range of DF, and the bottles were stirred continuously by an orbital shaker at 120 rpm until the gas production ceased and no additional gas production was detected.

4.2.2 Preparation of the substrate

The used substrate was constituted by an assortment of Organic Market Waste (OMW), whose merceological composition and constituents (i.e. water, total carbohydrates, sugars, fibres, proteins, lipids and minerals) are reported in **Table 4.1** and were evaluated using the USDA Food Composition Database [18] according to the method reported elsewhere [16]. OMW was collected from a local market and comminuted means of a kitchen food grinder, diluted with tap water in an approximate 1:1 w/w ratio and alkaline pre-treated. The chosen pre-treatment consisted in the addition of a 2N NaOH solution to stabilize the substrate at pH=12 and keeping the solution in a thermostatic chamber at $30 \pm 1^\circ\text{C}$ for 24 hours. This pre-treatment has been proved useful for highly lignocellulosic substrates, particularly to increase the biodegradation of such structures [19] and generate sufficient C5- and C6-sugars for the fermentation process [20]; in the selected feed, carbohydrates amount c. 83 % of the dry matter, composed roughly by 76 % sugars and 24 % fiber (see **Table 4.1**). After the application of the basic pre-treatment, the substrate was reset at pH=7 using a 2M HCl solution.

Table 4.1 Model composition of the Organic Market Waste (OMW) used for the tests.

Constituents	Mass (g)	wi/w _{total} (%)	Water (g)	Carbohydrates (g)	Sugar (g)	Fiber (g)	Proteins (g)	Lipids (g)	Minerals (g)
<i>Apple</i>	344.95	11.04	295.14	47.64	35.84	8.28	0.90	0.59	0.45
<i>Carrots</i>	104.00	3.33	91.82	9.96	4.93	2.91	0.97	0.25	0.49
<i>Eggplant</i>	272.25	8.72	251.29	16.01	9.61	8.17	2.67	0.49	0.76
<i>Fava Beans</i>	70.20	2.25	50.97	12.38	6.47	5.27	5.56	0.51	0.39
<i>Fennel</i>	168.00	5.38	151.55	12.26	6.60	5.21	2.08	0.34	0.98
<i>Kiwi</i>	232.20	7.43	192.89	34.04	20.87	6.97	2.65	1.21	0.93
<i>Lemon</i>	195.00	6.24	173.51	18.17	4.88	5.46	2.15	0.59	0.37
<i>Lettuce</i>	151.60	4.85	143.99	4.35	1.18	1.97	2.06	0.23	0.46
<i>Melon</i>	200.72	6.43	180.95	16.38	15.78	1.81	1.69	0.38	0.64
<i>Orange</i>	378.47	12.12	328.32	44.47	35.39	9.08	3.56	0.45	0.93
<i>Pepper</i>	217.00	6.95	190.40	20.53	11.07	3.26	4.34	0.43	0.95
<i>Strawberries</i>	192.62	6.17	175.19	14.79	9.42	3.85	1.29	0.58	0.40
<i>Tomato</i>	346.14	11.08	327.17	13.46	9.10	4.15	3.05	0.69	0.99
<i>Watermelon</i>	250.50	8.02	229.08	18.91	15.53	1.00	1.53	0.38	0.35
Total	3123.65	100.00	2782.26	283.36	186.66	67.38	34.48	7.11	9.09
% (w/w)			89.07	9.07			1.10	0.23	0.53

4.2.3 Preparation of the inoculum

The acidogenic inoculum was obtained by treating cow manure at pH=3, using 2 N HCl for 24 h at 35 °C, according to a previously reported procedure [21], in order to inhibit the growth of methanogens. The initial conditions of the inoculum, before the acid treatment, were as follows: pH = 7.5, density 973 kg/m³, Volatile Solids (VS) 113.99 g/L and Total Solid concentration (TS) 134.69 g/L. The treated manure was used as inoculum in all the DF tests at a ratio of 10% (v/v) of the working volume. The fermentation broth was composed of the pre-treated substrate, the inoculum and tap water to reach adequate initial *TS* and *VS* concentrations (see **Table 4.3**).

4.2.4 Analytical measurements

The water content, TS and VS were evaluated according to the standard procedure [22]. The pH was measured using a Consort P903 device (LAISS Apparecchi Scientifici, Turin, Italy). Cumulative gas production was assessed by means of the acid water-displacement (i.e. at pH=2 to prevent CO₂-capture) method, employing a filled gas meter flask connected to a collector bottle. The gas produced in both from the AC and DF series of tests referred to a working temperature of 30 °C (i.e. thermostatic chamber conditions) and the pressure was adjusted to the initial liquid within the gasometer (c. 7 cm H₂O). The quality of the produced gas was analysed, taking samples from each bottle head space, through off-line gas chromatography (Varian Micro-GC CP-4900, Palo Alto, USA) equipped with two columns: *i*) a Poroplot U column for CO₂ determination (85° C injection temperature, 200 KPa, Ar as the carrier) and *ii*) a molecular Sieve-type

device for H₂, CH₄, CO, O₂ and N₂ determination (95°C injection temperature, 200 KPa, He as the carrier). The energy content of the substrate was estimated through the Lower Heating Value (LHV) of the dry matter of the OMW, using a calorimetric bomb (Parr-Instrument 1261, Moline, USA).

4.2.5 Relaxation time approach

Roels demonstrated [23] that for a given phenomenon exhibiting first-order kinetics, the passage, under an external perturbation of matter or energy, from a steady state, C_{si} , towards a new steady state, C_{si}' , required a determined time (t_{∞}), but it could be considered to have occurred, or *relaxed*, after the elapse of the *relaxation time* (τ_R). The τ_R ($\tau_R \leq t_{\infty}$) for first-order systems corresponds to a time interval between C_{si} and a fraction of $(1-1/e)$ of C_{si}' , which represents a 63% achievement of the second stationary state (see **Figure 4.1**).

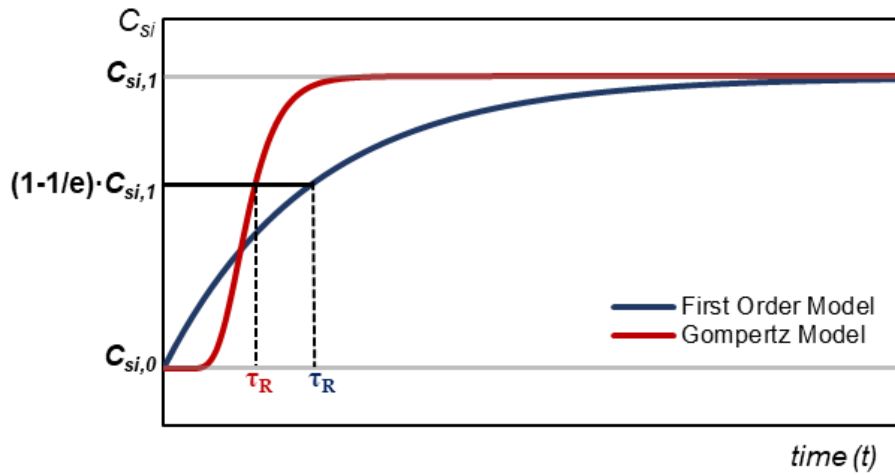


Figure 4.1 Relaxation times of phenomena

In the case of *apparent phenomena*, constituted by a combination of different mechanisms or contributions, according to Roels, only those with a τ_R of the same order of magnitude mutually affect the dynamics of each other. In addition, Roels suggested that mechanisms with τ_R that are different by more than one order of magnitude are not concurrent (i.e. there is no interaction between them), and therefore can be considered as frozen or relaxed. Hence, only phenomena which occur in the same time-window have the possibility to influence each other, and therefore should be taken into consideration for the description of a complex system. For example, oil reservoirs formation has a characteristic or relaxation time which is several orders of magnitude greater than the human life expectancy, thus the process, from the human perspective, is frozen on time (i.e. oil is therefore considered a non-renewable resource).

In general, for a first-order process, where the flux (J) is directly proportional to the driving force (ΔX):

$$J = k\Delta X \quad (4.1)$$

the relaxation time can be considered as:

$$\tau_R = \frac{1}{k} \quad (4.2)$$

which can be considered constant over the entire X range. However, first-order kinetics is rarely applicable in biological systems, hence the kinetic expression corresponds to a higher-order relationship:

$$r = f(\bar{A}) \quad (4.3)$$

where \bar{A} is the vector of the state variable that affects the system. In the case of higher-order systems, **Equation 4.3** can be linearized and written in a similar way to the flux equation:

$$r = \frac{f(\bar{A})}{A} * A \quad (4.4)$$

where A is the so-called “*probe parameter*” [21], an experimentally measurable parameter which provides information on the evolution and dynamics of systems themselves. Hence, the relaxation time analogously to the previous case, can be taken as:

$$\tau_R = \frac{A}{f(\bar{A})} \quad (4.5)$$

Since **Equation 4.5** is not constant for different combinations of the \bar{A} vector, an appropriate A value should be selected to evaluate the relaxation time, that is, one able to characterize the experimental observation interval. Ruggeri et al. [21] noted that **Equation 4.5** allows an actual value of τ_R to be estimated from experimental data. An acceptable estimation can be performed by evaluating the time that the system takes to reach an approximately $(1-1/e)$ fraction of the difference between the actual state and a new given steady-state. This experimental approach is useful for the prediction of the interaction between two phenomena, which can be achieved by calculating τ_R , using the same *probe parameter*, in two separate tests. A given complex phenomenon requires therefore for its dynamic description both concurrent separated phenomena if the values of the individual τ_R are of the same order of magnitude. This proposed approach has been used in this chapter to understand whether the Anaerobic Corrosion (AC) of zero-valent iron fillings (Fe^0) is a mechanism that can potentially influence the complex phenomena of biological hydrogen production through Dark Fermentation. In this regard, the experimental tests of the present work aimed at monitoring the evolution of H_2 as *probe parameter* in independent AC and DF tests and to assess the synergistic effects for combined Fe^0 -supplemented DF systems.

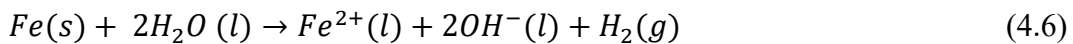
4.2.6 Fe⁰ Anaerobic Corrosion (AC)

First of all, an important consideration on the fluid dynamics of the system should be performed. Fe⁰ particles and the liquid phase, as well as the biotic phase, present a large difference in terms of specific gravity (around 1 for microorganisms and water, while for iron is around 7 kg/L). Therefore, a preliminary experimental evaluation was conducted to define the conditions necessary to reach a sufficiently homogeneous dispersion of the iron fillings in the fermenting broth, since it is important to reach a close contact between the microorganisms and Fe⁰. Several tests were performed at 120 rpm with three Fe⁰ concentrations: 1, 2 and 3 g/L in deionised water and a sample broth, to evaluate the maximum concentration of Fe⁰ which yields a sufficient uniform dispersion. The Fe⁰ concentrations were selected based on tested values found in literature and also taking into consideration the difficulties of dispersing iron in the broth.

Table 4.2 Chemical reactions involved in the water/iron system

	Reaction	Equation
a)	$2\text{Fe}^{3+} + 3\text{H}_2\text{O} \rightarrow \text{Fe}_2\text{O}_3 + 6\text{H}^+$	$\text{Log}(\text{a}_{\text{Fe}^{3+}}) = -0.72 - 3 \cdot \text{pH}$
b)	$\text{Fe}^{2+} \rightarrow \text{Fe}^{3+} + \text{e}^-$	$E_0 = 0.771 + 0.0591 \cdot \text{Log}(\text{a}_{\text{Fe}^{3+}} / \text{a}_{\text{Fe}^{2+}})$
c)	$2\text{Fe}^{2+} + 3\text{H}_2\text{O} \rightarrow \text{Fe}_2\text{O}_3 + 6\text{H}^+ + 2\text{e}^-$	$E_0 = 0.728 - 0.1773 \cdot \text{pH} - 0.0591 \cdot \text{Log}(\text{a}_{\text{Fe}^{2+}})$
d)	$2\text{Fe}_3\text{O}_4 + \text{H}_2\text{O} \rightarrow 3\text{Fe}_2\text{O}_3 + 2\text{H}^+ + 2\text{e}^-$	$E_0 = 0.221 - 0.0591 \cdot \text{pH}$
e)	$3\text{Fe}^{2+} + 4\text{H}_2\text{O} \rightarrow \text{Fe}_3\text{O}_4 + 8\text{H}^+ + 2\text{e}^-$	$E_0 = 0.98 - 0.2364 \cdot \text{pH} - 0.0886 \cdot \text{Log}(\text{a}_{\text{Fe}^{2+}})$
f)	$3\text{Fe}^0 + 4\text{H}_2\text{O} \rightarrow \text{Fe}_3\text{O}_4 + 8\text{H}^+ + 8\text{e}^-$	$E_0 = 0.085 - 0.0591 \cdot \text{pH}$
g)	$\text{Fe}^0 \rightarrow \text{Fe}^{2+} + 2\text{e}^-$	$E_0 = -0.440 + 0.0295 \cdot \text{Log}(\text{a}_{\text{Fe}^{2+}})$
h)	$\text{O}_2 + 4\text{H}^+ + 4\text{e}^- \rightarrow 2\text{H}_2\text{O}$	$E_0 = 1.223 - 0.0591 \cdot \text{pH}$
i)	$2\text{H}^+ + 2\text{e}^- \rightarrow \text{H}_2$	$E_0 = -0.0591 \cdot \text{pH}$

The thermodynamic equilibria of Fe⁰ particles with water, under either aerobic or anaerobic conditions, can easily be visualized using pH/Red-Ox potential plots or Pourbaix diagrams [24]. Pourbaix diagrams can be plotted for different metals and a wide range of environmental conditions (pH, ORP, temperature, pressure), and are a visual representation of the electrochemical equations presented in **Table 4.2**. Water has a thermodynamic stability region at standard conditions (i.e. 1 atm and 25 °C), but apart from this region, it can be reduced by the evolution of hydrogen or oxidized, with H₂O production, in the presence of oxygen. **Figure 4.2** shows the Pourbaix diagram of the water/iron system, at 25°C and atmospheric pressure, applying the procedure reported in [25] under the assumption that the dissolved species thermodynamic activity corresponds to the concentration around 10⁻⁶ M at initial conditions, and considering Hematite (Fe₂O₃), Magnetite (Fe₃O₄), Fe²⁺ and Fe³⁺ as the main corrosion products. Hence, the global Red-Ox reaction which governs the evolution of the system to reach thermodynamic equilibrium is:



with the production of the OH⁻, Fe²⁺ and H₂ species. Generally, corrosion tests are performed on metallic materials and alloys by exposing them to conditions which resemble different environments, and corrosion rates (CR) are expressed as the

mean corroded thickness of the material (mm/y) or as the mass loss rate (MR) as $\text{g}/(\text{m}^2 \cdot \text{y})$ [26]. In our case, the iron particles for these experiments were randomly structured and granular and it is therefore possible to suppose that the corrosion would not have proceeded uniformly from the surface of the fillings towards the core.

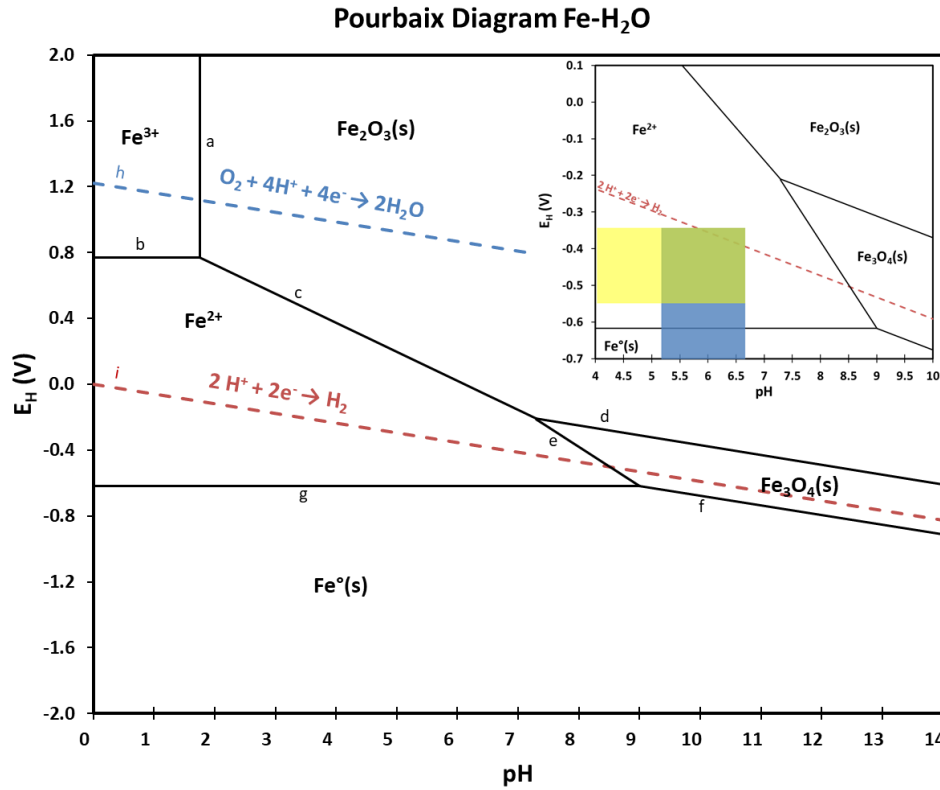


Figure 4.2 Pourbaix diagram of the Fe-H₂O system

The global corrosion reaction represented by **Equation 4.6** is a heterogeneous system, from a chemical reaction point of view, that is composed of different phases: a solid phase and a liquid phase, whose interaction generates a dissolved phase (Fe^{2+} and OH^- ions) and a gas phase, that is, H_2 . The progress of the corrosion reaction was observed from the experimental evaluation of one of the involved species; H_2 evolution was in fact selected for the reasons reported in **section 4.2.5**. The experimental observations suggest that the dynamics of the system follow a saturation equation:

$$H_{AC}(t) = H_{max} * \frac{t}{K_s + t} \quad (4.7)$$

where $H_{AC}(t)$ represents the cumulative specific hydrogen production (mL/g Fe°) at a given time, t represents the time in hours (h), and H_{max} is the overall quantity of produced gas (mL/g Fe°), which is the asymptotic value, while K_s is the half-saturation time-constant of the system (h) i.e. the time at which the cumulative

hydrogen production is equal to $H_{max}/2$. **Equation 4.7** was used to evaluate τ_R by means of a best-fitting of the experimental H_2 evolution.

4.2.7 Dark fermentation (DF)

The biological production of H_2 , especially through mixed cultures in DF, is an excellent technique for the energy recovery from organic sources, as it produces clean energy from different biomass and waste materials and offers the possibility for further process stages to recover compounds of interest, while contributing to decrease the exploitation of traditional fossil fuels [27]. Over the last decade, several papers appeared on the argument, thus increasing knowledge on either the fundamentals or on the application of DF [28]. The use of wastewaters and different organic substrates and mixed microorganism cultures makes the operation of DF very simple, which can also be operated at relatively rapid Hydraulic Retention Times (HRT) [29]. Furthermore, the use of biohydrogen produced from organic refuses, used as a bioenergy carrier, does not involve the generation of any net biogenic CO_2 , thus paving the way towards a circular economy [30].

Hydrogen Producing Bacteria (HPB) inocula, which are mainly dominated by fermentative organisms, used in DF, contain different microbial species in which no methanogenic species are present. The production is directed towards mainly volatile fatty acids (VFA), H_2 and CO_2 [15]. However, a pH-control is recommended to prevent the culture to enter a metabolic state (*solventogenesis*) in which the production of solvents (e.g. ethanol, butanol) is preferred over carboxylic acids (i.e. at $pH < 4.5$). Hence, the operative conditions of this type of bioreactor are slightly different from that of methanogenic ones. The HPB cultures in DF systems content strict or facultative anaerobic microorganisms [31] that are able to take several metabolic pathways, whose enzymatic mechanisms are similar. The H_2 yields of such processes depends primarily on the microbial culture (inoculum) and the substrate; theoretically, one mole of glucose yields from 2 up to 4 moles of H_2 , following the butyric or acetic acid pathway, respectively [32], while the productions are in the (0.15-0.06) L/g of VS or (0.20-0.48) L/g of Chemical Oxygen Demand (COD) ranges for complex structures, such as Organic Wastes [33]. Molecular hydrogen production is mediated at a cellular level through the action of an important enzyme family, *hydrogenases*, which can present different metallic active sites: Ni-Fe for [Ni-Fe]-hydrogenases and Fe-Fe for [Fe-Fe]-hydrogenases [34].

In order to model the H_2 production in DF, a saturative model was chosen, the modified Gompertz present as **Equation 4.8** has been used extensively [35][36]:

$$H_{DF}(t) = G_{max} * \exp \left\{ - \exp \left[\frac{R_{max} * e}{G_{max}} (\lambda - t) + 1 \right] \right\} \quad (4.8)$$

with $H_{DF}(t)$ representing the cumulative specific hydrogen production (mL/g of VS) at a given time t (h), G_{max} is the asymptotic value, i.e. the overall quantity of produced gas (mL/g of VS), R_{max} is the maximum rate of gas production in

(mL/(g·h)), λ is the time interval corresponding to the lag phase (h) and e is Euler's number ($\exp(I)$). **Equation 4.8** is a form of the Gompertz equation, which is *ad hoc* parameterized, in terms of three lumped constants (i.e. G_{max} , R_{max} and λ) to obtain a physical (and biological) interpretation that is useful to understand and compare the dynamics of the complex (saturative) systems. It is important to recall that **Equation 4.8** is, in the present context, a descriptive model in the time domain, where all the parameters that affect the phenomena under study (e.g. pH, temperature, quality and quantity of substrates, the nature of the microorganism consortium and the mixing rate, among others) are not elucidated explicitly, even though they affect the numerical values of the lumped parameters. Therefore, **Equation 4.8** was used to evaluate the dynamics of the control DF (DF_C) and Fe⁰-supplemented tests (DF₁ and DF₂), as well as the relaxation time (τ_R).

The calculation of the τ_R and the afore mentioned lumped parameters for DF is therefore a comprehensive approach, which involves the contribution of each subsystem:

- i) characteristics of the microorganisms (quality and relative abundance of the actual species, microbial species-species interactions),
- ii) substrate (composition, structure, pre-treatment effects, reactivity, inhibitory compounds),
- iii) the operational conditions (rpm of the mixing rotational speed, the initial pH, the initial Red-Ox potential and temperature) of the tests,
- iv) the effects due to the presence of Fe⁰, all of which affect the *macro-performance* of the system, in terms of H₂ production.

In this respect, the experimental tests tried to keep the contributions *i*), *ii*) and *iii*) constant and the *iv*) was scanned at different Fe⁰ concentrations to see the response of the systems.

4.3 Results and discussion

4.3.1 Anaerobic corrosion

The preliminary tests with water and an inactivated broth in the presence of Fe⁰, which were aimed at establishing the highest concentration of Fe⁰ dispersed uniformly in the liquid phase, showed that the 2 g/L concentration was almost uniformly dispersed; instead, the 3 g/L test showed that an important fraction of the dosed iron remained at the bottom of the bottle. This result is in contrast with the results reported in [11], where higher Fe⁰ doses (~17 g/L) of iron were used, placing 5 g of nano-structured Fe⁰ in 300 mL of water, and operating at 200 rpm. It is important to note that the suspension of iron in fermentation broths has not yet been sufficiently addressed in the literature, hence, this topic deserves further study.

The thermodynamic equilibria diagram of the iron/water system was plotted according to the methodology highlighted in **Section 4.2.6**, and it is reported in

Figure 4.2. The lines that define the stability region of the iron system are marked from *a)* to *g)* and correspond to the considered reactions presented in **Table 4.2**, while the oxidation and reduction reactions of water are represented by dashed lines. The iron exhibits the typical signs of corrosion, immunity, passivation zones and the speciation of solid oxides (e.g. magnetite and haematite), as well as dissolved ferrous and ferric compounds, which depend on the operative pH and Red-Ox potential values. The environmental conditions of the DF, which can be defined in terms of the acidity (pH) and the reduction potential (E_H), is highlighted in **Figure 4.2** (i.e. upper-right side). In the case under study, the anaerobic environment of DF is characterized by a pH that ranges from 5.2 to 6.6 and a Red-Ox potential that ranges from -350 to -470 mV [37], although particular conditions for different substrate and adapted inocula can differ from these values. The Pourbaix diagram for the above conditions indicates that the stable form of iron is the ferrous form (Fe^{2+}), while water is reduced with the production of H_2 gas, but only for a higher pH and more positive Red-Ox potential, which corresponds to the beginning of DF. The Pourbaix diagram indicates that iron will only be corroded at a low pH and low Red-Ox potential, if there are other species present (inorganic and organic compounds or microorganisms) that are able to scavenge the electrons produced by the AC of iron, hence inducing additional corrosion through the modification of the thermodynamic equilibrium.

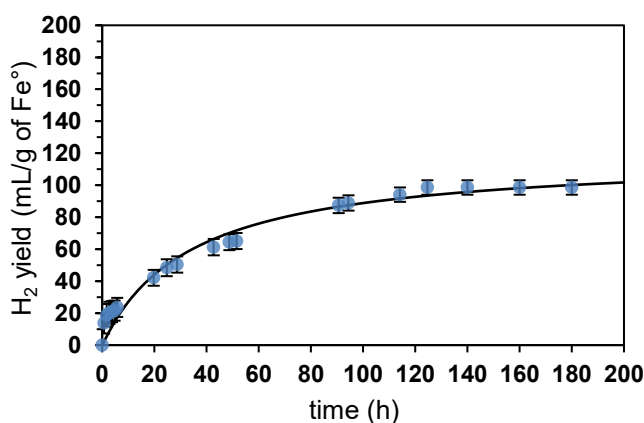


Figure 4.3 Cumulative specific H_2 gas evolution during Anaerobic Corrosion: (●) Experimental Data and (--) Curve fitting.

The quantified cumulative hydrogen evolution from the AC tests is shown in **Figure 4.3** for the tests at 1 and 2 g/L, (AC_1 and AC_2) tests, respectively. The quantity of H_2 is reported per unit mass of dosed Fe^0 for both tests, since no appreciable differences were observed among the tested concentrations. This result could be due to the superficial nature of the corrosion reaction, which depends on the specific surface of the material (i.e. exposed surface of the Fe^0 fillings). Since for both test the same quality of iron (same dimensions and shape) was used, the growth of the reactive surface is therefore proportional to the mass of the material. Besides the experimental H_2 production, **Figure 4.3** also presents the best-fit curve of the mean value of experimental data according to **Equation 4.7**, which yielded a correlation coefficient (**Table 4.4**) that can be considered acceptable, due to the

experimental uncertainties linked to the type of measurements, which primarily aims at evaluating the τ_R of AC. The fitting parameters are reported in **Table 4.4**, and the obtained τ_R for the AC tests was c. 58 h. As it is possible to see from **Figure 4.3**, the anaerobic corrosion of iron particles does not exhibit any lag phase, as expected, since no lag activation step is necessary for the corrosive phenomenon to occur, as is the case for the biological production of hydrogen. Hence, the corrosion reaction presents a reaction rate which is maximum at $t=0$ h, which then progressively decreases.

As stated above, the used iron powder in this study was not micro-structured, however, it still provided an experimental yield of 23 %, referring to the stoichiometric H_2 , considering that the total Fe^0 added had reacted. The yield is similar to the AC of the nanostructured iron reported in the references [11], and this result is in contrast with that of Reardon et al. [38], who hypothesized that the kinetics of Fe^0 corrosion is of an autocatalytic type in water and exhibits a more complex behaviour in moist sands.

4.3.2 Dark Fermentation

The cumulative specific biohydrogen production through DF from OMW with and without Fe^0 dosing, are shown in **Figure 4.4**, while **Table 4.3** reports the results of the proximate analysis of systems at the beginning and at the final state of the tests. The chromatographic analysis of the biogas revealed that there was no CH_4 , and that the gaseous mixtures were only composed of H_2/CO_2 . This indicates, as expected due to the applied basic treatment, that no *methanogens* were present in the initial HPB inoculum. The experimental data of the H_2 production dynamics (i.e. expressed as mL/g of added VS) were modelled satisfactorily ($R^2>0.99$) with the modified Gompertz model (**Equation 4.8**), and the parameters are reported in **Table 4.4**. From a comparison of the G_{max} parameter, which is an indicator of the maximum yield which is attainable, DF_1 and DF_2 resulted in higher values than the control sample (DF_C), with H_2 production which increases as the Fe^0 dosage increases.

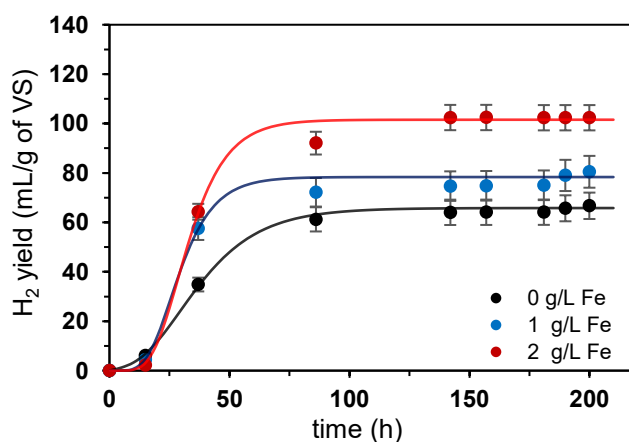


Figure 4.4 Cumulative specific H_2 production during Dark Fermentation

It should also be noted that the amount of added iron per g of VS (w/w), is rather modest: 1:35 and 2:35, unlike other Authors [11][39][40], who tested concentrations of Fe^0 in higher ratios compared to the organic content of the samples.

Table 4.3 Experimentally evaluated Dark Fermentation parameters.

Test		DF _C	DF ₁	DF ₂
TS (g/L)	Initial	43.46 ± 0.19	43.46 ± 0.19	43.46 ± 0.19
	Final	31.77 ± 1.13	33.75 ± 1.57	35.55 ± 0.36
	ΔTS	11.69 ± 1.32	9.71 ± 1.76	7.91 ± 0.55
VS (g/L)	Initial	34.98 ± 2.80	34.98 ± 2.80	34.98 ± 2.80
	Final	20.85 ± 0.91	22.17 ± 1.27	23.79 ± 0.29
	ΔVS	14.13 ± 3.71	12.81 ± 4.07	11.19 ± 3.09
pH	Initial	7.40 ± 0.01	7.40 ± 0.01	7.40 ± 0.01
	Final	5.75 ± 0.05	5.79 ± 0.22	6.03 ± 0.02
Energy (kJ)	Available Energy	63.17 ± 3.43	63.17 ± 3.43	63.17 ± 3.43
	Produced Energy	2.60 ± 0.33	2.98 ± 0.38	3.80 ± 0.49
Efficiency (%)		4.11 ± 0.75	4.72 ± 0.88	6.01 ± 1.1

It is worth mentioning the obtained VS and TS concentrations at the end of DF₁ and DF₂ increased, compared to DF_C. This rise seems to be correlated to the added quantity of Fe^0 , as presented in **Table 4.3**. The increase in VS at the end of fermentation means an increase in organic material, either as a mass of microorganism or as an organic molecule produced by biomass activity. This could be interpreted as an indication of the enhancement of biomass growth as a result of Fe^0 dosing. In addition, the values of pH in **Table 4.3** show a buffering effect on DF, due to the addition of Fe^0 , which may be related to the generation of OH^- ions during the AC reaction (**Equation 4.6**). This is an additional beneficial effect of the addition of iron because since it reduces the quantity of the pH control solution which is necessary to add to DF to limit *solventogenesis*.

Additionally, the total quantity of produced CO_2 is shown in **Figure 4.5** for each DF tests; CO_2 production in DF₁ and DF₂, compared to DF_C, decreased by about 11% and 35%, respectively, and consequently the H_2/CO_2 ratio increased from more than 1 up to almost 3. This effect should be considered as beneficial, since the largest quantity of produced H_2 occurs at the expense of CO_2 , hence the addition of Fe^0 could be considered as a promoter of *in loco* CO_2 sink.

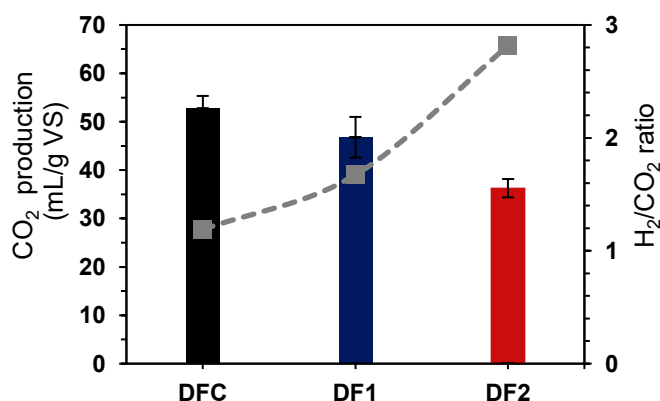


Figure 4.5 Cumulative specific CO_2 production (bars) and H_2/CO_2 ratio (■) in the gas produced during the DF tests, with and without the addition of Fe^0

In energetic terms, the efficiency (η) of the DF process was calculated, using the approach reported in [15], as:

$$\eta = \frac{n_{H_2} * LHV_{H_2}}{TS_{OMW} * LHV_{OMW}} \quad (4.9)$$

taking as reference for the initial available energy embedded in the substrate the calorific value of the dry mass ($LHV_{OMW}=14,538$ kJ/kg of TS) and for the produced energy the total (primary) energy output of the process, which is the total moles of produced hydrogen (n_{H_2}) multiplied by the lower calorific value of hydrogen (~ 239 kJ/mol). The efficiency parameter (η) is useful in for the overall evaluation of the energetic performance of the system, since it relates the two most important energy fluxes in the process under analysis; energy-recovery from DF occurs through dehydrogenation reactions which releases the chemical energy contained in organic substrates, while the produce energy corresponds to the effective produced hydrogen. The calculated η values for the tests resulted in 4.11, 4.72 and 6.01 % for DF_C, DF₁ and DF₂, respectively, which highlights, from an efficiency point of view, the positive effects of Fe⁰ supplementation.

4.3.3 Synergic effects and dynamic interaction of the involved phenomena

The dynamics of systems under study were analysed using **Equation 4.7** and **4.8**; the correspondent parameters for each case and the calculated τ_R values are reported in **Table 4.4**. The dynamics analysis resulted in τ_R of AC and DF_C which are of the same order of magnitude, that is, 58 and 45 h respectively, which is an indication of the concurrence of phenomena, according to the Roels approach. For the Fe⁰ supplemented samples (DF₁ and DF₂), the obtained values of τ_R are lower than those of the DF_C control test, which might be due to synergic effects between DF and AC. The effects of the concurrence of both phenomena may be highlighted quantitatively through a comparison of the Gompertz parameters reported in **Table 4.4**. The most marked difference can be observed through R_{max} values; for DF₁ and DF₂ increases by 2 and 2.5 times, compared to DF_C, while the lag phase, λ , increases by 25 % and 40 % for DF₁ and DF₂, respectively. The lumped parameter R_{max} is a measure of the gas production rate; the addition of Fe⁰ showed a positive effect, which doubled the rate at which gas is produced, while the λ parameter quantifies the time which is required for the inoculum (i.e. mainly constituted by spores) to germinate and reach an active metabolic state for the production of biohydrogen. Conversely, the supplementation of Fe⁰ induced longer activation phases, which is probably due to some interactions between the generated Fe²⁺ and OH⁻ ions and the microorganisms at early stage, as suggested in the literature [13].

On the other hand, the G_{max} values confirm the presence of synergic effects: increases of 15% and 46% were obtained for DF₁ and DF₂, respectively. However, to evaluate whether the observed H₂ surplus was not just a result of the simple addition of H₂ generated via AC and the total quantity of H₂ produced in DF_C, the

produced quantities in DF₁ and DF₂ were compared to “*summation of the effects*”, noted as DF₁* and DF₂*, which is the algebraic sum of volumes produced in the independent AC and DF_c tests (see **Figure 4.6**).

Table 4.4 Dynamic parameters evaluated by means of a best fitting procedure and calculated relaxation time values for each test.

Parameter		Fe ^o concentration (g/L)		
		0	1	2
AC ₁	H_{max} (mL/g of Fe)	-	119.0	
	K_s (h)	-	34.0	
AC ₂	τ_R (h)	-	58	
	R^2		0.966	
DF _C	G_{max} (mL/g of VS)	69.5	79.9	101.7
	R_{max} (mL/(h·g of VS))	1.38	2.86	3.42
DF ₁	λ (h)	12.6	15.8	17.7
DF ₂	τ_R (h)	45	34	37
	R^2	0.997	0.988	0.995

As shown in **Figure 4.6**, the comparison of the total quantity of H₂ produced in DF₁ and DF₂ is higher than the theoretical quantity of the DF₁* and DF₂* sums, which, in fact, might indicate the existence of synergism between AC and DF phenomena.

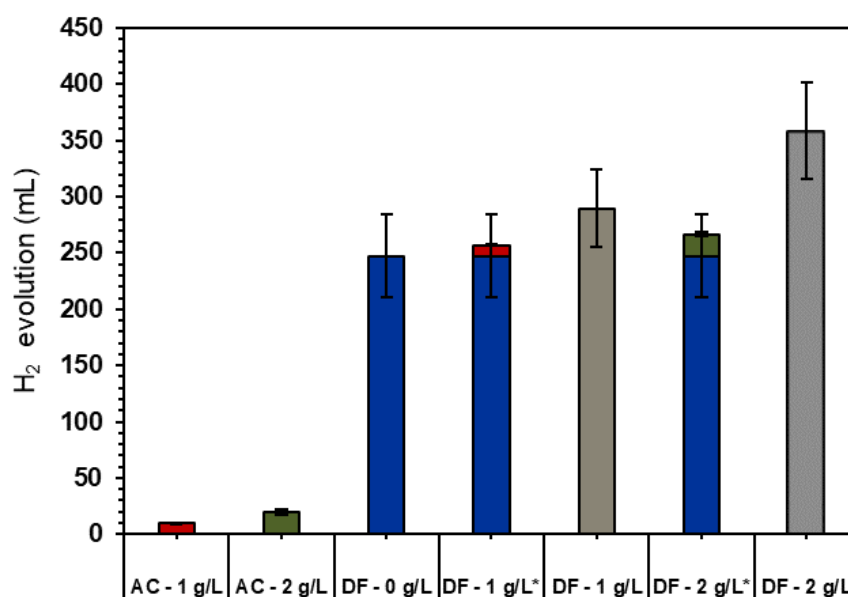


Figure 4.6 Total H₂ production for the AC and DF systems. (DF₁* and DF₂* represent the “*summation of the effects*”)

Since the quantity of H₂ generated by AC is very low (**Figure 4.6**), compared to the H₂ generated by DF, considering AC as a purely additive phenomenon to DF is not sufficient to explain the greater amount of H₂ obtained for DF₁ and DF₂. In order to evaluate the statistical significance of the obtained results, an ANOVA analysis of the experimental results was conducted (i.e. as paired Student's t-test) taking into consideration the mean experimental uncertainties (**Table 4.5**). ANOVA tests are commonly used in the biomedical field to test the response of

pharmaceutical compounds at different doses. In our case, the null hypothesis is that the average H₂ production is not the same for all groups; although the *t*-test among DF₁ and DF₁* resulted in $p=0.3933$ and for DF₁ and DF_C in $p=0.2661$, which suggests a probability of almost 60 % and 75 % for the samples to be equal, respectively, but the comparison among either DF₂ and DF_C or DF₂ and DF₂* resulted in $p=0.0057$ and $p=0.0202$, which indicate that the synergistic effects are present (i.e. with a probability > 97 %) in the supplemented systems and that the effects are presumably dose-dependent. Therefore, it is possible to conclude that the AC of iron and the DF of OMW are concurrent phenomena which show an acceptable statistical significance at a Fe⁰ concentration of 2 g/L.

Table 4.5 ANOVA analysis of the experimental results.

Compared tests	N ° of samples	H ₂ production (mL/g of VS)	R. error (%)	Student <i>t</i> -test	$p < 0.05$
DF _C	3	70.65	13 %	1.2915	0.2661
DF ₁	3	82.80	16 %		
DF _C	3	70.65	13 %	5.3894	0.0057
DF ₂	3	102.48	5 %		
DF ₁ *	3	73.47	14 %	0.9558	0.3933
DF ₁	3	82.80	16 %		
DF ₂ *	3	76.29	15 %	3.7336	0.0202
DF ₂	3	102.48	5 %		

DF₁* and DF₂* represent the “summation of the effects”.

4.3.4 Discussion on the nature of the synergic effects

Although the system under analysis presents a high degree of complexity, due to the use of a mixed undefined culture and OMW as feed, an interesting starting point to analyse the origin of the synergistic effects is the interaction of the Fe⁰ AC products with the biotic phase of the system. This is a particularly difficult task, but a brief compendium of the current state-of-the art of the knowledge on this topic and the possible reason for the synergism is given hereafter.

After the hydrolytic phase takes place, and the constituents (i.e. sugars, lipids and proteins) of the organic matter are released in soluble forms into the liquid phase, these compounds can then enter the cells (i.e. using different transport by diffusion) and be degraded through the different metabolic pathways. Following [16], the degradation of complex sugar molecules in short-chain carboxylic acids follows a common route in the species *Clostridium spp.s* (*acetobutylicum*, *butyricum*, *pasteranum*, etc.), which are one of the main fermentative classes of HPB involved in the production of biohydrogen through DF. Some of the key enzymes which mediated the catabolic degradation are: dehydrogenase (DH), Pyruvate: ferredoxin oxidoreductase (PFOR), phosphotransacetylase (PTA), acetate kinase (AK) and the redox mediator Ferredoxin (Fd) [16] (see **Figure 4.7**), whose actions are concatenated either for catabolic or anabolic pathways. PFOR and Fd two enzymes of interest that contain iron, whose active sites and catalytic activity depend to a great extent on the coordination of these Fe atoms. In fact, the expression of high levels Fd, and its role as main electron supplier towards

hydrogenases in fermentative bacteria have been related to the availability of iron, and especially to ferrous ions (Fe^{2+}) in the culture media [41].

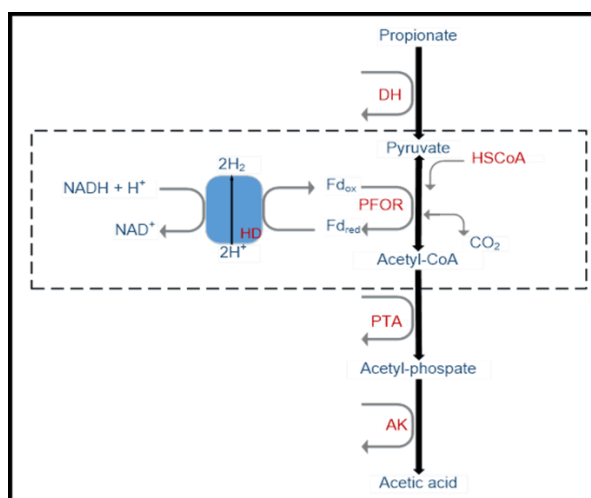


Figure 4.7 Simplified propionic acid degradation pathway into acetic acid for Clostridia

On the other hand, there is also experimental evidence [14] that suggests that PFOR is also responsible for the reverse reaction (i.e. the carboxylation of Acetyl-CoA into pyruvate with the fixation of CO_2 , see **Figure 4.7**), which is an important step in anabolic pathways, which in turn leads to biomass formation. The latter fact could help to elucidate the higher amount of VS found in the exhausted broths (**Table 4.3**) for Fe^0 -supplemented samples as well as to understand the lower observed CO_2 production.

In order to better understand the concurrence of AC and DF, it is important to consider the fate of iron corrosion products, namely ferrous ions (Fe^{2+}) and the electron flow (e^-). As far as the iron-cycle inside bacterial cells is concerned, different uptake mechanisms have been proposed for ferrous (Fe^{2+}) and ferric (Fe^{3+}) ions, since these ions have different solubilities in aqueous media. Various mechanisms have been proposed for the assumption of ferric ion (Fe^{3+}) by bacterial and eukaryotic cells, while the information concerning ferrous ions (Fe^{2+}) uptake mechanisms is rather ambiguous. By considering the Pourbaix diagram (**Figure 4.2**), it can be observed that Fe^{2+} and Fe^{3+} show different thermodynamic stability, and it should be noted that Fe^{3+} could only exist, for thermodynamic reasons, at a low pH and a high Red-Ox potential ($\text{pH} < 2$; $> 0.8 \text{ V}$) i.e. in oxic environments outside the DF range (see the upper part of **Figure 4.2**). In addition, as noted by Raymond et al. [42], Fe^{3+} has a solubility in water of 10^{-18} M at pH 7.4, while Fe^{2+} has a solubility of approximately 0.1 M. As a result of the very low solubility of Fe^{3+} , it has been observed that bacteria and fungi secrete siderophores, such as enterobactin or ferrichrome, which are very specific Fe^{3+} chelating agents [43]. The up-to-date proposed mechanisms hypothesize that ferric ions are complexed first (i.e. in the liquid media, outside from the cell) and then pass through outer membrane receptor proteins for complex ions (FeaA), interact with a binding protein at the periplasmic region and finally cross the cytoplasmic membrane

through ATP-driven pores conformed by FepG and FepD proteins [42]. For gram-positive bacteria, siderophores seem to be tightly anchored to the cytoplasmic membrane, and the complexed Fe^{3+} ions are shuttled towards the transport systems which are also present in the membrane [44].

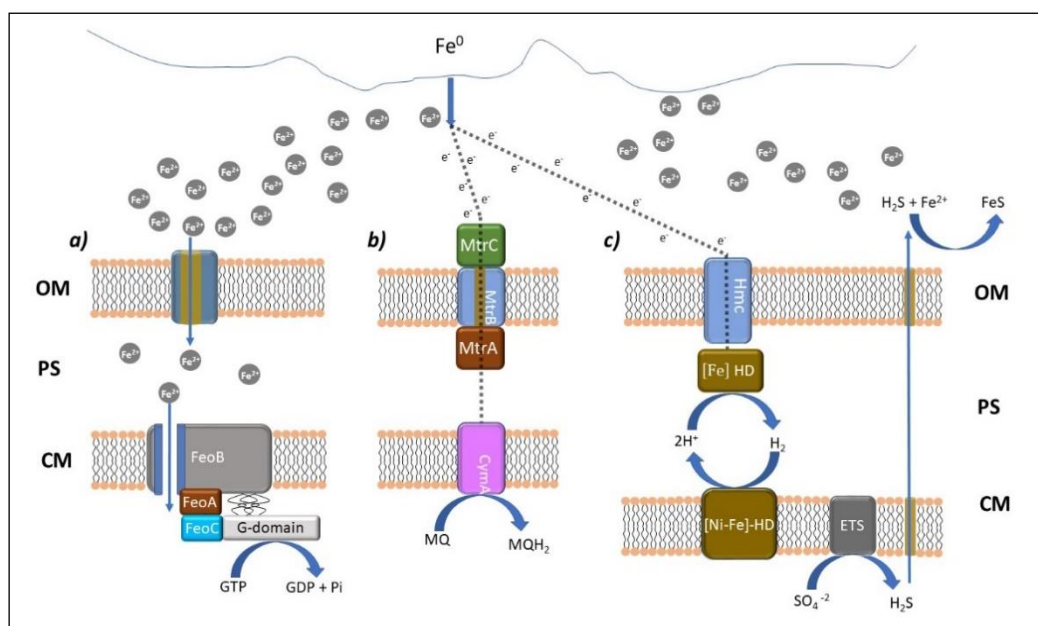


Figure 4.8. Possible fate of the anaerobic corrosion products (Fe^{2+} and e^-) and their interaction with HPB: *a)* Mechanism for ferrous uptake in Gram-negative bacteria; no siderophores are required to transport the Fe^{2+} ions, which diffuse across unidentified porins of the outer membranes, until the ferrous ions are captured by the Ferrous Uptake system (Feo), which is composed of the FeoA, FeoB and FeoC complex proteins; *b)* Electrons captured by the Mtr respiratory pathway. Electrons are initially transferred to the outer surface of MtrC, which then shifts the electrons towards MtrA, which are located at the periplasmic space, passing across the MtrB membrane protein. Most of the electron flow is then transferred to multi-heme CymA cytochromes, where they are eventually captured by the menaquinone pool and *c)* the electrons from corrosions are captured by outer membrane HMC (High molecular weight cytochromes) and are transferred to periplasmic Fe-hydrogenases, where H_2 is produced. At the cytoplasmic membrane, Ni-Fe hydrogenases reduce hydrogen and deviate electrons to the electron transfer systems (ETS), thus reducing sulphate (SO_4^{2-}) to hydrogen sulphide (H_2S); OM: outer membrane, PS: Periplasmic space and CM: cytoplasmic membrane. For more details, see **section 4.3.4**.

However, the uptake and/or assimilation mechanisms of Fe^{2+} are still under research. **Figure 4.8** depicts the possible fate of iron AC products: *a)* for Fe^{2+} , *b)* and *c)* for e^- . As noted above, since the solubility of Fe^{2+} is several orders of magnitude higher of Fe^{3+} , chelating agents are not likely to be required in the same proportion as in the case of Fe^{3+} , hence it is possible to hypothesize that Fe^{2+} ions diffuse across the outer membrane through unspecified porins (*a* mechanism in **Figure 4.8**). Moreover, different mechanisms (i.e. Feo, MntH, FutABC and Zupt, among others) have been identified to transport ferrous ions into the cytoplasm, once Fe^{2+} ions reach the periplasm [44]. Among these mechanisms, Feo (Fe^{2+} iron transport) has been reported to be extensively diffused for ferrous uptake in different types of bacterial cells [45].

There is currently a great deal of interest in the electrical interactions of biological systems and electrodes in several electro microbial devices and in bio-electrochemical systems (BES), hence the fate of the e^- flow constitutes an important step towards understanding the behaviour of the global system [46]. Most

of the research has been focused on electrically-active microorganisms such as *Geobacter* and *Shewanella spp.s*, which are gram-negative bacteria that possess different multiheme c-type cytochromes (MHCs) and which are partially exposed to the external part of the outer membrane [47], however, *Clostridium spp.s* are also believed to be able to express cytochromes [48]. Cytochromes possess prosthetic heme groups, consisting of an Fe atom centred within a porphyrin cyclic molecule. Cytochromes are widely diffused in prokaryotic organisms, with a higher occurrence in gram-negative than in gram-positive bacteria, and the expression of these metalloproteins does not seem to be correlated to particular environmental conditions or Red-Ox potentials [49]. The role of MHCs as electron transfer proteins, is due to their particular structure, where heme co-factors are arranged in particular non-linear sequences [50] to facilitate the flow of electrons in a specific direction. Marcus Theory [51] has been used to predict and model the intraprotein electron transfer (ET), and some authors have proposed that ET can be described, at an intraprotein and an interprotein level, as a through-space tunnelling phenomenon [50] due to weak electrical interactions present in biological systems [52].

Nevertheless, cathodic reaction mechanisms of electron donation to microorganisms are still under revision. Ross et al. [53] proposed the Mtr pathway (the *b* mechanism in **Figure 4.8**) after studying a culture of *Shewanella oneidensis* in contact with an electron donor graphite electrode; the growth of an electrically active biofilm was observed and electrons are believed to have been shifted through the quinone pool into the cytoplasm, coupled with fumarate reduction processes. The Mtr pathway, for example, relies on the function of the MtrA, MtrB and MtrC protein complexes, as well as on the action of the CymA and OmcA cytochromes. An early study conducted by Bryant and Laishley [54] investigated the role of hydrogenases in steel biocorrosion; hydrogenases were extracted from *Clostridium pasteurianum* (i.e. a H₂-producing microorganism) under environmental conditions where the AC of steel was expected to occur. The results suggested that the mechanism for biocorrosion included the reverse action of hydrogenases, which was achieved by depolarizing the outer surface of the steel rods, and hydrogenases then acted as a direct receptor for the flow of electrons produced by Fe⁰ corrosion, thus increasing the evolution of H₂ (the *c* mechanism in **Figure 4.8**). Furthermore, the addition of methyl-viologen, a biological redox intermediate, resulted in a delay in hydrogen production, which indicated the preference of this receptor for the electrons instead of hydrogenases, but after receptor exhaustion, the production of H₂ was resumed through the hydrogenases pool. Similar conclusions were drawn by Van Ommen Kloeke et al. [55], who examined a *Desulfovibrio vulgaris* culture, a sulphate reducing bacteria (SRB), to test the effects of biocorrosion on mild steel. The observations suggested that important differences in the protein bands of the outer membrane in the presence of steel arose, which is in agreement with the enzymatic pool enhancement and modification hypothesis proposed to support the present experimental results.

As mentioned before, H₂ production in HPB depends on the presence of the hydrogenases, which apparently can produce hydrogen by using exogenous

electrons, but a key aspect is the need for electrically-active enzymes (e.g. c-cytochromes) or shuttle compounds (i.e. such as conductive extracellular polymeric substances), which, via Red-Ox reactions, are able to capture the external electron flow and introduce it into the cells. The reviews presented by Rosenbaum et al. [56] and Patil et al. [57] provide a general overview on the subject of the microbial assumption of electrons at the cathode of BES for the production of reduced compounds. In the Authors' opinion, the presented mechanisms could support the experimental evidence presented in the present paper concerning the higher H_2 production in presence of the Fe^0 AC in a DF environments.

4.4 Conclusions

The Roels macro-analysis of experimental data of DF H_2 production under Fe^0 dosage has offered a clear indication of concurrent phenomena: Fe^0 AC and microbial activity. The H_2 yield increased by up to 46%, compared to the control test, hence metal supplementation in DF could enhance energy recovery in the form of bio- H_2 ; in efficiency terms, the energy recovery from OMW also showed an important improvement, since the efficiency of this type of process is always related to hydrogen productivity. In addition, Fe^{2+} ions are believed to be metabolized by the activity of microorganisms, which leads to an improvement in the capturing of CO_2 , probably due to an enhancement in the enzymatic activity of fermentative bacteria. The observed phenomena are in agreement with the most recent candidate mechanisms used to explain the bioelectrical activity of different microorganisms in novel microbial electrochemical devices.

Although the studies on Fe^0 supplementation in bioenergy production systems are quite novel, the rationalization of the involved biogeochemical cycles and the technical operating conditions is fundamental from the feasibility and sustainability points of view. In our case, the Fe^0 /VS ratios are modest, 1:35 and 2:35 (w/w) compared to other literature references; higher Fe^0 doses pose a design challenge on the mixing conditions of the bioreactors, which required further research. In this respect, iron suspension could be addressed by means of the deposition of the metal particles in beads of density similar to that of the fermentation broths. Additionally, no inhibitions due to Fe^0 addition in DF were found nor have been reported in literature, however, long-testing experimental campaigns can be suitable approach to test whether Fe^0 can lead to inhibitions of biomethane or biohydrogen production and/or to monitor the microbial changes either in the composition or the activity of the microbiome.

References

- [1] F. Fu, D. D. Dionysiou, and H. Liu, "The use of zero-valent iron for groundwater remediation and wastewater treatment: A review," *J. Hazard. Mater.*, vol. 267, pp. 194–205, 2014.
- [2] K. Güssow, A. Proelss, A. Oschlies, K. Rehdanz, and W. Rickels, "Ocean iron fertilization: Why further research is needed," *Mar. Policy*, vol. 34, no. 5, pp. 911–918, 2010.
- [3] C. E. Gomez Camacho and B. Ruggeri, "Syntrophic Microorganisms Interactions in Anaerobic Digestion (AD): a Critical Review in the Light of Increase Energy Production," *Chem. Eng. Trans.*, vol. 64, 2018.
- [4] T. Bond and M. R. Templeton, "History and future of domestic biogas plants in the developing world," *Energy Sustain. Dev.*, vol. 15, no. 4, pp. 347–354, 2015.
- [5] H. Jouhara et al., "Municipal waste management systems for domestic use," *Energy*, vol. 139, pp. 485–506, 2017.
- [6] M. Di Addario, A. C. L. Malavè, S. Sanfilippo, D. Fino, and B. Ruggeri, "Evaluation of sustainable useful index (SUI) by fuzzy approach for energy producing processes," *Chem. Eng. Res. Des.*, vol. 107, pp. 153–166, 2016.
- [7] I. G. Jensen and L. Skovsgaard, "The impact of CO₂-costs on biogas usage," *Energy*, vol. 134, pp. 289–300, 2017.
- [8] R. Lin, J. Cheng, J. Zhang, J. Zhou, K. Cen, and J. D. Murphy, "Boosting biomethane yield and production rate with graphene: The potential of direct interspecies electron transfer in anaerobic digestion," *Bioresour. Technol.*, vol. 239, pp. 345–352, 2017.
- [9] E. Abdelsalam, M. Samer, Y. A. Attia, M. A. Abdel-Hadi, H. E. Hassan, and Y. Badr, "Influence of zero valent iron nanoparticles and magnetic iron oxide nanoparticles on biogas and methane production from anaerobic digestion of manure," *Energy*, vol. 120, pp. 842–853, 2017.
- [10] Y. Yang, J. Guo, and Z. Hu, "Impact of nano zero valent iron (NZVI) on methanogenic activity and population dynamics in anaerobic digestion," *Water Res.*, vol. 47, no. 17, pp. 6790–6800, 2013.
- [11] Y. Hu, X. Hao, D. Zhao, and K. Fu, "Enhancing the CH₄ yield of anaerobic digestion via endogenous CO₂ fixation by exogenous H₂," *Chemosphere*, vol. 140, pp. 34–9, 2015.
- [12] E. Abdelsalam, M. Samer, Y. A. Attia, M. A. Abdel-Hadi, H. E. Hassan, and Y. Badr, "Comparison of nanoparticles effects on biogas and methane production from anaerobic digestion of cattle dung slurry," *Renew. Energy*, vol. 87, pp. 592–598, 2016.
- [13] X. Meng, Y. Zhang, Q. Li, and X. Quan, "Adding Fe⁰ powder to enhance the anaerobic conversion of propionate to acetate," *Biochem. Eng. J.*, vol. 73, pp. 80–85, 2013.

- [14] C. Furdui and S. W. Ragsdale, "The role of pyruvate ferredoxin oxidoreductase in pyruvate synthesis during autotrophic growth by the Wood-Ljungdahl pathway," *J. Biol. Chem.*, vol. 275, no. 37, pp. 28494–9, 2000.
- [15] A. C. Luongo Malave, D. Fino, C. E. Gomez Camacho, and B. Ruggeri, "Experimental tests on commercial Sweet Product Residue (SPR) as a suitable feed for anaerobic bioenergy (H₂+ CH₄) production," *Waste Manag.*, vol. 71, pp. 626–635, 2018.
- [16] B. Ruggeri, T. Tommasi, and S. Sanfilippo, *BioH₂ & BioCH₄ Through Anaerobic Digestion: From Research to Full-scale Applications*. Springer London, 2015.
- [17] G. Kvesitadze et al., "Two-stage anaerobic process for bio-hydrogen and bio-methane combined production from biodegradable solid wastes," *Energy*, vol. 37, no. 1, pp. 94–102, 2012.
- [18] United States Department of Agriculture, "USDA Food Composition Databases," 2016. [Online]. Available: <https://ndb.nal.usda.gov/ndb/search/list>. [Accessed: 07-Oct-2016].
- [19] M. T. Holtzapple, J. E. Lundeen, R. Sturgis, J. E. Lewis, and B. E. Dale, "Pretreatment of lignocellulosic municipal solid waste by ammonia fiber explosion (AFEX)," *Appl. Biochem. Biotechnol.*, vol. 34–35, no. 1, pp. 5–21, 1992.
- [20] B. Ruggeri, A. C. Luongo Malave, M. Bernardi, and D. Fino, "Energy efficacy used to score organic refuse pretreatment processes for hydrogen anaerobic production," *Waste Manag.*, vol. 33, no. 11, pp. 2225–2233, 2013.
- [21] B. Ruggeri, T. Tommasi, and G. Sassi, "Experimental kinetics and dynamics of hydrogen production on glucose by hydrogen forming bacteria (HFB) culture," *Int. J. Hydrogen Energy*, vol. 34, no. 2, pp. 753–763, 2009.
- [22] American Public Health Association, American Water Works Association, and Water Environment Federation, "Standard Methods for the Examination of Water and Wastewater," APHA, 1999.
- [23] J. A. Roels, *Energetics and kinetics in biotechnology*. Elsevier Biomedical Press, 1983.
- [24] M. Pourbaix, *Atlas of electrochemical equilibria in aqueous solutions*. Michigan, 1974.
- [25] J. D. Verink, "Simplified Procedure for Constructing Pourbaix Diagrams," in *Uhlig's Corrosion Handbook: Third Edition*, 2011, pp. 93–101.
- [26] ASTM, "ASTM: G102 – 89 Standard Practice for Calculation of Corrosion Rates and Related Information from Electrochemical Measurements," 2015.
- [27] F. Orecchini and E. Bocci, "Biomass to hydrogen for the realization of closed cycles of energy resources," *Energy*, vol. 32, no. 6, pp. 1006–1011, 2007.
- [28] D. Das and T. N. Veziroglu, "Hydrogen production by biological processes: a survey of literature," *Int. J. Hydrogen Energy*, vol. 26, no. 1, pp. 13–28, 2001.

- [29] K. Nath and D. Das, "Improvement of fermentative hydrogen production: Various approaches," *Appl. Microbiol. Biotechnol.*, vol. 65, no. 5, pp. 520–529, 2004.
- [30] S. Manish and R. Banerjee, "Comparison of biohydrogen production processes," *Int. J. Hydrogen Energy*, vol. 33, no. 1, pp. 279–286, 2008.
- [31] C. T. Gray and H. Gest, "Biological Formation of Molecular Hydrogen," *Science (80-.)*, vol. 148, no. 3667, pp. 186–192, 1965.
- [32] A. Yoshida, T. Nishimura, H. Kawaguchi, M. Inui, and H. Yukawa, "Enhanced hydrogen production from glucose using ldh- and frd-inactivated *Escherichia coli* strains," *Appl. Microbiol. Biotechnol.*, vol. 73, pp. 67–72, 2006.
- [33] I. K. Kapdan and F. Kargi, "Bio-hydrogen production from waste materials," *Enzyme Microb. Technol.*, vol. 38, no. 5, pp. 569–582, 2006.
- [34] P. M. Vignais, B. Billoud, and J. Meyer, "Classification and phylogeny of hydrogenases," *FEMS Microbiol. Rev.*, vol. 25, no. 4, pp. 455–501, 2001.
- [35] M. Di Addario et al., "Development of Fuzzylogic model to predict the effects of ZnO nanoparticles on methane production from simulated landfill," *J. Environ. Chem. Eng.*, vol. 5, no. 6, pp. 5944–5953, Dec. 2017.
- [36] K. M. C. Tjørve and E. Tjørve, "The use of Gompertz models in growth analyses, and new Gompertz-model approach: An addition to the Unified-Richards family," *PLoS One*, vol. 12, no. 6, pp. 1–17, 2017.
- [37] A. C. Luongo Malave', M. Bernardi, D. Fino, and B. Ruggeri, "Multistep anaerobic digestion (MAD) as a tool to increase energy production via H₂ + CH₄," *Int. J. Hydrogen Energy*, vol. 40, no. 15, pp. 5050–5061, 2015.
- [38] E. J. Reardon, R. Fagan, J. L. Vogan, and A. Przepiora, "Anaerobic Corrosion Reaction Kinetics of Nanosized Iron," *Environ. Sci. Technol.*, vol. 42, no. 7, pp. 2420–2425, 2008.
- [39] Y. Feng, Y. Zhang, X. Quan, and S. Chen, "Enhanced anaerobic digestion of waste activated sludge digestion by the addition of zero valent iron," *Water Res.*, vol. 52, pp. 242–250, 2014.
- [40] G. Zhen, X. Lu, Y. Y. Li, Y. Liu, and Y. Zhao, "Influence of zero valent scrap iron (ZVSI) supply on methane production from waste activated sludge," *Chem. Eng. J.*, vol. 263, pp. 461–470, 2015.
- [41] E. Knight, A. J. D'Eustachio, and R. W. F. Hardy, "Flavodoxin: A flavoprotein with ferredoxin activity from *Clostridium pasteurianum*," *Biochim. Biophys. Acta - Enzymol. Biol. Oxid.*, vol. 113, no. 3, pp. 626–628, 1966.
- [42] K. N. Raymond, E. A. Dertz, and S. S. Kim, "Enterobactin: An archetype for microbial iron transport," *Proc. Natl. Acad. Sci.*, vol. 100, no. 7, pp. 3584–3588, 2003.
- [43] J. B. Neilands, "Siderophores : Structure and Function of Microbial Iron Transport Compounds," *J. Biol. Chem.*, vol. 270, no. 45, pp. 26723–26726, 1995.

- [44] C. K. Y. Lau, K. D. Krewulak, and H. J. Vogel, "Bacterial ferrous iron transport: The Feo system," *FEMS Microbiol. Rev.*, vol. 40, no. 2, pp. 273–298, 2016.
- [45] M. L. Cartron, S. Maddocks, P. Gillingham, C. J. Craven, and S. C. Andrews, "Feo - Transport of ferrous iron into bacteria," *BioMetals*, vol. 19, pp. 143–157, 2006.
- [46] S. Bajracharya et al., "An overview on emerging bioelectrochemical systems (BESs): Technology for sustainable electricity, waste remediation, resource recovery, chemical production and beyond," *Renew. Energy*, vol. 98, pp. 153–170, 2016.
- [47] K. Richter, M. Schicklberger, and J. Gescher, "Dissimilatory reduction of extracellular electron acceptors in anaerobic respiration," *Appl. Environ. Microbiol.*, vol. 78, no. 4, pp. 913–921, 2012.
- [48] A. Poehlein, F. R. Bengelsdorf, B. Schiel-Bengelsdorf, G. Gottschalk, R. Daniel, and P. Dürre, "Complete Genome Sequence of Rnf- and Cytochrome-Containing Autotrophic Acetogen *Clostridium acetivum* DSM 1496," *Genome Announc.*, vol. 6, no. 5, pp. e00786-15, 2015.
- [49] S. Sharma, G. Cavallaro, and A. Rosato, "A systematic investigation of multiheme c-type cytochromes in prokaryotes," *J. Biol. Inorg. Chem.*, vol. 15, no. 4, pp. 559–571, 2010.
- [50] M. Breuer, K. M. Rosso, and J. Blumberger, "Electron flow in multiheme bacterial cytochromes is a balancing act between heme electronic interaction and redox potentials," *Proc. Natl. Acad. Sci.*, vol. 111, no. 2, pp. 611–616, 2014.
- [51] F. Burggraf and T. Koslowski, "Charge transfer through a cytochrome multiheme chain: Theory and simulation," *Biochim. Biophys. Acta - Bioenerg.*, vol. 1837, no. 1, pp. 186–192, 2014.
- [52] W. Kurlancheek and R. J. Cave, "Tunneling through weak interactions: comparison of through-space-, H-bond-, and through-bond-mediated tunneling," *J. Phys. Chem. A*, vol. 110, no. 51, pp. 14018–14028, 2006.
- [53] D. E. Ross, J. M. Flynn, D. B. Baron, J. A. Gralnick, and D. R. Bond, "Towards electrosynthesis in *Shewanella*: Energetics of reversing the Mtr pathway for reductive metabolism," *PLoS One*, vol. 6, no. 2, p. e16649, 2011.
- [54] R. D. Bryant and E. J. Laishley, "The role of hydrogenase in anaerobic biocorrosion.," *Can. J. Microbiol.*, vol. 36, no. 4, pp. 259–264, 1990.
- [55] F. Van Ommen Kloeke, R. D. Bryant, and E. J. Laishley, "Localization of cytochromes in the outer membrane of *Desulfovibrio vulgaris* (Hildenborough) and their role in Anaerobic Biocorrosion," *Anaerobe*, vol. 1, no. 6, pp. 351–358, 1995.
- [56] M. Rosenbaum, F. Aulenta, M. Villano, and L. T. Angenent, "Cathodes as electron donors for microbial metabolism: Which extracellular electron transfer mechanisms are involved?," *Bioresour. Technol.*, vol. 102, no. 1, pp. 324–333, 2011.

- [57] S. A. Patil, C. Hägerhäll, and L. Gorton, “Electron transfer mechanisms between microorganisms and electrodes in bioelectrochemical systems,” *Bioanal. Rev.*, vol. 4, no. 2–4, pp. 159–192, 2012.

5. Continuous Two-Step Anaerobic Digestion (TSAD) of Organic Market Waste: rationalising process parameters

5.1 Introduction

The feasibility of the use of mixed microbial consortia in Anaerobic Digestion (AD) for a wide range of organic substrates has been demonstrated during the last decades. In fact, AD is one of the most widespread energy-recovery processes throughout the world and it reached 16.6 Mtoe of primary energy production in Europe in 2016 [1], which represented 1.12 % of the total EU primary energy consumption for that year. Moreover, different ongoing developments have also integrated AD in biorefinery context processes [2].

Currently, the most frequently used feedstock for AD is that of organic material, that is, either agro-industrial production residues or the Organic Fraction of Municipal Solid Waste (OFMSW), which is mainly constituted by: cellulose, hemicellulose and lignin. Biomethane is produced using different inocula containing a wide variety of microorganisms, which progressively adapt to degrade the different organic constituents: carbohydrates, proteins and lipids [3]. Large macromolecules are first hydrolysed to small-chain carbohydrates, while proteins are hydrolysed to amino acids and lipids to long-chain fatty acids. In acidogenesis, volatile fatty acids (VFA) are produced simultaneously with H_2 and CO_2 through dehydrogenation and decarboxylation reactions. Later, the acetogenic phase takes place converting the primary fermented products into acetic acid and CO_2 , which are used in methanogenesis by hydrogenotrophic methanogens (CO_2 and H_2) and acetoclastic methanogens (acetic acid) together with other substances (methylated compounds), albeit to a lesser extent [4]. All the above-mentioned phenomena are not independent; they are possible in AD microbiomes thanks to the fascinating syntrophic relationships that are established between fermenting bacteria and archaea. These bacteria produce surplus reducing power under the form of electrons, which is used by methanogens; these in turn need electrons, and this process is often referred to as interspecies electron transfer IET [5]. Moreover, several IET mechanisms, such as H_2 and formate, have been proposed as shuttled and direct interspecies for electron exchange [6].

Microbial Community Engineering (MCE) is a growing topic of interest within the biotechnological field which comprehends species-species and species-environment interactions, including symbiotic associations (i.e. mutualistic,

parasitic or commensalistic), competition and predation within species and strains. MCE has a high potentiality, which could be exploited for the production of chemicals [7], energy [8] and materials [9]. Species-species and species-environment interactions are related to the application of external stressors (*selective pressure*) to microbiomes, a process that can be applied using different approaches of a dynamic nature. The stability of a microbiome under environmental changes is therefore of the utmost importance. Two-Stage Anaerobic Digestion (TSAD) has recently been exploited using different microbiomes for each stage [10]. TSAD is conducted in one or two physically separated bioreactors, the latter in the case of continuous runs and the former for batch runs. The first step, i.e. bio- H_2 production, is referred in the literature as Dark Fermentation (DF) and it has been studied extensively [11], while only a few studies are available on TSAD, and most of these are on the batch mode. TSAD permits more energy to be recovered than a one-stage process [12], not only due to the energy produced as hydrogen, but also because of the higher methane production. The reason for this enhancement is that the first stage serves as a biological pre-treatment, thus making the substrates more easily biodegradable by methanogens, and hence increasing the energy efficiency of the whole process [13][14]. As suggested in [10], the microbial consortia used to produce bio- H_2 and bio- CH_4 can be divided into two main groups, according to the pivotal role of H_2 in AD: Hydrogen Producing Bacteria (HPB) and Hydrogen Consuming Bacteria (HCB). The first group is mainly composed of hydrolytic and fermentative microorganisms, and the second of fermentative microorganisms and methanogens.

In this context, continuous TSAD is a process that has been designed to separate the AD microbiomes into two bioreactors: *i*) a first one, aimed at producing H_2 plus CO_2 and a mixture of volatile fatty acids (VFA) that are present in the liquid phase, which is mainly carried out by HPB and *ii*) a second one, which is fed with the liquid output stream from the first, and targets CH_4 and CO_2 production, and which contains a consortium of HCB and HPB. In the case of TSAD, it is mandatory to keep HPB separate from HCB in the first bioreactor. The separation can be obtained through the use of certain operational parameters (external stressors), such as: pH, temperature, mixing rate, Organic Loading Rate (OLR), Red-Ox potential, Hydraulic Retention Time (HRT), concentration of inhibitory compounds and kinetic selection of the microorganisms. The batch operation mode for TSAD systems was previously studied in [13]; however, it is necessary to pay more attention to the dynamics of the systems as far as the continuous mode is concerned, in particular for HRT [15] and OLR, which determine the growth kinetics of the microbial species, and hence the performances of the whole system.

The aim of this study was to experimentally evaluate the energetic performance and the stability of biogas production, using a quasi-pilot TSAD system operating in continuous mode, by selecting and maintaining the process parameters that are suitable for the microbiome present at each stage. Continuous operation was conducted using Organic Market Waste (OMW), taken from a local market, as the feed, under different HRT and OLR conditions. The performance of the TSAD system was evaluated by recording the amount of energy produced as H_2 and CH_4

in each step and the total recovered energy (H_2+CH_4), compared to the energy obtained in one-stage AD using the efficiency and efficacy parameters. The stability analysis of quasi-steady-state condition was conducted over 120 days of operation by evaluating the index of dispersion of fluctuations using Fano factors (FF).

5.2. Materials and methods

5.2.1 Experimental set-up of the TSAD system

The TSAD system consists of two CSTRs connected in series: a first bioreactor (S1), Minifors I (Infors HT, Bottmingen, Switzerland), with a total volume of 2 L, which operates with a working volume of approximately 1.34 L, and a second bioreactor (S2), Chemap Fermenter (Chemap AG, CH-8708, Manedorf, Switzerland), with a volume of 14 L and a fermentation volume of approximately 13.4 L, i.e. with a reactor volume ratio (S1:S2) of 1:10. Both reactors operate under anaerobic conditions, which are reached by flushing N_2 through the fermentation broth for 10 minutes, and under mesophilic conditions at 35 °C, which is controlled by means of an electrical heater loop device. Different pH conditions have been applied to S1 and S2 to maintain different microbiomes in each reactor. In S1, the set point is $pH_{S1}=5.5$, which was set in order to prevent solventogenesis at $pH < 5$ [16], while the set point in S2 is $pH_{S2}=7$, chosen to prevent the lowering of methanogen activity at $pH < 6.5$ [17]. The pH values are controlled within the bioreactors (S1 and S2) by means of 405-DPAS-SC-K8S/225 and 9816 Viscolyt, sensors made by (Mettler Toledo) for S1 and S2, respectively, and by means of two control loop devices, which act on peristaltic pumps using a 2N NaOH solution. In addition, mixing rates of 300 and 50 rpm are applied in S1 and S2, respectively, and are maintained constant for the duration of the tests. A high mixing rate is necessary in S1 to degas the H_2 dissolved in the liquid, which inhibits the bioreaction [6], and to prevent the formation of the aggregates between HPB and HCB consuming H_2 .

On the other hand, S2 requires a low mixing rate to favour the formation of the aggregates containing HPB and HCB and to prevent high hydrodynamic stress on the methanogens. The Red-Ox potential is measured in continuous mode by means of sensors inserted into S1 and S2 (Pt4805-DPAS-SC-K8S/225 and Pt4805-DPAS-SC-K8S made by, Mettler Toledo). Both bioreactors are operated in continuous mode with a slight overpressure (<50 mbar), which is maintained by means of two gas-over-flow valves, to avoid oxygen from infiltrating into the system. The complete system is only fed through the Minifors reactor, using a peristaltic pump with a feed frequency of 6 h. The output stream from S1 reaches S2, without any pH adjustment, by means of gravity-driven overflow, due to the difference in elevation between S1 and S2, which is about 50 cm, as shown in the schematic representation of the experimental set-up (**Figure 5.1a**) and in the presented picture (**Figure 5.1b**).

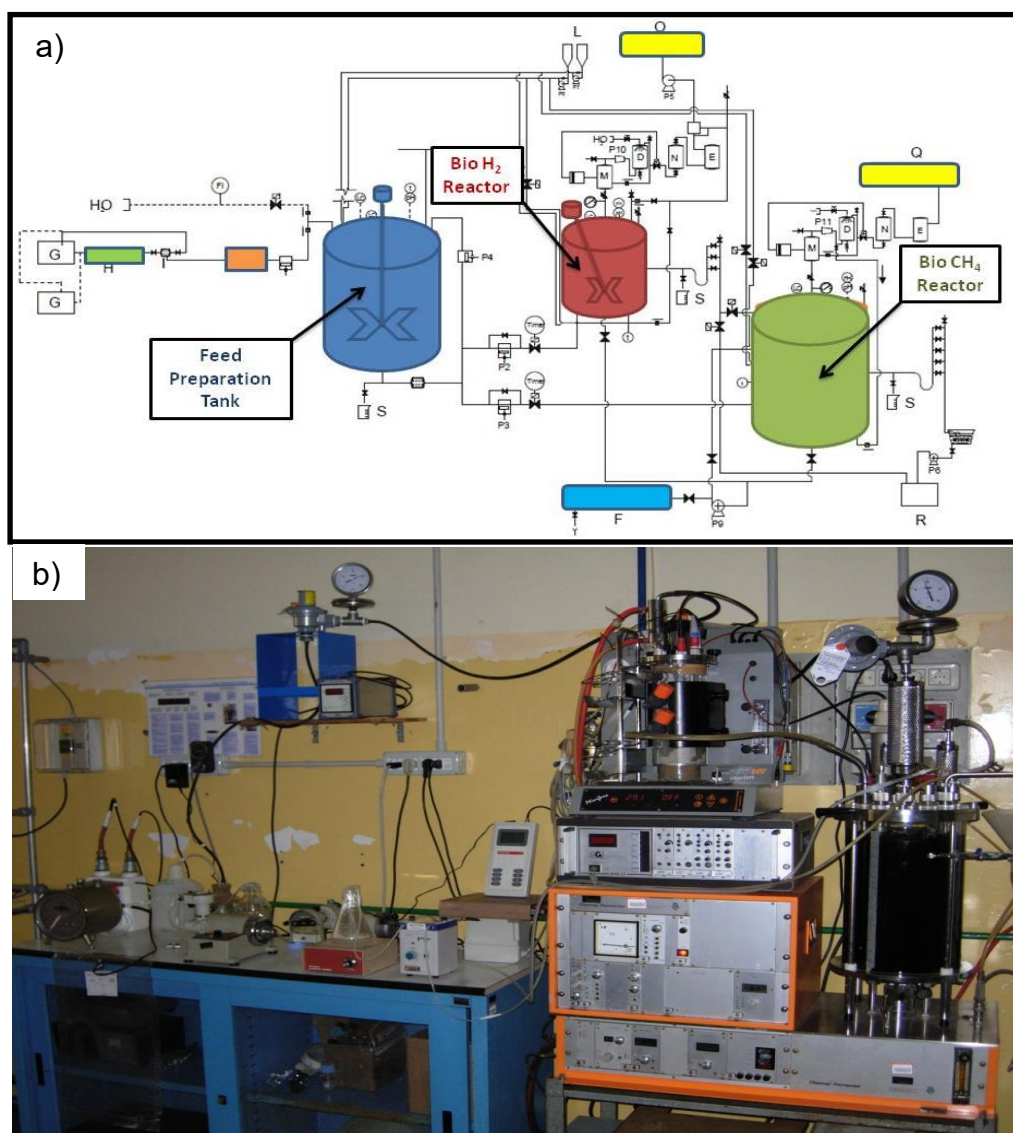


Figure 5.1 a) Scheme of the used pilot plant in continuous mode with A: feed preparation tank; B: H₂ reactor (S1) C: CH₄ reactor (S2); D: absorption column; E: activated carbon adsorption column; F: heating system; G: Feed tank (one running, one in stand-by); H: crush screw; I: on line filter; L: control pH reservoirs; M: pressure control device; N: silica gel drying column; O: hydrogen gas rich storing tank under pressure; Q: biogas storing system at 1 Atmosphere; R: digestate reservoir tank; S: liquid sampling device and **b)** Pilot plant picture.

Considering that AD is not only an energy recovery technique, as is also satisfies other environmental sustainability constrains, such as water consumption, the effluent of the process - the digestate - which is the output of the CH₄ reactor and is not suitable for discharging into a receiving water body, has to undergo a separation step in order to recover the water (dewatering) and produce the dried digestate (about 40 % w/w of humidity). The thus obtained water is then recycled and mixed with the fresh feed to avoid any unnecessary water expenditure and to satisfy the water content requirements for the DF process for wet fermentation. However, in the case of TSAD, the water recycling stream also contains some HCB concentrations, which should not introduce any significant perturbations to the microbial composition in S1. In this respect, the output stream of S2 is filtered using 125 µm nylon filters (Carl Roth GmbH, Karlsruhe, Germany) and used to dilute the feed for S1.

5.2.2 Preparation and pre-treatment of the substrate

The selected substrate used for the tests was Organic Market Waste (OMW), which was constituted by a random mixture of fruit and vegetables collected from an open market (the Racconigi Market, Turin, Italy). The OMW presented an elevated water content, of approximately 89-90 % w/w, which made it suitable for wet fermentation processes. Furthermore, the dry matter (DM) was mainly constituted by carbohydrates (sugars and fibres), of 70-90 % w/w, proteins of around 10-35 % w/w, lipids of 2 – 9 % w/w and minerals of 3-5 % w/w_{DM}. The collected refuses were ground and diluted with tap water to reach the desired Total Solids concentration (35-40 g/L) for the first preparation, without the addition of any substances, to obtain a homogenous solution which was then fed to the system.

Table 5.1 Model composition of the feed to S1

	w/w [%]	Water [%]	Carbohydrates [%]	Proteins [%]	Lipids [%]	Fiber [%]	Other [%]	Energy [Kcal/g]
<i>Strawberry</i>	13.79	90.50	5.30	0.90	0.40	1.60	1.30	0.27
<i>Pear</i>	16.13	87.40	8.40	0.30	0.10	3.80	0.00	0.35
<i>Apple</i>	9.14	86.90	10.70	0.40	0.10	1.70	0.20	0.43
<i>Tomato</i>	22.98	93.16	3.53	0.88	0.22	1.99	0.22	0.19
<i>Zucchini</i>	6.33	93.60	1.40	1.30	0.10	1.20	2.40	0.11
<i>Peppers</i>	9.05	92.30	4.20	0.90	0.30	1.90	0.40	0.31
<i>Onion</i>	11.29	92.10	5.70	1.00	0.10	1.00	0.10	0.26
<i>Celery</i>	2.04	88.30	2.40	2.30	0.20	1.60	5.20	0.20
<i>Potato</i>	4.20	78.50	16.80	2.10	1.00	1.60	0.00	0.85
<i>Orange</i>	1.77	87.20	7.80	0.70	0.20	1.60	2.50	0.34
<i>Parsley</i>	1.41	87.20	1.00	3.70	0.60	5.00	2.50	0.20
<i>Lettuce</i>	1.87	94.30	2.20	1.80	0.40	1.30	0.00	0.19
<i>Mean %</i>		89.29	5.79	1.36	0.31	2.02	1.24	
<i>Mean % (dry basis)</i>			54.01	12.67	2.89	18.90	11.53	

As a result of the long duration of the experimental campaign, different batches of substrate were prepared, following the procedure already reported in [17], but diluted with the filtered liquid discharged from methanogenic reactor S2 [18]. A representative composition of the feed sent to reactor S1 can be found in **Table 5.1.**, evaluated using the USDA Food Composition Database (i.e. following the procedure reported in **Chapter 4**, section 4.2.2).

5.2.3 Preparation of the inocula

The initial inocula used for both systems were cow manure. In the first stage (S1), the HPB inoculum was prepared by treating fresh manure at $pH=3$ with a 2 M solution of HCl at 35 °C for 24 h to reduce the population of methanogens (non-spore forming) following a procedure already reported in [19], in order to promote the enrichment of such spore-forming HPB as *Clostridium spp.* Fresh cow manure was used for the methanogenic reactor (S2), due to the suitability of its anaerobic microbial consortium. Both bioreactors were inoculated with a 10 % v/v fraction of the working volume.

5.2.4 Analytical Measurements

The proximate analysis consisted of the measurement of the dry matter (DM) and Volatile Solids (VS) according to the standard procedures [20]. The pH was measured using a pH-meter (Laiss CONSORT P903, Turin, Italy). Cumulative gas production was assessed for each bioreactor using calibrated milligas counters (Ritter MGC-1 v3.2, Bochum, Germany). Both gas outputs were collected in plastic sampling bags (SKC Inc., Pennsylvania, USA) and analysed through off-line gas chromatography, using a Micro-GC (Varian Micro-GC CP-4900, Palo Alto, USA) equipped with a Thermal Conductivity Detector (TCD) and two columns: a poroplot U column for CO₂ determination (85 °C, 200 KPa and Argon as the carrier) and a molecular sieve-type column for H₂, CH₄, O₂ and N₂ determination (95 °C, 200 KPa and Helium as the carrier). The Lower Heating Values (LHV) of the substrates after dehydration at 105 °C for 24 h and pelletisation of the DM were measured by means of a calorimetric bomb (Parr-Instrument 1261, Moline, USA).

5.2.5 Start-up of the TSAD system

Bioreactors S1 and S2 were both inoculated with different consortia of microorganisms (section 2.3) as seeds, since the generation of bio-hydrogen and bio-methane takes place in different microorganism populations (i.e. HPB and HCB). Considering that the necessary lag phase and duplication times are different in both cases, it was decided to first initiate the methanogenic bioreactor. Hence, the start-up procedure first involved the inoculation of S2 in batch-mode, with the aim of establishing the microbial culture in the exponential-production phase of biogas (CH₄+CO₂), which lasted more than 30 days.

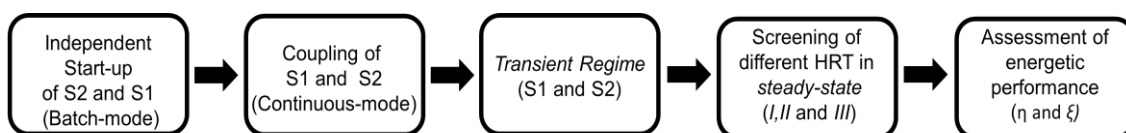


Figure 5.2 Block diagram of the experimental design

On the 20th day after the start-up of S2, the first stage (S1) was also inoculated to start in batch-mode in order to let the microbial culture adapt to fermentative conditions. OWM, prepared as reported in **section 5.2.2**, was used in S1 and S2 under different operational parameters (**section 5.2.1**). When S1 had approximately reached the time corresponding to the exponential phase independently (i.e. 3-4 days), the two bioreactors were connected by opening the connection liquid valve (**Figure 5.1**), and the continuous operation of the two-stage (TSAD) system was launched (see **Figure 5.2** for the experimental design sequence). After the system had been run for a time approximately equal to that of the longer HRT (15 days), in continuous mode, corresponding to 1 cycle of HRT for S2 and 10 cycles of HRT for S1, tests were carried out on the system in quasi-steady-state conditions, starting with the higher HRT tested of 15 days.

5.2.6 Screening of the different Hydraulic Retention Times (HRT)

After the system had been started, three operative HRT namely I, II, III, which are reported in **Table 5.2**, were tested. Considering that the volume of the broth in S2 was 10 times that in S1, and that the total liquid discharged from S1 was fed to S2, the $HRT_{S1}: HRT_{S2}$ ratio was 1:10. Hence, the $HRT_{S1}: HRT_{S2}$ was fixed at 1:10 during the experiments since HPB and HCB are constituted by ecologically different microorganisms with different specific growth rates (μ_{max}), that is, of approximately 0.215 and 0.010 h⁻¹, respectively [10]. Considering that a biohydrogen/biomethane CSTR reactor could reach pseudo-steady-state conditions after approximately 3 HRT, due to the variability of μ_{max} of the different species present in the consortia, the evaluation of the performance of S2 lasted at least 3 cycles of the tested HRT condition, while it lasted 30 cycles of each HRT for S1, which can be considered a sufficiently long time to separate HPB from HCB. The first set of tested HRT corresponds to 1.5 and 15 days for S1 and S2, respectively; these are the longest retention times (the lowest feeding rates) and they were progressively decreased. Although literature references [10] suggest that S1 (i.e. Dark Fermentation) can be operated at $HRT_{S1} < 24$ h, due to the fixed above introduced relation of HRT ($HRT_{S1}: HRT_{S2}$), this would represent a $HRT_{S2} < 10$ d, which in turn could bring S2 into washout conditions of the methanogenic population (see **section 5.2.7** and **Figure 5.3**).

5.2.7 Kinetic selection of the microorganisms based on HRT

In order to assure the long-term stability of HPB and HCB populations, not only were such process parameters as the pH and the mixing rate kept different in S1 and S2, but the so-called *kinetic selection* was also tested, due to its fundamental role in continuous plant operation [21]. This involves the application of the wash-out criterium of a chemostat containing different microorganism species, each with its own specific growth rate. The growth rates (μ) are inversely related to the doubling times of the microorganisms, e.g. $t_d = \ln(2)/\mu_{max}$, which is a more intuitive parameter. As previously mentioned, HPB presents shorter doubling times than HCB, and hence a greater μ_{max} , while HCB has a longer t_d , and therefore requires a longer HRT to reproduce. The large temporal differences necessary for HCB and HPB to reproduce promote a kinetic selection of different microbiomes. It is possible to understand this selection if we consider, for simplicity, an ideal continuous stirred tank reactor (CSTR) containing only one bacteria species (X) and only one organic substrate (S). Considering that bacterial growth follows Monod kinetics, in a steady-state (ss) condition, the constitutive mass balance equations become:

$$S_{ss} = \frac{K_S * D}{(\mu_{max} - D)} \quad (5.1)$$

$$X_{SS} = Y_{X/S} * (S_0 - S_{SS}) \quad (5.2)$$

where μ_{max} is the maximum specific growth rate of the microorganism (h^{-1}), D is the dilution rate $D=Q/V=HRT^{-1}$ (h^{-1}), Q is the flow rate (L/h) and V the volume (L), K_s is the affinity constant (g_S/L), $Y_{X/S}$ (g_X/g_S) is the yield coefficient of the biomass and S_0 (g_S/L) is the substrate concentration in the feed stream. From equations (1) and (2), as D approaches μ_{max} , S_{SS} approaches S_0 , hence X_{SS} approaches zero. This condition means that the bioreactor goes into *wash-out* ($X_{SS} \rightarrow 0$): no microorganisms are then present in the bioreactor and the bioreaction stops. Since $HRT=D^{-1}$, in the case of a bioreactor containing two species of microorganisms, working with a shorter HRT than doubling time t_d of one species will promote the wash-out of the second one.

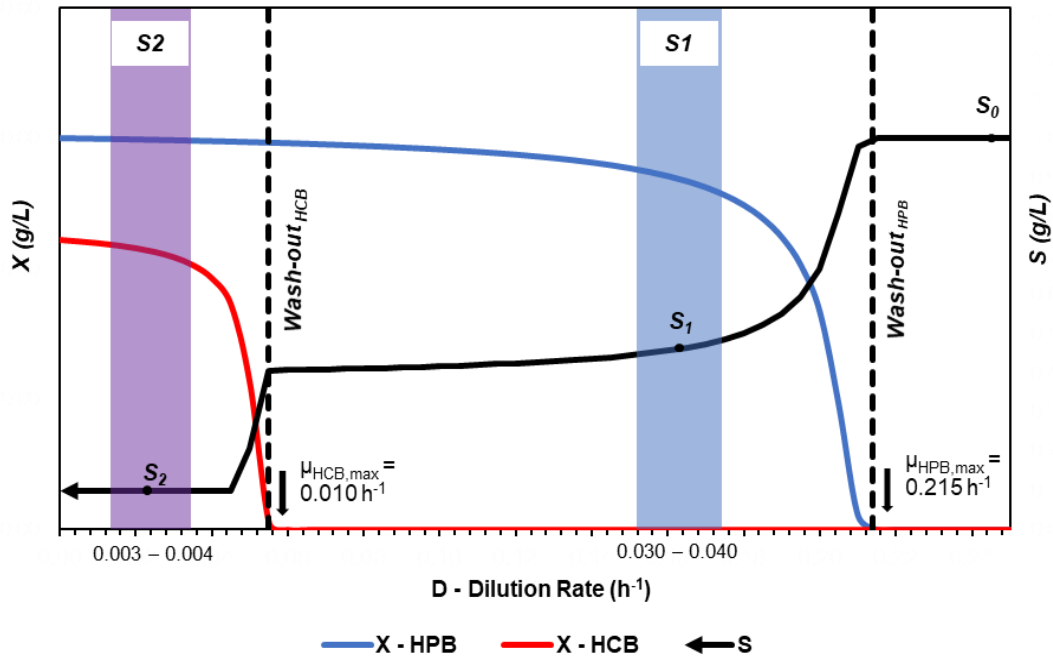


Figure 5.3 Graphical representation of **Equation 5.1** and **5.2**, evidencing the kinetic selection of microorganisms based on HRT

In the present case, the two populations of interest (HPB and HCB) are constituted by hundreds of species, each with a particular value of t_d , and experimental reference values should therefore be considered to represent all the involved species. **Figure 5.3** shows, in a qualitative way, the application of kinetic selection to a TSAD system, where the nominal trends for the substrate concentrations (S) and biomass (X) are presented under steady-state conditions. The dashed vertical lines represent the wash-out of each species, while the vertical bands represent possible operative ranges of HRT for S1 and S2. As can be observed in **Figure 5.3**, an adequate separation of HPB and HCB occurs: only HPB species are present in S1, while a balance between HPB and HCB in S2 allows syntrophy to be reached between the microbial populations of interest. The substrate concentration

decreases as it passes through the cascade of bioreactors: S_0 is the feed substrate concentration for S1, S_1 is the outlet concentration of S1 and is also the inlet concentration for S2 and, finally, S_2 is the concentration of the second stage (S2).

5.2.8 Efficiency (η) and Efficacy (ζ) evaluations

The energetic performance of the continuous TSAD system was evaluated using two parameters: *i*) efficiency (η), which considers the produced energy as the sum of the obtained $H_2 + CH_4$, compared to the amount of energy present in the OMW fed to the system, through its LHV (kJ/g_{DM}) and *ii*) efficacy (ζ), which takes into consideration the energy produced with the TSAD system, compared with the energy produced under an exclusively methane form in the one-stage AD for the same substrate. The concepts of this approach have been previously introduced in [13], and it is here sufficient to highlight the low experimental uncertainty linked to the determination of LHV, which is valid for any type of organic refuse. This approach is preferred than the use of Biological Methane Potential (BMP) since the energy in TSAD is produced under the form of $H_2 + CH_4$, and mainly because the former step modifies the efficiency of the methanogenic step [12].

The efficiency was evaluated as follows:

$$\eta = \frac{\frac{\dot{v}_{S1}}{22.41} * y_{S1,H2} * LHV_{H2} + \frac{\dot{v}_{S2}}{22.41} * y_{S2,CH4} * LHV_{CH4}}{Q_{S1} * S_{OMW} * LHV_{OMW}} \quad (5.3)$$

where \dot{v}_{S1} and \dot{v}_{S2} are the experimentally measured (NL/h) mean biogas flow rates from S1 and S2; $y_{S1,H2}$ and $y_{S2,CH4}$ are the gas mole fractions (mol/mol) of the gas for each stage (i.e. H_2 in S1 and CH_4 in S2), LHV_{H2} and LHV_{CH4} are the molar LHVs of hydrogen and methane, respectively (239.2 kJ/mol and 800.29 kJ/mol); 22.41 NL/mol is the volume occupied by 1 mol of ideal gas; Q_{S1} corresponds to the mean feeding flow rate (L/h) for each tested HRT condition of S1, S_{OMW} is the mean concentration of the volatile matter (g_{VS}/L) present in the OMW and $LHV_{OMW} = (14.538 \pm 150)$ KJ/g_{VS}, as experimentally determined. The efficacy of TSAD was calculated as:

$$\zeta = \frac{Ep_{TSAD}}{Ep_{AD}} \quad (5.4)$$

where Ep_{TSAD} is the energy produced by the TSAD systems (i.e. the numerator of Equation 5.3) and Ep_{AD} (Equation 5.5) is the energy produced by the same feed in the one-stage AD. In the present case, Ep_{AD} was experimentally evaluated in batch mode (test not shown) and a mean value of 0.151 L_{CH4}/g_{VS} was obtained, hence:

$$Ep_{AD} = \frac{0.151}{22.41} * LHV_{CH4} * Q_{S1} * S_{OMW} \quad (5.5)$$

permits the energy produced in the one-step AD to be evaluated as a reference value for each tested HRT, where Q_{SI} (L/h) is the feed for each condition and S_{OMW} the correspondent volatile matter concentration (gvs/L).

5.3. Results and discussion

5.3.1 Volatile Solid (VS) concentrations along the TSAD system

During the continuous test, the operative conditions were kept constant, as mentioned in **Section 5.2.1**. The fed substrate had variable characteristics, since it was prepared periodically (i.e. every Monday) from refuses to simulate full-scale conditions, and it was used during the following days. **Figure 5.4** shows the monitored concentration of VS for the three tested *HRT* in the feed, as well as the output from S1 and the digestate (output from S2) to help understand the behaviour of the TSAD system. It is important to note that the time axis considered and reported in the figures only regards the time of operation in pseudo-steady-state, hence 3 HRT for S2 and 30 HRT for S1. The mean VS concentrations in the feeds for each condition (I, II and III) were 29.2 ± 8.5 , 32.1 ± 3.8 and 29.1 ± 1.6 gvs/L, for each case (**Figure 5.4**). In order to simulate the behaviour of the full plant, due to the variations of the feed characteristics as a consequence of the periodical collection of the refuses, the feeds were only treated as reported in **Section 5.2.2**, this explains the constant OLR for only certain lapses. It is evident that the system can absorb the very large variations of OLR for all the cases. In case I, that is, the system with the longest HRT, the variability in the feed was greater, hence higher oscillations were observed and for some days the difference between the input and output of S2 was very narrow.

Table 5.2 Performance results and operative conditions for each tested condition I, II and III

	I	II	III
<i>S1 - HRT [d]</i>	1.5	1.2	1.1
<i>S2 - HRT [d]</i>	15	12	11
<i>S1- Feed [L/d]</i>	0.89 ± 0.05	1.12 ± 0.05	1.21 ± 0.05
<i>S1 - OLR [gvs/(L·d)]</i>	19.39 ± 5.65	26.84 ± 1.71	19.54 ± 2.00
<i>S2 - OLR [gvs/(L·d)]</i>	1.33 ± 0.19	1.27 ± 0.11	1.95 ± 0.14
<i>S1 - H₂ Productivity [NLH₂/(L_{broth}·d)]</i>	1.437 ± 0.431	1.428 ± 0.291	1.219 ± 0.152
<i>S2 - CH₄ Productivity [NLCH₄/(L_{broth}·d)]</i>	0.299 ± 0.030	0.320 ± 0.019	0.471 ± 0.088
<i>S1 - H₂ Yield [NLH₂/gvs]</i>	0.074 ± 0.029	0.053 ± 0.011	0.050 ± 0.006
<i>S2 - CH₄ Yield [NLCH₄/gvs]</i>	0.154 ± 0.055	0.119 ± 0.007	0.179 ± 0.033
<i>Mean daily produced energy [kJ/d]</i>	163.89 ± 14.50	173.79 ± 1.30	243.15 ± 4.44
<i>Mean daily available energy [kJ/d]</i>	579.75 ± 145.42	717.73 ± 41.45	750.78 ± 80.45
<i>Efficiency [η]</i>	0.28 ± 0.08	0.24 ± 0.01	0.32 ± 0.04
<i>Efficacy [ξ]</i>	1.18 ± 0.34	0.90 ± 0.04	1.29 ± 0.16

It should be noted that even when the VS concentration had more variability, the mean OLR showed a variability of between 10 and 25 % (see **Table 5.2**), which is the same range as that of full-scale digesters, and was always within ranges commonly found in literature for wet fermentation conditions [22]. The response of S2 was also smoother for the three tested conditions, a result that could be related

to the lower activity of the HCB consortia compared to HPB and the longer HRT (see Section 5.3.2).

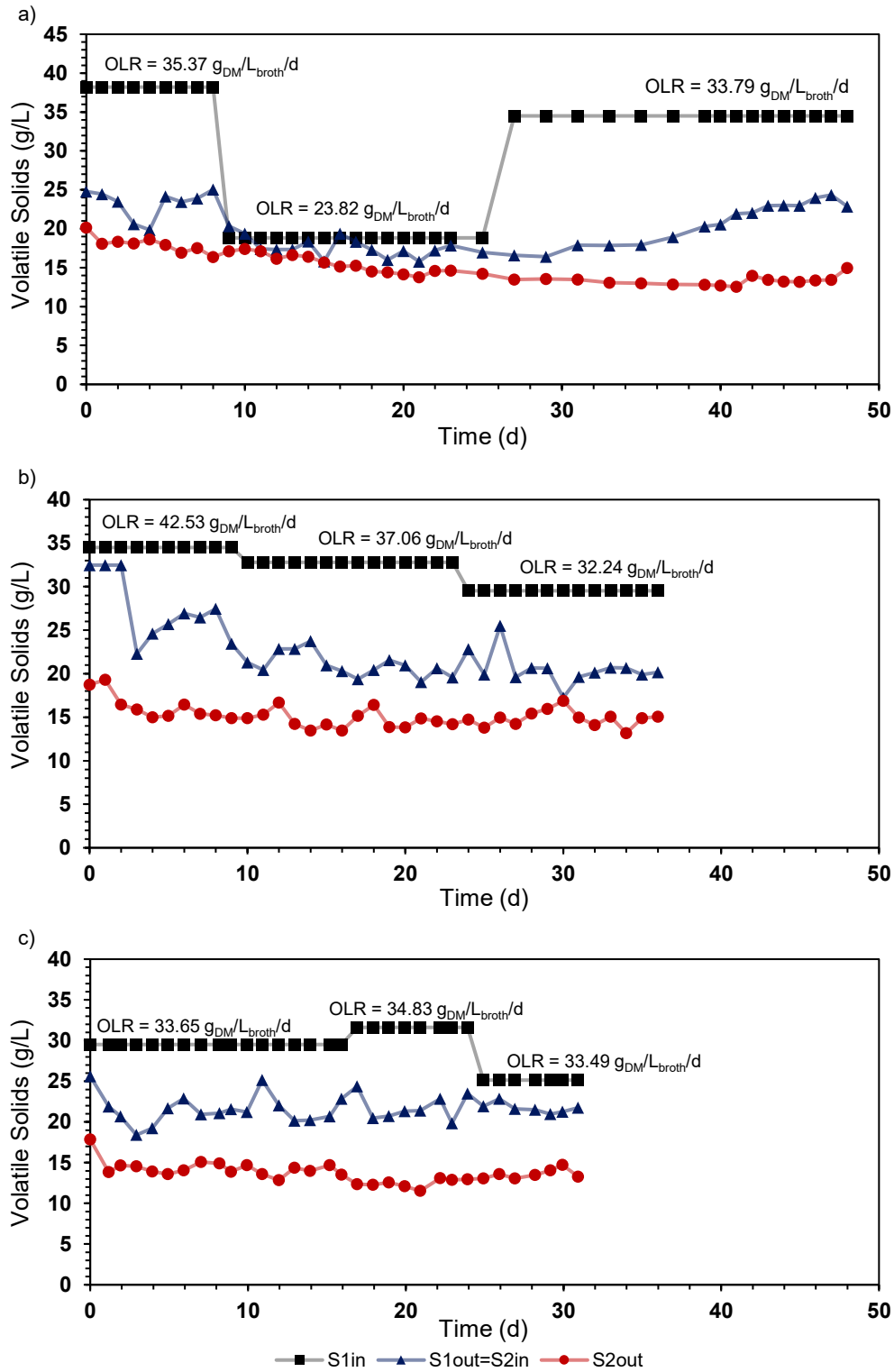


Figure 5.4 Behaviour of Volatile Solids concentrations under different HRT: **a) I**, **b) II** and **c) III**

5.3.2 H₂ and CH₄ production in S1 and S2 for different HRT

As previously mentioned, the produced energy was evaluated considering the energy produced under the form of H₂ and CH₄. To this end, the specific daily productivity $NL_{gas}/(L_{broth} \cdot d)$ was recorded for each stage (S1 and S2) for the tested conditions of HRT (I, II, III). The trends are presented in **Figure 5.5**, where the durations of the tests (3 cycles of each HRT condition for S2 and 30 cycles per HRT for S1) are reported on the time axis. Oscillatory behaviour can be observed for both reactors. The observed oscillations in the case of H₂ productivity are larger than CH₄, probably due to the larger feed variations, and are remarkable unstable under the three tested HRT. On the other hand, the CH₄ productivity presents a lower amplitude than H₂ but the oscillations are quite smooth, and the productivity appears almost constant at HRT = 15 days. The oscillation could be related to many different aspects, such as the dynamics of synergic interactions of the microorganisms and reactor phenomena.

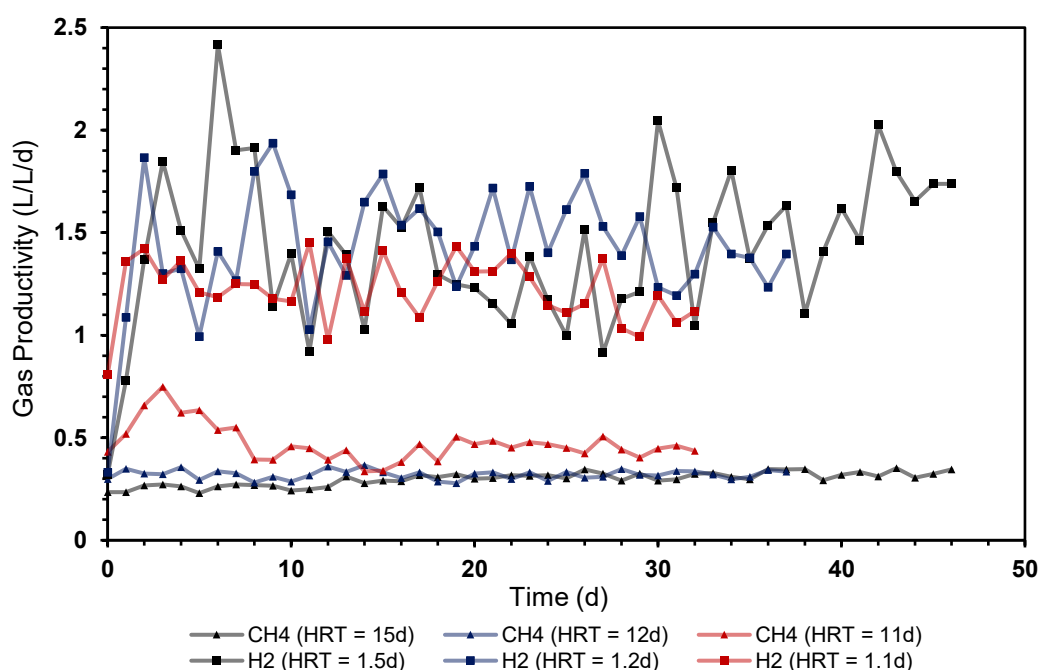


Figure 5.5 Specific H₂ (▲) and CH₄ (■) productivity at the different tested HRT

Since the consortia in S1 and S2 required different adaptation times, the specific growth rate of the microbiome depends on the microorganism's synergies, while other relevant reactor phenomena, such as the residence time, the circulation and mixing times in the vessel as well as the local viscosity and its temporal variations, could affect too the magnitude of oscillation in both bioreactors. As the experimental procedure evolved from I → II → III, the HRT is decreased, therefore the overall adaptation of the system should move towards case III. The mean H₂ productivity amounted to (1.437 ± 0.431) , (1.429 ± 0.291) and (1.219 ± 0.152) $L_{H_2}/(L_{broth} \cdot d)$, while for CH₄ it amounted to (0.299 ± 0.030) , (0.320 ± 0.019) and (0.471 ± 0.088) $L_{CH_4}/(L_{broth} \cdot d)$ for I, II and III HRTs, respectively. The relative

variability for H₂ productivity lay around 12-30 %, while for the case of CH₄ it was about 6-18 %, values which are within the previously reported range of experimental data [14]. Moreover, very complex higher-order phenomena such as those recalled above, could affect the oscillations in both S1 and S2, which are always observed in the case of full-plant scale AD, it is very difficult to provide an explanation for each case. However, it is possible to hypothesise that, in conditions where the system is operated for shorter HRT, these variations are likely to be more related to macroscopic operating conditions, such as: fluctuating OLR, differences between HRT and the microorganism retention time, non-ideal mixing conditions and the amplitude of the spatial gradients in the vessel. On the other hand, when the feed is replaced less frequently at longer HRT, the system could be dominated by microbiological behaviour, such as competition, selection among the microorganisms and metabolic shifts between different species present in both bioreactors. However, the role of the S1 as a pre-treatment step that is able to absorb, to some extent, the perturbations of the feed entering methanogenic bioreactor S2 can be observed from **Figure 5.5**. Given the difficulties to explain in detail the mechanisms that generate the oscillations, a macro-analysis is presented in the following section.

5.3.3 Statistical analysis of the TSAD in a pseudo-steady-state condition

A statistical analysis was conducted to analyse the oscillatory behaviour reported in **Figure 5.5**, even though the size of the sampling data is limited (i.e. about 30-50 points for each tested conditions). Conducting a stochastic analysis in the present context means studying the properties of random time series or, more precisely, of complex erratic phenomena. This includes the study of the mean, variance and correlation functions, as traditional measures of the properties of random data. When the time series are such that the variance and/or the mean diverge over the observation parameters, as occurs for the productivities reported in **Figure 5.5**, it is necessary to analyse the heterogeneity properties of a measurement by determining how the variance depends on the size of the units used to measure the time series. In other words, attention needs to be oriented towards the assessment of the temporal heterogeneity of the phenomena. A parameter that is able to give information on the intermittent increases and decreases in an activity or the frequency of an event is called *burstiness*. One of the measures of burstiness is: $FF = \sigma^2/M$ over a specified time scale, i.e. the ratio of the variance of the events over the mean value of the events that occur over a certain counting time, which is called the Fano Factor (FF). It is also called index of dispersion and was introduced by the Italian mathematician Ugo Fano in 1947 [23] to analyse the number of ions produced in a volume of gas by the absorption of such radiation.

The FF has recently gained popularity in a variety of applications in different fields [24], including genetics [25] and biochemical enzyme pathway predictions [26]. As far as physical significance is concerned, it is possible to argue that the lower the FF is, the more the system obeys a deterministic law i.e. when the noise

disturbance is low, the higher the FF, and the more the system is of a statistical nature, the greater the noise effects.

Although the average performance for each HRT tested condition (I, II and III) are presented in **Table 5.2**, the information about the oscillations within each cycle for the tested HRTs deserve a further consideration. In the present case, the FF was evaluated by computing the σ^2 of the spikes of productivity and the mean value (M) of the data reported in **Figure 5.5**. FF was evaluated for two situations: *i*) for the entire duration of the test in pseudo-state-state for each HRT reported in **Table 5.3** (i.e. based on the average performance of each HRT) and *ii*) for a single time interval of observation equal to one cycle of HRT for S2, for each tested HRT condition, for both S1 and S2, as shown in **Figure 5.6**.

Table 5.3 Fano Factor evaluate considering the total data for each HRT

$FF \times 10^2$	HRT I	HRT II	HRT III
<i>S1</i>	9.8541	6.0562	1.8761
<i>S2</i>	0.3625	0.1551	1.7216

As a first consideration, it is possible to see, from **Table 5.3**, that the FF for S2 for all the tested HRT is much lower than that of S1, meaning that methane bioreactor S2 is stabilised by S1, as a result of the lowering of the disturbance, due to the variations of the above quoted operative variables. A second consideration regards the selection of the operative HRT.

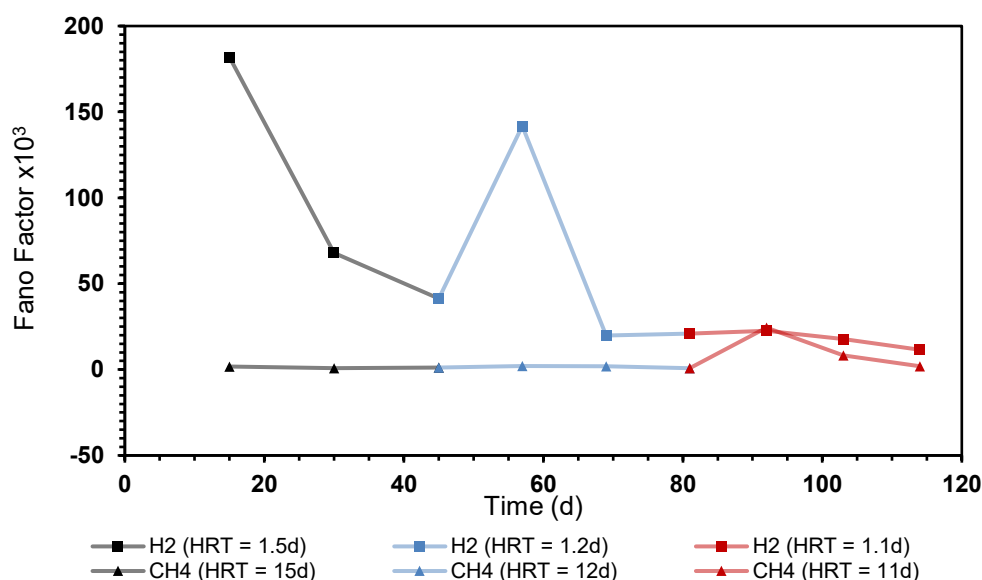


Figure 5.6 Fano Factor evaluated for each HRT unit time for the tested HRT I, II and III

As is possible to see from **Table 5.3**, as the HRT decreases from I to II and III, the stability of S1 increases, as can be seen from the decreases in FF. This means that the biohydrogen bioreactor could be operated even at $HRT < 1.1$ days. Instead, for S2, the stability increases from I to II and decreases from II to III; in fact, the

FF decreases from I to II, while it increases from II to III. This is a clear indication that $HRT = 12$ days could be the lowest acceptable HRT for the methanogenic bioreactor in TSAD using OMW as the feed. It should be pointed out that this value is about 1/3 or lower than the HRT used in a one-step AD (30-40 days), hence the volume of the vessel decreases as do the capital and operative costs. **Figure 5.6** shows the FF variations along the three tested HRT, which were evaluated at each time interval equal to the HRT for S2. From **Figure 5.6**, it is possible to argue that, after the occurrence of a perturbation it is necessary to wait for a time that is at least equal about 2 times HRT for the perturbation to be assimilated, as is possible to see for S2 for $HRT=11$ days, where the instability is smoothed out in the subsequent 2 HRT.

5.3.4 Energetic Performance of the TSAD

As a result of the different biological pathways that lead to hydrogen and methane production at a cellular level, the productivity (i.e. $L_{gas}/L_{broth}/d$) of H_2 in S1 is higher than that of CH_4 in S2, over the 4:1 to 5:1 range (see **Figure 5.5**). Considering that molar LHV_{CH_4} is more than 3.4 times greater than LHV_{H_2} , and that the volume of S2 is 10 times that of S1, the most important contribution to the overall energy production is the methanogenic one. The cumulative energy produced in S1 and S2 is shown in **Figure 5.7**; the slopes of the curves provide an estimation of the mean daily rate at which the energy is produced for each operative HRT, while the correlation coefficients (R^2) judges the goodness of the estimations. The daily energy production rate for methane is more than one order of magnitude higher than that of hydrogen. The CH_4 slope (MJ/day) increases as HRT decreases, probably due to the higher OLR, while the energy produced daily for H_2 is not affected significantly by the operative HRT. Although the CH_4 production shows a larger standard deviation (R^2) for condition III, due to the transition II \rightarrow III, this deviation is in agreement with the FF value of $1.72 \cdot 10^{-2}$ reported in **Table 5.3**. Finally, the III condition ($HRT=11$ days) produces more energy per day, but it is more unstable than the longer HRT.

Table 5.2 offers a compendium of the operative conditions tested along with the mean performance results obtained for S1 and S2 for the TSAD system. The share of H_2 that contributes to the overall cumulative produced energy represents only 12.15 % for I, 12.25 % for II and 7.6 % for III, and it can be estimated from the ratio of the slopes of the hydrogen and methane curves presented in **Figure 5.7**. Luo et al. [27] studied a TSAD with different HRT relations between S1 and S2, that is, of 3:14 and 1:14, and they achieved an energy recovery of H_2 accounting for 14 % of the overall energy, an outcome which is in agreement with the results of this work. The daily energy production data, presented in **Table 5.2**, represent the mean values, computed on a daily basis, and they therefore differ marginally from the slopes in **Figure 5.7**. In addition, from **Table 5.2** it is possible to see that TSAD is able to manage higher OLR than one-step-AD, which is of 3-4 gvs/(L·d), which is a very important aspect for the full-scale application [28].

In order to apply the energy performance evaluation procedure highlighted in **Section 5.2.8**, the experimental measurement of the *LHV* of OMW was used to determine the energy content of the substrate. In the biogas technology field, different methods have been proposed to evaluate the maximum amount of energy that can be obtained from organic wastes. The use of *LHV* values offers a more standard approach than BMP tests, which can be ambiguous as a result of the lack of a generally accepted standard measurement protocol [29] and due to the difficulties associated with the replicability of these tests, which can generate large uncertainties, which in some cases are beyond acceptable thresholds. Instead, the experimental evaluation of *LHV* follows a standard procedure that can be employed for any kind of fuel, of either a biological or chemical nature [30].

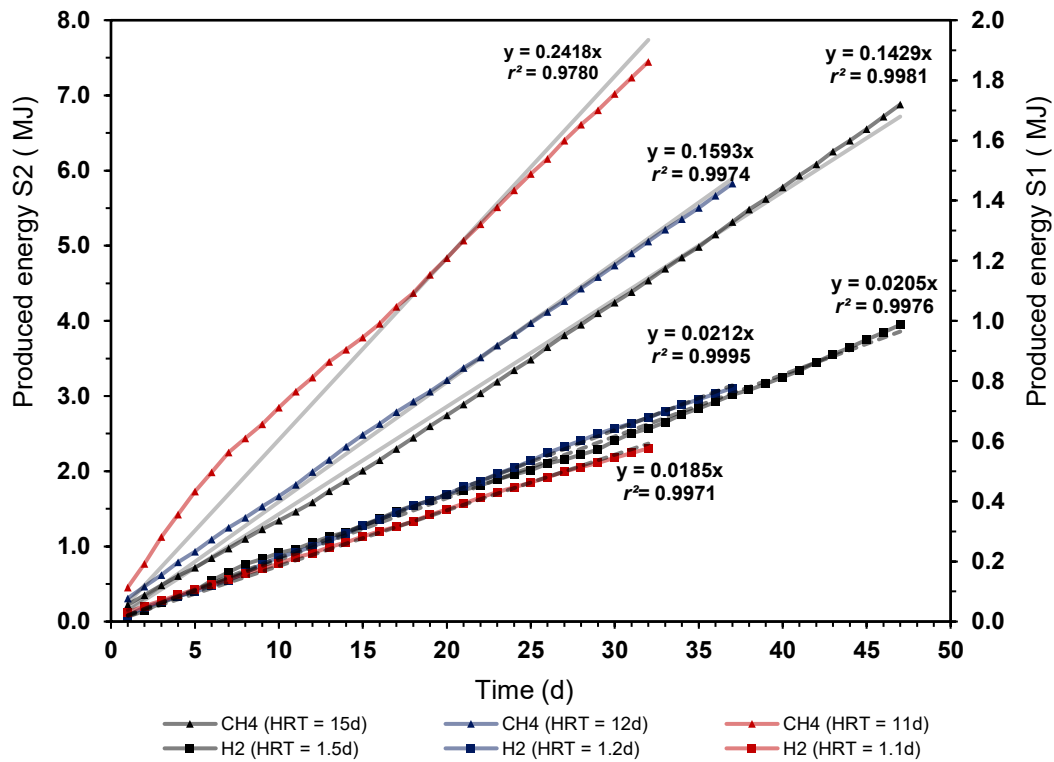


Figure 5.7 Cumulative energy production for the tested HRT

In fact, *LHV* has been related to the degree of reduction of biological systems [31] and different empirical correlations have been proposed to link *LHV* to the measurement of the chemical oxygen demand (COD) and to the DM or VS for sewage sludges [30]. The experimentally tested LHV_{OMW} was around 14,538 kJ/kg_{DM}, with a relative uncertainty of $\pm 10\%$, which was due to the fluctuations in the composition of the mixed collected fruit and vegetables, along with seasonal changes. The application of **Equation 5.3** led to the results of η reported in **Table 5.2** for each tested HRT. These results showed that the best energetic performance of the TSAD system was achieved at operative condition III, i.e. for the shortest *HRT* and the highest OLR for S2. As far as the efficacy ζ of the TSAD compared to the classic one-step AD is concerned, **Table 5.2** reports the results of the application of Equation 4, with reference values (**Equation 5.5**) of Ep_{AD} of 139.27,

192.67 and 188.55 (kJ/d) for I, II and III, respectively. From **Table 5.2**, it is possible to see that the quantity of energy produced in the TSAD process, even though affected by the different HRT conditions, is about 20% higher than that of one-step AD. The efficacy indicator quantifies the improvements, albeit only in terms of energetic performance. In fact, the lower bioreactor volume in TSAD, as a consequence of the lower HRT than in one-step-AD, also needs to be considered, as reported above.

Some authors have suggested that TSAD is not suitable for all substrates. Linder *et al.* [32] have recently tested TSAD for different feedstocks and concluded that it is more suitable for sugar-rich feeds. However, in their experimental set-up, it is difficult to understand whether a clear difference of HRT between the acidogenic and the methanogenic bioreactor was considered. HRT plays a fundamental role in ensuring the separation of microbiome HPB and HCB in S1, along with process parameters that should be controlled. The present experimental tests were conducted with OMW, which is a very complex feed containing carbohydrates, lignocellulose and other organic material, and the obtained results confirm that the microbiome in either S1 or S2 adapted well to the used materials as a substrate for the vital activities assure a stable bioenergy recovery. In addition, the obtained discharge water, used after a filtration of the S2 effluent to dilute the OMW feed in S1, certainly contained HCB microbiomes, albeit at low concentrations. Considering that no CH₄ was detected in the gas output stream from S1 means that the adopted strategy, mainly the kinetic selection of HCB and HPB, was effective in the separation of HCB microbiome in S1.

Table 5.4 Comparison among continuous TSAD systems from literature

Ref.	Substrate	Yield	OLR		HRT		Time ^a	Temp.		
		[NL/g _{vs}]		[g _{vs} /(L/d)]		[d]		[d]	[°C]	
		S1 (H ₂)	S2 (CH ₄)	S1 (H ₂)	S2 (CH ₄)	S1	S2		S1	S2
[33]	Food Waste	–	0.48	–	–	30	30	120	55	55
[34]	Swine manure + OMW	0.14	0.35	11.24	1.16	3	22	25	55	55
[35]	Food Waste	0.01	0.37 - 0.42	6.00 -15.00	2.00 - 5.00	4	12	-	55	55
[36]	Food Waste	–	0.31 - 0.61	–	0.81 - 4.84	1-5	5 -30	30	38	38
[37] ^b	Whey permeate	0.03 – 0.16	0.05 – 0.11	21.32 - 37.31	4.31 - 7.97	1	3	75	35	35
[38] ^b	POME	0.11 – 0.13	0.14 – 0.19	13.33 – 40.00	4.95 – 5.07	2	15	120	55	31
[39] ^b	POME	0.14	0.21	50	5.16	2	5	120	55	37
[40] ^c	Maize Silage	0.02 – 0.05	0.11 – 0.16	4.90 – 6.30	1.40 – 1.60	16.9	16.9	60	38	38
[41]	Food Waste	0.05 – 0.16	0.03 – 0.81	16.3	2.2 – 5.6	5	8-30	270	55	35
<i>This Study</i>	OMW	0.05 – 0.07	0.12 – 0.18	19.39 – 26.84	1.27 – 1.95	1.1-1.5	11-15	140	35	35

a) Overall testing time in days.

b) Data were converted from COD to VS using the mean composition given for the substrate.

c) The feed was semi-continuous, but both bioreactors were operated in continuous-mode.

Table 5.4 shows the results of this study compared with literature data. The study of TSAD literature selected for comparison purposes only considered tests pertaining to different organic substrates, and only in continuous mode. The study by [30] did not consider hydrogen production in the first stage, since no hydrogen was produced in their system under steady-state operation conditions, due to the

fact that both bioreactors were operated at the same HRT. It is interesting to note, in **Table 5.4**, that TSAD leads to flexibility, in terms of the variation of the organic substrate, that is, OLR and HRT, and that the obtained yields of hydrogen and methane depend on the substrate feed.

Finally, the process parameters for S1 and S2 are summarised in **Table 5.5**, where the experimental observations of this work and the choices made in order to guarantee the long-term stability of the TSAD process towards a scale-up procedure are pointed out. TSAD is a growing technology in the field of bioenergy production, but also for material recovery.

Moreover, it is gaining ground as one of the most interesting applications of MCE principles and it can help in the development of innovative processes designs. The separation of microbiomes occurs in continuous TSAD to some extent as a result of the different initial inocula, but the process parameters and stressors (or selective pressure) are also critical aspects for the stability and the performance of the system over the long term; therefore, linking biological knowledge with process engineering can offer an opportunity for sustainable solutions based on the emerging field of MCE.

Table 5.5 Suggested process parameters of the TSAD configuration for S1 and S2

<i>Process Parameter</i>	<i>S1</i>	<i>S2</i>	<i>Highlights</i>
T [°C]	35 - 55	35 - 55	<ul style="list-style-type: none"> • Mesophilic and Thermophilic operations are possible, even combinations of them; possible competition among mesophilic and thermophilic microorganisms • Convenience of energy-recovery should be carefully evaluated at thermophilic conditions
OLR [gvs/(L·d)]	1 - 40	1 - 5	<ul style="list-style-type: none"> • HPB are less sensitive than HCB to substrate inhibitions, therefore S1 consent operation at higher OLR • Indirect influence on the bioreactor volume
HRT [d]	0 - 3	10 - 20	<ul style="list-style-type: none"> • The choice of HRT should be based on the characteristic of the feed and growth kinetics of the microbiome for each stage • HRT can be scanned for particular substrates, but operation should maintain fixed HRT values to promote microbiome stability (HPB in S1 and HPB+HCB in S2)
Power Input [W/m ³]	100	50	<ul style="list-style-type: none"> • HPB are more sensitive to product inhibition (H₂) and therefore higher mixing is required (degassing) • HCB present a lower shear stress resistance than HPB • In S2, granules formation (HPB+HCB) is favoured at low mixing intensities
pH	5 - 6	7 - 7.5	<ul style="list-style-type: none"> • Optimal pH is different for S1 and S2 • Lower HRT in S1 can cause process instabilities due to shifts in pH and microbiomes (VFA acids accumulation and solvents production)
Red-Ox [mV]	+100 - (-200)	< - 330	<ul style="list-style-type: none"> • HPB can be either anaerobes or facultative aerobes, while HCB and especially methanogens are strictly anaerobes

5.4. Conclusion

The assessment of the energetic performance of the TSAD system is a laborious task, due to the considerable number of variables, such as feed variabilities (OMW), which is constituted by complex organic substrates, the inherent complexity of the biological systems of a mixed cultures and bioreactor spatial heterogeneities problems. The selection of the microbial consortia for S1 and S2, through an acidic treatment to enrich HPB, and the use of adequate stressors, mainly HRT based on the kinetic selection of the microorganism parameters were effective, as no CH_4 was found in the produced gas in the hydrogen reactor. The correct selection of the microbiome for each bioreactor of the TSAD is fundamental to maintain the performance of the system for a long operational time at full-scale. The choice to test the TSAD system for at least 3 cycles for each HRT condition of S2 proved to be useful, since S1 acts as a damping system, by ensuring a stable CH_4 production under steady-state conditions. A very low amplitude of oscillations and progressive reduction were in fact observed in the methanogenic bioreactor, as quantified by the Fano factor over time. As far as the stability analysis of the steady-state condition is concerned, $\text{HRT}=11$ days seems to be more unstable than $\text{HRT}=12$ days, and an even higher energy production resulted in the latter condition. In terms of energy production, Two-Step Anaerobic Digestion intended as a process to produce biohydrogen (Dark Fermentation) and biomethane (Anaerobic Digestion) resulted in about 20% more than one step-AD, while the rationalisation and optimisation of HRT could result in significant reductions of the volume (and costs). As concerns the CH_4 fermenter, which is the largest one, could be reduced to 1/3 or more, of the volume of a one-step AD. Finally, the managed OLR could be of 4-5 times that of one-step-AD. The present results are very promising for the full-scale application of TSAD, even though additional experimental tests are still necessary for various substrates.

References

- [1] EurObserv'ER, "Press Release: Biogas Barometer," Paris, 2017.
- [2] J. Ben-Iwo, V. Manovic, and P. Longhurst, "Biomass resources and biofuels potential for the production of transportation fuels in Nigeria," *Renew. Sustain. Energy Rev.*, vol. 63, pp. 172–192, 2016.
- [3] I. H. Franke-Whittle, A. Walter, C. Ebner, and H. Insam, "Investigation into the effect of high concentrations of volatile fatty acids in anaerobic digestion on methanogenic communities," *Waste Manag.*, vol. 34, no. 11, pp. 2080–2089, 2014.
- [4] Y. Liu and W. B. Whitman, "Metabolic, phylogenetic, and ecological diversity of the methanogenic archaea," *Ann. N. Y. Acad. Sci.*, vol. 1125, pp. 171–189, 2008.
- [5] Z. Bagi *et al.*, "Biotechnological intensification of biogas production," *Appl. Microbiol. Biotechnol.*, vol. 76, no. 2, pp. 473–482, 2007.
- [6] C. E. Gomez Camacho and B. Ruggeri, "Syntrophic Microorganisms Interactions in Anaerobic Digestion (AD): a Critical Review in the Light of Increase Energy Production," *Chem. Eng. Trans.*, vol. 64, 2018.
- [7] J. Bader, E. Mast-Gerlach, M. K. Popović, R. Bajpai, and U. Stahl, "Relevance of microbial coculture fermentations in biotechnology," *J. Appl. Microbiol.*, vol. 109, no. 2, pp. 371–387, 2010.
- [8] C. Koch, S. Müller, H. Harms, and F. Harnisch, "Microbiomes in bioenergy production: From analysis to management," *Curr. Opin. Biotechnol.*, vol. 27, pp. 65–72, 2014.
- [9] C. S. S. Oliveira, C. E. Silva, G. Carvalho, and M. A. Reis, "Strategies for efficiently selecting PHA producing mixed microbial cultures using complex feedstocks: Feast and famine regime and uncoupled carbon and nitrogen availabilities," *N. Biotechnol.*, vol. 37, pp. 69–79, 2017.
- [10] B. Ruggeri, T. Tommasi, and S. Sanfilippo, *BioH₂ & BioCH₄ Through Anaerobic Digestion: From Research to Full-scale Applications*. Springer London, 2015.
- [11] R. Łukajtis *et al.*, "Hydrogen production from biomass using dark fermentation," *Renew. Sustain. Energy Rev.*, vol. 91, pp. 665–694, 2018.
- [12] Z. Siddiqui, N. J. Horan, A. R. Sahito, J. Abdulkadir, and S. A. Memon, "Optimising the production of energy from coblended food waste and biosolids using batch reactor studies," *Water Environ. J.*, vol. 28, no. 4, pp. 483–489, 2014.
- [13] A. C. Luongo Malave, M. Bernardi, D. Fino, and B. Ruggeri, "Multistep anaerobic digestion (MAD) as a tool to increase energy production via H₂ + CH₄," *Int. J. Hydrogen Energy*, vol. 40, no. 15, pp. 5050–5061, 2015.
- [14] A. C. L. Malave, D. Fino, C. E. Gómez Camacho, and B. Ruggeri, "Experimental tests on commercial Sweet Product Residue (SPR) as a suitable feed for anaerobic bioenergy (H₂+ CH₄) production," *Waste Manag.*, vol. 71, pp. 626–635, 2018.

- [15] M.-K. H. Winkler, P. Boets, B. Hahne, P. Goethals, and E. I. P. Volcke, "Effect of the dilution rate on microbial competition: r-strategist can win over k-strategist at low substrate concentration," *PLoS One*, vol. 12, no. 3, pp. 1–12, 2017.
- [16] C. E. Gómez Camacho, F. I. Romano, and B. Ruggeri, "Macro approach analysis of dark biohydrogen production in the presence of zero valent powered Fe⁰," *Energy*, vol. 159, pp. 525–533, 2018.
- [17] B. Ruggeri, A. C. Luongo Malave, M. Bernardi, and D. Fino, "Energy efficacy used to score organic refuse pretreatment processes for hydrogen anaerobic production," *Waste Manag.*, vol. 33, no. 11, pp. 2225–2233, 2013.
- [18] E. Angelonidi and S. R. Smith, "A comparison of wet and dry anaerobic digestion processes for the treatment of municipal solid waste and food waste," *Water Environ. J.*, vol. 29, no. 4, pp. 549–557, 2015.
- [19] B. Ruggeri, T. Tommasi, and G. Sassi, "Experimental kinetics and dynamics of hydrogen production on glucose by hydrogen forming bacteria (HFB) culture," *Int. J. Hydrogen Energy*, vol. 34, no. 2, pp. 753–763, 2009.
- [20] American Public Health Association, American Water Works Association, and Water Environment Federation, "Standard Methods for the Examination of Water and Wastewater," *APHA*, 1999.
- [21] H. Veldkamp and H. Jannasch, "Mixed culture studies with the chemostat," *J. Appl. Chem. Biotechnol.*, vol. 22, pp. 105–123, 1972.
- [22] R. M. W. Ferguson, F. Coulon, and R. Villa, "Organic loading rate: A promising microbial management tool in anaerobic digestion," *Water Res.*, vol. 100, pp. 348–356, 2016.
- [23] U. Fano, "Ionization Yield of Radiations. II. The Fluctuations of the Number of Ions," *Phys. Rev.*, vol. 72, no. 1, pp. 26–29, 1947.
- [24] D. R. Cox and V. Isham, *Point Processes*. London: Taylor & Francis, 1980.
- [25] M. Thattai and A. van Oudenaarden, "Intrinsic noise in gene regulatory networks," *Proc. Natl. Acad. Sci.*, vol. 98, no. 15, pp. 8614–8619, 2001.
- [26] A. C. Barato and U. Seifert, "Universal Bound on the Fano Factor in Enzyme Kinetics," *J. Phys. Chem. B.*, vol. 119, no. 22, pp. 6555–6561, 2015.
- [27] G. Luo, L. Xie, Q. Zhou, and I. Angelidaki, "Enhancement of bioenergy production from organic wastes by two-stage anaerobic hydrogen and methane production process," *Bioresour. Technol.*, vol. 102, no. 18, pp. 8700–8706, 2011.
- [28] D. Deublein and A. Steinhauser, *Biogas from Waste and Renewable Resources: An Introduction*. Weinheim: Wiley, 2011.
- [29] G. Esposito, L. Frunzo, F. Liotta, A. Panico, and F. Pirozzi, "Bio-Methane Potential Tests To Measure The Biogas Production From The Digestion and Co-Digestion of Complex Organic Substrates," *Open Environ. Eng. J.*, vol. 5, no. 1, pp. 1–8, 2012.
- [30] C. Schaum, D. Lensch, and P. Cornel, "Evaluation of the energetic potential of sewage sludge by characterization of its organic composition," *Water Sci. Technol.*, vol. 73, no. 12, pp. 3072–3079, 2016.

- [31] C. Gary, J. Frossard, and D. Chenevard, "Heat of combustion, degree of reduction and carbon content: 3 interrelated methods of estimating the construction cost of plant tissues," *Agronomie*, vol. 15, no. 1, pp. 59–69, 1995.
- [32] J. Lindner, S. Zielonka, H. Oechsner, and A. Lemmer, "Is the continuous two-stage anaerobic digestion process well suited for all substrates?," *Bioresour. Technol.*, vol. 200, pp. 470–476, 2016.
- [33] B. Xiao *et al.*, "Comparison of single-stage and two-stage thermophilic anaerobic digestion of food waste: Performance, energy balance and reaction process," *Energy Convers. Manag.*, vol. 156, pp. 215–223, 2018.
- [34] M. A. Voelklein, A. Jacob, R. O' Shea, and J. D. Murphy, "Assessment of increasing loading rate on two-stage digestion of food waste," *Bioresour. Technol.*, vol. 202, pp. 172–180, 2016.
- [35] Y. Tan, X. Wang, and Y. Zheng, "Modeling and daily operation optimization of a distributed energy system considering economic and energy aspects," *Int. J. Energy Res.*, May 2018.
- [36] G. H. Wang, L. Wang, X. J. Tan, Y. X. Wang, and F. Wang, "Two-Phase Mesophilic Anaerobic Co-Digestion of Food Waste and Sewage Sludge: Effect of Hydraulic Retention Time," *Adv. Mater. Res.*, vol. 852, pp. 789–796, 2014.
- [37] M. Kisielewska, I. Wysocka, and M. R. Rynkiewicz, "Continuous biohydrogen and biomethane production from whey permeate in a two-stage fermentation process," *Environ. Prog. Sustain. Energy*, vol. 33, no. 4, 2013.
- [38] S. O-Thong, W. Suksong, K. Promnuan, M. Thipmune, C. Mamimin, and P. Prasertsan, "Two-stage thermophilic fermentation and mesophilic methanogenic process for biohythane production from palm oil mill effluent with methanogenic effluent recirculation for pH control," *Int. J. Hydrogen Energy*, vol. 41, no. 46, pp. 21702–21712, 2015.
- [39] S. Krishnan *et al.*, "Process enhancement of hydrogen and methane production from palm oil mill effluent using two-stage thermophilic and mesophilic fermentation," *Int. J. Hydrogen Energy*, vol. 41, no. 30, pp. 12888–12898, 2016.
- [40] P. C. Benito Martin, M. Schlienz, and M. Greger, "Production of biohydrogen and methane during semi-continuous digestion of maize silage in a two-stage system," *Int. J. Hydrogen Energy*, vol. 42, no. 9, pp. 5768–5779, 2017.
- [41] D. E. Algapani *et al.*, "Long-term bio-H₂ and bio-CH₄ production from food waste in a continuous two-stage system: Energy efficiency and conversion pathways," *Bioresour. Technol.*, vol. 248, pp. 204–213, 2018.

6. Energy Sustainability Analysis (*ESA*) of distributed H₂ production

6.1 Introduction

According to Georgescu-Roegen, the mastery of fire was one of the first promethean innovations of the human species [1]. Although for a long period there was strong scepticism about the influence of cooking in human and society evolution, nowadays the use of fire for cooking purposes is widely recognized since it not only made food more familiar and tasteful, but also safer to our organisms, decreasing the presence of pathogens, shaping the composition of gut microbiota and improving the quantity and quality of assimilated nutrients. Hence, it can be said that the use of fire in the early stages of human evolution increased the amount of available energy, which initially could be used for basic needs such as nourishment and heating (*endosomatic needs*) and later diverted to found and forge metals, substituting stone tools (*exosomatic needs*).

The real breakthrough that combustion represents is the exploitation of a phenomenon which resembles a naturally occurring one - aerobic respiration -, but at higher rate; the energy embedded in chemical bonds is transformed into heat (oxidised by atmospheric O₂) and creates a positive feedback loop which further triggers the reaction by supplying the activation energy to nearby combustible molecules. Although there are no absolutely perfect technologies, understanding the working conditions and the maximum potential that can be extracted is essential to determine their validity and range of application of them, and is of utmost importance when sustainability is concerned. For example, aerobic respiration and combustion could only be possible after the Great Oxidation Event, where the composition of the terrestrial atmosphere significantly changed from water vapor, sulphur compounds, hydrogen and methane to a nitrogen- and oxygen- rich atmosphere probably due to multiple factors affecting the fluxes within geochemical and biogeochemical cycles, giving rise to the proliferation of eukaryotic and multicellular organisms [2].

The next technological milestone in the development of current patterns of energy use and the exosomatic societal energy-dependence was the industrial revolution, where the energy of coal combustion is seized in steam-engines, generating physical work. Steam engines eventually evolved into steam turbines, which coupled to generators started the revolution of one of the most versatile and expensive commodities that modern society uses to supply energy services, electricity. However, even from the nineteenth and early twentieth century the

question of societal patterns of energy consumption and energy efficiency has been raised by different authors [3][4][5][6].

During the last decades, there has been an accelerated growth in human exosomatic energy consumption, which is reflected as an increasing pressure on the energy sector. In general terms, the stages of energy life can be described as: *i) primary energy*, which is a resource extracted from the ground, sun, air, sea (i.e. primary energy sources), which can be converted into *ii) secondary energy*, as energy carrier to be transported or stored, until finally distributed to consumers as *iii) final energy*. At the end-use, other technologies convert the delivered useful energy into energy services such as food production, mobility, heating, cooling, lighting, among others (see **Figure 6.1**).

PRIMARY ENERGY	SECONDARY ENERGY	ENERGY SERVICES
<p>Non-renewable: (fossil and nuclear)</p> <ul style="list-style-type: none"> • Coal • Natural Gas • Nuclear • Oil • Oil Sands • Oil Shale • Shale gas <p>Renewable: («clean» sources)</p> <ul style="list-style-type: none"> • Biomass • Geothermal • Hydroelectric • Solar • Tidal • Wind 	<p>Energy Carriers & Storage Systems</p> <ul style="list-style-type: none"> • Chemical: <ul style="list-style-type: none"> ☐ Fossil Fuels ☐ Biofuels ☐ Synthetic fuels • Electrical and electrochemical: <ul style="list-style-type: none"> ☐ Batteries ☐ Supercapacitors ☐ Fuel Cells • Mechanical: <ul style="list-style-type: none"> ☐ Flywheels ☐ Compressed Air ☐ Pumped Hydropower • Thermal: <ul style="list-style-type: none"> ☐ Liquid Storage ☐ Phase Change ☐ Molten Salts ☐ Cryogenic Storage ☐ Pumped Heat 	<p>Societal Needs</p> <ul style="list-style-type: none"> • Food Industry • Water Supply • Ambient conditioning • Chemicals production • Materials production • Chemicals and Materials transport • Mobility, public and private transportation • Goods production, assembly and transport • Lightening • Communications • Construction • Appliances • Research • Education • Waste Management • Entertainment

Figure 6.1 Life stages of energy in our modern society: from primary energy to energy services

However, an important aspect that plays a fundamental role in the modern energy scenario is decarbonization. The use of fossil fuels in thermoelectric plants or for transportation purposes is associated with a constant emission of CO₂, which is currently tackled to be reduced at all costs. One of the most recurrent proposals is the complete electrification of energy services. This solution, although at first sight seems quite evident and adequate, requires a more careful analysis to evaluate its effectiveness and avoid indirect CO₂ emissions, which can ultimately lead to an unsustainable scenario. One of the most interesting proposals, which has been on the table for more than twenty years is the question of hydrogen. Hydrogen has been under continuous investigation due to its potential to be a key player in the energy transition, mainly because of the versatility of this energy carrier, which can be potentially be integrated in different areas such as power generation, transport, heating, fuel-cell electric vehicles, energy storage, among others.

On the other hand, and contrary to fossil fuels, molecular hydrogen (H₂) is not present in large deposits in the earth's crust, nor is it found in significant concentrations in the atmosphere. Even though H₂-reservoirs have recently been

discovered with relatively high concentrations of entrained hydrogen in different basements and sediments [7], the majority of the hydrogen used nowadays (>90%) is produced from fossil fuels, mainly via reforming of liquid fuels or natural gas and coal gasification and in a lesser proportion (<10%) from water electrolysis and from biomass sources.

An important part of shaping the future energy services outlook is the required and/or proposed technology involved in each life stages of energy. As mentioned above, the future networks are likely to include not only the production of distributed power from mixed primary sources, but also to combine different technologies for storage, avoiding unnecessary steps which ultimately reduce the overall efficiency. The monitoring of these technologies used to harvest primary energy and the successive transformations are required to delivery efficient energy services is fundamental for a transition which is really in line with the precepts of sustainable development. Although sustainability's pillars stress the need to balance the pressure on the environment with profitable solutions which have positive effects on the human population, *energy sustainability* should be evaluated *in primis* due to its hierarchical importance in the quantification of the useful energy that can be diverted from societal uses into sustainable innovations and policies. Unlike other industrial processes, energy-production processes require a more detailed study, since an approach similar to the quantification of emissions (CO₂, CO, NO_x, CH₄, etc), typically assessed using environmental indexes via Life Cycle Assessments (LCA) as, for example, Global Warming Potential in equivalent CO₂ units at a fixed period, is not consistent with the methodology of energy sustainability. Industrial processes can be classified and compared considering as benchmark the amount of emitted and/or captured CO₂, which can result ultimately in a positive or negative net balance according to the boundaries and methodology of analysis; while for the sustainable energy-production processes the balance should be always positive.

In this context, there has been a growing interest in evaluating the net energy production of renewable and non-renewable sources. One of the most extended approaches proposes the calculation of different indicators, which are often used in economic analysis, but adapted to energy flows. For example, different authors have proposed the use of the EROI (Energy Return on Invested) criteria, which relates the amount of produced energy to the total invested energy, to score energy production processes, using different system boundaries (i.e. society, *point-of-use*, extended) [8]. Other important sustainability parameter is the Energy Payback Time (EPT), which indicates the time framework that a particular technology requires for the compensation of the energy diverted for its construction and/or assembly.

EROI has been used as a common ground for the comparison of fossil fuels and renewable energies [9], it has been linked to societal welfare and development [10][11][12], it has been revisited in the light of the Peak-Oil paradox [13], it has been hypothesized to be key driver of biological evolution [14] and, recently, it has been proposed by the International Energy Agency (IEA) in the methodology for the Net Energy Analysis of Photovoltaic Systems [15]. However, there is still much debate about the correct use of energy units and its respective weighting factors

when analysing complex systems involving the use of electric power, heat and chemical energy, as well as discriminating among primary energy sources [16]. In any case, it is clear that energy sustainability evaluation is a concern which is currently under revision worldwide due to its importance for the current and future energy scenarios. In this respect, Ruggeri et al. [17] developed a methodology which is useful for the evaluation of the *energy sustainability* of energy producing processes, combining in the Fuzzy domain different deterministic indicators, such as EROI and EPT.

The present work aims at evaluating the energy sustainability of three different technological choices: *i*) Steam-Methane Reforming (SMR), *ii*) Solar-Powered Water Electrolysis (SPWE) and *iii*) Two-Stage Anaerobic Digestion (TSAD), using experimental data collected over long experimental campaigns, for the production of hydrogen at “*the point of use*” (i.e. distributed hydrogen production).

6.2 Methodology

6.2.1 Energy Sustainability Analysis (ESA)

As previously introduced in [17], the methodology for *ESA* for different technologies is based on the concept of viability, resembling the feature of living organisms of harnessing energy to sustain and reproduce themselves. In this context, a viable technology or an energy sustainable technology for energy production/recovery should be able to produce an energy surplus, *useful energy*, sufficient to cover direct and indirect energy costs of the technology and yield back a surplus to society. Hence, the *ESA* is of utmost importance in the context of energy recovery or production process, where the gross produced or recovered energy is contrasted with the direct energy expenditures on site and/or to the indirect energy, which is the share of diverted energy from society (off-site) to provide the materials flow and services. In order to quantify all energy fluxes, a Life Cycle Assessment (LCA) approach is used, setting proper boundaries of analysis. Moreover, since the *ESA* seeks the evaluation of a technology, a bottom-up approach is adopted to quantify the overall performance of each system under analysis, compiling the necessary data and expressing energy flows in terms of consistent functional units.

6.2.2 Boundaries of analysis

One of the most critical aspects of sustainability studies, such as Life Cycle Assessment (LCA), is the boundaries of analysis and correspondent adopted approach. The boundaries of analysis must be well defined and should be in line with the purposes of the study in question.

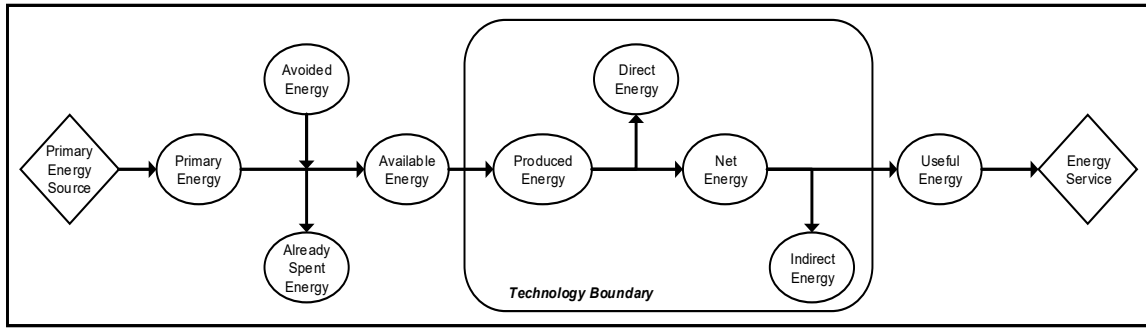


Figure 6.2 Analogical Model (AM) used to simplify the energy fluxes of each technology

The present methodology of energy sustainability uses the Analogical Model (AM), where the key energy fluxes are located. The *ESA* includes the technological boundaries, in order to assess the internal use of energy of the given technology, but also tracks the external energy flows which go through the technological boundaries. Moreover, the methodology of *ESA* can also be used to rationalize the Materials Input (MI) and energy intensity that a specific technology requires, to monitor its intrinsic energy performance. The most relevant energy flows are depicted in the AM in **Figure 6.2**.

6.2.3 Energy Sustainability Index (ESI)

After the process is studied in general terms, the first indicator of interest is the *Energy Sustainability Index* (ESI). This Index is dimensionless, since it is expressed as an energy quotient that aims to compare, in a first screening, two physical energy quantities: the produced energy (E_{prod}) and the spent direct energy (E_{dir}). In the case that system under analysis comprehends additional relevant energy fluxes, such as *already spent energy* and/or *avoided energy*, these quantities should be either subtracted or added to the E_{prod} (**Equation 6.1**).

$$ESI = \frac{E_{\text{prod}} - E_{\text{already spent}} + E_{\text{avoided energy}}}{E_{\text{dir}}} \quad (6.1)$$

The ESI indicator is useful to discriminate between technologies at different stages of development, even at the infancy level. Obviously, for an accurate calculation, it is necessary to use the values that correspond to average or steady-state operation conditions, or it can be done as well in different time points if there are significant variations in the energy output or the energy requirements of the process. That is, if a technology requires a growing flow of direct energy for maintaining a relative constant energy production, as it advances in its useful life, (i.e. besides the energy expenditures for maintenance) the ESI value will not be constant but will decrease over time.

In the first instance, for energy production and/or recovery processes, the ESI index should be greater than one ($ESI > 1$). For other types of processes, where in addition to energy production there are also material flows involved, ESI could be less than one, but for both cases it represents the aforementioned relationship

between energy flows. Although the units might seem inconsistent, i.e. due to the sum of direct energy flows either from thermal and electrical nature, the purpose of the ESI is analogous to the economic parameter cash flow, but presented in terms of relationship and not as a net term, which does not differentiate between types of energy (i.e. all physical quantities of energy) and serves to assess, in a first scan, the energy sustainability of the process.

For example, a water boiler which consumes electricity and produces heated water. This is an energy service (heated water) rather than an energy production process. However, the direct energy which is used comprehends the energy which is given for the flow of water (i.e. using pumps) and the energy for the electric resistance. The calculation of the ESI would therefore require the assessment of the produced energy (i.e. thermal energy absorbed by the water) and the direct electricity expenditures. While the efficiency indicator would represent the fraction of the maximum attainable heat exchange which actually occurs, the ESI in this case would reflect the intrinsic use of energy of the water boiler and serve for comparing purposes with substitute technologies and/or process configurations.

6.2.4 Analogical Model (AM)

The following step in the *ESA* is the rationalization of all energy flows that are present in the process/technology under analysis, besides the *direct energy* flux and *produced energy*, which are used in the calculation of the ESI. Following [17], a suitable way to perform this step is through the use of the AM, used typically in LCA studies, combined with a bottom-up approach. The AM comprehends a careful look at the process, within the chosen boundaries, to calculate the different components of the indirect energy (E_{ind}) as shown in **Equation 6.2** and in **Table 6.1**.

$$E_{ind} = \sum_{i=1}^n E_{ind,i} \quad (6.2)$$

Some of these terms, presented in **Table 6.1**, are difficult to estimate; the importance and weight strongly depend on the process under analysis and the chosen approach. However, useful recommendations are found in [18]. An exhaustive study should therefore include the relevant flows of energy, chemicals and materials, which are generally monitored (i.e. through mass balances or input-output accounting) but is also necessary to express these terms as energy costs, which is the scope of the *ESA*. These energy fluxes can be calculated using tabulated Cumulative Energy Demand (CED) values and estimating the total mass of required materials and chemicals (i.e. m_{chem} and m_{mat} , respectively) over the useful lifetime of the plant, as follow:

$$E_{chem} = \sum_{i=1}^n CED_i \cdot m_{chem,i} \quad (6.3)$$

$$E_{mat} = \sum_{i=1}^n CED_i \cdot m_{mat,i} \quad (6.4)$$

Through the AM, each component can be identified and quantified, detecting limiting steps and also allowing rational modifications, substitutions or improvements of the process.

Table 6.1 Relevant components of the *indirect energy* (modified from [18]).

x_i	Description
E_{chem}	Indirect energy used to produce the <i>chemicals</i> of the process
E_{mat}	Indirect energy used to produce the <i>materials</i> of the process
$E_{ind\ to\ prod\ edir}$	Indirect energy used to produce the <i>direct energy</i> of the process
E_{maint}	Indirect energy used for <i>maintenance</i> purposes
E_{labour}	Indirect energy used to sustain the <i>human labour</i>
E_{constr}	Indirect energy used for <i>construction</i> purposes
E_{decomm}	Indirect energy used for <i>decommissioning</i> purposes
E_{amort}	Indirect energy allocated for the <i>amortisation</i> of a future similar facility

One of the most critical factors is the energetic footprint of materials and chemicals. Even though materials enter the system as “matter”, its production and/or assembly also has an energetic cost; i.e. a share of the societal *useful energy* was devoted for its construction, in some cases at different geographical locations.

For example, an installed solar panel in Germany but produced in China, has an energetic burden to society in terms of *useful energy* that should be able to repay the initial construction cost and produce an additional surplus, whose energy sustainability can be assessed through the *ESA*. However, in monetary terms, the differences also include the disparity in salaries and services costs between the two countries, which can be misleading in certain sustainability studies.

A difficult term to evaluate, which integrates the different dimensions of sustainability, is the energy used to sustain human labour (E_{labour}). The consumption of energy by human force corresponds, first of all, to food (i.e. daily endosomatic human energy requirement ~ 10 MJ, while the Cumulative Energy Demand is 5-10 MJ_{eq}/MJ_{food} [19]). However, in energy-producing facilities, human capital and its energy consumption tend to be very low compared to the other relevant energy fluxes. Only if an energy production plant is not even able to pay, in energy terms, the energy quota corresponding to the food of its workers, it will hardly deliver an extra benefit for society. In addition, the E_{labour} not only includes the food provided to workers, but also energy services necessary for the correct performance of the required tasks, i.e. heating, air conditioning, transportation, ventilation, uniforms, etc.

Another important term, and that is fundamental for the present methodology for the study of the *vitality* of energy production processes, is the term E_{amort} . This energy contribution is assumed to correspond to the sum of the E_{mat} and E_{chem} and serves to amortise, over the useful life of a technology, a similar plant that replaces it at the end of its useful life. In this sense, the *ESA* for a specific technology aims to establish not only the net energy balance taking into consideration the direct and indirect energy expenses, but also the continuity of the supply of energy services at societal level, which can only be assured if part of the produced energy is stored for the production of the necessary materials and chemicals to reproduce a similar plant, possibly with higher energy efficiency.

6.2.5 Energy Return on Invested (EROI) and Energy Payback Time (EPT)

The final phase of the *ESA* includes the calculation of two indicators that are very important to understand the relationship of energy flows, Energy Return On Investment (EROI) and Energy Payback Time (EPT). Once the AM has been constructed and the indirect energy has been quantified, two relevant derived energy fluxes can be calculated:

$$E_{net} = E_{prod} - E_{dir} \quad (6.5)$$

$$E_{useful} = E_{net} - E_{ind} \quad (6.6)$$

which can be used for the calculation of EROI and EPT, as follow:

$$EROI = \frac{E_{net}}{E_{ind}} \quad (6.7)$$

$$EPT = \frac{E_{ind}}{\frac{E_{net}}{n}} \quad (6.8)$$

The EROI (**Equation 6.7**) is the ratio between the *net energy* (**Equation 6.5**) and the indirect energy, whose particular components were discussed previously in **section 6.2.4**. In order to calculate the EPT (**Equation 6.8**), it is necessary to compare the total indirect energy to be used in the useful life of the plant to the average annual rate of net energy production, in order to determine the time (i.e. years, months, etc.) that will take the system under analysis to repay the indirect energy that was diverted from other societal purposes for its construction and operation.

6.3 Case study: distributed H₂ production

The case study under analysis is the production of distributed hydrogen, using three different technologies, and the comparison of the energy sustainability of each them. The collected data for each case corresponds to long experimental campaigns, which assessed the performance of the systems, the materials and chemicals input, the relevant outputs, the energy expenses and monitored the key parameters that are required to perform an energy sustainability analysis.

6.3.1 Steam-Methane Reforming (SMR)

A general flow diagram of the SMR systems is depicted in **Figure 6.3**. The experimental tests were conducted in an Ultraformer compact fuel processor unit

(Catator AB, Lund, Sweden), whose design allows flexible feeds, either gaseous such as biogas, natural gas and methane or liquids fuels as liquified petroleum gas, naphtha, methanol and ethanol.

Table 6.2 Reactions of interest for each section of the Ultraformer

<i>Combustion Reaction (CATBUR)</i>	$\text{CH}_4 + 2\text{O}_2 \rightarrow \text{CO}_2 + 2\text{H}_2\text{O}$
<i>Reforming reaction (SREF)</i>	$\text{CH}_4 + \text{H}_2\text{O} \rightarrow \text{CO} + 3\text{H}_2$
<i>Water-Shift reaction (WGS)</i>	$\text{CO} + \text{H}_2\text{O} \rightarrow \text{CO}_2 + \text{H}_2$
<i>Oxidation reactions (PROX)</i>	$\text{C} + \text{O}_2 \rightarrow \text{CO}_2$
	$2\text{CO} + \text{O}_2 \rightarrow 2\text{CO}_2$
	$2\text{H}_2 + \text{O}_2 \rightarrow 2\text{H}_2\text{O}$
	$\text{CH}_4 + 2\text{O}_2 \rightarrow \text{CO}_2 + 2\text{H}_2\text{O}$

The system comprehends four wire mesh catalytic units, integrated in a compact block, to carry out the process of SMR:

- I. Catalytic Burner (CATBUR), where methane is fed from a gas cylinder (i.e. high purity > 99.995 % mol/mol) and mixed with air, in an excess of O_2 of 50-60 % of the stoichiometric ratio, to provide the temperature conditions of the highly endergonic reaction of steam-reforming,
- II. the proper Steam-REFormer (SREF); water or water vapor are mixed with methane, and the steam-reforming reaction takes place (see **Table 6.2**) using the heat produced in the burner ($\Delta H_{\text{reaction}} = +206 \text{ kJ/mol CH}_4$);
- III. the output gases are then sent to the Water-Gas Shift (WGS) reactor, where carbon monoxide is further oxidized to carbon dioxide; water is required for this step as a reactant and as cooling agent due to the temperature differences with the previous units (i.e. based on the thermodynamic requirements, $\Delta H_{\text{reaction}} = -41 \text{ kJ/mol CO}$),
- IV. the final unit is the Preferential Oxidation unit (PROX), which aims at oxidizing some of the reaction by-products of the previous stages into CO_2 , in order to meet the gas output stream specifications. This unit requires air input (O_2) and cooling water and it is composed by two sections (PROX1 and PROX2), which operate at different temperatures, in the range 125-130 °C and 100-105 °C, respectively.

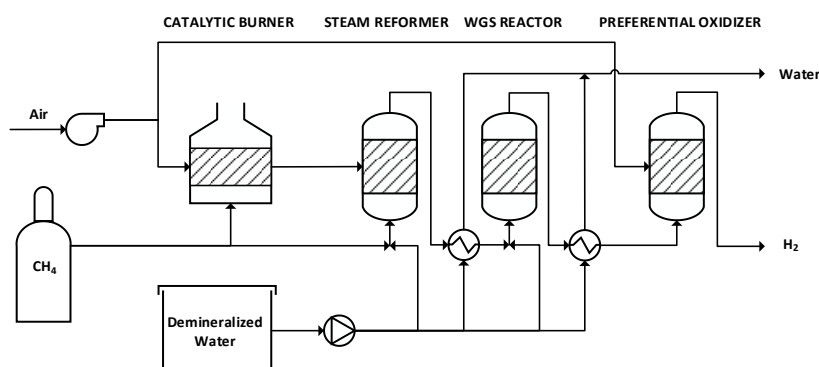


Figure 6.3 Simplified flow diagram of the Steam-Methane Reforming (SMR) process

Other process configurations often include pre-treatment units, such as hydrodesulfurization, to remove impurities prior to the SMR, while others also include in the downstream phase NO_x and CO₂ capture units, which in the experimental set-up under analysis were not present since the feed to the system was high purity grade methane.

Table 6.3 Collected data from the Ultraformer.

	CATBUR	SREF	WGS	PROX
<i>Dimensions [cm]</i>	10x10x10	23x8x8	13x7x10	7x4x10 8x5x10
<i>Catalysts mesh [cm]</i>	7x7	7x30	7x7	7x7 7x7
<i>Catalysts [% w/w Me]</i>	Pd5%/Al ₂ O ₃	Pt5%/Al ₂ O ₃	Pt5%/ZrO ₂	Rh5%/Al ₂ O ₃
<i>Working Temperature [°C]</i>	900-920	360 - 645	390 – 440	105 – 125
Chemicals Flow				
<i>CH₄ [NL/min]</i>	6.000	16.000	-	-
<i>Air [NL/min]</i>	107.000	-	-	7.500
<i>Demineralized water [L/min]</i>	0.051	-	0.024	-

6.3.2 Solar-Powered Water Electrolysis (SPWE)

The second technology which was tested for the production of hydrogen consists in a combined system of photovoltaic panels and water electrolyser. The photovoltaic system is composed by commercially available photovoltaic cells (Sunways Plus, Anhui Sheng, China), placed in a wave-form array to optimize the capture of solar radiation at the Environment Park of Turin (Italy; 45°05'14.1"N 7°40'25.7"E).

The support consists in a triple-glazed double-glass (i.e. glass thickness 22mm; 80 kg/m² max. wind load and 190 kg/m² max. snow load) semi-transparent structure covering c. 190 m², containing 160 modules of 100x100 mm polycrystalline cells (i.e. 78 cells per module). The PV modules are arranged in 8 parallel strings; Solar Irradiance (SI) is measured at the bottom, therefore proportional values of SI were estimated through the ratio of the curvature, dividing the total area in five key strings as presented in **Table 6.4**.

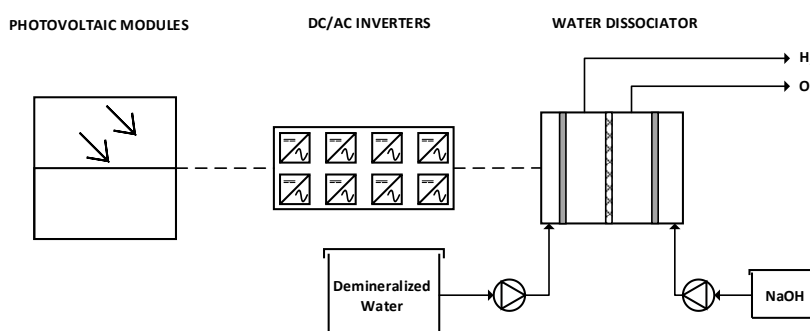


Figure 6.4 Simplified flow diagram of the Solar-Powered Water Electrolysis (SPWE) process

The DC output from the photovoltaic modules is connected to a series of eight inverters (SMA Sunny Boy 1700E, Niestetal, Germany) in order to convert the DC

to AC, which is fed directly into the Water Dissociator (Idroenergy Spa. 3.7, Livorno, Italy), a general diagram of the system is shown in **Figure 6.4**.

Table 6.4 Curvature-weighted Irradiated Surface for each string of the PV array

String	Curvature [m ⁻¹]	Curvature ratio [%]	Irradiated Surface [m ²]
I	0.057107	59.86	23.75
II, III	0.058582	61.41	47.50
IV, V	0.044705	46.86	47.50
VI, VII	0.094688	99.26	47.50
VIII	0.095393	100.00	23.75

Coupling PV power generation to water electrolysis is difficult due to variations in the daily and seasonal SI; this produces a variable power output from the PV modules and leads to underutilization of the capacity of the electrolyser, which is supplied ultimately by grid electricity (**Figure 6.5**).

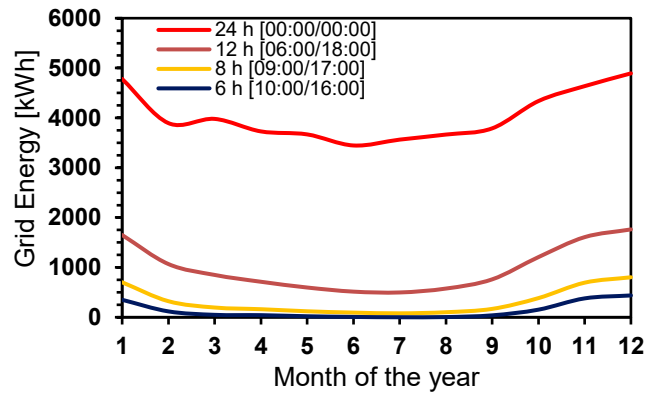


Figure 6.5 Monthly grid power demand for the operation of the electrolyser, considering different operation time slots of operation.

Hence, the components of the experimental set-up were carefully selected; the maximal nominal power of the electrolyser is c. 80 % of the maximum output from the photovoltaic arrange, further technical data of the main equipment can be found in **Table 6.5**.

Table 6.5 Technical Specifications and dimensions of the main equipment of the SPWE system

PV cells		Inverter		Water Dissociator	
Dimensions					
Size [mm]	801x1491	Size [mm]	434x295x214	Size [cm]	115x95x140
Weight [kg]	66	Weight [kg]	25	Weight [kg]	420
Units [-]	160	Units [-]	8	Units [-]	1
Technical Specifications					
Power - P_{MPP} [W]	102.2	$P_{AC, nominal}$ [W]	1500	$H_2 Flow_{MAX}$ [Nm ³ /h]	2.47
Voltage - U_{MPP} [V]	18.9	$P_{AC, max}$ [W]	1700	$O_2 Flow_{MAX}$ [Nm ³ /h]	1.23
Current - I_{MPP} [A]	5.4	Harm. Dist. Max [%]	< 4 %	Pressure _{MAX} [bar]	1.80
$V_{Open\ Circuit}$ [V]	23.4	Output Voltage - V_{AC} [V]	198 - 251	Gas purity [%]	≥ 99.5
$I_{Short-Circuit}$ [A]	5.8	Frequency _{Output} - f_{AC} [Hz]	49.8 - 50.2	Consumption _{MAX} [kW]	13.5
		Max. efficiency – η_{MAX}	≥ 93.5	Supply Voltage _{AC} [V]	400
		Power Consumption [W]	< 5	Frequency [Hz]	50 - 60
		Power _{Stand-by} [W]	< 0.1	Distillated Water _{MAX} [L/h]	2.20
				Electrolyte Solution [L]	25
				Electrolyte [% w/w]	18 NaOH

6.3.3 Two-Stage Anaerobic Digestion (TSAD)

Finally, the third technology belongs to the biotechnological field and is the utilization of a Two-Stage Anaerobic Digestion (TSAD) system for the production of bio- H_2 and bio- CH_4 , using organic waste as feed. The flow diagram of the system is presented in **Figure 6.6**; the process configuration comprehends two CSTR operated in series. The experimental data (i.e. yield and optimal parameters) was collected using a laboratory setup composed by a Minifors I bioreactor (Infors HT, Bottmingen, Switzerland) for bio- H_2 production and a Chemap fermenter (Chemap AG, CH-8708, Manedorf, Switzerland), for bio- CH_4 production with a working volume ratio of 1:10. Both bioreactors were inoculated with adequate microbial consortia for the optimize production of each biofuel; the tested substrate was the Organic Fraction of Municipal Solid Waste (OFMSW).

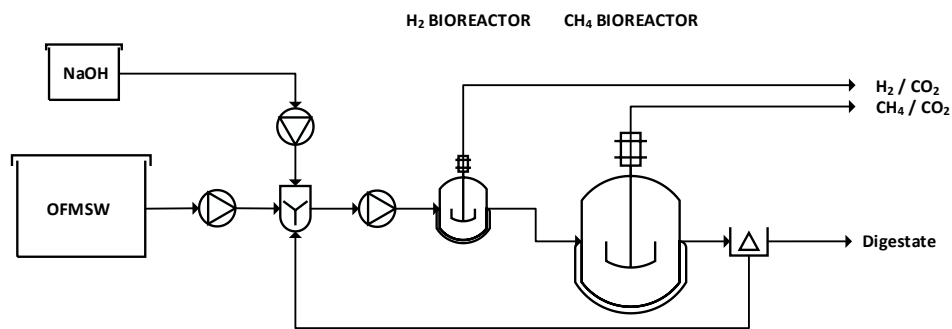


Figure 6.6 Simplified flow diagram of Two-Stage Anaerobic Digestion (TSAD) process

In order to perform a more adequate comparison, the obtained yields in laboratory scale (see **Table 6.6**) were used as design specifications for a system whose production is comparable to the other technologies tested for the present case study (i.e. in the range 10 -20 kW H_2), following the procedure presented in [20][21] (see **Table 6.7**).

Table 6.6 Performance of the laboratory TSAD using OFMSW as feed

	H_2 - bioreactor	CH_4 - bioreactor
Working Temperature [°C]	35.0	35.0
Mean Ambient temperature [°C]	13	13
Power input, pre-treatment [kW/m ³]	0.2	-
Power input, mixing [kW/m ³]	0.1	0.20
Mixing application time [h/h]	1/1	0.25/1
Hydrogen potential [NL _{H₂} / kg _{DM}]	79.04	-
Methane potential [NL _{CH₄} /kg _{DM}]	-	247.32
Hydraulic Retention Time [d]	2	15
Mean gas composition [%]	CH_4 : < 1 CO_2 : 65±5 H_2 : 35±5	CH_4 : 72±5 CO_2 : 28±5 H_2 : < 1

Table 6.7 Feed considerations for the design

	10 000
Population [p]	
MSW [kg/d/p]	1.50
Separate Collection [%]	50.00
OFMSW [%]	55.00
LHV_{OFMSW} [MJ/kg_{DM}]	17.00

Finally, the sizing (see **Table 6.8**) of the plant was performed in order to carry out the *ESA*. For this case, sizing is required to quantify the amount of materials and chemicals (*indirect energy*) that are necessary for a plant of the required conditions.

Table 6.8 Sizing of the TSAD system

	H₂ - bioreactor	CH₄ - bioreactor
D/h	3	3
V [m³]	21.175	158.813
D [m]	4.325	8.465
h [m]	1.442	2.822
Cement - ϵ_1 [m]	0.300	0.300
Insulator - ϵ_2 [m]	0.080	0.080

6.4 Results and Discussion

The *ESA* was carried out using Cumulative Energy Demand (CED) from a LCA software (SimaPro 7.2.4) database (Ecoinvent, 2007), to estimate the amount of energy used for extraction, manufacturing and transport of the materials of interest. CED values were used as reported in the data based, using the cumulative terms for all energy sources without any weighting factor. Furthermore, in the case of hydrogen and fossil fuels (e.g. CH₄), the assigned energy content corresponds to the Lower Heating Value (MJ/mol).

As a temporary reference framework, a useful lifetime of 20 years for the three technologies was set and the corresponding assessment of the elements that must be replaced when their useful life is inferior to that of the technology was included.

Even though the *ESA* is aimed at evaluating the energy sustainability of a given technology, the quantification of indirect energy also allows to shed light on the MI. **Table 6.9** shows the main materials considered for each case. In the case of SMR, the use of materials is low, in fact, the employed technology (Ultraformer) is designed for small-scale applications, mainly domestic use and/or urban transportation, which requires a compact structure and limited quantities of materials. On the other hand, some of the materials are very energy intensive (i.e. high CED), such as the metals used in the catalytic meshes, which are also subject to deactivation over operation and must therefore be replaced periodically.

For the SPWE technology, the MI and their corresponding energy footprint was performed considering not only the photovoltaic panels and the structure, but also taking into account the corresponding CED for the necessary electrical components. As reported in **Table 6.9**, the MI used for the panels and the bracket, which cover

an area of approximately 190 m², is quite high (i.e. in the order of 10⁴ kg), while the other components present a rather low MI in the 10²-10³ kg range. Finally, the case of the TSAD presents a large MI (i.e. also in the order of 10⁴ kg), mainly dedicated for the construction of both fermenters, in particular large amounts of cement and insulating material and lower amounts of steel for auxiliary equipment and pipelines.

Table 6.9 Main Materials Input (MI) considered for the *ESA*

Component		Amount [kg]	CED [MJ/kg]	Material Description
<i>Steam-Methane Reforming (SMR)</i>				
Block Unit	Total	1.12E+01	5.25E+01	Stainless Steel 304 X5CrNi18 (304)
	CATBUR	9.12E-02	9.50E+03	Pd5%/Al ₂ O ₃ ; Replacement each 8 months
	SREF	1.01E-01	9.84E+03	Pt5%/Al ₂ O ₃ ; Replacement each 8 months
	WGS	4.78E-01	9.89E+03	Pt5%/ZrO ₂ ; Replacement each 8 months
	PROX	3.37E-02	1.45E+04	Rh5%/Al ₂ O ₃ ; Replacement each 12 months
Auxiliaries	Total	1.00E+01	5.25E+01	Pumps, blower and pipelines
<i>Solar-Powered Water Electrolysis (SPWE)</i>				
PV		1.06E+04	6.64E+01	Materials covering 190 m ² ; Polycrystalline silicon
Structure		3.17E+03	1.10E+01	70% Wood Class II /30% Construction Steel Fe520 I
Inverter		4.00E+02	1.36E+02	Inverter 1500W; (Replacement 10 years)
Electrolyzer		1.68E+03	2.39E+01	Electrolyser; (Replacement 5 years)
<i>Two-Stage Anaerobic Digestion (TSAD)</i>				
S1	Mixer	2.32E+02	5.25E+01	Stainless Steel 304 X5CrNi18 (304)
	Cement	2.36E+04	3.58E+00	General purpose cement
	Insulation	2.85E+03	9.52E+01	Polystyrene foam slab
	PVC	3.82E+01	6.86E+01	PVC calendered sheet (Digester Dome)
	Auxiliaries	2.65E+02	5.25E+01	Integrated value pumps and pipelines
S2	Cement	9.06E+04	3.58E+00	General purpose cement
	Insulation	1.09E+04	9.52E+01	Polystyrene foam slab
	PVC	1.46E+02	6.86E+01	PVC calendered sheet (Digester Dome)
	Auxiliaries	1.02E+03	5.25E+01	Integrated value pumps and pipelines

After calculating the different components of the indirect energy, the relevant energy flows for the *ESA* can be obtained, by applying **Equations 6.2 – 6.9** and according to the flow diagrams depicted in **Figure 6.3**, **Figure 6.4** and **Figure 6.6**, and are shown in **Table 6.10**.

First of all, the amount of *primary energy* available in each technology was estimated; for the SMR and TSAD, the LHV of CH₄ and biomass (OFMSW) is used as a reference, respectively. For SPWE, the *primary energy* is calculated based on the yearly average irradiance in the coordinates where the photovoltaic panels are installed. However, for SMR, there is an energy flow of *already spent energy* associated with the methane production phase, which includes extraction, pre-treatment and transport to the point of use (CED_{CH4}=0.07 MJ_{eq}/mol CH₄, which represents a fraction of 8-9 % of the total LHV_{CH4}). In the case of TSAD, the OFMSW is obtained from the total of the differentiated MSW collection, hence there is an energy cost associated to the MSW collection and sorting step (~100 kWh/ton_{MSW}) and an important flux of *avoided energy* that corresponds to the energy saved for the avoided waste to landfill scenario (~117 kWh/ton_{OFMSW}). The produced energy for SMR, SPWE and the first stage (S1) of the TSAD corresponds

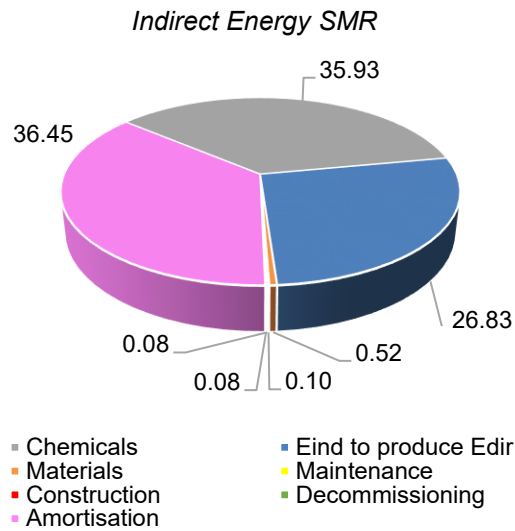
to the primary energy contained in H_2 , while for the two-step system TSAD (S1 + S2) the sum of $H_2 + CH_4$ was considered.

The *direct energy* in each case corresponds to the energy expenses during operation, which ideally consume a fraction of the *produced energy*. SMR is a technology that requires high working temperatures, due to the thermodynamics of the reactions involved in the process along with a continuous flow of gases, which also requires a high-power input for the compressors. On the other hand, the photovoltaic system (PV) has few *direct energy* expenses, mainly the power consumption of the inverters (i.e. with different threshold during operation and stand-by conditions), which in any case is rather modest. When the system is coupled to the water electrolyser, the *direct energy* significantly increases, since the system requires a continuous supply of electricity, not only during the hours of irradiance, to operate in optimized conditions, hence the deficit is supplied by the electric grid. The experimental tests conducted on the water dissociator showed a long start-up time until operative conditions were achieved (i.e. lasting approximately 50-60 minutes) and resulted in an average power demand of 7.81 kW, a H_2 flow rate of $0.92 \text{ Nm}^3/\text{h}$ and an average yield of 39.63 % which contrasts with the values for steady-state operation, i.e. 8.11 kW, $1.83 \text{ Nm}^3/\text{h}$ and 72.17%, respectively. In the TSAD case, the *direct energy* corresponds to: *i)* the expenses to heat up the feed (i.e. diluted OFMSW) to the conditions of exercise (35°C) of the bioreactors *ii)* to compensate the environmental thermal losses and *iii)* the power input to the agitators, which is a requirement in both stages (S1 and S2), although in different proportions and to other auxiliary equipment (e.g. mixer). Alone S1, as shown in **Table 6.10**, the energy produced (H_2) is not enough to cover *direct energy* expenses, whereas when the complete system is considered with both fermenters, the *produced energy* can supply the *direct energy*.

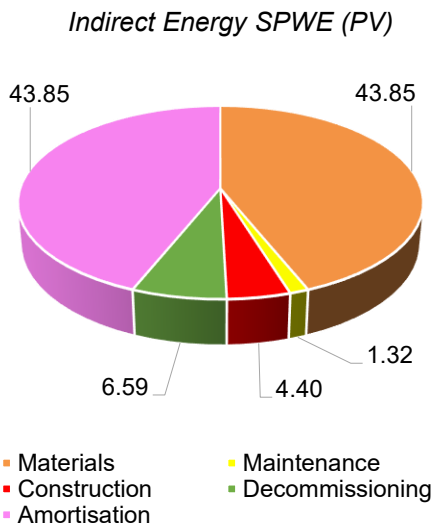
The *indirect energy* was calculated using the materials presented in **Table 6.9**, the flows of chemicals required for the operation and estimating the corresponding energy quotas for maintenance, construction and decommissioning, in addition to the *indirect energy* needed to produce the *direct energy*. The E_{labour} was only considered for the TSAD system, considering the cumulative energy demand to provide the daily calories of human diet (see **section 6.2.4**). On the contrary, SMR and SPWE do not have allocated E_{labour} quotas, because the daily operation does not require dedicated human operators. As stated before, the Ultraformer (SMR) is designed to be used, for example, in the transport sector, so the required human labour is allocated to $E_{\text{maintenance}}$. The SPWE case is similar, labour force is only required for some special operations (e.g. start-up, maintenance, replacement of PV panels). The contribution of E_{amor} was calculated for each case under analysis, as explained in **section 6.2.4**, including in the E_{ind} an energy quota corresponding to the sum of indirect energy of materials and chemicals.

The percentage share of each component of the *indirect energy* are presented in **Figure 6.7**. The most important contributions for indirect energy are:

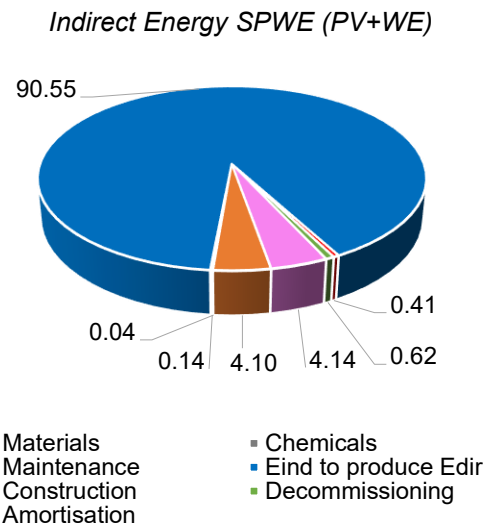
a)



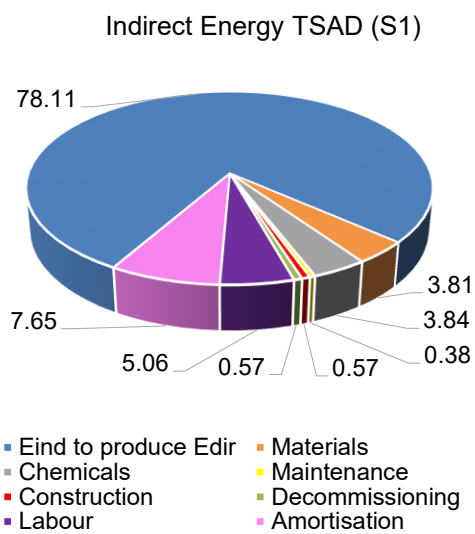
b)



c)



d)



e)

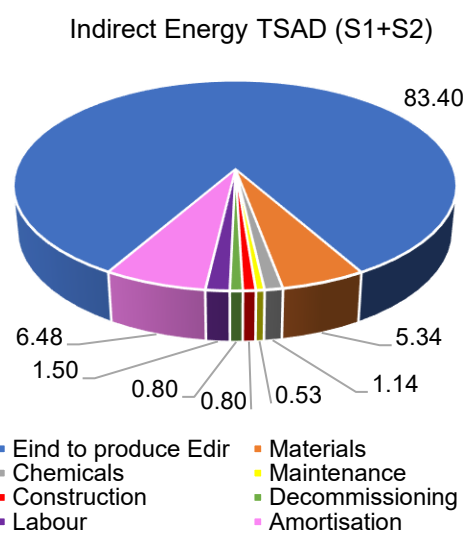


Figure 6.7. Percentage composition of the *indirect energy* for each technology configuration under analysis

- SMR: indirect energy is mainly constituted by three key contributions: the energy of chemicals (35.93%), the E_{amor} which is 36.45% and the *indirect energy* to produce direct energy (26.83%), which corresponds to the energy costs of methane production (see **Figure 6.7a**).

- SPWE: for the PV system, most of the indirect energy (87.70%) corresponds to materials and amortisation in equally proportions since there is no chemicals flow requested for operation; the $E_{\text{maintenance}}$ and $E_{\text{construction}}$ fraction is low, together representing 5.72%, while the $E_{\text{decommissioning}}$ corresponds to 6.59% (**Figure 6.7b**). For the case that is considered the PV system coupled to the electrolyser (**Figure 6.7c**), the flow of *indirect energy* increases significantly, mainly due to the grid power input, which is necessary to supply the water dissociator during the hours where there is no solar irradiance. For this configuration (PV+WE), the distribution of the *indirect energy* changes, and the E_{ind} to produce E_{dir} amounts to 90.55%, the E_{amor} 4.14% and the E_{mat} 4.10%

- TSAD: The system configuration of only one-stage (S1) and two-stages (S1 + S2) present a distribution of *indirect energy* mainly constituted (78.11-83.40%) by the E_{ind} to produce E_{dir} , which is the energy required for maintaining operative mixing and temperature conditions, while materials represent a modest fraction (3.80-5.34%), as well as the share of chemicals (1.14- 3.84%). The $E_{\text{construction}}$ and $E_{\text{decommissioning}}$ are relatively low (<1%) for both cases under analysis. The E_{labour} , which was assumed to be an operator during the 365 days of the year, results in a fraction of 5.06 % for the case of S1, while for the mixed system (S1 + S2) it represents only 1.50%. Finally, the share of amortisation energy resulted in 7.65% for S1 and the S1+S2 system in 6.48 (see **Figure 6.7d** and **Figure 6.7e**).

The last step of the *ESA* is the calculation of the indicators presented in **section 6.2.3** and **6.2.5**. The first calculated indicator (ESI), resulted > 1 for all the systems except for the S1 configuration of the TSAD, where a value of 0.12 was obtained (see **Table 6.10**). This means that the energy produced in the form of hydrogen is enough to cover only 12% of direct energy costs and therefore no further analysis can be conducted for this configuration (i.e. S1 alone). On the other hand, for the combined configuration (S1+S2), the resulting ESI value is 3.63, which respects the first step of the *ESA* methodology for the subsequent phases. For SPWE, the only use of PV panels has a high ESI value ($\text{ESI} \sim 180$); and it is due to the rather low energy expenditure that the PV system has during operation (i.e. with ESI being calculated on produced power instead of hydrogen), while for the coupled system of (PV + WE), the ESI is very close to 1 (calculated as produced H_2 on supplied *direct energy*), which indicates that the technology is debatable in terms of energy sustainability. The SMR technology, which is currently the most widespread to produce H_2 , resulted in an ESI value close to 2.5.

Finally, the EROI and EPT indicators were calculated. For SMR and TSAD, EROI values of 2.47 and 2.24 were obtained, respectively. For SPWE, the PV system yielded an EROI value of 1.25, while the combined system resulted in 0.01, which means that for every 100 units of invested energy, only 1 or less than one is obtained (i.e. hence energy sustainability should be revised for this technology). Finally, the estimated EPT amounted to 8.09 (SMR), 15.97 (only PV) and 8.94

(TSAD) years. Since the combined SWPE system (PV + WE) technology yielded a low EROI value (i.e. $\ll 1$), the EPT is unrealistic in comparison to the relative useful life of the technology. In addition, the dimensionless EPT was calculated, taking as reference the estimated useful life of the plant, to determine the fraction of the useful life that each technology will devote to repay the invested energy (see Table 6.10).

Table 6.10 Main energy flows considered for the *ESA*

<i>Primary Energy Source</i>		<i>Fossil</i>			<i>Biomass</i>	
		<i>(SMR)</i>	<i>(PV)</i>	<i>(PV+WE)</i>	<i>(S1)</i>	<i>(S2)</i>
<i>Primary Energy [MJ]</i>		6.01E+06	2.50E+07	2.50E+07	1.79E+08	1.79E+08
<i>Avoided Energy [MJ]</i>		-	-	-	1.26E+07	1.26E+07
<i>Already Spent Energy [MJ]</i>		5.56E+05	-	-	1.97E+07	1.97E+07
<i>Available Energy [MJ]</i>		5.46E+06	2.50E+07	2.50E+07	1.72E+08	1.72E+08
<i>Produced Energy [MJ]</i>		6.15E+06	2.27E+06	6.15E+06	8.96E+06	1.02E+08
<i>Direct Energy</i>	<i>Heat [MJ]</i>	2.25E+06	-	-	1.27E+07	1.69E+07
	<i>Power [MJ]</i>	3.57E+00	1.26E+04	6.02E+06	2.58E+06	9.26E+06
	<i>Materials [MJ]</i>	8.19E+03	7.91E+05	8.31E+05	3.85E+05	1.81E+06
	<i>Chemicals [MJ]</i>	5.66E+05	-	8.49E+03	3.88E+05	3.88E+05
	<i>Maintenance [MJ]</i>	1.64E+03	2.38E+04	2.78E+04	3.85E+04	1.81E+05
<i>Indirect Energy</i>	<i>E_{ind} to produce E_{dir} [MJ]</i>	4.23E+05	-	1.84E+07	7.89E+06	2.83E+07
	<i>Construction [MJ]</i>	1.23E+03	7.93E+04	8.33E+04	5.77E+04	2.72E+05
	<i>Decommissioning [MJ]</i>	1.23E+03	1.19E+05	1.25E+05	5.77E+04	2.72E+05
	<i>Labour [MJ]</i>	-	-	-	5.11E+05	5.11E+05
	<i>Amortisation [MJ]</i>	5.74E+05	7.91E+05	8.39E+05	7.73E+05	2.20E+06
<i>E net [MJ]</i>		3.90E+06	2.26E+06	1.28E+05	-6.33E+06	7.60E+07
<i>E ind [MJ]</i>		1.58E+06	1.80E+06	2.03E+07	1.01E+07	3.40E+07
<i>E useful [MJ]</i>		2.32E+06	4.55E+05	-2.01E+07	-1.64E+07	4.20E+07
<i>H₂ production [Nm³]</i>		5.72E+05	-	5.72E+05	8.33E+05	-
<i>ESI [-]</i>		2.48	180.01 ^{a)}	1.02	0.12	3.63
<i>EROI [-]</i>		2.47	1.25 ^{a)}	< 1	-	2.24
<i>EPT [y]</i>		8.09	15.97 ^{a)}	-	-	8.94
<i>EPT [-]^{c)}</i>		0.40	0.80 ^{a)}	-	-	0.45

^{a)} Produced energy is accounted as electricity.

^{b)} Produced energy is accounted as the sum of H₂ + CH₄.

^{c)} Corresponds to the fraction on the estimated useful life (20 years) used for this study that the EPT represents.

6.5 Conclusions

The study of energy sustainability is of great importance in our modern society, where sustainable solutions are sought for the momentous problem of sustainable energy supply. The case study of the H₂ production serves to evaluate different processes, taking a closer look at the way in which each technology requires and produces energy, either directly or indirectly. Each case under analysis (SMR, SPWE and TSAD), has different characteristics such as primary energy source, intermediate carriers, *direct* and *indirect energy* expenditures and, in addition, produces different *useful energy* flows, whose performance can be compared through global indicators such as the ESI, EROI and EPT. SMR resulted as the best-performing in energy sustainability terms with higher EROI value and lower EPT (2.47 and 8.09 years, respectively) than TSAD (2.24 and 8.94 years, respectively),

although TSAD produces not only hydrogen, but also an important flow of CH₄ which influences the obtained results since the production of biohydrogen alone resulted in no surplus of *useful energy* to society.

On the other hand, the combined SPWE resulted in very low EROI values (0.01), while the PV system for the production of electricity present a better performance (1.25). However, after the application of the *ESA*, other relevant Life Cycle Assessments (LCA) should be performed to quantify additional environmental aspects regarding sustainability.

Lastly, the present methodology (*ESA*) offers a consistent approach, which encompasses the different energetic flows that cross the boundaries of a determined technology and that can be of great importance in the future mixed system of energy services to quantify the physical scarcity of energy sources.

References

- [1] N. Georgescu-Roegen, “The Promethean Condition of Viable Technologies,” *Mater. Soc.*, vol. 7, pp. 425–435, 1983.
- [2] D. C. C. Catling, “The Great Oxidation Event Transition,” *Treatise on Geochemistry*, vol. 6, pp. 177–195, 2014.
- [3] E. Sacher, *Grundzüge einer Mechanik der Gesellschaft*. Salzburg: Fischer, 1881.
- [4] P. Geddes, “An Analysis of the Principles of Economics,” *Proc. R. Soc. Edinburgh*, vol. 12, pp. 943–980, 1884.
- [5] R. Clausius, *Über die Energievorräte der Natur und ihre Verwertung zum Nutzen der Menschheit*. Bonn: Max Cohen & Sohn, 1885.
- [6] F. Soddy, *Cartesian Economics: The Bearing of Physical Science Upon State Stewardship*. Students’ Unions of Birkbeck College and the London School of Economics, 1922.
- [7] J. Parnell and N. Blamey, “Global hydrogen reservoirs in basement and basins,” *Geochem. Trans.*, vol. 18, no. 2, 2017.
- [8] C. A. S. Hall, S. Balogh, and D. J. R. Murphy, “What is the minimum EROI that a sustainable society must have?,” *Energies*, vol. 2, no. 1, pp. 25–47, 2009.
- [9] F. Fizaine and V. Court, “Energy expenditure, economic growth, and the minimum EROI of society,” *Energy Policy*, vol. 95, pp. 172–186, Aug. 2016.
- [10] R. S. Atlason, “EROI and the Icelandic society,” *Energy Policy*, vol. 120, no. May, pp. 52–57, 2018.
- [11] J. G. Lambert, C. A. S. Hall, S. Balogh, A. Gupta, and M. Arnold, “Energy, EROI and quality of life,” *Energy Policy*, vol. 64, pp. 153–167, 2014.
- [12] J. Feng, L. Feng, J. Wang, and C. W. King, “Modeling the point of use EROI and its implications for economic growth in China,” *Energy*, vol. 144, pp. 232–242, Feb. 2018.
- [13] C. A. S. Hall, J. G. Lambert, and S. B. Balogh, “EROI of different fuels and the implications for society,” *Energy Policy*, vol. 64, pp. 141–152, 2014.
- [14] C. A. S. Hall, “Energy Return on Investment as Master Driver of Evolution BT - Energy Return on Investment: A Unifying Principle for Biology, Economics, and Sustainability,” C. A. S. Hall, Ed. Cham: Springer International Publishing, 2017, pp. 59–72.
- [15] M. Raugei, R. Frischknecht, C. Olson, P. Sinha, and G. Heath, “Methodological Guidelines on Net Energy Analysis of Photovoltaic Electricity,” International Energy Agency - Photovoltaic Power Systems Programme, 2016.
- [16] R. Frischknecht, F. Wyss, S. Büsser Knöpfel, T. Lützkendorf, and M. Balouktsi, “Cumulative energy demand in LCA: the energy harvested approach,” *Int. J. Life Cycle Assess.*, vol. 20, no. 7, pp. 957–969, 2015.
- [17] M. Di Addario, A. C. L. Malavè, S. Sanfilippo, D. Fino, and B. Ruggeri, “Evaluation of sustainable useful index (SUI) by fuzzy approach for energy producing processes,” *Chem. Eng. Res. Des.*, vol. 107, pp. 153–166, 2016.
- [18] B. Ruggeri, T. Tommasi, and S. Sanfilippo, *BioH₂ & BioCH₄ Through Anaerobic Digestion: From Research to Full-scale Applications*. Springer

- London, 2015.
- [19] S. Sanfilippo, A. Raimondi, B. Ruggeri, and D. Fino, "Dietary vs. transport: An analysis of environmental burdens pertaining to a typical workday," *Int. J. Consum. Stud.*, vol. 36, no. 2, pp. 133–140, 2012.
 - [20] G. Lombardelli, R. Pirone, and B. Ruggeri, "LCA Analysis of different MSW treatment approaches in the light of energy and sustainability perspectives," *Chem. Eng. Trans.*, vol. 57, pp. 469–474, 2017.
 - [21] B. Ruggeri, S. Sanfilippo, and T. Tommasi, "Sustainability of (H₂ + CH₄) by Anaerobic Digestion via EROI Approach and LCA Evaluations," in *Life Cycle Assessment of Renewable Energy Sources*, Springer, London, 2013, pp. 169–194.

List of Figures

Figure 1.1 Primary energy production from biogas for the main European players during 2010-2016 [26].	5
Figure 1.2 Electricity generation from biogas for the main European players during 2010-2016 [26].	6
Figure 1.3 Historic [2000-2016] prices of regional standards of Natural Gas.	8
Figure 2.1 General scheme of the Two-Stage Anaerobic Digestion (TSAD) process	12
Figure 2.2 Hydrolysis first order kinetics for pre-treated and non-pre-treatment Organic Market Waste (OMW)	17
Figure 2.3 Picture of the Retsch MM 400 bead milling device.	22
Figure 2.4 Photograph of the rotor-stator system	23
Figure 2.5. Graphical representation of the key components of the ultrasonication device for the different types of operation.	23
Figure 2.6 Photograph of a cultivating plate and binary contrast image of the area occupied by the cells on the same plate	24
Figure 2.7 Photograph of the front view of the experimental set-up used for the <i>in situ</i> laser black reflection measurements and Schematic design of the working principle and main components of the probe.	25
Figure 2.8 Colonized area on cultivation plates a function of the application time of the bead milling pre-treatment on a culture of <i>B. subtilis</i> .	26
Figure 2.9 Normalized area of colonized area on agar plates after the application of rotor-stator pre-treatment at different intensity conditions	27
Figure 2.10 Percentage of colonized area on agar plates after the application of batch sonication at different conditions	27
Figure 2.11 Percentage of colonized area on agar plates after the application of continuous sonication at different conditions of amplitude.	28
Figure 2.12 Comparison of residual cell viability at different threshold of energy input for the different mechanical pre-treatments.	29
Figure 2.13 Particle size distribution (PSD) of <i>C. acetobutylicum</i> samples treated with ultrasonication at 20 % amplitude	30
Figure 2.14 Cumulative Particle size distribution (PSD) of <i>C. acetobutylicum</i> samples treated with ultrasonication at 20 % amplitude.	31
Figure 2.15 Particle size distribution (PSD) of <i>C. acetobutylicum</i> samples treated with ultrasonication at 50 % amplitude	32
Figure 2.16. Photograph of the macro-flocs present in the stock culture of <i>C. acetobutylicum</i>	32
Figure 2.17 Cumulative Particle size distribution (PSD) of <i>C. acetobutylicum</i> samples treated with ultrasonication at 50 % amplitude.	33
Figure 2.18 Particle size distribution (PSD) of Agricultural Waste samples treated with ultrasonication at 50 % amplitude	34

Figure 2.19 Particle size distribution (PSD) of Agricultural Waste samples treated with ultrasonication at 50 % amplitude	34
Figure 2.20 Particle size distribution (PSD) of Agricultural Waste samples treated with bead mill	35
Figure 2.21 Cumulative Particle size distribution (PSD) of Agricultural Waste samples pre-treated with bead mill	36
Figure 2.22 Particle size distribution (PSD) of Agricultural Waste samples pre-treated with rotor-stator	37
Figure 2.23 Particle size distribution (PSD) of Agricultural Waste samples pre-treated with rotor-stator	37
Figure 3.1 Possible process integration for Dark Fermentation (DF).....	44
Figure 3.2 Map showing the geographical location of different types of biorefineries in Europe for the year 2017	46
Figure 3.3 Basic reference scheme of a third generation biorefinery, producing chemicals and energy	47
Figure 3.4 Proposed cellular stages of bacterial viability, comprehending reversible and irreversible damages and bacterial features which can be used to track cell viability	49
Figure 3.5 Schematic representation of the flow cytometry apparatus.....	52
Figure 3.6. Schematic representation of the measuring cell for polarizability anisotropy measurements.....	54
Figure 3.7 Agricultural waste used as substrate.....	56
Figure 3.8 Photograph of Gas Analysis system and collector bottles on analytical balances for the quantification of the gas flow.	57
Figure 3.9 Behaviour of pH and hydrogen yield throughout a dark fermentation with and without pH control	59
Figure 3.10 Ethanol, formic, acetic, propionic and butyric acid concentrations throughout dark fermentation with and without pH control	60
Figure 3.11 Results of the FDPA measurements 3D and 2D electrooptical measurements of cell polarizability with and without pH control.....	62
Figure 3.12 Histogram plots of the Forward Scatter Channel, at time point I for the system A and B	63
Figure 3.13 Combined plot of the bivariate FSC vs SSC signals, along with histograms for each channel.	63
Figure 3.14 Evolution of the percentual relative abundance of each sub-population	64
Figure 3.15 Bivariate (FSC vs SSC) density plots at different time points showing the evolution of sub-populations.....	65
Figure 3.16 Regions of polarized and depolarized cells discriminated using the SSC vs BOX plots in FC.....	68
Figure 3.17 Fraction of depolarized cells for each system at different time points, calculated using the BOX probe in FC analysis.	68
Figure 3.18 Correlation of FDAP measurements vs % of BOX stained cells.	69
Figure 4.1 Relaxation times of phenomena	79
Figure 4.2 Pourbaix diagram of the Fe-H ₂ O system.....	82

Figure 4.3 Cumulative specific H ₂ gas evolution during Anaerobic Corrosion ...	85
Figure 4.4 Cumulative specific H ₂ production during Dark Fermentation	86
Figure 4.5 Cumulative specific CO ₂ production and H ₂ /CO ₂ ratio in the gas produced during the DF tests, with and without the addition of Fe ⁰	87
Figure 4.6 Total H ₂ production for the AC and DF systems	89
Figure 4.7 Simplified propionic acid degradation pathway into acetic acid for Clostridia.....	91
Figure 4.8. Possible fate of the anaerobic corrosion products (Fe ²⁺ and e ⁻) and their interaction with HPB	92
Figure 5.1 Scheme of the used pilot plant in continuous mode and Pilot plant picture.	104
Figure 5.2 Block diagram of the experimental design	106
Figure 5.3 Graphical representation of Equation 5.1 and 5.2 , evidencing the kinetic selection of microorganisms based on HRT	108
Figure 5.4 Behaviour of Volatile Solids concentrations under different HRT ...	111
Figure 5.5 Specific H ₂ and CH ₄ productivity at the different tested HRT	112
Figure 5.6 Fano Factor evaluated for each HRT unit time for the tested HRT ..	114
Figure 5.7 Cumulative energy production for the tested HRT	116
Figure 6.1 Life stages of energy in our modern society: from primary energy to energy services.....	124
Figure 6.2 Analogical Model (AM) used to simplify the energy fluxes of each technology.....	127
Figure 6.3 Simplified flow diagram of the Steam-Methane Reforming (SMR) process	131
Figure 6.4 Simplified flow diagram of the Solar-Powered Water Electrolysis (SPWE) process	132
Figure 6.5 Monthly grid power demand for the operation of the electrolyser, considering different operation time slots of operation.	133
Figure 6.6 Simplified flow diagram of Two-Stage Anaerobic Digestion (TSAD) process	134
Figure 6.7. Percentage composition of the <i>indirect energy</i> for each technology configuration under analysis.....	138

List of Tables

Table 1.1. Produced primary energy and electrical and thermal efficiency from biogas in Europe during 2016.....	7
Table 1.2 Total primary energy consumption and biogas share for 2016 in Europe.....	7
Table 2.1 Main hydrolases responsible for the degradation of specific organic substrates.....	14
Table 2.2 Literature review of Hydrolysis Models	19
Table 2.3 Taxonomic classification of the fermentative microorganisms used during the tests.	21
Table 2.4 Medium composition for <i>Clostridium acetobutylicum</i> and <i>Bacillus subtilis</i> cultures.	21
Table 2.5 Characteristic <i>D values</i> of interest for the ultrasound pre-treatment on Agricultural Waste.....	35
Table 2.6 Characteristic <i>D values</i> of interest for the bead mill pre-treatment on Agricultural Waste.....	36
Table 2.7 Characteristic <i>D values</i> of interest for the rotor-stator pre-treatment on Agricultural Waste.....	37
Table 2.8 Specific Energy consumption for each tested pre-treatment on Agricultural Waste.....	38
Table 3.1 Fresh feedstock characterization.....	56
Table 3.2 Relative abundance of each sub-population for both systems.	64
Table 3.3 Settings for the BOX dye on treated, non-treated and control samples	67
Table 4.1 Model composition of the Organic Market Waste (OMW) used for the tests.	78
Table 4.2 Chemical reactions involved in the water/iron system	81
Table 4.3 Experimentally evaluated Dark Fermentation parameters.....	87
Table 4.4 Dynamic parameters evaluated by means of a best fitting procedure and calculated relaxation time values for each test.	89
Table 4.5 ANOVA analysis of the experimental results.....	90
Table 5.1 Model composition of the feed to S1	105
Table 5.2 Performance results and operative conditions for each tested condition I, II and III.....	110
Table 5.3 Fano Factor evaluate considering the total data for each HRT.....	114
Table 5.4 Comparison among continuous TSAD systems from literature	117
Table 5.5 Suggested process parameters of the TSAD configuration for S1 and S2	118
Table 6.1 Relevant components of the <i>indirect energy</i>	129
Table 6.2 Reactions of interest for each section of the Ultraformer	131
Table 6.3 Collected data from the Ultraformer.....	132

Table 6.4 Curvature-weighted Irradiated Surface for each string of the PV array	133
Table 6.5 Technical Specifications and dimensions of the main equipment of the SPWE system.....	133
Table 6.6 Performance of the laboratory TSAD using OFMSW as feed.....	134
Table 6.7 Feed considerations for the design.....	135
Table 6.8 Sizing of the TSAD system.....	135
Table 6.9 Main Materials Input (MI) considered for the <i>ESA</i>	136
Table 6.10 Main energy flows considered for the <i>ESA</i>	140